342

SEPARATION OF GAS MIXTURE IN A SUPERSONIC JET

by

Hisashi Mikami

January 1970

TABLE OF CONTENTS

ACKNOWLEDGEMENT

The auther wishes to express his gratitude to Professor Y. Takashima, for the opportunity to pursue this investigation, for his valuable guidance and supervision, and for his patient encouragement.

Thanks are also due to Dr. Y. Ooyama, former Director of the Research Laboratory of Nuclear Reactor, who suggested the problem in the first place.

The auther is also indebted to Professors Y. Mori, S. Ito, M. Shindo, and S. Aoki for their helpful suggestions.

I would also like to thank the staff and students of the section of the Nuclear Chemical Engineering, for their invaluable assistance, particularly, for the assistance recieved from Mr. Y. Endo during the experiment.

SUMMARY

Separation phenomena in supersonic jets of gas mixture were investigated.

The integral mass flux which can be obtained by integrating mass flux of a relevant species over a streamtube in a jet, with the aid of the Chapman-Enskog theory of diffusion, was used for evaluating the degree of separation in this work.

Several experimental data on the separation of binary gas mixture in axisymmetric and two-dimensional supersonic jets were obtained. In addition to these data, Becker's experimental results were refered to comparing with the theoretical results.

Two kinds of flow fields of axially symmetric and two-dimensional supersonic jets were computed by using the numerical method of characteristics. Then, on the basis of these calculation results, the integral mass flux along a supersonic streamtube and along that acompanying with an oblique shock wave was calculated and compared with the values obtained from the experimental data.

It was confirmed that the proposed method of calculation was widely useful to know the characteristics of species separation in supersonic jets.

NOTATION

Unless otherwise noted, all quantities are dimensionless.

A	area of nozzle exit, cm^2
A	area of heat-transfer surface, cm^2
a	sonic velocity, cm/s
a	shock strength defined by Eq. (3.25)
B	thermistor constant, °K
D	characteristic length of thermistor, cm
D	diameter of nozzle exit, cm
D_{ij}	multicomponent diffusion coefficient, cm^2/s
D_i^T	thermal diffusion coefficient of species i, g/cm.s
$\mathcal{D}_{ij}$	binary diffusion coefficient, cm^2/s
Div	divergent operator, cm^{-1}
f	velocity distribution function, s^3/cm^3
f	mole fraction of heavier species in a shock wave of binary gas mixture
G	mass flow rate through nozzle, g/s
Grad	gradient operator, cm^{-1}
h	heat transfer coefficient, $cal/s.cm^2.°K$
I	electric current, A
J_i	total mass flux of species i, g/s
j	mechanical equivalent of heat, J/cal
$\underset{\sim}{j}_i$	mass flux vector of species i, $g/cm^2.s$
$\tilde{K}$	proportional constant in Maxwell's inverse fifth power law, $cm^6/g.s^2$
Kn	= L/D, Knudsen number
k	Boltzmann constant, erg/°K
k_T	thermal diffusion ratio
L	mean free path of gas, cm
L_{mix}	mean free path of gas mixture, cm
M	molecular weight, g/mol
M	= q/a, local Mach number
M^*	= q/a*, critical Mach number

M^{**}	$= 2M_1M_2/(M_1+M_2)$, reduced molecular weight, g/mol
M_i	molecular weight of species i, g/mol
$\overline{M}$	mean molecular weight, g/mol
Δm	$= m_2 - m_1$, difference of molecular mass, g
$\overline{m}$	$= \sum_{i=1}^{n} m_i N_i$, average mass of gas mixture, g
m_i	mass of species i, g
$\overline{m}_A$	average mass of argon isotope mixture, g
$\left(\frac{\Delta m}{\overline{m}}\right)_{\mathcal{D}}$	$= \left(\frac{\mathcal{D}_{12}}{\mathcal{D}_{13}} - 1\right) + \left(\frac{m_3}{\overline{m}} - \frac{\mathcal{D}_{12}}{\mathcal{D}_{13}}\frac{m_2}{\overline{m}}\right)$, modified molecular mass difference, g
N_i	mole fraction of species i
Nu	$= \frac{hD}{\lambda}$, apparent Nusselt number
Nu*	actual Nusselt number calculated by Eq. (5.11)
n	$= \sum_{i=1}^{n} n_i$, number density of molecules, n/cm^3
n_i	number density of species i, n/cm^3
P	pressure, $dyne/cm^2$ or mm Hg
Pe	$= R^*a^0/D$, Péclet number
Pe	$= R^*a^0/\mathcal{D}_{23}^{\circ}\chi^{\circ}$, Péclet number
Pe_{13}	$= R^*a^0/\mathcal{D}_{13}^{\circ}$, Péclet number
Pr	$= C_p\mu/\lambda$, Prandtl number
Q	heat transfer from thermistor by any mechanism other than conduction through gas, cal/s
Q_i^*	molar flow rate of species i through nozzle, mol/s
Q_i^M	molar flow rate of species i of peripheral stream, mol/s
Q_i^K	molar flow rate of species i of core stream, mol/s
Q_A^*	molar flow rate of argon isotopes, mol/s
q	numerical value of gas velocity, cm/s
q_r	radial heat flux, $cal/s.cm^2$
R	resistance of thermistor, ohm
R	universal gas constant, erg/°K.mol
R*	radius of nozzle exit, cm
R*	half width of two-dimensional nozzle exit, cm
R	resistance of thermistor at temperature T, ohm
R_0	radius of sphere, cm
Re	$= R^*a^0/\nu^{\circ}$, Reynolds number
Re	$= WD/\nu^{\circ}$, Reynolds number
r	distance from jet axis, cm

r	distance from cone surface, cm
$\bar{r}$	$= r/R^*$
r	radial distance, cm
$\bar{r}$	normalized radial distance
Sc	$= \frac{\mu}{\rho \mathcal{D}_{12}}$, Schmidt number
Sh	= St Pe, Sherwood number
St	$= J/m^*Q^*$, Stanton number
s	coordinate along cone wall, cm
s	coordinate along streamline, cm
T	absolute temperature, °K
T^*_{ij}	$= T/\varepsilon_{ij}/k$, reduced temperature
T_w	wall temperature of thermistor, °K
t	temperature, °C
u	internal energy, erg/molecule
V	velocity of molecule, cm/s
$\bar{\mathbf{V}}_i$	diffusion velocity of species i with respect to $\mathbf{v}_0$, cm/s
$\bar{V}_i$	absolute value of $\bar{\mathbf{V}}_i$
$\bar{\mathbf{V}}_i'$	diffusion velocity of species i with respect to $\mathbf{V}_A$, cm/s
v	dimensionless velocity in shock wave
v_0	velocity on cone surface, cm/s
$\mathbf{V}_0$	$= \frac{1}{\rho}\sum_{i=1}^{n} \rho_i \bar{\mathbf{V}}_i$, mass average velocity of gas mixture, cm/s
$\mathbf{V}_A$	$= \frac{1}{\rho_A}\sum_{i=2}^{3} \frac{N_i}{N_2+N_3}\rho_i \bar{\mathbf{V}}_i$, mass average velocity of argon isotopes, cm/s
$\bar{\mathbf{V}}_i$	average velocity of species i, cm/s
W	$= \sqrt{\frac{p_0}{\rho_0}}$, characteristic velocity, cm/s
X	external force, dyne
x	distance along jet axis, cm
$\bar{x}$	$= x/R^*$
y	distance from jet axis, cm
$\bar{y}$	y/R^*
z	stream function

Greek symbols

α	$= (N_1^M/N_2^M)/(N_1^0/N_2^0)$, separation coefficient
α	$= \cos^{-1} R_0/r$

α	accommodation coefficient
α	thermal diffusion coefficient
α_{mix}	accommodation coefficient of gas mixture
β	$= 1/\tan \mu$
Γ	discharge coefficient
γ	ratio of specific heat
δ	angle between V_0 and $\overline{V}_2$, see Fig. 8, radian
ε	distance between shock and cone surface
ε	angle between V_0 and $\overline{V}_3$, see Fig. 8, radian
ε_A	$= \dfrac{N_1^M N_2^K}{N_2^M N_1^K} - 1$, separation effect
ε_{ij}	potential parameter for interaction between molecules i and j, erg
ζ	= tan
η	coordinate in characteristic coordinate system
Θ	angle between centerline and line perpendicular to cone surface (Fig. 32)
Θ	$= \dfrac{\overline{m}^M Q^M}{\overline{m}^* Q^*}$, cut relevant to gas mixture
Θ_A	$= \dfrac{\overline{m}_A^M Q_A^M}{\overline{m}_A^* Q_A^*}$, cut relevant to argon isotope mixture
θ	inclination of velocity vector
θ	molecular mass ratio of binary gas mixture
κ	curvature, cm^{-1}
κ	$= (\gamma - 1)/(\gamma + 1)$
κ	ratio of internal energy to translational energy
Λ	Prandtl-Meyer function, radian
λ	root of Eq. (3.29)
λ_g	thermal conductivity of gas
λ_{mix}	thermal conductivity of gas mixture
μ	$= \sin^{-1} 1/M$, Mach angle, radian
μ	viscosity of gas, g/cm.s
μ_{mix}	viscosity of gas mixture
ν	kinematic viscosity, cm^2/s
$\boldsymbol{\nu}$	unit vector normal to surface element d
$\boldsymbol{\nu}_A$	unit vector normal to streamline element of argon isotope mixture
ξ	coordinate in characteristic coordinate system, cm

ρ	density, g/cm^3
ρ_A	density of argon isotope mixture, g/cm^3
$d\Sigma$	surface element, cm^2
σ	angle of shock inclination, radian
σ_{ij}	collision diameter between molecules i and j, A
τ	dimensionless temperature in shock wave
χ	$= \dfrac{\mathcal{D}_{13}}{N_1\mathcal{D}_{23} + N_2\mathcal{D}_{13} + N_3\mathcal{D}_{12}}$
χ	$= \dfrac{\pi}{2} - \mu_{\xi=1}$
φ	angle between streamline and normal to shock wave
$\mathcal{G}$	$= p/\rho^{\gamma}$, Entropy function
ψ	stream function
$\Omega^{(1,1)*}$	$= \Omega^{(1,1)}/\Omega^{(1,1)}_{\text{rigid sphere}}$ collision integral
ω	$= 4y_4/\theta_3$
ω	integration constant

Superscripts

0,M,K	quantities relevant to conditions prevailing upstream, peripheral stream, and core stream, respectively
*	quantities at sonic condition

Subscripts

i	relating to species i
1,2	indicate lighter and heavier species of binary gas mixture
1,2,3	components He, ^{36}Ar, ^{40}Ar
A	quantities relevant to argon isotope mixture
Σ	quantities in shock wave
$\mathcal{E}$	quantities just behind shock
∞	quantities at infinity

I Introduction

The steep pressure gradient induced in a supersonic free jet causes pressure diffusion which in turn brings about separation of species. This phenomena was first applied to a practical separation process by Tahourdin and Dirac (1) at Oxford University in 1946. Similar effects were observed by Dickens et al. in 1948 in U.S.A.. They passed a H_2/N_2 gas mixture (43.9% H_2 - 56.1% N_2) through a nozzle to form a jet and found an increased concentration (68.5% H_2 - 31.5% N_2) in the peripheral stream of the divided jet. Thus, their invention of this apparatus was authorized as the U.S. patent in 1952(2). However, the process was not taken more attention until it was rediscovered independently by Becker, et al. at the University of Marburg, Germany, in 1954 (3), in the process of their basic study aimed at creating molecular beams of high intensity. Subsequently, Becker's group, now at Karsruhe, Germany, have been developing a process for the separation of isotopes for various configurations of the apparatus, and have published numerous experimental results. Furthermore, they have recently developed a new process for the separation of uranium isotopes using curved walls and adding helium into uranium hexafluoride. This jet separation pilot plant has been operated successfully (4). They are expecting this process to become economically competitive to the gaseous diffusion process.

On the other hand, several experiments on the separation of gas mixture in a free jet at very low pressure, were performed by the low pressure research group at University of California. They attempted a fundamental investigation of the jet separation based on the fluid dynamics of gas mixture. Chow, one of the members, measured the concentration distribution of the heavier species in the binary gas mixture throughout the jet by traversing a small sampling probe. (5)

Reis and Fenn (6), however, demonstrated that the gaseous constituents were a function of the way how to draw samples from the jet, because a curved shock, standing in front of the sampling tube could cause species separation. Also Waterman and Stern(7,8) measured the degree of separation on various gas mixtures in a free jet.

There have appeared several attempts to give a theoretical account of the jet separation. Nardelli and Repanai (9) made theoretical analysis which deals with the prediction of separation coefficients taking account of the pressure diffusion, when the supersonic jet of a gas mixture is separated by means of a skimmer into peripheral stream and central stream. All the analyses by Zigan (10), Mikami (11), and Sherman (12) were later developed on the basis of Nardelli and Repanai's analytical procedure. Recently Sherman has made an analytical study on the separation of a binary gas mixture in an axially symmetric free jet, and has given an equation for the mole fraction along the jet axis (12). Very recently, Rothe (13) measured the degree of separation in a helium-argon jet by an electron beam fluorescence method, and the separation results on the axis of the jet were in fairly good agreement with the Sherman' theory. Anderson et al. (14) also made measurements of diffusive separation of argon-helium mixtures in a free jet by means of a mass spectrometer detector, and obtained reasonable agreement between experimental results on the jet axis and the Sherman' equation.

The object of the work reported here was the more reliable prediction of the characteristics of jet separation process, aimed at some practical application in the design of facilities of this process.

II Theoretical Considerations

2.1 Diffusive Separation of Binary Gas Mixture in a Supersonic Jet

We first briefly describe the basic feature of diffusive separation in a supersonic jet. As shown in Fig. 1 , an isotope gas mixture is introduced into a nozzle at an inlet pressure p^0 and ejected from the nozzle exit at mass flow rate G . The supersonic jet thus created is separated by means of a skimmer into peripheral stream ΘG and central stream $(1-\Theta)G$, and then pumped away by vacuum pumps. The static pressure is p^M and p^K, respectively in the peripheral and central streams. The peripheral stream is thereby enriched in the light component and the central stream correspondingly enriched in the heavy component.

The enrichment of the lighter component in the peripheral stream can be explained qualitatively by the fact that a large pressure gradient created in a jet causes pressure diffusion of components and species separation.

Proposed Equation for Integral Mass Flux

To calculate mean concentration of peripheral and central streams, detailed information with respect to the concentration distribution in the jet is not necessary, but it is sufficient if we know the integral mass flux, which is obtained by integrating mass flux over the border surface between the peripheral and the central streams, from the nozzle exit to the skimmer.

Referred to coordinates moving along with the gas mixture flow, the mass flux of the lighter component $\dot{j}_1$ is given from the kinetic theory of gases as (15) :

$$\dot{j}_1 = \frac{n^2}{\rho} m_1 m_2 \mathcal{D}_{12} \left\{ \operatorname{grad} N_1 - \frac{\Delta m}{\bar{m}} N_1 N_2 \operatorname{grad} \ln p \right\} - D_1^T \operatorname{grad} \ln T \tag{2.1}$$

If both the first term of ordinary diffusion and the third term of thermal diffusion are neglected because of the relatively small variation of concentration in space and the very small value of thermal diffusion coefficient, the mass flux

$$\dot{j}_1 = -\frac{n^2}{\rho} m_1 m_2 \mathcal{D}_{12} \frac{\Delta m}{\bar{m}} N_1 N_2 \frac{1}{p} \operatorname{grad} p \tag{2.2}$$

The total mass flux into the peripheral stream J_1 can be obtained by integrating $\dot{j}_1 \cdot \nu \, d\Sigma$ from the nozzle exit to the skimmer over the border surface between the peripheral and the core streams, where ν denotes the unit vector normal to the surface element (see Fig. 2).

Thus

$$J_1 = -\int_0^S \frac{n^2}{\rho} m_1 m_2 \mathcal{D}_{12} \frac{\Delta m}{\bar{m}} N_1 N_2 \frac{1}{p} \operatorname{grad} p \cdot \nu \, 2\pi r \, ds \tag{2.3}$$

For two-dimensional jet,

$$J_1 = -\delta \int_0^s \frac{n^2}{\rho} m_1 m_2 \mathscr{D}_{12} \frac{\Delta m}{\overline{m}} N_1 N_2 \frac{1}{p} \operatorname{grad} p \cdot \nu \, ds \qquad (2.4)$$

where δ is the thickness of the jet.

The mutual diffusion coefficient is given by (16)

$$\mathscr{D}_{12} = 2.662 \cdot 10^3 \frac{\sqrt{T^3 / M^{**}}}{p\, \sigma^2 \Omega^{(1,1)*}(T^*)} \qquad (2.5)$$

The collision integral $\Omega^{(1,1)*}(T^*)$ has been calculated by Hirschfelder, et al. (17), with the Lennard-Jones potential assumed for the intermolecular force. Fig. 3 shows the relationship between $\Omega^{(1,1)*}$ and reduced temperature T^* for the Lennard-Jones potential. It is seen that the approximation

$$\Omega^{(1,1)*} \simeq 1.439\, T^{*-\frac{1}{2}} \qquad (2.6)$$

holds in a range of T^* between a certain small value and about 2.5. Thus, the relation between the collision integral and absolute temperature can be expressed as

$$\Omega^{(1,1)*} = c\, T^{-\frac{1}{2}} \qquad (2.7)$$

For example, the force constants σ and ε for the interaction between argon molecules are found in a table by the same author (18):

$$\sigma = 3.418\ \mathring{A}, \qquad \varepsilon/k = 124^\circ K$$

The self-diffusion coefficient in gaseous argon was measured as a function of temperature by Winn (19) and by de Paz, et al. (20). Their data are plotted in Fig. 4, in which the solid line represents the values predicted by Eqs. (2.5) and (2.7) with potential parameters $\sigma = 3.54\mathring{A}$, $\varepsilon/k = 124^\circ$K. The line is seen to fit the plots extremely well.

On the other hand, when the modified Buckingham potential is assumed for the intermolecular force, the values of $T^{*\frac{1}{3}}\Omega^{(1,1)*}(T^*)$ calculated by Mason (21) are approximately constant over a fairly wide range of T^*, as shown in Fig. 5.

The potential parameters for the Lennard-Jones potential between UF_6 molecules are found in a survey report by Dewitt (22):

$$\sigma = 5.2232\ \mathring{A}, \qquad \varepsilon/k = 439^\circ K$$

Thus, the relation between $\Omega^{(1,1)*}$ and T^* for UF_6 may be approximated by

$$\Omega^{(1,1)*} = c\, T^{-\frac{1}{3}} = 11.67\, T^{-\frac{1}{3}} \qquad (2.8)$$

below room temperature ($T^* = 0.67$).

The mutual diffusion coefficient of $^{235}UF_6$ and $^{238}UF_6$ has recently been measured by Brown, et al. (23) Their data are reproduced in Fig. 6 in which the solid line shows values predicted by Eqs. (2.5) and (2.8). The line is seen to fit the plots well.

Now, from the equation of motion in the natural coordinate system, the following expression is given

$$\operatorname{grad} p \cdot \nu = -\kappa \rho q^2 = -\frac{d\theta}{ds} \rho q^2 \tag{2.9}$$

where q and θ denote the numerical value of the gas velocity and the angle of inclination of the velocity vector, respectively. By substitution of Eq. (2.9) into Eq. (2.3) and with the aid of the equation of state for ideal gas,

$$J_1 = \int_0^s \frac{m_1 m_2 \Delta m}{\bar{m}} N_1 N_2 \cdot 2.662 \cdot 10^3 \sqrt{\frac{M_1 + M_2}{2 M_1 M_2}} \frac{\sqrt{T^3}}{\sigma_{12}^2 \Omega^{(1,1)*}} \frac{q^2}{(RT)^2} \frac{d\theta}{ds} 2\pi r \, ds \tag{2.10}$$

For convenience of calculation, a variable known as the Prandtl-Meyer function is introduced to substitute s :

$$\Lambda = \int_1^M \frac{\sqrt{M^2 - 1}}{1 + \frac{\gamma - 1}{2} M^2} \frac{dM}{M}$$

$$= \sqrt{\frac{\gamma+1}{\gamma-1}} \tan^{-1} \sqrt{\frac{\gamma-1}{\gamma+1}(M^2 - 1)} - \tan^{-1} \sqrt{M^2 - 1} \tag{2.11}$$

where M represents local Mach number. As Λ can be regarded as a function of s along a streamline, Eq. (2.10) becomes

$$J_1 = \int_0^\Lambda \frac{m_1 m_2}{\bar{m}} \Delta m \, N_1 N_2 \cdot 2.662 \cdot 10^3 \cdot \sqrt{\frac{M_1 + M_2}{2 M_1 M_2}} \frac{\sqrt{T^3}}{\sigma_{12}^2 \Omega^{(1,1)*}}$$

$$\times \frac{q^2}{(RT)^2} \frac{d\theta}{d\Lambda} 2\pi r \, d\Lambda \tag{2.12}$$

To reduce the above expression to nondimensional form, the following nondimensional quantities are introduced:

$$\bar{r} = \frac{r}{R^*}, \quad St = \frac{J_1}{\bar{m}^0 Q^*}, \quad Re = \frac{R^* a^0}{\nu^0}$$

$$Sc = \frac{\nu^0}{\mathscr{D}_{12}^0}, \quad M^* = \frac{q}{a^*}, \quad Pe = Re \; Sc$$

where $a^0, \nu^0, \bar{m}^0, \mathscr{D}_{12}^0$ and Q^* denote the sonic velocity, the kinematic viscosity, the average mass of gas mixture, the mutual diffusion coefficient under upstream stagnant condition and the total molar flow rate of gas mixture through the nozzle, respectively. The Stanton number St is defined as the ratio between the total diffusion mass flux into the peripheral stream and the total mass flux through the nozzle. Equation (2.12) then reduces to

$$St = \frac{J_1}{\overline{m}^* Q^*} = \frac{1}{P_e} \frac{2 m_1 m_2 \Delta m}{\overline{m}^{o\,3}} \gamma \left(\frac{\gamma+1}{2}\right)^{1/(\gamma-1)} \left(\frac{2}{\gamma+1}\right)^{\frac{1}{2}} I \quad (2.13)$$

$$I = \int_0^{\Lambda} M^{*2} \frac{d\theta}{d\Lambda} \pi \frac{\overline{m}^{o}}{\overline{m}} N_1 N_2 \left(\frac{T^o}{T}\right)^{\frac{1}{2}} \frac{\Omega^{(1,1)*o}}{\Omega^{(1,1)*}} d\Lambda \quad (2.14)$$

The integral I depends on both Λ and θ. By applying the Eq. (2.7) or Eq. (2.8), Eq. (2.14) is rewritten in the forms:

$$I = \int_0^{\Lambda} M^{*2} \frac{d\theta}{d\Lambda} \pi \frac{\overline{m}^{o}}{\overline{m}} N_1 N_2 \, d\Lambda \quad (2.15)$$

or

$$I = \int_0^{\Lambda} \left(\frac{T^o}{T}\right)^{\frac{1}{6}} M^{*2} \frac{d\theta}{d\Lambda} \pi \frac{\overline{m}^{o}}{\overline{m}} N_1 N_2 \, d\Lambda \quad (2.16)$$

In the first order approximation, both the mole fraction N_1, N_2 and the average mass of gas mixture can be assumed equal to their values at the nozzle inlet. Thus, the integral I can be evaluated numerically if the flow field of the jet is known.

The separation coefficient α is expressed by definition as a function of mass flux J_1 in the form

$$\alpha = \frac{Q_1^M / Q_2^M}{N_1^o / N_2^o} = \frac{N_2^o}{N_1^o} \frac{m_2}{m_1} \frac{m_1 N_1^o \Theta Q^* + J_1}{m_2 N_2^o \Theta Q^* - J_1} \quad (2.17)$$

where Q_i^M is the molar flow rate of the i-th component of the peripheral stream and Θ is the cut defined by the ratio of the mass flow rate of the peripheral stream to that through the nozzle. Then the relationship between the Stanton number and the separation coefficient is given by

$$St = \frac{m_1 N_1^o}{\overline{m}^o} \Theta \frac{\alpha - 1}{1 + \alpha \frac{m_1 N_1^o}{m_2 N_2^o}} \quad (2.18)$$

The separation coefficient α can be calculated from separation effect ε_A by the equation

$$\alpha - 1 = \frac{\varepsilon_A (1 - \Theta)}{1 + \Theta \varepsilon_A (1 - N_1^M)} \simeq \frac{\varepsilon_A (1 - \Theta)}{1 + \Theta \varepsilon_A (1 - N_1^o)} \quad (2.19)$$

The Péclet number is given by

$$p_e = \frac{R^* a^o}{\mathcal{D}_{12}^o} = R^* \sqrt{\gamma \frac{1}{\overline{m}^o} k T^o} \; \frac{1}{\mathcal{D}_{12}^o}$$

$$= R^* \sqrt{\gamma \frac{1}{\overline{m}^o} k \; T^o} \quad \frac{1}{\dfrac{2.662 \cdot 10^3 \sqrt{T^3 (M_1 + M_2)/2 M_1 M_2}}{p^o \sigma_{12}^2 \; \Omega_{12}^{(1,1)*}(T_{12}^*)}} \tag{2.20}$$

2.2 Diffusive Separation of Three Component Gas Mixture in a Supersonic Jet

For a three-component gas mixture, the mass flux vector of species is given by

$$\dot{j}_i = n_i \ddot{m}_i \overline{V}_i = \frac{n^2}{\rho} \sum_{j=1}^{3} m_i m_j D_{ij} d_j - D_i^T \operatorname{grad} \ln T \tag{2.21}$$

where

$$d_j = \operatorname{grad}\left(\frac{n_j}{n}\right) + \left(\frac{n_j}{n} - \frac{n_j m_j}{\rho}\right) \operatorname{grad} \ln p \tag{2.22}$$

The diffusion velocity of species i is denoted by $\overline{V}_i$, the rate of flow of molecules of i with respect to the mass average velocity of gas, —that is,

$$\overline{V}_i = \overline{\mathbf{V}}_i - \mathbf{V}_o \tag{2.23}$$

where $\overline{\mathbf{V}}_i$ is the average velocity of species i and

$$\mathbf{V}_o = \frac{1}{\rho} \sum_{i=1}^{3} \rho_i \overline{\mathbf{V}}_i \tag{2.24}$$

The above set of equations is written in the alternate form

$$\sum_{\substack{j=1 \\ j \neq i}}^{3} \frac{n_i n_j}{n^2 \mathcal{D}_{ij}} (\overline{V}_j - \overline{V}_i) = d_i - \operatorname{grad} \ln T \sum_{j=1}^{3} \frac{n_i n_j}{n^2 \mathcal{D}_{ij}} \left(\frac{D_j^T}{n_j m_j} - \frac{D_i^T}{n_i m_i}\right) \tag{2.25}$$

where $\mathcal{D}_{ij}$ denotes the usual binary diffusion coefficients (16). These equations are a generalized form of the Stefan-Maxwell equations.

If both terms of ordinary diffusion flux and thermal diffusion flux are neglected in comparison with pressure diffusion flux, the expression for the mass flux becomes

$$j_i = \frac{n^2}{\rho} \sum_{j=1}^{3} m_i m_j D_{ij} \left(\frac{n_j}{n} - \frac{n_j m_j}{\rho} \right) \operatorname{grad} \ln p \tag{2.26}$$

and Eq. (2.25) reduces to

$$\sum_{\substack{j=1 \\ j \neq i}}^{3} \frac{n_i n_j}{n^2 \mathcal{D}_{ij}} \left(\overline{V}_j - \overline{V}_i \right) = \left(\frac{n_j}{n} - \frac{n_j m_j}{\rho} \right) \operatorname{grad} \ln p \tag{2.27}$$

Consider following a three-component gas mixture of helium, argon-36, and argon-40. We denote quantities relevant to He, ^{36}Ar, and ^{40}Ar by subscripts 1, 2, and 3, respectively, and define the new diffusion velocity of species i, $\overline{V}_i'$ with respect to the mass average velocity of argon gas V_A by the equations:

$$\overline{V}_j' = \overline{V}_j - V_A \tag{2.28}$$

$$V_A = \frac{1}{\rho_A} \left(\rho_2 \overline{V}_2 + \rho_3 \overline{V}_3 \right) \tag{2.29}$$

$$\rho_A = \rho_2 + \rho_3 \tag{2.30}$$

By definition,

$$n_2 m_2 \overline{V}_2' - n_3 m_3 \overline{V}_3' = 0 \tag{2.31}$$

Then, the integral mass flux of ^{36}Ar over a surface of a stream tube of argon

$$J = \int_0^{S_A} n_2 m_2 \overline{V}_2' \cdot \nu_A \, 2 \pi r_A \, d S_A \tag{2.32}$$

where ν_A denotes the unit vector normal to the surface element (see Fig. 7).

The separation coefficient of argon isotopes α, when the jet is separated by means of a skimmer into peripheral and central stream, is given by

$$\alpha = \frac{N_2^M / N_3^M}{N_2^o / N_3^o} = \frac{N_3^o}{N_2^o} \cdot \frac{m_3}{m_2} \cdot \frac{m_2 N_2^o \Theta_A Q_A^* + J}{m_3 N_3^o \Theta_A Q_A^* - J} \tag{2.33}$$

and

$$\Theta_A = \frac{Q_A^M \, \overline{m}_A^M}{Q_A^* \, \overline{m}_A^o} \tag{2.34}$$

where Q_A^* and Q_A^M denote the total molar flow rate of argon gas through the nozzle and the molar flow rate of the peripheral stream of argon gas, respectively.

As the mole fraction of ^{36}Ar is much smaller than the mole fraction of ^{40}Ar, $\bar{V}_A$ is close to $\bar{V}_3$, and hence

$$\bar{V}_1' \cdot \nu_A = (\bar{V}_1 - \bar{V}_A) \cdot \nu_A \simeq$$

$$(\bar{V}_1 - \bar{V}_3) \cdot \nu_A = (\bar{V}_1 - \bar{V}_3) \cdot \nu_A = V_n \tag{2.35}$$

The geometrical relationship among these quantities is illustrated in Fig. 8 in which

$$\bar{V}_n = (\bar{V}_3 - \bar{V}_2)\sin(\delta + \varepsilon),$$

$$\bar{V}_2 = |\bar{V}_2| \quad , \quad \bar{V}_3 = |\bar{V}_3| \tag{2.36}$$

where δ and ε denote the angles between $\bar{V}_0$ and $\bar{V}_3$, and $\bar{V}_0$ and $\bar{V}_3$, respectively. On the other hand, from Eq. (2.21) and the equation:

$$\sum_{i=1}^{3} \dot{j}_i = 0 \tag{2.37}$$

we get

$$\bar{V}_3 - \bar{V}_2 = \frac{n_1 \mathcal{D}_{23}}{n_1 \mathcal{D}_{23} + n_2 \mathcal{D}_{13} + n_3 \mathcal{D}_{12}} \times$$

$$n^2 \left(\frac{\mathcal{D}_{12}}{n_1 n_2} d_2 - \frac{\mathcal{D}_{13}}{n_1 n_3} d_3 \right) \tag{2.38}$$

where

$$d_i = \frac{n_i}{n}\left(1 - \frac{m_i}{\bar{m}}\right) \operatorname{grad} \ln p \tag{2.39}$$

$$\bar{V}_3 - \bar{V}_2 = \mathcal{D}_{23} \frac{\mathcal{D}_{13}}{N_1 \mathcal{D}_{23} + N_2 \mathcal{D}_{13} + N_3 \mathcal{D}_{12}} \left[\left(\frac{\mathcal{D}_{12}}{\mathcal{D}_{13}} - 1 \right) \right.$$

$$\left. + \left(\frac{m_3}{\bar{m}} - \frac{\mathcal{D}_{12}}{\mathcal{D}_{13}} \frac{m_2}{m} \right) \right] \left| \operatorname{grad} \ln p \right| \tag{2.40}$$

From the equation of motion in the streamline coordinate system, we have

$$\operatorname{grad} p \cdot \nu = -\frac{d\theta}{ds} \rho q^2 \tag{2.41}$$

where q, θ, and ν, respectively, denote the numerical values of the velocity, the angle of inclination of velocity vector, and unit vector normal to the streamline element, relevant to the gas mixture.

Hence, (Fig. 9)

$$\left| \text{grad}\, p \right| = \rho q^2 \frac{d\theta}{ds} \frac{1}{\sin \delta} \tag{2.42}$$

From Eqs. (2.35), (2.36), (2.40) and (2.41)

$$n_2 m_2 V_2' \cdot \nu_A = n_2 m_2 \mathcal{D}_{23} \frac{\mathcal{D}_{13}}{N_1 \mathcal{D}_{23} + N_2 \mathcal{D}_{13} + N_3 \mathcal{D}_{12}} \times$$

$$\left[\left(\frac{\mathcal{D}_{12}}{\mathcal{D}_{13}} - 1 \right) + \left(\frac{m_3}{\overline{m}} - \frac{\mathcal{D}_{12}}{\mathcal{D}_{13}} \frac{m_2}{\overline{m}} \right) \right] \frac{\sin(\delta + \varepsilon)}{\sin \delta} \rho q^2 \frac{d\theta}{ds} \frac{1}{p} \tag{2.43}$$

The binary diffusion coefficient

$$\mathcal{D}_{ij} = 2.662 \times 10^3 \frac{\sqrt{T^3 (M_1 + M_2)/2 M_1 M_2}}{p\, \sigma_{ij}^2\, \Omega^{(1,1)*}(T_{ij}^*)} \tag{2.44}$$

where

$$T_{ij}^* = \frac{T}{\varepsilon_{ij}/k} \tag{2.45}$$

The force constants σ_{ij} and ε_{ij} for the interaction between i and j molecules are found in a table of Hirschfelder (18):

$$\sigma_{12} = \sigma_{13} = 3.059\ \text{A} \qquad \varepsilon_{12}/k = \varepsilon_{13}/k = 21.3\ {}^\circ\text{K}$$

$$\sigma_{23} = 3.418\ \text{A} \qquad \varepsilon_{23}/k = 124.0\ {}^\circ\text{K}$$

By substituting Eq. (2.43) into Eq. (2.32) and with the aid of the equation of state for ideal gas,

$$J = 2\pi m_2 \overline{m}^\circ \mathcal{D}_{23}^\circ \frac{p^\circ}{k^2 T^{\circ 2}} \int_0^{S_A} N_2 \left(\frac{T^\circ}{T}\right)^{\frac{1}{2}} \frac{\Omega^{(1,1)*^\circ}}{\Omega^{(1,1)*}} \chi \left(\frac{\Delta m}{\overline{m}}\right)_{\mathcal{D}} \frac{\overline{m}}{\overline{m}^\circ} \times$$

$$\times \frac{\sin(\delta + \varepsilon)}{\sin \delta} q^2 \frac{d\theta}{ds} r_A\, ds_A \tag{2.46}$$

where

$$\chi = \frac{\mathcal{D}_{13}}{N_1 \mathcal{D}_{23} + N_2 \mathcal{D}_{13} + N_3 \mathcal{D}_{12}} \tag{2.47}$$

$$\left(\frac{\Delta m}{\overline{m}}\right)_{\mathcal{D}} = \left(\frac{\mathcal{D}_{12}}{\mathcal{D}_{13}} - 1 \right) + \left(\frac{m_3}{\overline{m}} - \frac{\mathcal{D}_{12}}{\mathcal{D}_{13}} \cdot \frac{m_2}{\overline{m}} \right) \tag{2.48}$$

It is convenient to reduce the above expression to nondimensional form by introducing the following dimensionless quantities:

$$\bar{r} = \frac{r}{R^*} , \quad St = \frac{J}{Q_A^* \bar{m}_A^o} , \quad P_e = \frac{R^* a^o}{\mathcal{D}_{23}^o \chi}$$

where a^o and a^* denote the sonic velocity of gas mixture under the upstream stagnant condition and at the sonic nozzle exit, respectively. As a first-order approximation, N_2, $\bar{m}$, χ, and $(\Delta m/\bar{m})_{\mathcal{D}}$ are assumed equal to their values at the nozzle inlet. Then, Eq. (2.46) reduces to

$$St = \frac{2}{P_e} \frac{m_2}{m_3} \left(\frac{\Delta m}{m}\right)_{\mathcal{D}}^o \frac{N_2^o}{N_3^o} \gamma \left(\frac{\gamma+1}{2}\right)^{\frac{1}{\gamma-1}} \left(\frac{2}{\gamma+1}\right)^{\frac{1}{2}} I \tag{2.49}$$

where

$$I = \int_0^{\bar{x}_A} \left(\frac{T^o}{T}\right)^{\frac{1}{2}} \frac{\Omega^{(1,1)*^o} \sin(\delta+\varepsilon)}{\Omega^{(1,1)*} \sin\delta} M^{*2} \frac{d\theta}{ds} \bar{r}_A \frac{1}{\cos(\theta-\varepsilon)} d\bar{x}_A \tag{2.50}$$

The above integration should be carried out along the streamline of argon, while the quantities in the integrand are relevant to the gas mixture except for $\bar{r}_A$. The integral I can be evaluated numerically if the flow field of the supersonic jet is known.

The streamlines of argon were calculated in the manner described below. The differential equation for a streamline of argon becomes

$$\frac{dr_A}{dx} = \tan(\theta - \varepsilon) \tag{2.51}$$

and further the following equations hold (Figs. 8 and 10).

$$q = W \cos\varepsilon + \bar{V}_3 \cos\delta \tag{2.52}$$

$$W = \sqrt{q^2 + \bar{V}_3^2 - 2q\bar{V}_3 \cos\delta} \tag{2.53}$$

From Eqs. (2.51) and (2.52) we get

$$\varepsilon = \tan^{-1} \frac{\sin\delta}{(R - \cos\delta)} \tag{2.54}$$

where

$$R = \frac{q}{\bar{V}_3} \tag{2.55}$$

From Eq. (2.27), we obtain

$$\overline{V}_3 = \frac{1}{n_3}\frac{n^2}{\rho} m_1 \mathcal{D}_{13} \left[1 - \frac{n_2 \left(\frac{m_2}{m_1} \mathcal{D}_{23} - \mathcal{D}_{13} \right)}{n_1 \mathcal{D}_{23} + n_2 \mathcal{D}_{13} + n_3 \mathcal{D}_{12}} \right] \times$$

$$\times \frac{n_1}{n} \left(1 - \frac{m_1}{\overline{m}} \right) |grad\ ln p| + \frac{1}{n_3}\frac{n^2}{\rho} m_2 \mathcal{D}_{23} \times$$

$$\times \left[1 + \frac{n_1 \left(\frac{m_1}{m_2} \mathcal{D}_{13} - \mathcal{D}_{23} \right)}{n_1 \mathcal{D}_{23} + n_2 \mathcal{D}_{13} + n_3 \mathcal{D}_{12}} \right] \frac{n_2}{n} \left(1 - \frac{m_2}{\overline{m}} \right) |grad\ ln p| \simeq$$

$$\frac{n_3^0}{n_1^0} \frac{m_1}{\overline{m}^0} \mathcal{D}_{13}^0 \left(1 - \frac{m_1}{\overline{m}^0} \right) \frac{1}{p} \frac{1}{\sin\delta} \rho q^2 \frac{d\theta}{ds} \tag{2.56}$$

and hence

$$\frac{V_3}{q} = \frac{1}{P_{e_{13}}} \frac{N_1^0 m_1}{N_3^0 m^0} \left(1 - \frac{m_1}{m^0} \right) \gamma \left(\frac{2}{\gamma + 1} \right)^{\frac{1}{2}} \times$$

$$\times \frac{1}{\sin\delta} M^* \frac{d\theta}{ds} \left(\frac{T}{T^0} \right)^{\frac{1}{2}} \frac{\Omega^{(1,1)*^0}(T_{13}^0) p^0}{\Omega^{(1,1)*}(T_{13}) p} \tag{2.57}$$

where

$$P_{e_{13}} = \frac{R^* a^0}{\mathcal{D}_{13}^0} \tag{2.58}$$

On the other hand, making use of the equation:

$$\tan\delta = \frac{\left|\frac{dp}{dn}\right|}{\left|\frac{dp}{ds}\right|} = \frac{\rho q^2 \frac{d\theta}{ds}}{-\frac{dp}{ds}} = -\rho q^2 \left(\frac{d\theta}{dp} \right)_s \tag{2.59}$$

we obtain

$$\delta = \tan^{-1} \left[-\frac{2\gamma}{\gamma + 1} M^* \frac{\rho}{\rho^0} \left(\frac{d\theta}{d\, p/p^0} \right) \right] \tag{2.60}$$

Then, the right-hand side of Eq. (2.51) can be calculated as a function of by using the computed results for the flow field of the gas mixture (see Section III), with the aid of Eqs. (2.54) and (2.60), where the values of $d\theta/ds$ and $d\theta/d(p/p^0)$ were calculated by a numerical differentiation formula for nonequidistant nodes by using the solution at four neighboring mesh points. Thus, the numerical solution to Eq. (2.51) was obtained by the Runge-Kutta-Gill method, under the initial condition:

$$\bar{\eta}_A = \sqrt{1 - \Theta_A}\,, \qquad x = 0 \tag{2.61}$$

On the other hand, Eq. (2.33) reduces to

$$St = \frac{m_2 N_2^0}{m_A^0} \Theta_A \frac{\alpha - 1}{1 + \alpha \frac{m_2 N_2^0}{m_3 N_3^0}} \tag{2.62}$$

Then, with the aid of the equation:

$$\alpha - 1 = \frac{\varepsilon_A (1 - \Theta_A)}{1 + \Theta_A \varepsilon_A (1 - N_2^0)} \tag{2.63}$$

the value of

$$\frac{St \cdot P_e}{2 \frac{m_2}{m_3} \left(\frac{\Delta m}{m}\right)_{\mathfrak{D}}^0 \gamma \left(\frac{\gamma + 1}{2}\right)^{\frac{1}{\gamma - 1}} \left(\frac{2}{\gamma + 1}\right)^{\frac{1}{2}}}$$

can be calculated from experimental data for the separation effect

$$\varepsilon_A = \frac{N_2^M / N_3^M}{N_2^K / N_3^K} - 1 \tag{2.64}$$

2.3 Diffusive Separation of Binary Gas Mixture in a Shock Wave

The steep pressure and temperature gradients induced in a shock wave cause pressure diffusion as well as thermal diffusion which in turn bring about separation of species. The expression for the integral mass flux, J over a stream tube which passes through a oblique shock wave in an axisymmetric supersonic flow is given as follows:
By definition,

$$J = \int_{\Sigma} \dot{j}_1 \cdot \nu \, d\Sigma = \int_{\Sigma} \dot{j}_1 \cdot \nu \, 2\pi r_{\Sigma} \, ds \qquad (2.65)$$

where the symbol Σ represents the region in the shock wave. (see Fig. 11)
From Eq. (2.1), we have

$$\dot{j} \cdot \nu = -\frac{n^2}{\rho} m_1 m_2 \mathcal{D}_{12} \left(\frac{dN_1}{dx} + \frac{\Delta m}{\bar{m}} N_1 N_2 \frac{1}{p} \frac{dp}{dx} + k_T \frac{1}{T} \frac{dT}{dx} \right) \sin\varphi \qquad (2.66)$$

where the x-axis is in the direction of the normal to the shock and φ denotes the angle between a streamline and the x-axis. By substituting Eq. (2.66) into Eq. (2.65) and with the aid of the equation of state for ideal gas,

$$J = -2\pi m_1 m_2 \frac{p^0}{kT^0} \frac{\mathcal{D}_{12}^0}{\bar{m}^0} \int_{\Sigma} \frac{p}{p^0} \frac{T^0}{T} \frac{\mathcal{D}_{12}}{\mathcal{D}_{12}^0} \frac{\bar{m}^0}{\bar{m}} \sin\varphi F \, r_{\Sigma} \, ds \qquad (2.67)$$

where

$$F = \frac{dN_1}{dx} - N_1 N_2 \frac{\Delta \bar{m}}{\bar{m}} \frac{1}{p} \frac{dp}{dx} + \frac{1}{T} \frac{dT}{dx} \qquad (2.68)$$

and subscript 0 denotes quantities relevant to stagnant condition.
The above equation is rewritten in the following form by using the same dimensionless quantities as introduced in the section 2-1 :

$$\frac{St \cdot Pe}{\frac{2 m_1 m_2 \Delta m}{\bar{m}^{0\,3}} \left(\frac{\gamma+1}{2} \right)^{\frac{1}{\gamma-1}} \left(\frac{2}{\gamma+1} \right) \gamma} = \frac{\bar{m}^0}{\Delta m} \frac{1}{\gamma} \left(\frac{\gamma+1}{2} \right) I_{\Sigma} \qquad (2.69)$$

and

$$I_{\Sigma} = \int_{\Sigma} \left(\frac{T}{T^0} \right)^{\frac{1}{2}} \frac{\Omega^{(1,1)*0}}{\Omega^{(1,1)*}} \frac{\bar{m}^0}{\bar{m}} F \, \bar{r}_{\Sigma} \tan\varphi \, d\bar{x}_{\Sigma} \qquad (2.70)$$

The integral I_Σ can be calculated if the flow properties as well as the concentration distribution in the shock are known. As a first order approximation, the solution for a normal shock wave (24) can be utilized since this solution always applies locally to any shock surface. Thus, a dimensionless velocity, v in a normal shock is introduced to substitute x, for convenience of calculation. Then,

$$I_\Sigma = \int_\Sigma \left(\frac{T}{T^0}\right)^{\frac{1}{2}} \frac{\Omega^{(1,1)*0}}{\Omega^{(1,1)*}} \frac{\overline{m}'}{\overline{m}} G\, \overline{n}_\Sigma \tan \varphi \, dv \qquad (2.71)$$

where

$$G = \frac{dN_1}{dv} + N_1 N_2 \frac{\Delta m}{m} \frac{1}{p} \frac{dp}{dv} + k_T \frac{1}{T} \frac{dT}{dv} \qquad (2.72)$$

The latter equation is rewritten in the form:

$$G = f(1-f) \left\{ \frac{\theta - 1}{1+(\theta-1)f} \left[-\frac{1}{v} + \frac{1}{\tau}\frac{d\tau}{dv} - \frac{(\theta-1)}{1+(\theta-1)f}\frac{df}{dv} \right] \right.$$

$$\left. - \frac{1}{f(1-f)}\frac{df}{dv} - \alpha \frac{1}{\tau}\frac{d\tau}{dv} \right\} \qquad (2.73)$$

where τ , f and θ , respectively denotes dimensionless temperature, mole fraction of heavy species and molecular mass ratio.

III Calculation for Flow of Supersonic Jet

3.1 Flow Field of Axially Symmetric Supersonic Jet

In this section, the flow field of an axially symmetric supersonic jet into vacuum is computed by using the numerical method of characteristics (25, 26) and both $d\theta/d\Lambda$ and I which appeared in Eq. (2.14) are calculated along various streamlines.

The computing procedure used in this study is briefly described below. The equations of motion in the characteristic coordinate system, are given in the following form (27)

$$\frac{\partial}{\partial \eta}(\Lambda - \theta) = \sin\mu \frac{\sin\theta}{r} \tag{3.1}$$

$$\frac{\partial}{\partial \xi}(\Lambda + \theta) = \sin\mu \frac{\sin\theta}{r} \tag{3.2}$$

where ξ and η denote coordinates, and r and $\mu\left(= \sin^{-1}\frac{1}{M}\right)$ denote the distance from jet axis and Mach angle, respectively. The equations for the directions of the characteristic curves are

$$\left(\frac{dr}{dx}\right)_{\pm} = \tan(\theta \pm \mu) \tag{3.3}$$

and the elementary increments of characteristic curves, $d\xi$, $d\eta$ are given by

$$\left.\begin{matrix} d\xi \\ d\eta \end{matrix}\right\} = dr\sqrt{1 + \left(\frac{dx}{dr}\right)^2_{\pm}} \tag{3.4}$$

With the Eqs. (3.3) and (3.4), the equations of motion along characteristic curves become

$$d\Lambda \mp d\theta = \frac{\sin\mu \cdot \sin\theta}{r\sin(\theta \pm \mu)}\, dr \tag{3.5}$$

By introducing new variables, $\beta = \frac{1}{\tan\mu} = \sqrt{M^2 - 1}$ and $\zeta = \tan\theta$ we have

$$d\zeta \mp \frac{2\beta^2(1+\zeta^2)\,d\beta}{(\gamma+1)(1+\beta^2)(1+K\beta^2)} \pm \frac{\zeta(1+\zeta^2)\,dr}{(\beta\zeta \pm 1)r} = 0, \tag{3.6}$$

$$K = \frac{\gamma - 1}{\gamma + 1}$$

Then, the familiar step by step method of characteristics was applied in which the known solution at two points P_1, P_2 leads to the solution at point P_3 (see Fig.12). The difference equations based on Eq. (3.6) are given in Appendix A.

It is necessary for obtaining the solution at an unknown point P_3 to use an iterative process which is started with an initial assumption for the coefficients, m, E, K, L, n, F, I, J in the difference equations and is continued until the criterion

$$max \left(\left| \frac{r_3^n - r_3^{n-1}}{r_3^{n-1}} \right| \left| \frac{x_3^n - x_3^{n-1}}{x_3^{n-1}} \right| \left| \frac{\beta_3^n - \beta_3^{n-1}}{\beta_3^{n-1}} \right| \left| \frac{\zeta_3^n - \zeta_3^{n-1}}{\zeta_3^{n-1}} \right| \right) \leqq 10^{-6} \quad (3.7)$$

is satisfied. The initial estimation of the coefficients m, E, K, L was made by assuming that $\zeta_3 = \zeta_1$, $\beta_3 = \beta_1$, $r_3 = r_1$, $x_3 = x_1$ and of the coefficients n, F, I, J by assuming that $\zeta_3 = \zeta_2$, $\beta_3 = \beta_2$, $r_3 = r_2$, $x_3 = x_2$.

The initial set of the data were obtained from the table presented by Katskova (26) who computed the flow field of an axially symmetric supersonic jet near the nozzle exit.

The change in the stream function, ψ along a characteristics curve is given by

$$d\psi = \frac{d\psi}{dr} dr + \frac{d\psi}{dx} dx = \frac{2\rho}{\rho^*} r\, dx \left[u\left(\frac{dr}{dx}\right)_\pm - v \right] \quad (3.8)$$

From Eq. (3.3)

$$\left(\frac{dr}{dx}\right)_\pm = \tan(\theta \pm \mu) = \frac{\beta\zeta \mp 1}{\beta + \zeta} \quad (3.9)$$

Substitution of Eq. (3.9) into Eq. (3.8) gives

$$d\psi = -2\frac{\rho}{\rho^*} r M^* \frac{(1+\zeta^2)^{\frac{1}{2}}}{(\beta + \zeta)} dx \quad (3.10)$$

Then the difference equation for ψ_3 is given by

$$\psi_3 = \psi_2 - \left(\frac{r_2 \rho_2 M_2^*}{\zeta_2 + \beta_2}(1+\zeta_2^2)^{\frac{1}{2}} + \frac{r_3 \rho_3 M_3^*}{\zeta_3 + \beta_3}(1+\zeta_3^2)^{\frac{1}{2}} \right)(x_3 - x_2) \quad (3.11)$$

The number of computed points was so determined that the increments of both x/R^* and r/R^* are maintained less than 0.02.

In Fig.13 the results of computation for streamlines for $\gamma = 1.4$ are plotted with the value of cut as a parameter. Fig.14 gives $d\theta/d\Lambda$ calculated along streamlines with the aid of the numerical differentiation formula for non-equidistant nodes (28) by using four neighbouring points, as a function of Λ with the cut as a parameter. The streamlines for $\gamma = 1.66667$ are shown with the value of cut as parameter in Fig.15, in which the experimental data by Becker, et al. (29) are also plotted. Figure16 gives $d\theta/d\Lambda$ along various streamlines, and the Mach number distribution along the streamlines is shown in Fig.17.

3.2 Flow Field of Two-Dimensional Supersonic Jet

The flow field of two-dimensional supersonic jet can be calculated by the numerical method of characteristics if the flow properties near sonic nozzle exit are known.

The equations of motion in the characteristic coordinate system are written in the form

$$d\zeta \mp \frac{2\beta^2(1+\zeta^2)}{(\gamma+1)(1+\beta^2)(1+\kappa\beta^2)} = 0 \qquad (3.12)$$

Then, the familiar step-by-step method was used in which the known solution at two points P_1 and P_2 leads to the solution at point P_3 (see Fig.12)

The difference equations based on Eq. (3.12) are given in Appendix B.

The initial set of data of the flow properties near sonic nozzle exit was obtained by the same procedure as adopted by Katskova et al. (25) for the axially axisymmetric case as described briefly below.

Near the sonic nozzle exit, flow variables μ, θ and y are expressed in terms of parameter χ in the forms

$$\mu \sim \frac{\pi}{2} + \mu_1(z)\chi, \qquad (3.13)$$

$$\theta \sim \theta_3(z)\chi^3, \qquad (3.14)$$

$$y \sim z + y_4(z)\chi^4, \qquad (3.15)$$

$$x = -\int_1^z \left(\frac{2}{\gamma+1}\right)^{\frac{1}{2}\frac{\gamma+1}{\gamma-1}} \left(\frac{\gamma-\cos 2\mu}{1-\cos 2\mu}\right)^{\frac{1}{2}\frac{\gamma+1}{\gamma-1}} \cos(\theta-\mu)\,dz, \qquad (3.16)$$

where μ, θ, x, y and ψ denote Mach angle, flow inclination, Cartesian coordinates and stream function, respectively. The coefficients are given as functions of ψ by

$$\mu_1 = \omega' \tag{3.17}$$

$$\theta_3 = \frac{2}{3(\gamma+1)} \omega'(\omega\omega'' - \omega'^2) \tag{3.18}$$

$$y_4 = \frac{1}{6(\gamma+1)} \omega\omega'(\omega\omega'' - \omega'^2) \tag{3.19}$$

where $\omega(\psi)$ is the solution of the differential equation

$$\omega''' = \frac{1}{\omega\omega'} \omega''(5\omega'^2 - \omega\omega'') \tag{3.20}$$

under the boundary conditions

$$\begin{gathered} \omega'(1) = -1, \qquad \omega(1) = 0 \\ \omega(0)\,\omega''(0) - \omega'^2(0) = 0 \end{gathered} \tag{3.21}$$

The numerical solution of the above equation was obtained by the Runge-Kutta-Gill method. Details of the above calculation are described in Appendix C.

Based on the above procedure of calculation, a computer program was prepared and actual computations were carried out for a supersonic jet into vacuum for $\gamma = 1.4$ and $\gamma = 1.067$. In Figs. 18 and 19 the results of computation for streamlines are plotted with the value of cut Θ as parameter. Figures 20 and 21 give $d\theta/d\Lambda$ along various streamlines and the Mach number distribution is shown in Figs. 22 and 23 .

3.3 Flow Properties in a Normal Shock Wave of a Binary Gas Mixture

The solution to the shock structure of a binary gas mixture based on the continuum Navier-Stokes equations, has been given by Sherman. (24,30) Since this solution can be utilized to calculate approximately the integral mass flux in any curved shock wave, the flow properties and concentration distribution in a normal shock of He/Ar and H_2/N_2 gas mixtures were calculated by using the Sherman's formula. (Appendix D)

The differential equations determining the temperature, τ and mole fraction of heavy species, f as a function of the velocity, v are given by

$$\frac{d\tau}{dv} = \frac{\frac{\gamma-1}{2\gamma} P_r \left\{ 2v - v^2 - a + 2\tau \left[\frac{\gamma}{\gamma-1} - \frac{1+(\theta-1)f_\infty}{1+(\theta-1)f} + (f_\infty - f)\alpha \right] \right\}}{\frac{3}{4}\left\{ v + \frac{1+(\theta-1)f_\infty}{1+(\theta-1)f}\frac{\tau}{v} - 1 \right\}} \tag{3.22}$$

$$\frac{df}{dv} = -\frac{4}{3} S_c \frac{(f_\infty - f)[1+(\theta-1)f]^3}{[1+(\theta^2-1)f][1+(\theta-1)f_\infty]\left\{ v + \frac{1+(\theta-1)f_\infty}{1+(\theta-1)f}\frac{\tau}{v} - 1 \right\}}$$

$$- \frac{f(1-f)[1+(\theta-1)f]}{1+(\theta^2-1)f}\left\{ (\theta-1)\frac{1}{v} - \left[(\theta-1) - \alpha\{1+(\theta-1)f\}\right]\frac{1}{\tau}\frac{d\tau}{dv} \right\} \tag{3.23}$$

where a, α and θ, respectively denote the shock strength, thermal diffusion coefficient and molecular mass ratio and subscript ∞ means the quantity outside the shock. The shock strength a is expressed as

$$a = \frac{\gamma^2 M_\infty^2 \left(M_\infty^2 + \frac{2}{\gamma-1} \right)}{(\gamma M_\infty^2 + 1)} \tag{3.24}$$

where M_∞ represents the initial Mach number.

The boundary conditions are written as follows:

$$\text{at } v = v_\infty = \frac{\frac{2\gamma}{\gamma+1} + \sqrt{\left(\frac{2\gamma}{\gamma+1}\right)^2 - 4\frac{\gamma-1}{\gamma+1}a}}{2} \tag{3.25}$$

$$\tau_\infty = v_\infty(1 - v_\infty) \tag{3.26}$$

$$\left(\frac{d\tau}{dv}\right)_{v=v_\infty} = \frac{(a_1-\lambda)b_2 - a_2 b_1}{a_3 b_2 - a_2(b_3 - \lambda)} \tag{3.27}$$

$$\left(\frac{df}{dv}\right)_{v=v_\infty} = \frac{(b_3-\lambda)(a_1-\lambda) - b_1 a_3}{(b_3-\lambda)a_2 - b_2 a_3} \tag{3.28}$$

The expression for a_i, b_i and c_i (i=1,2,3) are given in Appendix D and λ is a minus real root of the following algebraic equation:

$$\lambda^3 - (a_1 + b_2 c_3 + b_3 + c_2 + a_2 c_1)\lambda^2$$
$$+ (a_1 b_2 c_3 + a_1 b_3 + a_1 c_2 + b_3 c_2 - a_2 b_1 c_3 + a_2 c_1 b_3$$
$$- a_3 b_1 - a_3 b_2 c_1)\lambda + (a_3 b_1 c_2 - a_1 b_3 c_2) = 0 \qquad (3.29)$$

The calculated values of λ are shown as a function of ν_∞ in Figs. 24 and 25.

The solution to Eqs. (3.22) and (3.23) was obtained numerically by the Runge-Kutta-Gill method. Figs. 26, 27, 28 and 29 respectively give the results of calculation for τ and f as a function of v, with the initial Mach number as a parameter. With the aid of the above results of computation, the mass flux integral I_Σ in an oblique shock defined by Eq. (2.71) was calculated and plotted in Figs. 30 and 31 as a function of wave angle β with the normal component of initial Mach number as a parameter.

3.4 The Shock Wave Formed by a Cone in a Supersonic Jet

In order to evaluate the separation effect of jet separation process, it is indispensable for determining the shock shape in a supersonic jet. The method of integral relations proposed by Dorodnitsgn (31) is well suited for this objective. In this section, numerical results are obtained for the shape of attached shock ahead of a cone of half-angle 22.5°, placed in an axisymmetric supersonic jet of Ar/He mixture (γ =1.66667) by following the same procedure of Bartyenev and Shirshov (32). The flow of jet is assumed to be a modified source flow proposed by Sherman (33). Then, the distribution of flow variables can be calculated with the aid of the following equations :

$$\rho(r, x) = \rho(0, x) \cos^2\theta \cos^2\left(\frac{\pi}{2} \frac{\theta}{\phi}\right) \qquad (3.30)$$

$$M_c = A\left(0.5\bar{x} - \frac{x_0}{D}\right)^{\gamma-1} - \frac{1}{2}\left(\frac{\gamma+1}{\gamma-1}\right) \Big/ A\left(0.5\bar{x} - \frac{x_0}{D}\right)^{\gamma-1}$$
$$+ C\left(0.5\bar{x} - \frac{x_0}{D}\right)^{-3(\gamma-1)} \qquad (3.31)$$

with
$$\frac{x_0}{D} = 0.075$$
$$A = 3.26$$
$$C = 0.31$$

where M_c represents the centerline Mach number.

In the method of integral relations, the governing equation of motion are written in divergence form :

$$\frac{\partial A}{\partial r} + \frac{\partial B}{\partial s} = C \tag{3.32}$$

$$\frac{\partial D}{\partial r} + \frac{\partial E}{\partial s} = 0 \tag{3.33}$$

where

$$A = R\left(\rho u^2 + \frac{\gamma-1}{2\gamma} p\right), \quad B = \rho u v R$$

$$C = \frac{\gamma-1}{2\gamma} p \sin\Theta, \quad D = \rho u R, \quad E = \rho v R$$

and s axis is in the direction of the wall, the r axis perpendicular to it. (Fig. 32)
By integrating with respect to r, from r=0 to r= ε we obtain the following integral relations

$$A_\varepsilon - A_0 + \frac{d}{ds}\int_0^s B\, dr - B_\varepsilon \frac{d\varepsilon}{ds} = \int_0^\varepsilon C\, dr \tag{3.34}$$

$$D_\varepsilon - D_0 + \frac{d}{ds}\int_0^\varepsilon E\, dr - E_\varepsilon \frac{d\varepsilon}{ds} = 0 \tag{3.35}$$

Furthermore, if we assume that the integrand is a linear function of r, these relations yield a set of ordinary differential equations for σ, v_0 and ε in terms of s, (Appendix E) where σ, v_0 and ε, respectively denote angle of shock inclination, velocity on cone surface and distance to shock along r axis. The boundary conditions are calculated from the relations for a cone in a uniformstream, that is,

$$\left[\frac{p_0}{\varphi}\right]^{\frac{1}{\gamma}} \sqrt{1 - \left(p_0\, \varphi^{\frac{1}{\gamma-1}}\right)^{\frac{\gamma-1}{\gamma}}}\, \cos\Theta + \rho_\varepsilon u_\varepsilon \left[\frac{\cos\Theta}{\tan(\sigma_0 + \Theta - \frac{\pi}{2})} + \sin\Theta\right] = 0 \tag{3.36}$$

$$p_0 = \frac{2\rho_\varepsilon u_\varepsilon^2 \left[\cos\Theta + \sin\Theta \tan(\sigma_0 + \Theta - \frac{\pi}{2})\right]}{\frac{\gamma-1}{2\gamma}\left[\sin\Theta \tan(\sigma_0 + \Theta - \frac{\pi}{2}) + 2\cos\Theta\right]} + p_\varepsilon \tag{3.37}$$

with

$$\varphi = \frac{p_\varepsilon}{\rho_\varepsilon^\gamma}, \quad p_0 = (1 - v_0^2)^{\frac{\gamma}{\gamma-1}}\, \varphi^{-\frac{1}{\gamma-1}}$$

From Eqs. (3.36) and (3.37), the shock angle and pressure coefficient versus Mach number for various cone angles are calculated and compared with the exact solution by Taylor and Maccoll (Figs. 33 and 34) It is seen that there is good agreement between both results. The numerical solution of the above set of differential equations was obtained by the Runge-Kutta-Gill method. The results for the shock shape for different location of the cone in a jet are shown in Fig. 35 .

IV Experimental Methods and Results

4.1 Description of Jet Separation Apparatus and Procedure

The experiments on the separation of binary gas mixture in an axisymmetric supersonic jet were performed by using the apparatus consisting of a convergent nozzle and a skimmer which were similar to those of Waterman et al. (7) Details of this system are shown in Fig.36. The nozzle and the skimmer used in this experiment are 0.3 mm and 2 mm in diameter, respectively. The distance between the nozzle exit and the skimmer can be varied by means of a micrometer screw and measured by a dial gauge to an accuracy of the order of 0.01 mm. The nozzle and the skimmer are so arranged that their centers are on a line with the aid of a travelling microscope.

A flow diagram of the experimental apparatus is illustrated in Fig 37. A binary gas mixture of known concentration was introduced to the nozzle at the inlet pressure p^o through a needle valve and ejected at the nozzle exit at mass flow rate G. The supersonic jet thus created was separated into the peripheral stream ΘG and the central stream $(1-\Theta)G$ by a skimmer and were pumped away by the mechanical boosters and rotary vacuum pumps, at the static pressure of p^M and p^K, respectively. The pressures p^o, p^M and p^K were measured by a di-octylphtalate oil manometer to an accuracy of the order of 0.01 mmHg. The volume flow rate of gas mixture was obtained by means of a soap film flow meter jointed to the delivery tube of the rotary vacuum pump, in which the displacement rate of a soap film meniscus in a calibrated burette was measured. A small amount of gas mixture was sampled from the peripheral flow into a sample bulb after slight compression by the mechanical booster. The flow of gas was maintained for about 15 min prior to sampling in order to attain a steady-state condition. The sample bulb was evacuated by a mercury diffusion pump to a pressure of about 10^{-5} mmHg before sampling. The flow rate and the concentration were measured for the peripheral stream, because a preliminary test confirmed that the calculated values on the basis of mass balance agree very well with the experimental values.

The constructional details of the apparatus of jet separation in a two-dimensional jet are shown in Fig.38.

This apparatus is similar to above mentioned one. A small modification consisted in mounting the nozzle and the gas inlet tube on a adjustable support provided with micrometer screws to arrange the nozzle and skimmer system. The convergent slit nozzle of 0.129 mm in width and 20 mm in length was made of razor blades in the manner as shown in Fig.39. An extremely narrow (i.e. 0.1 mm) and parallel slit was successfully made by this process. Two kinds of slit skimmers each of length 15 mm are also made of razor blades, which are 1.5 mm and 3.0 mm in width, respectively.

A flow diagram of the experimental equipments is illustrated in Fig.40. The main modification consisted in providing the automatic Töpler pump to compress the sample gas from the peripheral stream to sample bulb.

4.2 Concentration Measurements of Binary Gas Mixture at Low Pressure

In this experiments, it was required to determine the concentration of gas mixtures such as H_2/N_2, He/N_2 at low pressure to an accuracy of the order of 0.1% so that it may evaluate the separation effect.

In the early experiments, the low pressure constant volume method was applied to measure concentration (34), in which the gas mixture containing hydrogen as one of two constituents was determined in the following manner. The gas mixture was circulated through a heated column packed with cupper oxide by a mercury diffusion pump, after the pressure and the gas volume were measured. (see Fig.41) Water vapour produced by the reaction of H_2 with cupper oxide was removed by the liquid nitrogen trap. Non-reacting gas (N_2) was compressed to the original volume by the Töpler pump. Thus the composition could be determined reading the pressure. It was satisfied with the accuracy, however, the time required was over 90 minutes for one sample.

In order to shorten the time required in the measurement as well as to obtain better accuracy, we tried to apply the thermal conductivity method to the gas analysis at low pressure, which has been used at atmospheric pressure.

It was found that this type of device was applicable for low pressure with a fair degree of accuracy, and also possible to shorten the required time down to about 10 minutes. The principle of the method is based on the measurement of the resistance of a nearly spherical thermistor, placed in a rarefied gas mixture at various pressures. The rate of generation of heat in the thermistor under a steady state, is equal to the rate of dissipation from the thermistor. This becomes

$$(jRI^2 - Q) = hA(T - T_\infty) \tag{4.1}$$

where
R = Resistance of thermistor
I = Electric current which passes through thermistor
T = Temperature of thermistor
T_∞ = Temperature of the wall of the block
A = Surface area of thermistor
h = Heat transfer coefficient
Q = heat transfer from thermistor by any mechanism other than conduction

The relation between R and T for a thermistor is expressed by

$$R = R_\infty \exp\left[B\left(\frac{1}{T} - \frac{1}{T_\infty}\right)\right] \tag{4.2}$$

The sensitivity of thermistor to small temperature change is extremely high, in comparison with the other material. The value of B is in the range of 2000°K 5000°K.

From Eqs. (4.1) and (4.2)

$$T = \frac{1}{\frac{1}{B}\ln\frac{R}{R_0} + \frac{1}{T_0}} = \frac{1}{B^{-1}\ln R + T^{*-1}}, \quad T^{*-1} = T_0^{-1} - B^{-1}\ln R_0 \tag{4.3}$$

and

$$RI^2 = hA\left(\frac{1}{B^{-1}\ln R + T^{*-1}} - T_\infty\right) \tag{4.4}$$

Then we find that a unique relation between h and R is obtained if I is maintained to be constant. The value of h depends on the pressure and the concentration. Hence, the relation between the resistance of the thermistor and the concentration of gas mixture could be determined if resistance measurements are carried out under constant pressure, using gas mixtures of various concentration. In our experiment, resistance was measured as a function of pressure for each gas mixture and the value of resistance at a given pressure was calculated by means of interpolation.

Electronic circuit

A balanced type bridge circuit was used to measure the resistance of the thermistor R as shown in Fig.42. The thermistor employed in the measurement was produced by the Gow-Mac Instrument Company in U.S.A. (35) and has about 7000 Ω resistance at room temperature. Its form is beads coated by glass as small as about 0.5 mm in diameter, and inserted into the cylindrical hole of diameter 6 mm, drilled in 50 x 50 x 50 mm^3 cell block made from brass (Fig.43). A line power source of a.c. 100 V was stabilized through a commercial magnetic voltage regulator. It was supplied to the high precision d.c. voltage regulator. The circuit indicated in Fig.44 is the same one as designed by Takahei (36). The output of about 350 V d.c. is supplied to the constant d.c. current regulator. The circuit shown in Fig.44 was designed by referring to the circuit proposed by Shimoda (37). The output current to the bridge was chosen to be 3.8 mA. The ripple was attenuated to a degree not appreciable by a galvanometer and by a milliammeter. Furthermore, the output current can be kept constant even if the variation of the resistance of the thermistor brought large variation of the load impedance.

Thermostat

It is quite necessary to regulate the variation of the temperature of the cell block as small as possible, because of the large sensitivity of the thermistor to temperature variation. The cell block was placed in water bath stirred by a jet agitation machine. The temperature of water was carefully regulated by on-off control of heating current by a transistor relay. The variation of temperature was detected by a specially designed toluen-thermostat in which a capillary part is smaller in diameter than that in the commercial one. Furthermore, the waterbath was placed in an air bath. A wooden wall of the air bath was lined by styro-foam plates for insulation. Air was stirred by a fan and temperature was regulated in a similar way. From the measurement by Beckmann thermometer, it was found the variation of the temperature of water was able to be reduced to below 1/1000°C.

Assembly of vacuum system

The assembly of vacuum system and gas introduction system are shown in Fig.42 . The following experimental procedure was employed. A gas mixture of known composition in a sample bulb was admitted into the cylindrical hole in the cell block by means of a Töpler pump after the system was evacuated by a mercury diffusion pump and a rotary vacuum pump. The gas mixture first compressed to the pressure of about 18 mmHg and isolated from the vacuum system by keeping the stop cock 1 closed. Then the pressure of the gas mixture was measured by a di-octylphtalate oil manometer to an accuracy of the order of 0.1 mmHg. The electric current was supplied to the thermistor and maintained for several minutes prior to the measurement of resistance, in order to insure the attainment of steady state condition, which can be confirmed from the zero deflection of the galvanometer. After the measurement, the pressure of the gas mixture was lowered slightly by opening the stop cock 1 and letting the small part of the gas mixture sucked out by the evacuating pump. Then the same experimental procedure was repeated. In this manner, the relation of the resistance of thermistor to the pressure can be obtained for each gas mixture.

Results of experiment

The thermistor constant β was determined in the following way. Firstly, the resistance of the thermistor was measured for various electric currents and the extrapolated value at zero current was taken as the true resistance at the thermostat temperature. Secondly, the same procedure was repeated changing the thermostat temperature. The relation between R/R_∞ and $(T_\infty - T)/T_\infty T$ was obtained as shown in Fig.45 . Thus, the value of constant β was determined to be 3500°K.

The effect of air pressure on the thermistor resistance was measured to confirm its reproducibility as indicated in Fig.46 . The results obtained before and after a series of experiments with hydrogen and nitrogen gas mixtures were quite satisfactory.

The relation between the resistance of the thermistor and the pressure for H_2-N_2 gas mixtures is shown in Fig. 47 in which the concentration was taken as a parameter. The same relation for He-N_2 gas mixtures is shown in Fig.48 . The relation of the resistance and the concentration was plotted in Figs.49 and 50 in the cases of both 15 mmHg and 10 mmHg. It is evident that the relation can be approximated by a straight line with a fair degree of accuracy.

It seems that small scatter of the experimental data is not due to the errors from the resistance measurement but ascribed to the errors originated in the mixing process of pure gases for making a sample. Mixing was carried out by using the Töpler pump in such a way as shown in Fig. 51 . A pure gas was contained in a given constant volume and the pressure was measured (a). Then the gas was isolated by a mercury cut-off (b). After the remained gas was sucked out, another pure gas was added to the first one and total pressure was measured (c). Then the expansion and compression of the mixed gas was repeated several times by raising and lowering the mercury in the Töpler pump, until the mixing was accomplished. It is likely that the errors would be rather introduced from the pressure measurement and from the incomplete mixing process.

The experimental results presented above show that the concentration of H_2/N_2 and He/N_2 gas mixture can be determined to an accuracy of the order of 0.1% by thermal conductivity method, even if the pressure is as small as about 10 ~ 15 mmHg. This method has the advantage that the time interval required in the measurement is very short and the procedure is simple. Moreover, there is room for improvement to obtain better accuracy because the resistance measurement will be attainable to an accuracy of the order of 0.1 ohm. In this study, the electric current supplied to thermistor was chosen to be 1.9 mA, although the safe maximum current of about 6 mA is allowed. It is clear that much higher sensitivity could be obtained with the higher heating current at least up to 5 mA.

4.3 Critical Mass Flow of Rarefied Gas Mixtures

It is well known that for invicid flow, there exists a definite critical pressure ratio $(p^*/p^\circ)_c$ beyond which no additional increase in mass flow rate can be accomplished by decreasing the back pressure. The critical pressure ratio and maximum flow rate for a smooth nozzle is given by

$$\left(\frac{p^*}{p^\circ}\right)_c = \left(\frac{\gamma+1}{2}\right)^{\frac{\gamma}{\gamma-1}} \tag{4.5}$$

$$G = \left(\frac{2}{\gamma+1}\right)^{\frac{1}{2}\frac{\gamma+1}{\gamma-1}} \rho^\circ A\,(\gamma R T)^{\frac{1}{2}} \tag{4.6}$$

where γ denotes the ratio of specific heats.

In this section, the experimental results on the critical mass flow rate of several gas mixtures are presented.

Figure 52 shows the experimental values of volume flow rate through the circular nozzle as a function of inlet pressure. The ratio of downstream pressure to inlet pressure p^*/p° is very small and the downstream condition ceases to influence the upstream condition. The discharge coefficient Γ are calculated from these data and plotted as a function of Reynolds number in Fig. 53 where Γ and Re are defined by the following expressions. (38)

$$G = \Gamma \rho^\circ W A \tag{4.7}$$

$$Re = \frac{WD}{\nu^\circ} \tag{4.8}$$

$$W = \left(\frac{p^\circ}{\rho^\circ}\right)^{\frac{1}{2}} \tag{4.9}$$

where ν° is the kinematic viscosity of a gas mixture evaluated at the equilibrium upstream condition and given with the aid of Wilke's formula in the following form:

$$\nu^o = \frac{1}{\rho}\sum_{i=1}^{n} \frac{x_i \mu_i}{\sum_{j=1}^{n} x_i \Phi_{ij}} \tag{4.10}$$

$$\Phi_{ij} = \frac{1}{\sqrt{8}}\left(1 + \frac{M_i}{M_j}\right)^{-\frac{1}{2}}\left[1 - \left(\frac{\mu_i}{\mu_j}\right)^{\frac{1}{2}}\left(\frac{M_j}{M_i}\right)^{\frac{1}{4}}\right]^2 \tag{4.11}$$

Figure 54 shows the experimental values of volume flow rate through a slit nozzle as a function of the inlet pressure for several gas mixtures.

These experimental results for various gas mixtures can be correlated uniquely by using the dimensionless quantities Γ and Re as shown in Fig. 55 .

4.4 Measurements of Diffusive Separation of Mixtures

Separation of H_2/N_2 Mixtures in an Axisymmetric Supersonic Jet

In Fig. 56 , the experimental data of separation coefficients are shown as a function of the distance between the nozzle exit and the skimmer with the inlet pressure as a parameter. The separation coefficient is defined by

$$\alpha = \frac{N_1^M/N_2^M}{N_1^0/N_2^0} \tag{4.12}$$

The experimental conditions are: converging nozzle; 0.3 mm I.D., skimmer; 2 mm I.D., stagnation temperature; 300°K, initial composition; 48.92 mole per cent hydrogen. Other experimental conditions are shown in Table 1 in which the sizes of barrel shock and Mach disk are calculated values (see section 5.2)

Table 1 Experimental conditions

P^0 mm Hg	P^M mm Hg	P^0/P^M	x_M/R^*	$y_M/2R^*$	$y/2R^*$	$y/2R^*$	$y_s/2R^*$
221.8	0.2	1109	46.4	16.7	19.9	1-10	6 2/3
381.8	0.2	1909	58.6	23.1	27.5	1-10	6 2/3
700.0	0.3	2333	77.4	26.0	30.9	1-10	6 2/3

x_M, axial distance to the Mach disk; y_M, diameter of the Mach disk;
y_B maximum diameter of barrel shock; x_s, axial distance of skimmer;
y_s, diameter of skimmer.

The cut Θ_G which means the ratio of the mass flow rate of the peripheral stream to the total mass flow rate through the nozzle is given in Fig. 57 . It becomes evident that same supersonic profiles are formed for this range of inlet pressure.

Separation of H_2/N_2 and He/N_2 Mixtures in a Two-Dimensional Supersonic Jet

The composition of the mixtures employed in the experiment was as follows:

(1) 48.9% H_2 - 51.1% N_2
(2) 21.8% He - 78.2% N_2

The separation of these mixtures was determined as a function of the distance, X_s between the nozzle and the skimmer at different inlet pressure and downstream pressures. Figs. 58 and 59 are the relation found between the separation coefficient and the distance between the nozzle and the skimmer. In Figs. 60 and 61, the experimental data of the cut are shown as a function of the distance between the nozzle and the skimmer with the inlet pressure as a parameter. It is seen that the cut reaches a finite value as X_s tends to zero. The portion of the jet, Θ_G^0 flows into the peripheral stream without changing its composition.
Hence, it is necessary to make some corrections in order to obtain the actual value of the separation coefficients as well as the cut. As a simple approximation, the portion of the jet not subjet to variation of composition can be assumed to be constant and equal to Θ_G^0 regardless of the change of the nozzle to skimmer distance.
Then, the actual values of the separation coefficient and the cut are calculated from the following equations:

$$\Theta_G = \frac{\Theta_G^{obs.} - \Theta_G^0}{1 - \Theta_G^0} \tag{4.13}$$

$$\alpha = \frac{N_2^0}{N_1^0} \frac{N_1^0 \dfrac{(1 - \Theta_G^0)\Theta_G}{m^0} + \dfrac{J}{G}\dfrac{1}{m_1}}{N_2^0 \dfrac{(1 - \Theta_G^0)\Theta_G}{m^0} - \dfrac{J}{G}\dfrac{1}{m_2}} \tag{4.14}$$

$$\frac{J}{G} = \frac{m_1 N_1^0}{m^0} \Theta_G^{obs.} \frac{\alpha^{obs.} - 1}{1 + \alpha^{obs.} \dfrac{m_1 N_1^0}{m_2 N_2^0}} \tag{4.15}$$

where superscript obs. represents the experimentally observed values. The corrected values of the separation coefficient and the cut are shown in Figs. 62, 63, 64, and 65.

V Comparison of Theoretical Predictions with Experimental Data

5.1 Heat Transfer from a Sphere to Rarefied Gas Mixtures

The graphs in Figs. 47 and 48 presented in the section 4.2 show in essence the variation of the heat transfer coefficient of a sphere in a rarefied gas as a function of Knudsen number, where Knudsen number Kn is defied as the ratio of the mean free path of the gas and the radius of the sphere.

From these results, it seems possible to obtain the relation between Nusselt number and Knudsen number with the help of Eqs. (4.1) and (4.2). Thus, the expression for the Nusselt number is given as follows:

$$Nu = \frac{hD}{\lambda_{mix}} = \frac{(jRI^2 - Q)}{\pi T_\infty \lambda_{mix} D} \times \frac{\left[1 - \frac{T_\infty}{B} \ln \frac{R_\infty}{R}\right]}{\frac{T_\infty}{B} \ln \frac{R_\infty}{R}} \qquad (5.1)$$

However, it is necessary to take into account the effect of thermal resistance of the coated glass on the thermistor, for hydrogen or helium, because of their high thermal conductivity. The correction for Nusselt number due to this effect can be made.

The apparent Nusselt number was evaluated as a function of Knudsen number by using the experimental results with the aid of Eq. (5.1). The thermal conductivity of a gas mixture λ_{mix} at the surface temperature of the thermistor can be evaluated from the experimental results presented in reference (39) and from the method of Mason and Saxena (40)

$$\lambda_{mix} = \sum_{i=1}^{n} \frac{N_i \lambda_i}{\sum_{j=1}^{n} N_i \phi_{ij}} \qquad (5.2)$$

in which N_i is mole fraction and λ_i is the thermal conductivity of the pure component . The coefficient ϕ_{ij} is given as follows:

$$\phi_{ij} = \frac{1}{\sqrt{8}} \left(1 + \frac{M_i}{M_j}\right)^{-\frac{1}{2}} \left[1 - \left(\frac{\mu_i}{\mu_j}\right)^{\frac{1}{2}} \left(\frac{M_j}{M_i}\right)^{\frac{1}{4}}\right]^2 \qquad (5.3)$$

The thermal conductivity data at a given temperature are available from the table in references (39, 41). The surface temperature was approximated by the thermistor temperature.

The characteristic length D was determined from the following equation which means that πD^2 is equal to the surface area of a spheroidal thermistor;

$$\pi D^2 = 2\pi b^2 \left\{1 + \left(\frac{a}{b}\right)^2 \frac{1}{\sqrt{1 - \left(\frac{a}{b}\right)^2}} \times \ln \frac{1 + \sqrt{1 - \left(\frac{a}{b}\right)^2}}{\frac{a}{b}}\right. \qquad (5.4)$$

where a, b denote short radius and long radius respectively, and was 0.0419 cm in this experiment.

The heat loss Q , that is, the heat conduction from the thermistor through platinum wire leads 27.6 μ in diameter and 10 mm in total length, (see Fig. 43) was calculated from the following simple expression on the assumption that the heat conduction from the wire to the gas can be neglected. The above assumption is valid if the wire is placed in an infinite medium.

$$Q = 2\pi\delta^2\lambda_M \frac{T - T_\infty}{L} \tag{5.5}$$

in which δ , λ_M , L denote the radius of platinum wire, the thermal conductivity of platinum and the length of platinum wire, respectively. Corrections for radiation and free convection were neglected because the maximum value of the correction in the present investigation were about 0.1 per cent, and 1 per cent, respectively.

Knudsen number for pure gas and gas mixtures was calculated from the following expression at the wall temperature of the cell block T_∞ (42)

$$Kn'' = 85.89 \frac{\mu_{mix}}{Dp}\sqrt{\frac{T_\infty}{\overline{M}}} \tag{5.6}$$

where μ_{mix} = viscosity of gas mixture
$\overline{M} = M_1N_1 + M_2N_2$; mean molecular weight.

The viscosity of gas mixtures is obtained from the analogous equation to the previously given expression for the thermal conductivities, (40) or from the experimental results presented in reference (39)

$$\mu_{mix} = \sum_{i=1}^{n} \frac{N_i\,\mu_i}{\sum_{j=1}^{n} N_i\,\phi_{ij}} \tag{5.7}$$

The actual Nusselt number Nu^* can be obtained by considering of the heat conduction in the glass region surrounded by two concentric spheres, that is,

$$Nu = \frac{Nu^*}{1 + Nu^*C\lambda_{mix}} \tag{5.8}$$

$$C = \frac{S_2 - S_1}{2S_1\lambda_s} \tag{5.9}$$

where λ_s : the thermal conductivity of glass. S_1 , S_2 denote the radii of inner and outer spheres respectively (see Fig. 66). From Eq. (5.8) it is found that Nu depends on λ_{mix} as follows:

$$Nu = \frac{c_1}{1 + c_2\lambda_{mix}} \tag{5.10}$$

Figure 67 indicates Nu as a function of λ_{mix} for various gas mixtures when $Kn = 0.01$. The constants C_1 and C_2 appearing in Eq. (5.10) were determined from these results to be 1.79 and 0.103 respectively. The solid line in Fig. 67 expresses the relation between Nu and λ_{mix} calculated from Eq. (5 10) with these constants. Thus the actual Nusselt number was obtained as follows:

$$Nu^* = \frac{Nu}{1 - 0.0577 \cdot 10^4 \lambda_{mix} Nu} \tag{5.11}$$

Figure 68 gives the Nu^* for various gas mixtures and pure gas in the form of a function of Kn.

On the other hand, solving the Maxwell's integral equation of transport, we can obtain the analytical expression for the relation between Nusselt number and Knudsen number in the form:

$$Nu^* = \frac{2}{1 + \frac{15}{2} \alpha_{mix}^{-1} Kn} \tag{5.12}$$

Details are described in Appendix F.

The above relation with various values of α are shown by solid lines in Fig. 68. The results for some pure gases were in good agreement with Eq. (5.12) as indicated in Fig. 68, where the values of α for hydrogen, helium and nitrogen were chosen as 0.3, 0.35 and 0.8 respectively. It seems that these values of the accommodation coefficients are reasonable in comparison with the values obtained by other investigators, as given in Table (references (43, 44, 45) and the tables presented in the survey report on accommodation coefficient by Hartnett (46)).

For a multi-component gas mixture, the accommodation coefficient is expressed by the following equation from the energy balance

$$\alpha_{mix} = \frac{\sum_i \frac{N_i \alpha_i}{\sqrt{m_i}}}{\sum_i \frac{N_i}{\sqrt{m_i}}} \tag{5.13}$$

where α_i is the accommodation coefficient for pure gas, and N_i is a mole fraction. (47)

Figure 69 indicates the relation between Nu^* and $\alpha_{mix}^{-1} Kn$ for various gas mixtures, in which α_{mix} is evaluated from Eq. (5.13).

5.2 Comparison of Experimental Data with Theoretical Predictions

Separation of Hydrogen and Nitrogen Mixtures

From the experimental results for α and Θ, the value of

$$\frac{St \cdot Pe}{\frac{2 m_1 m_2 \Delta m}{m^{o\,3}} \gamma \left(\frac{\gamma+1}{2}\right)^{\frac{1}{\gamma-1}} \left(\frac{2}{\gamma+1}\right)^{\frac{1}{2}}}$$

is calculated with the aid of following equation:

$$St'' = \frac{m_1 N_1^o}{m^o} \Theta_G \frac{\alpha - 1}{1 + \alpha \frac{m_1 N_1^o}{m_2 N_2^o}} \tag{5.14}$$

The Péclet number is given by

$$Pe = \frac{R^* a^o}{\mathscr{D}_{12}^o} = R^* \sqrt{\gamma \frac{1}{m^o} k T^o} \frac{1}{\mathscr{D}_{12}^o}$$

$$= \frac{1}{2.662 \cdot 10^3 \frac{\sqrt{T^3 (M_1 + M_2)/2 M_1 M_2}}{p^o \sigma_{12}^2 \Omega_{12}^{(1,1)*}(T_{12}^{*o})}} \tag{5.15}$$

The force constants σ_{12} and ε_{12} associated with the Lennard-Jones potential for interaction between hydrogen and nitrogen molecules are found in the reference (48) to be

$$\sigma_{12} = 3.305 \text{ A}, \qquad \varepsilon_{12}/k = 58.1\,^{o}\text{K}.$$

The experimental values of the above dimensionless quantity are plotted as a function of nozzle to skimmer distance with the inlet pressure as a parameter in Fig. 70 It is indicated, in Fig. 70 , that experimental results for various inlet pressures can be summarized with a single relation by using the above dimensionless quantities.

If the leading edge of the skimmer is located inside the region bounded by both the barrel shock and the Mach disk (see Fig. 71), the cut will not be affected by the change of inlet pressure as shown in Fig. 57 Bier and Schmidt have reported a photographic study on the shape and size of the barrel shock and Mach disk (49). Their observed values on the Mach disk diameter, $y_M/2R^*$ and the maximum diameter of the barrel shock, $y_s/2R^*$ can be expressed as a function of the pressure ratio, p^0/p^1 by the following equations, over the range of p^0/p^1 of $10-10^3$.

$$\frac{y_M}{2R^*} = 0.252 \left(\frac{p^\circ}{p'}\right)^{0.598} \tag{5.16}$$

$$\frac{y_B}{2R^*} = 0.316 \left(\frac{p^\circ}{p'}\right)^{0.591} \tag{5.17}$$

The relationship between the axial distance to the Mach disk and the pressure ratio has been given by Ashkenus and Sherman as follows (50):

$$\frac{x_M}{R^*} = 1.34 \left(\frac{p^\circ}{p'}\right)^{\frac{1}{2}}, \quad 15 \leqslant \frac{p^\circ}{p'} \leqslant 17000 \tag{5.18}$$

Under our experimental condition, these values were calculated from the above equations as shown in Table 1 Hence, the flow field of supersonic jet into vacuum can be directly used for calculating the mass transfer up to the skimmer, regardless of the change of jet boundary.

The calculated relationship between the cut and the nozzle to skimmer distance when the distance from the axis r/R^* is $2.0/0.3$, is plotted in Fig. 57 for comparison with the experimental results. With the aid of the results for $d\theta/d\Lambda$, the integral, I was calculated for $r/R^* = 2.0/0.3$, by using Simpson integration formula. As the first order approximation, both the mole fraction N_1, N_2 and the average mass of gas mixture $\overline{m}$ were assumed to be constant and equal to their values at the nozzle inlet. Then, the integral, I is given by

$$I = N_1^\circ N_2^\circ \int_0^\Lambda \left(\frac{T^\circ}{T}\right)^{\frac{1}{6}} M^{*2} \frac{d\theta}{d\Lambda}\, \overline{n}\, d\Lambda \tag{5.19}$$

The results of calculation are shown in Fig. 70 by a solid line.

As indicated in Fig. 57 the experimental results on the relationship between the cut and the axial distance to the skimmer were in fairly good agreement with the results of calculation based on the flow pattern of axially symmetric supersonic jet into vacuum, which is computed by using the method of characteristics. This agreement has led to the conclusion that the flow properties up to the skimmer are unaffected by the jet boundary, that is, the leading edge of the skimmer is located inside the region bounded by both the barrel shock and the Mach disk under our experimental condition. The results on diffusive separation of hydrogen and nitrogen mixtures in an axially symmetric supersonic jet were also in fairly good agreement with the results of calculation by the proposed Eqs. (2.13) and (2.14) which were derived by taking account of the pressure diffusion in the jet.

Separation of H_2/N_2 and He/N_2 Mixtures in a Two-Dimensional Supersonic Jet

In Figs. 72 and 73, we show the measurement of expansion pressure ratio as a function of the cut for idfferent inlet pressures and for different nozzle to skimmer distances. It is seen that the experimental condition can be classified into two groups in this experiment. With the aid of the experimental data for expansion pressure ratio, the approximate shape of the barrel shock was calculated by assuming the shock profile to be expressed as

$$y = 1 + \tan^{-1}(\theta^M - \mu^M)\,x + c_1 x^2 + c_2 x^3 \tag{5.20}$$

where

$$\theta^M = \sqrt{\frac{\gamma+1}{\gamma-1}}\tan^{-1}\sqrt{\frac{\gamma-1}{\gamma+1}(M^{M^2}-1)} - \tan^{-1}\sqrt{M^{M^2}-1} \tag{5.21}$$

$$M^M = \sqrt{\frac{2}{\gamma-1}\left\{\left(\frac{p^o}{p^M}\right)^{\frac{\gamma-1}{\gamma}} - 1\right\}} \tag{5.22}$$

, the constants c_1 and c_2 being determined from the following condition:

$$x = x_B\ ;\quad y = y_B \qquad \frac{dy}{dx} = 0$$
$$x = x_M\ ;\quad y = y_M \tag{5.23}$$

The values of x_B, y_B, x_M, and y_M were chosen from the experimental data presented by Bier and Schmidt (49). In Fig. 74, the approximate shock profile is shown with the expansion pressure ratio as a parameter. Thus, it becomes evident that the leading edge of the skimmer located outside the barrel shock in this two-dimensional experiment.

If the leading edge of the skimmer locate far outside the barrel shock, the integral mass flux will be independent of the width of the skimmer, since the flow behind the shock will have little effect on species separation. From the experimental data for α and Θ, the value of

$$\frac{St\cdot p_e}{\frac{m_1 m_2 \Delta m}{m^{o3}}\,\gamma\left(\frac{\gamma+1}{2}\right)^{\frac{1}{\gamma-1}}\left(\frac{2}{\gamma+1}\right)^{\frac{1}{2}}}\;\frac{\Gamma}{\Gamma_\infty}$$

is calculated and plotted as a function of the cut in Figs. 75 and 76

Furthermore, the value of $\dfrac{St\, p_e}{\frac{m_1 m_2 \Delta m}{m^{o3}}\,\gamma\left(\frac{\gamma+1}{2}\right)^{\frac{1}{\gamma-1}}\left(\frac{2}{\gamma+1}\right)^{\frac{1}{2}}}\;\dfrac{\Gamma}{\Gamma_\infty}\;\dfrac{1}{N_1^o N_2^o}$

is plotted for both H_2/N_2 gas mixture and He/N_2 gas mixture in Fig. 77. The experimental data are summarized well into two groups, and it is seen that the width of the skimmer has no effect on the integral mass flux. However, these values of integral mass flux are extremely smaller than those predicted by integrating theoretical mass flux inside the barrel shock. This means that the absolute value of the integral mass flux in the shock is nearly equal to that in the isoentropic core. Bier also has obtained the similar result as shown in Fig. 78. On the other hand, when the expansion pressure ratio is relatively large, and simultaneously the width of the skimmer is small, the relationship between the integral mass flux and the cut becomes different as shown in Fig. 79. In this case, the leading edge located in the broaden shock wave. It is seen that the experimental values tend toward calculated values when the effect of shock is decreased.

5.3 Comparison of Theoretical Predictions with Existing Data Given by Becker et al.

Diffusive Separation of Argon Isotope Mixture

Becker, et al. have given experimental data for the separation effect $\mathcal{E}_A$ for an $^{36}Ar/^{40}Ar$ mixture as a function of the nozzle-skimmer distance, with the cut Θ as parameter (see Figs. 80 and 81 (30,51)). The separation effect is defined by

$$\mathcal{E}_A = \frac{N^M (1 - N^K)}{N^K (1 - N^M)} - 1$$

where N^M and N^K are the mole fractions of the lighter component of a binary mixture in the peripheral stream and the core stream, respectively.

From the experimental results for $\mathcal{E}_A$ and Θ given by Becker, et al., the value of

$$\frac{St \cdot Pe}{\frac{2 m_1 m_2 \Delta m}{\overline{m}^{o\,3}} \gamma \left(\frac{\gamma+1}{2}\right)^{\frac{1}{\gamma-1}} \left(\frac{2}{\gamma+1}\right)^{\frac{1}{2}}}$$

is calculated with the aid of Eqs. (2.13), (2.15) and (2.20) and plotted in Figs. 82 and 83 as a function of nozzle-to-skimmer distance x/R^* with Θ as parameter.

The flow field of axially symmetric supersonic jet into vacuum was computed by using the numerical method of characteristics; $d\theta/d\Lambda$ and I appearing in Eq. (2.14) were calculated along various streamlines. The details of the method of computation are described in the previous section. The streamlines obtained are shown with the value of cut as parameter in Fig. 84 in which the experimental data by Becker, et al. are also plotted. Figure 16 gives $d\theta/d\Lambda$ along various streamlines, and the Mach number distribution along the streamlines is shown in Fig. 17 .

If the leading edge of the skimmer is located inside the region bounded by both the barrel shock and the Mach disk (see Fig. 71), the value of cut will not be affected by changes in the inlet pressure, that is, by the changes in the position of jet boundary, so that the flow field of supersonic jet into vacuum can be directly used for calculating the mass transfer up to the skimmer, regardless of changes in jet boundary.

Bier & Schmidt (49) have published a photographic study on the shape and size of the barrel shock and Mach disk for argon gas. Their observed values of the Mach disk diameter $y_M/2R^*$, the maximum diameter $y_B/2R^*$ of the barrel shock, the axial distance $x_B/2R^*$ at which the diameter of the barrel shock becomes maximum, and the axial distance $x_M/2R^*$ to the Mach disk can all be expressed as functions of the pressure ratio p^o/p' over a range of p^o/p' between 10 and 10^3 :

$$\frac{y_M}{2R^*} = 0.205 \left(\frac{p^o}{p'}\right)^{0.620} \qquad (5.24)$$

$$\frac{y_B}{2R^*} = 0.245 \left(\frac{p^o}{p'}\right)^{0.624} \qquad (5.25)$$

$$\frac{x_M}{R^*} = 1.31 \left(\frac{p^o}{p'}\right)^{0.520} \qquad (5.26)$$

$$\frac{x_B}{R^*} = 0.81 \left(\frac{p^o}{p'}\right)^{0.526}$$

Table 2 shows these values calculated from the above equations under the same conditions as Becker's experiment. Hence, the leading edge of the skimmer may be located inside the barrel shock except in the case of the small values of cut.

With the aid of the results of computation for $d\theta/d\Lambda$, the integral I was calculated as a function of Λ along various streamlines. As first order approximation, both the mole fraction N_1, N_2 and the average mass of gas mixture $\overline{m}$ were assumed to be constant and equal to their values at the nozzle inlet, that is, $N_1^o = 0.00337$, $N_2^o = 0.996$. Then

$$I = N_1^o N_2^o \int_0^{\Lambda} M^{*2} \frac{d\theta}{d\Lambda} \bar{\pi}\, d\Lambda \qquad (5.27)$$

The results of calculation are shown by the solid lines in Figs. 82 and 83.

As indicated in Fig. 84 experimental results on the streamline by Becker, et al. are in fairly good agreement with the results of calculation on the flow pattern of axially symmetric supersonic jet into vacuum, except for $\Theta = 0.1$. This agreement permits us to affirm that the flow properties upstream of the skimmer are affected neither by the skimmer itself nor by the jet boundary, which means that the leading edge of the skimmer was located inside the barrel shock.

The results on diffusive separation of $^{36}Ar/^{40}Ar$ isotope mixture in an axially symmetric supersonic jet are in reasonably good agreement with the results of calculation by the proposed Eqs. (2.13) and (2.15) as indicated by Figs. 82 and 83 except for small values of cut.

Diffusive Separation of Three-Component Gas Mixture of ^{36}Ar, ^{40}Ar, and He

Becker et al. (30) have given experimental results on the separation of argon isotopes, when the supersonic jet of an ^{36}Ar-^{40}Ar-He(H_2) mixture is separated by means of a skimmer into peripheral and central streams. Further experimental results on the separation of a $^{235}UF_6$-$^{238}UF_6$-He mixture were also presented (52, 4). Figure 85 shows typical results for the separation effect, ε_A, for argon isotopes, as a function of the nozzle skimmer distance, x_s, with the cut, Θ_A, as a parameter. The above results were obtained under the condition of constant feed rate of argon gas through a nozzle, while the separation effect, ε_A, increases appreciably with increasing helium concentration. Similar results were obtained for separation of uranium isotopes using a curved jet containing gaseous uranium hexafluoride and helium. A jet separation pilot plant working with a $He-UF_6$ mixture was built in Karlsruhe in Germany and has been operated successfully (4).

The gas dynamic characteristics of an invicid free jet of a helium-argon mixture are independent of its composition because their ratios of specific heats are the same. Thus, the flow field of an axially symmetric supersonic jet into vacuum for $\gamma = 1.66667$—computed—in the previous section can be used directly. The streamlines of argon gas were obtained by solving Eq. (2.51) numerically, and shown by solid lines in Figs. 86 and 87 with the value of cut, Θ_A, as a parameter, in which the mole fractions N_1^o, N_2^o, and N_3^o, and the inlet pressure, p^o, are assumed to be similar to the values in Becker's experiment:

Case I			Case II		
N_1^o	$= 0.52$		N_1^o	$= 0.89$	
N_2^o	$= 0.48$	0.00337	N_2^o	$= 0.11$	0.00337
N_3^o	$= 0.48$	0.99663	N_3^o	$= 0.11$	0.99663
p^o	$= 24$ torr		p^o	$= 60$ torr	

In this calculation, the light component consists of pure helium, although a small quantity of hydrogen was also included in Becker's experiment.

The experimental data are plotted in Figs. 86 and 87 . Then, the mass flux integral, I, was calculated from Eq. (2.50) by the Simpson formula. The results of calculation are shown by solid lines in Figs. 88 and 89 .

If the leading edge of the skimmer is located inside the region bounded by the barrel shock and the Mach disk, the flow field of the supersonic jet into vacuum can be directly used for calculating the mass transfer up to the skimmer regardless of the value of the expansion pressure ratio. As indicated in Figs. 86 and 87 the results of calculation on the flow pattern of an axisymmetric supersonic jet into vacuum are in fairly good agreement with experimental results, except for small values of cut. This agreement permits us to affirm that the flow properties upstream of the skimmer are affected neither by the skimmer itself nor by the jet boundary, which means that the leading edge of the skimmer was located inside the barrel shock.

From the experimental results for $\mathcal{E}_A$ and Θ_A given by Becker et al., the value of

$$\frac{St \cdot Pe}{2\,\frac{m_2}{m_3}\left(\frac{\Delta m}{\overline{m}}\right)^o_{\mathcal{D}} \gamma \left(\frac{\gamma+1}{2}\right)^{\frac{1}{\gamma-1}} \left(\frac{2}{\gamma+1}\right)^{\frac{1}{2}}}$$

is calculated with the aid of Eqs. (2.62) and (2.63) and plotted in Figs. 88 and 89 as a function of nozzle-to-skimmer distance with Θ_A as parameter. As can be seen, there is reasonable agreement between theory and experiment, for $\Theta_A > 0.3$.

As indicated in Figs.88 and 89, a numerical analysis on the diffusive separation of three-component gas mixtures of ^{36}Ar, ^{40}Ar, and He in an axisymmetric supersonic jet gave reasonable agreement between calculated and experimental results. The enhancement of the separation effect of argon isotopes when helium is added as a third component can be attributed to the decrease of the average mass of the gas mixture and the apparent increase of the mutual diffusion coefficient between argon isotopes (Eq.2.47). A similar analysis could be used to analyze the process for separation of uranium isotopes using a jet containing gaseous uranium hexafluoride and helium.

Diffusive Separation of $^{235}UF_6/^{238}UF_6$ Mixture in a Two-Dimensional Supersonic Jet

Becker et al. (53) have given experimental results on the separation effect ε_A for $^{235}UF_6/^{238}UF_6$ mixture as a function of nozzle inlet pressure, as reproduced in Fig.90 Table 3 gives their experimental conditions. From these data, the values of

$$\frac{St \cdot p_e}{\frac{m_1 m_2 \Delta m}{m^{o3}}\, \gamma \left(\frac{\gamma+1}{2}\right)^{\frac{1}{\gamma-1}} \left(\frac{2}{\gamma+1}\right)^{\frac{1}{2}}}$$

are calculated with the aid of Eqs.(2.18) and (2.20) and plotted in Fig.91 as a function of inlet pressure.

The flow field of supersonic jet of UF_6 gas from a two-dimensional sonic nozzle was calculated numerically by the method of characteristics.

Based on the results obtained therefrom the pressure diffusion flux was calculated along various streamlines. Figure 92 presents the integral I along various streamlines as a function of x/R*.

Comparison of diffusive separation between experimental data and theoretical prediction is shown in Fig.91, and a comparison of cut is shown in Fig.93. It is seen from these figures that the experimental values of the pressure diffusion flux as well as cut tend toward calculated values with increasing inlet pressure, that is, expansion pressure ratio.

Table 2 Becker's experimental condition

P^0 mm Hg	P^0/P^M mm Hg	x_M/R^*	$y_M/2R^*$	y_B/R^*	$y_A/2R^*$
30	$1.5\cdot10^3$	58.7	19.1	37.9	23.5
80	$4.0\cdot10^3$	97.8	35.1	63.6	43.3
16	10^3	47.4	14.9	30.8	18.2

Table 3 Geometry of Becker's jet separation apparatus

	A	B	C
Width of nozzle exit mm	0.085	0.045	0.049
Width of skimmer mm	0.29	0.19	0.25
Distance between nozzle exit and skimmer mm	0.1	0.08	0.11

Separation of Gas Mixture in a Shock Wave

Bier et al. (54) have given experimental results on the separation of helium-argon mixtures in a oblique shock wave which is formed ahead of a cone of half angle 22.5 placed in an axisymmetric free jet (Fig. 94). Their data for the separation coefficient and the cut for different nozzle inlet pressure and the distance between the nozzle exit and the vertex of the cone are reproduced in Figs. 95 and 96. It is seen that the separation coefficients are increased appreciably during passage of shock front through the leading edge of the skimmer.
From these data, the value of

$$\frac{St \cdot p_e}{\frac{2 m_1 m_2 \Delta m}{m^{o3}} \gamma \left(\frac{\gamma+1}{2}\right)^{\frac{1}{\gamma-1}} \left(\frac{2}{\gamma+1}\right)^{\frac{1}{2}}}$$

are calculated with the aid of Eqs. (2.18) and (2.20) and plotted in Fig. 97 as a function of the distance between the nozzle exit and the vertex of the cone.
Now, consider following the streamline which issues from the nozzle exit and just reaches the leading edge of the skimmer after crossing the oblique shock.
If we assume that the flow behind shock has little effect on species separation, the total integral mass flux can be obtained by summing the integral mass flux in the shock and that in the part of jet before the shock.
The conditions at the crossing point of the streamline and the shock can be determined by utilizing the results of calculation on the shock shape described in the section 3.4 and with the aid of the experimental data for the cut. Thus, the integral mass flux I_s was calculated from the results presented in the section 3.3.
The calculated results on the total integral mass flux are shown by a solid curve in Fig. 97 in which a dotted curve represents the integral mass flux in the part of jet before the shock. It is encouraging that there is reasonable agreement between experimental data and calculated values. However, it is further necessary to calculate flow field behind shock in order to make true comparison between the experimental data and theoretical prediction.

VI Evaluation of Jet Separation Process

Separation performance of a separating element is generally expressed in terms of separative power, δU (58). When the separation effect is very small, δU is expressed as

$$\delta U = \frac{G}{2} \varepsilon_A^2 \Theta (1 - \Theta) \tag{6.1}$$

where separation effect, ε_A is defined by

$$\varepsilon_A = \frac{N_1^M / N_2^M}{N_1^K / N_2^K} - 1 \tag{6.2}$$

It is of importance to find an optimum operating condition in which the finantial input for the separating element is minimaized relative to the separative power. The finantial input mainly consists of the cost of the electric energy for the compressor, and the capital cost. The former is roughly proportional to the isothermal compression energy, E, which is written in the form:

$$E = GRT \left(\Theta \ln \frac{p^o}{p^M} + (1 - \Theta) \ln \frac{p^o}{p^K} \right) \tag{6.3}$$

The optimum condition is approximately determined by minimizing the specific cost of energy, $E/\delta U$, as the jet separation process demands the high power consumption.

The separation effect, ε_A is given in terms of integral mass flux, J, as follows:

$$\varepsilon_A = \frac{\frac{N_1^o m_1}{\bar{m}^o} G\Theta + J}{\frac{N_2^o m_2}{\bar{m}^o} G\Theta - J} \times \frac{\frac{N_2^o m_2}{\bar{m}^o} G(1-\Theta) + J}{\frac{N_1^o m_1}{\bar{m}^o} G(1-\Theta) - J} - 1$$

$$= \frac{GJ}{\left(\frac{N_1^o m_1}{\bar{m}^o} G(1-\Theta) - J\right)\left(\frac{N_2^o m_2}{\bar{m}^o} G\Theta - J\right)} \tag{6.4}$$

If J is very small, Equation (6.4) becomes

$$\varepsilon_A = \frac{\bar{m}^{o\,2}}{m_1 m_2 N_1^o N_2^o} \frac{J}{G\Theta(1-\Theta)}$$

$$= \frac{\bar{m}^{o\,2}}{m_1 m_2 N_1^o N_2^o} \frac{St}{\Theta(1-\Theta)} \tag{6.5}$$

Therefore, the separation effect is proportional to the Stanton number. Thus, the specific cost of nergy is given by

$$\frac{E}{\delta U} = 2\left(\frac{m_1 m_2 N_1^\circ N_2^\circ}{\bar{m}^{\circ 2}}\right)^2 \Theta(1-\Theta) RT \left(\Theta \ln\frac{p^\circ}{p^M} + (1-\Theta)\ln\frac{p^\circ}{p^K}\right) St^2 \tag{6.6}$$

Now, let's consider first, the influence of a third component on the separation of isotopes. As shown in the previous sections, the degree of separation, that is, the separative power is enhanced by adding a light component like helium, while the energy consumption increases due to the increase of the flow rate.

To find out the optimum fraction of the light component, the value of $(Q^*/\delta U)/(Q^*/\delta U)_+$ has been calculated as a function of the mole fraction of helium, for two examples of He-^{36}A -^{40}A, and He -^{235}UF$_6$ -^{238}UF$_6$. The suffix + represents values for three component mixture and values for pure isotope mixture are represented without any suffix.

From Eq. (6.5), we get

$$\frac{\mathcal{E}_{A,+}}{\mathcal{E}_A} = \frac{I_+}{I}\frac{P_e}{P_{e+}}\frac{\bar{m}}{\bar{m}_+} = \frac{I_+}{I}\frac{\dfrac{a^\circ}{\mathcal{D}_{21}^\circ}}{\dfrac{a^\circ_+}{\mathcal{D}_{23+}^\circ \chi}}\frac{\bar{m}}{\bar{m}_+} \tag{6.7}$$

When the flow rate of isotope mixture is maintained constant, we have the following relation between inlet pressures, p° and p_+°.

$$\frac{p^\circ}{p_+^\circ} = \frac{\sqrt{\bar{m}}}{\sqrt{\bar{m}_+}}(1 - N_1) \tag{6.8}$$

and furthermore, if I_+ is assumed equal to I, we get

$$\frac{\mathcal{E}_{A+}}{\mathcal{E}_A} = \frac{\bar{m}}{\bar{m}_+}\frac{\mathcal{D}_{13}^\circ}{N_1\mathcal{D}_{23}^\circ + N_2\mathcal{D}_{31}^\circ + N_3\mathcal{D}_{12}^\circ}(1-N_1) \tag{6.9}$$

Hence,

$$\frac{\left(\dfrac{Q^*}{\delta U}\right)}{\left(\dfrac{Q^*}{\delta U}\right)_+} = \left(\frac{\bar{m}}{\bar{m}_+}\frac{\mathcal{D}_{13}^\circ}{N_1\mathcal{D}_{23}^\circ + N_2\mathcal{D}_{31}^\circ + N_3\mathcal{D}_{12}^\circ}\right)^2 \times (1-N_1)^3 \tag{6.10}$$

Figure 98 shows the dependence of $\left(\frac{Q^*}{\delta U}\right)/\left(\frac{Q^*}{\delta U}\right)_+$ on the fraction of helium. Each curve has a maximum at N = 0.4 for He-^{36}A-^{40}A mixture, and at N = 0.93 for He-^{235}UF$_6$ -^{238}UF$_6$ mixture.

It is noteworthy that the effect of addition of light component is remarkable for uranium hexafluoride isotope mixture, while the effect is not appreciable for argon isotope mixture, as shown in Fig.98 . The optimum value of the fraction of helium for uranium hexafluoride accidentally agreed with the value assigned by Becker et al. (4). Under the optimum condition, the specific cost of energy reduces down to about 1/5 comparing to the case of no addition of light component.

In the next place, let's consider the influence of the expansion pressure ratio, p°/p^{M} on the specific cost of energy. If the value of expansion pressure ratio is given, the shape of barrel shock can be determined in the manner as described in 5-2. Then the cross point of a relevant streamline at the barrel shock determines the location of the leading edge of the skimmer. When the value of expansion pressure ratio is increased, the cross point is shifted from upstream to downstream. Hence, the integral mass flux, that is, the separation effect increases as the expansion pressure ratio increases, while the power consumption also increases. If the stagnant condition at the nozzle inlet is fixed, and if p^{M} is assumed equal to p^{K}, the specific cost of energy is proportional to the quantity,

$$\frac{\log\left(\frac{p^{\circ}}{p^{M}}\right)}{\left(\frac{I}{N_1^{\circ}N_2^{\circ}}\right)^2}$$

Figure 99 shows the value of $\log\frac{p^{\circ}}{p^{M}}/\left(I/N_1^{\circ}N_2^{\circ}\right)^2$ as a function of p°/p^{M} for cut $\Theta = 1/2, \sim 1/3, 1/4$, in the case of two-dimensional jet of $\gamma=1.4$. It is seen that the specific cost of energy becomes nearly constant beyond $p^{\circ}/p^{M}=50$. As the pressure recovery through the shock can hardly be evaluated, the real optimum expansion pressure ratio is still obscure at the present stage.

VI Conclusion

Based on the results of the present investigation, following concluding remarks can be made.

By using the integral mass flux, which can be obtained by integrating mass flux of a relevant species over a streamtube in a jet, it has been possible to deal with the separation phenomena in supersonic jets even with shocks.

Explicit expressions for evaluating the integral mass flux were introduced in a dimensionless form which included several dimensionless quantities, and were applied for the pressure diffusion flux in a jet of binary and ternary gas mixtures and also in an oblique shock wave of binary gas mixture. These were found useful to plot the experimental data on a single curve regardless of the physical properties, inlet pressure and initial concentration.

Two kinds of flow fields of axially symmetric and two-dimensional jets into vacuum were computed by using the numerical method of characteristics. The calculated results for flow pattern were in fairly good agreement with the results of skimmer experiments. This agreement leads to the conclusion that the flow properties in a jet can be well predicted even by assuming the fluid invicid and the flow pattern is not disturbed by the existence of the skimmer. This is probably true if the leading edge of the skimmer is located within the region bounded by the barrel shock and the Mach disk or Rieman wave.

The experimental results on diffusive separation of various gas mixtures were also in fairly good agreement with the calculation results from the proposed equation derived by taking account of the pressure diffusion in a jet. This means that the separation of species in a supersonic jet of gas mixture is mainly due to the pressure diffusion in the expanding jet or in the shock wave.

The effect of isotope separation by adding the third component like helium was analized numerically and was confirmed to be in good agreement with the experimental data given by Becker et al. The enhancement of the separation effect of isotopes when helium is added as a third component should be attributed to the apparent increase of the mutual diffusion coefficient between isotopes, and to the decrease of the average mass of the gas mixture.

In the case that the leading edge of the skimmer located outside from the intercepting shock in a two-dimensional supersonic jet, the experimental values of integral mass flux were found very small. This means that the magnitude of the integral mass flux in the shock counterbalances that in the potential core. An elongated and narrow intercepting shock is usually formed in a two-dimensional jet. Therefore, it becomes difficult to design the apparatus in a fashon as the leading edge of the skimmer is placed in the potential core so that the negative effect of the shock wave may be avoided.

The calculated results on the total integral mass flux in an oblique shock wave were in fairly good agreement with the experimental results presented by Bier et al. Thus, the present method of calculation was found useful to predict the species separation in a shock wave, too.

A thermal conductivity method which is based on measuring the heat transfer coefficient from a sphere to rarefied gas mixtures, was applied successfully to gas analysis at low pressure. The experimental data on the heat transfer coefficient were in good agreement with the analytical result obtained by solving Maxwell's integral equation of transport.

References

1. Tahourdin, P.A. — Oxford Report, No.36, Br.694, Clarendon Laboratory, Oxford, England (1946).

2. Dickens, S.P., Coghlan, C.A., Morrow, P.G. — Separation of Gases from Mixtures thereof, U.S. Patent, 2,607,439 (1952).

3. Becker, E.W., Bier, K. — Die Erzeugung eines intensiven teilweise monochromatisieren Wasserstoff-Molecularstrahles mit einer Laval-Düse, Zeitschrift für Naturforschung, 9a, 975 (1954).

4. Becker, E.W., Frey, G., Seidel, D. — Ten Stage Cascade Nozzle Enrichment, Nuclear Engineering, 13, 770 (1968).

5. Chow, R.R. — On the Separation Phenomena of a Binary Gas Mixture in an Axisymmetric Jet, University of California, Institute of Engineering Research Report HE-150-175, Nov. (1959).

6. Reis, V.H., Fenn, J.B. — Separation of Gas Mixtures in Supersonic Jets, Journal of Chemical Physics, 39, 3240 (1963).

7. Waterman P.C., Stern, S.A. — Separation of Gas Mixtures in a Supersonic Jet, Journal of Chemical Physics, 31, 405 (1959).

8. Stern, S.A., Waterman, P.C., Sinclair, T.F. — Separation of Gas Mixtures in a Supersonic Jet II. Behavior of Helium-Argon Mixtures and Evidence of Shock Separation, Journal of Chemical Physics, 33, 805 (1960).

9. Nardelli, G., Repanai, A. — I Principi Fisici del Metodo della Trenndüse, II., Energia Nucleare, 5, 247 (1958).

10. Zigan, F. — Gasdynamische Berechnung der Trenndüsenentmischung, Zeitschrift für Naturforschung, 17a, 772 (1962).

11. Mikami, H., Takashima, Y. — Separation of Isotope Gas Mixture in a Supersonic Jet, Bulletin of the Tokyo Institute of Technology, No. 61, 67 (1964).

12. Sherman, F.S. — Hydrodynamical Theory of Diffusive Separation of Mixtures in a Free Jet, The Physics of Fluids, 8, 773 (1965).

13. Rothe, D.E. — Electron Beam Studies of the Diffusive Separation of Helium-Argon Mixtures, The Physics of Fluids, 9, 1643 (1966).

14. Anderson, J.B. — Separation of Gas Mixtures in Free Jets, AICHE Journal, 13, 1188 (1967).

15. Hirschfelder, J.O., Curtiss, C. O., Bird, R.B. — Molecular Theory of Gases and Liquids, P.516. John Wiley, New York (1960).

16. Hirschfelder, J.O., Curtiss, C.O., Bird, R.B. — ibid., P.539.

17. Hirschfelder, J.O., Curtiss, C.O., Bird, R.B. — ibid., P.1126.

18. Hirschfelder, J.O., Curtiss, C.O., Bird, R.B. — ibid., P.1110.

19. Winn, E.B. — The Temperature Dependence of the Self-Diffusion Coefficients of Argon, Neon, Nitrogen, Oxygen, Carbon Dioxide, and Methane, Physical Review, 80, 1024 (1950).

20. De Paz, M., Turi, B., Klein, M.L. — New Self Diffusion Measurements in Argon Gas, Physica, 36, 127 (1967).

21. Mason, E.A. — Transport Properties of Gases Obeying a Modified Buckingham (Exp-Six) Potential, Journal of Chemical Physics, 22, 169 (1954).

22. DeWitt, R. — Uranium Hexafluoride, A Survey of the Physicochemical Properties, Goodyear Atomic Corporation, Portsmouth, Ohio (1960).

23. Brown, M., Murphy, E.G. — Measurements of the Self-Diffusion Coefficient of Uranium Hexafluoride, Transactions of the Faraday Society, 61, Part II, 2442 (1965).

24. Sherman, F.S. — Shock Wave Structure in Binary Mixtures of Chemically Inert Perfect Gases, Journal of Fluid Mechanics, 8, 465 (1960).

25. Katskova, O.N., Shmyglevskii, Y.D. — Axisymmetric Supersonic Flow of a Freely Expanding Gas with Plane Transition Surface, Sbornik Vychislitelnoi Matematiki, 2, 45 (1957).

26. Katskova, O.N. — On Axisymmetric Supersonic Expansion of a Real Gas, Zhrnal Vychislitelnoi Matematiki i Matematicheskoi Fiziki, 1, 301 (1961).

27. Liepmann, H.W., Roshko, A. — Elements of Gas Dynamics, P.292. John Wiley, New York (1960).

28. Berezin, I.S., Zhidkov, N.P. — Computing Methods, Vol.1, P.196. Pergamon Press, Oxford (1965).

29. Becker, E.W., Bier, K., Bier, W. — Trenndüsenverfahren mit leightem Zusatzgas, Zeitschrift für Naturforschung, 17a, 778 (1962).

30. Talbot, L., Sherman, F.S. — Structure of Weak Shock Waves in a Monoatomic Gas, NASA, MEMO 12-14-58W (1959).

31. Belotserkovskii, O.M., Chuskin, P.I. — The Numerical Solution of Problems in Gas Dynamics, in Basic Development in Fluid Dynamics, edited by M. Holt, Vol.1, P.1. Academic Press, New York (1965).

32. Bartyenev, D.A., Shirshov, V.P. — Calculation of Flow around a Body of Revolution with Sharp Leading Edge in a Non-Uniform Axisymmetric Flow of Gas, in Izvestiya Vyshikh Ychebnykh Zavedyenii Aviatsionnaya Tekhnika, No.1. P.3 (1968).

33. Sherman, F.S. — Self-Similar Development of Invicid Hypersonic Free-Jet Flows, Lockheed Missiles and Space Company, AD 618954 (1963).

34. Meiville, H.W., Gowenlock, B.G. — Experimental Method in Gas Reactions, P.223. MacMillan, London (1964).

35. Gow-Mac Thermistor Type Thermal Conductivity Cells, Specifications and Operating Instructions, Gow-Mac Instrument Company, U.S.A.

36. Takahei, T. — Electronics in Mechanical Engineering, P.103. Corona, Tokyo (1961).

37. Shimoda, K. — Fundamentals of Electronics, P.160. Shokabo, Tokyo (1958).

38. Liepmann, H.W. — Gaskinetics and Gasdynamics of Orifice Flow, Journal of Fluid Mechanics, 10, 65 (1961).

39. Hirschfelder, J.O., Curtiss, C.O., Bird, R.B. Molecular Theory of Gases and Liquids, P.577. John Wiley, New York (1964).

40. Bird, R.B., Stewart, W.E., Lightfoot, E.N. Transport Phenomena, PP.24 and 258. John Wiley, New York (1960).

41. Hirsenrath, J. et al. Tables of Thermodynamic and Transport Properties of Air, Argon, Carbon Dioxide, Carbon Mono-oxide, Hydrogen, Nitrogen, Oxygen, and Steam, PP. 284 and 357. Pergamon Press, New York (1960).

42. Kennard, E.H. Kinetic Theory of Gases, P.147. MacGraw-Hill, New York (1938).

43. Kennard, E.H. ibid., P.323.

44. Springer, G.S., Tsai, S.W. Method of Calculating Heat Conduction from Spheres in Rarefied Gases, The Physics of Fluids, 8, 1561 (1965).

45. Grilly, E.R., Taylor, W.J., Johnstone, H.L. Accommodation Coefficients for Heat Conduction between Gas and Bright Platinum, for Nine Gases between 80°K (or Their Boiling Points) and 380°K, Journal of Chemical Physics, 14, 435 (1946).

46. Hartnett, J.P. A Survey of Thermal Accommodation Coefficients, in Rarefied Gas Dynamics, edited by L. Talbot, P.1. Academic Press, New York (1961).

47. Mikami, H. Thermal Accommodation Coefficient for Gas Mixture, Kagaku Kogaku, 32, 715 (1968).

48. Waldmann, L. Transporterscheinungen in Gasen von mittlerem Druck, in Handbuch der Physik, edited by S. Flügge, XII, 429 (1958).

49. Bier, K., Schmidt, B. Zur Form der Verdichtungsstösse in frei expandierenden Gasstrahlen, Zeitschrift für angewandte Physik, 13, 493 (1961).

50. Ashkenus, H., Sherman, F.S. The Structure and Utilization of Supersonic Free Jet in Low Density Wind Tunnels, in Rarefied Gas Dynamics, edited by J.H. Leeuw, Vol.2, P.91. Academic Press. New York (1966).

51. Becker, E.W., Beyrich, W., Bier, K., Burghoff, H., Zigan, F. — Das Trenndüsenverfahren II, Die physikalischen Grundlagen des Trenneffektes und die spezifischen Aufwandsgrössen des Verfahrens, Zeitschrift für Naturforschung, 12a, 609 (1957).

52. Becker, E.W., Bier, K., Bier, W., Schütte, R. — Trenndüssenentmischung der Uranisotope bei Verwendung leichter Zusatzgase, Zeitschrift für Naturforschung, 18a, 246 (1963).

53. Becker, E.W., Schütte, R. — Das Trenndüsenverfahren III. Entmischung der Uranisotope, Zeitschrift für Naturforschung, 15a, 336 (1960).

54. Bier, K., Zeller, R. — Zur partiellen Entmischung von Gas- und Isotopengemischen durich Verdichtungsstösse, Zeitschrift für Naturforschung, 20a, 1519 (1965).

55. Motulevich, V.P. — Flow of Gas from a Nozzle Cut in an Oblique Plane, in Physical Gas Dynamics, edited by A.S. Predvoditelev, P.108. Pergamon Press, New York (1961).

56. Lees, L., Liu, C.Y. — Kinetic-Theory Description of Conductive Heat Transfer from a Fine Wire, The Physics of Fluids, 5, 1137 (1962).

57. Lees, L. — A Kinetic Theory Description of Rarefied Gas Flows, GALCIT Hypersonics Research Project, Memorandum No.51 (1959).

58. Cohen, K. — The Theory of Isotope Separation as applied to the Large Scale Production of U^{235}. MacGraw-Hill, New York (1951).

Author's Publication

a. Separation of Isotope Mixture by Nozzle Process: U.S.AEC Report, AEC-Tr-5069, July (1962).

b. Separation of Isotope Mixture by Nozzle Process (2), Bull. Tokyo Inst. Technol., No.49, 167 (1962).

c. Separation of Isotope Gas Mixture in a Supersonic Jet: Bull. Tokyo Inst. Technol., No.61, 67 (1964).

d. Analysis of Two Component Gas Mixture at Low Pressure by a Thermistor-Actuated Thermal Conductivity Cell: Bull. Tokyo Inst. Technol., No.69, 39 (1965).

e. Separation of Isotope Mixture in a Free Molecular Jet: J. Nucl. Sci. Technol., 3, 120 (1966).

f. Heat Transfer from a Sphere to Rarefied Gas Mixtures: Int. J. Heat Mass Transfer, 9, 1435 (1966).

g. Thermal Accommodation Coefficients for Gas Mixture: Chemical Engineering Japan, 32, 91 (1968).

h. Critical Mass Flow of Rarefied Gas Mixture through a Slit Nozzle: Bull. Tokyo Inst. Technol., 83, 103 (1968).

i. Separation of Gas Mixture in an Axisymmetric Supersonic Jet: Int. J. Heat Mass Transfer, 11, 1597 (1968).

j. Separation of Argon Isotope Mixture in an Axisymmetric Supersonic Jet: J. Nucl. Sci. Technol., 5, 572 (1968).

k. Separation of Isotope Mixture in a Two-Dimensional Supersonic Jet: J. Nucl. Sci. Technol., 6, 452 (1969).

l. Separation of a Three-Component Gas Mixture in an Axisymmetric Supersonic Jet: I/EC Fundamentals, 9, 121 (1970).

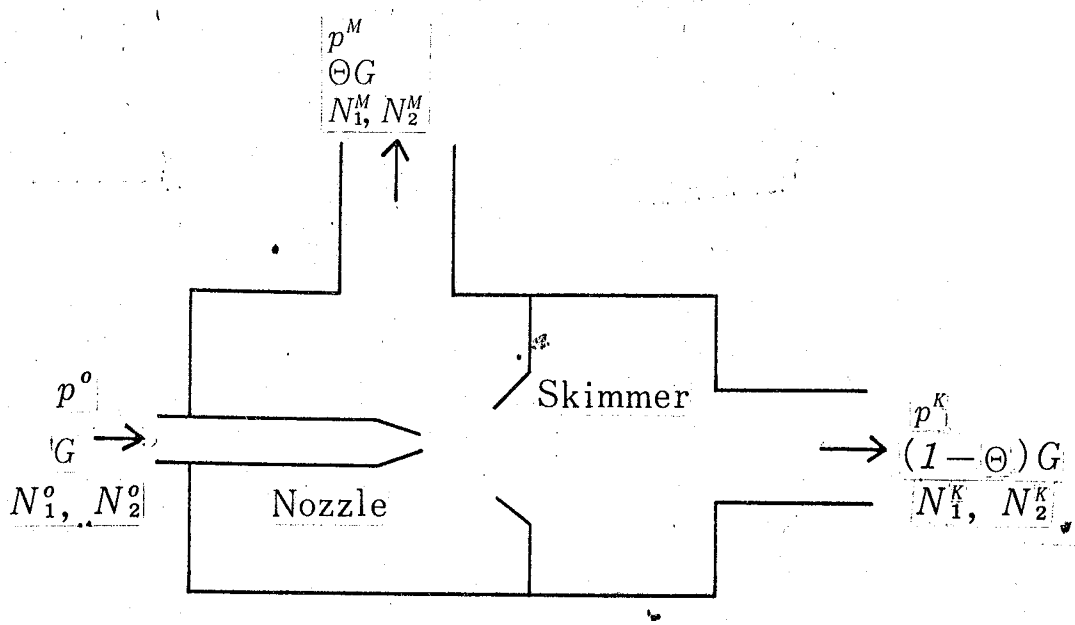

FIG.1 DIAGRAM OF APPARATUS FOR JET SEPARATION

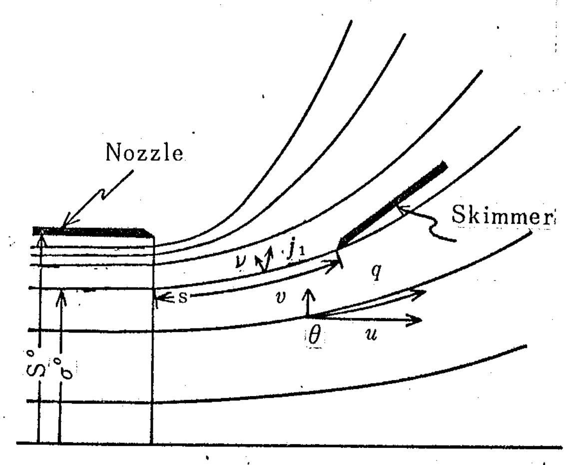

FIG.2 COORDINATES FOR AXIALLY SYMMETRIC FLOW

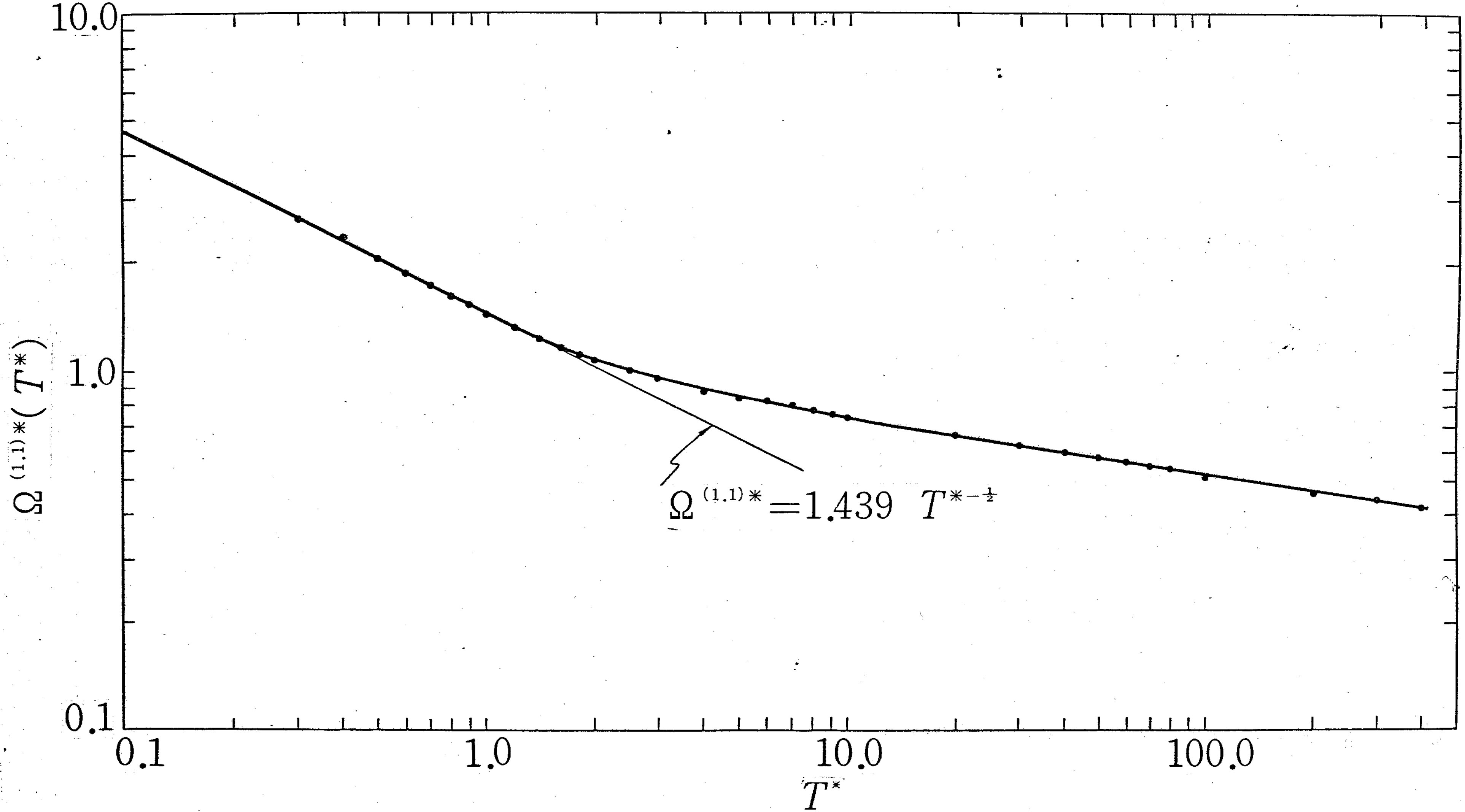

FIG.3 RELATIONSHIP BETWEEN COLLISION INTEGRAL AND REDUCED TEMPERATURE FOR LENNARD-JONES POTENTIAL

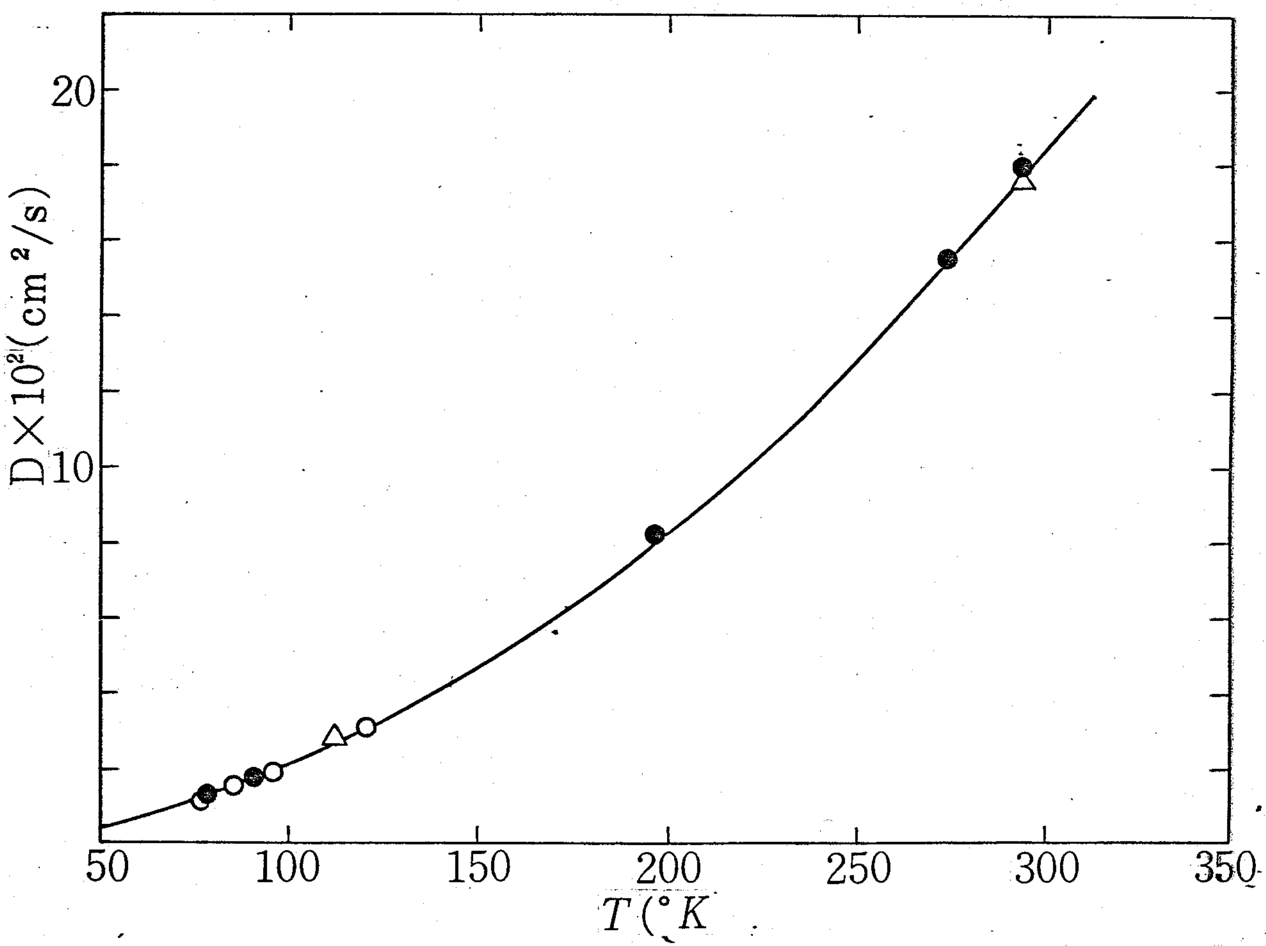

FIG.4 EXPERIMENTAL DATA ON SELF-DIFFUSION COEFFICIENT IN GASEOUS ARGON OBTAINED BY WINN(19) AND BY DE PAZ, ET AL.(20)

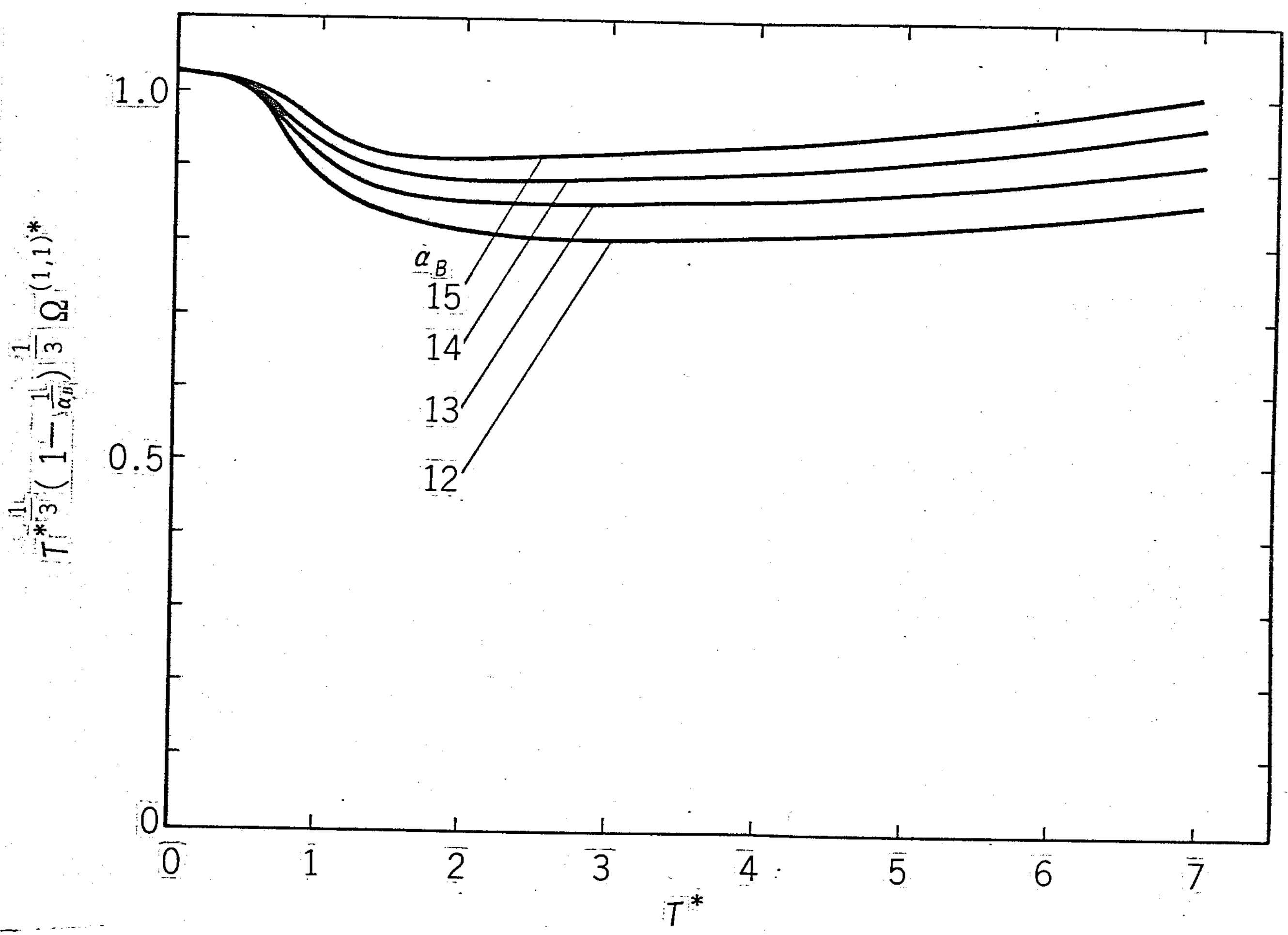

FIG.5 RELATION BETWEEN COLLISION INTEGRAL AND REDUCED TEMPERATURE, WHERE α_B DENOTES A POTENTIAL PARAMETER ASSOCIATED WITH THE MODIFIED BUCKINGHAM POTENTIAL

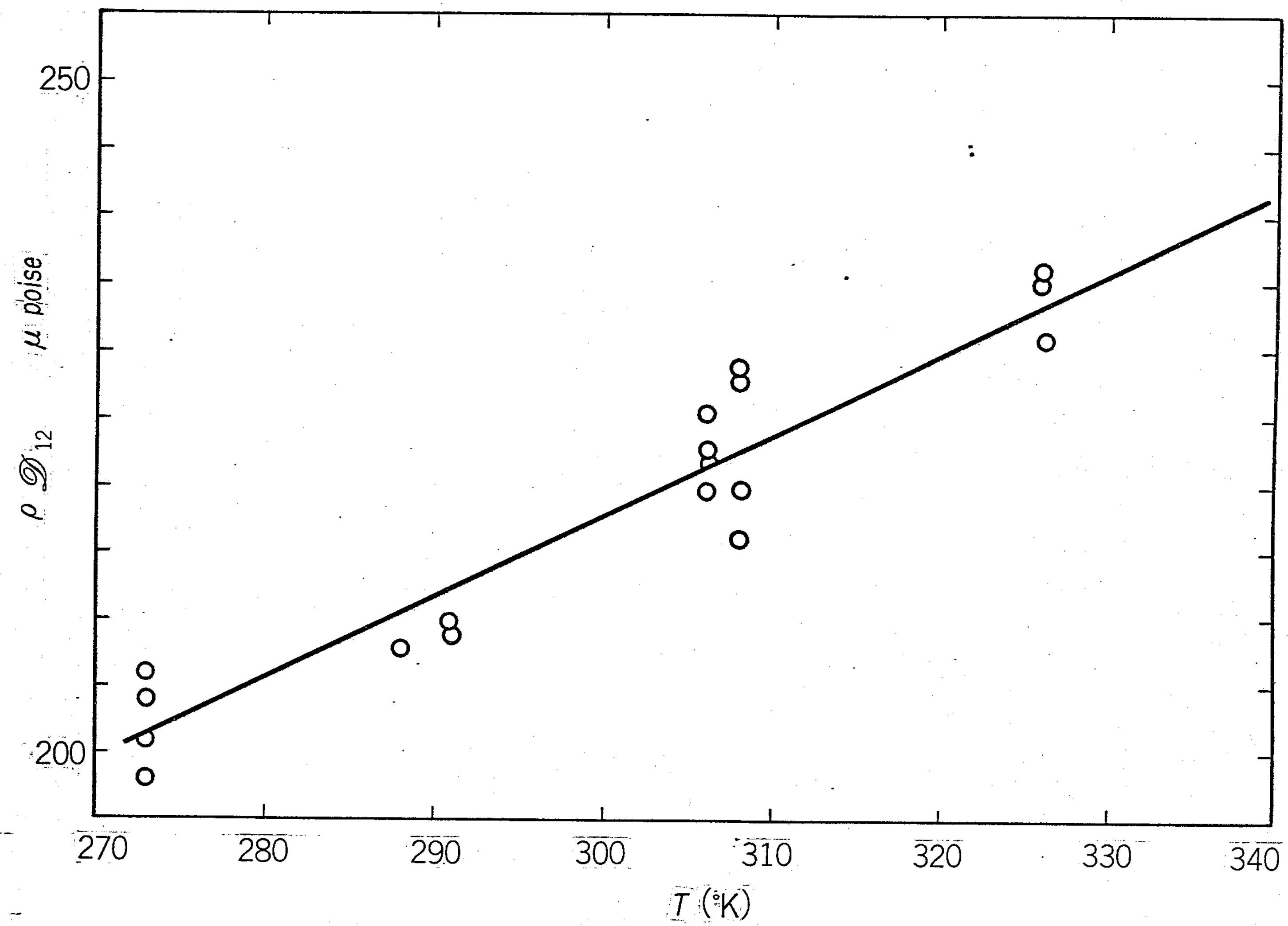

FIG.6 EXPERIMENTAL DATA OF MUTUAL DIFFUSION COEFFICIENT OF $^{235}UF_6$ $^{238}UF_6$, AFTER BROWN AND MURPHY(23)

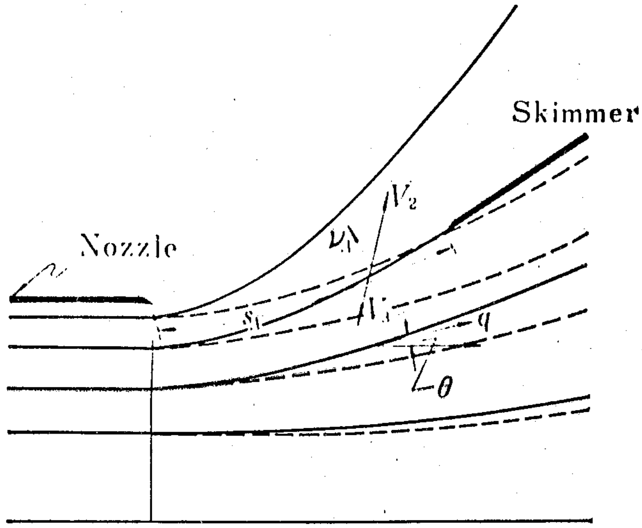

FIG.7 .. SCHEMATIC DRAWING OF SUPERSONIC JET

—— GAS MIXTURE

----- ARGON ISOTOPE GAS MIXTURE

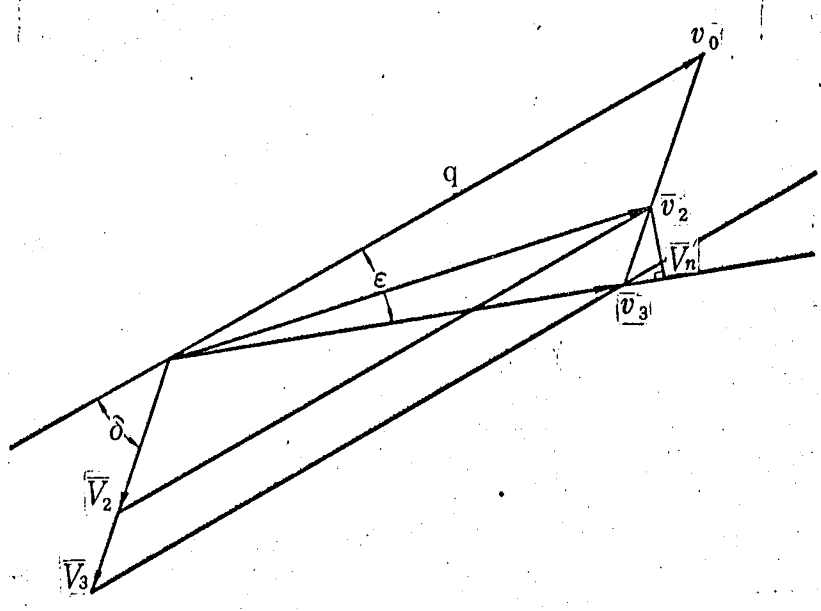

FIG.8 GEOMETRICAL REPRESENTATION OF DIFFUSION VELOCITY AND MASS AVERAGE VELOCITY

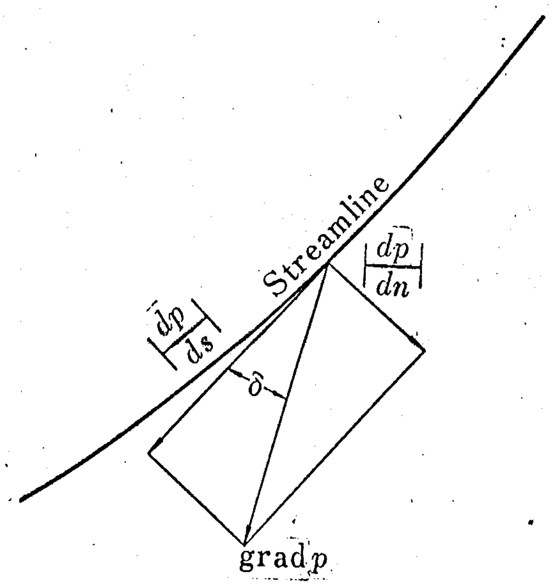

FIG.9 SYSTEM OF REFERENCE FOR PRESSURE GRADIENT

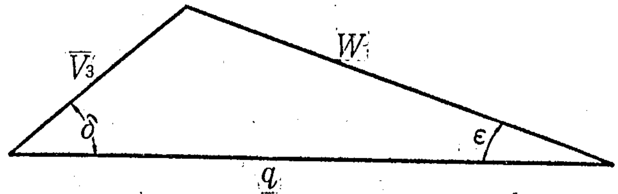

FIG.10 SYSTEM OF REFERENCE FOR δ AND ε

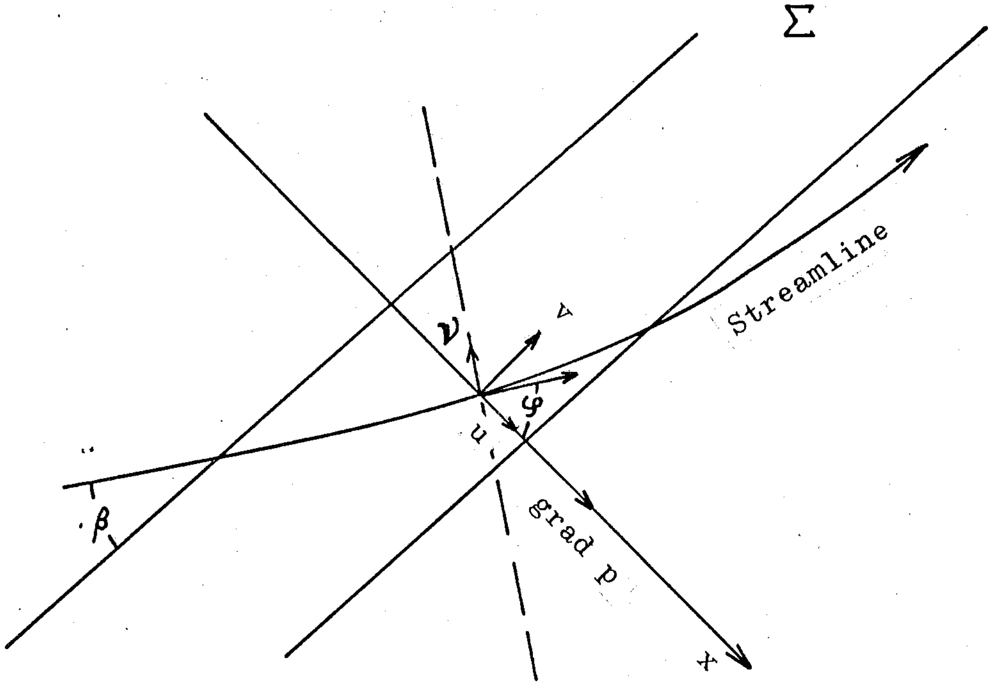

FIG.11 COORDINATES FOR OBLIQUE SHOCK WAVE

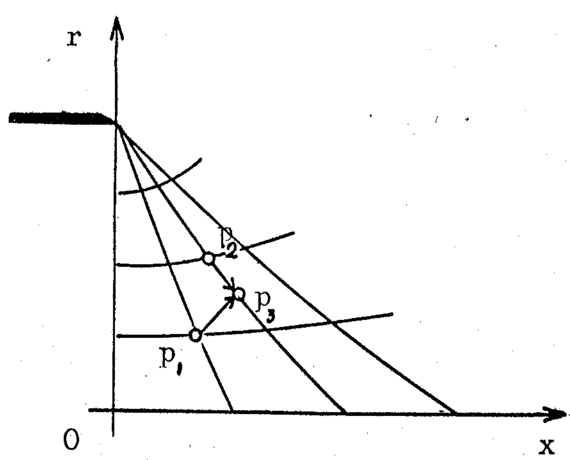

FIG.12 COMPUTATION OF UNKNOWN POINT 3 FROM TWO KNOWN POINTS 1,2

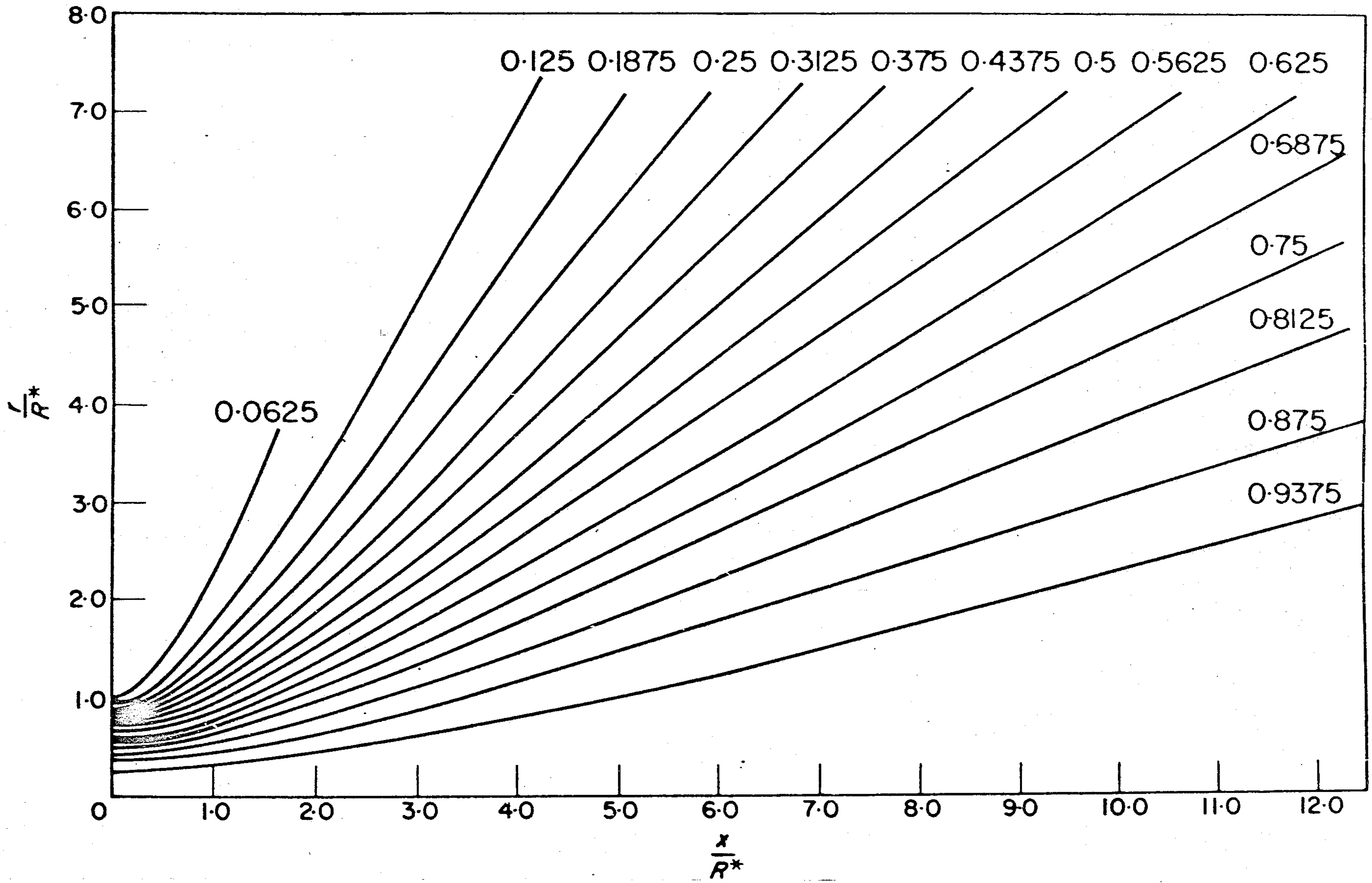

FIG.13 STREAMLINES OF AN AXISYMMETRIC FLOW OF A FREELY EXPANDING GAS
$\gamma = 1.4$

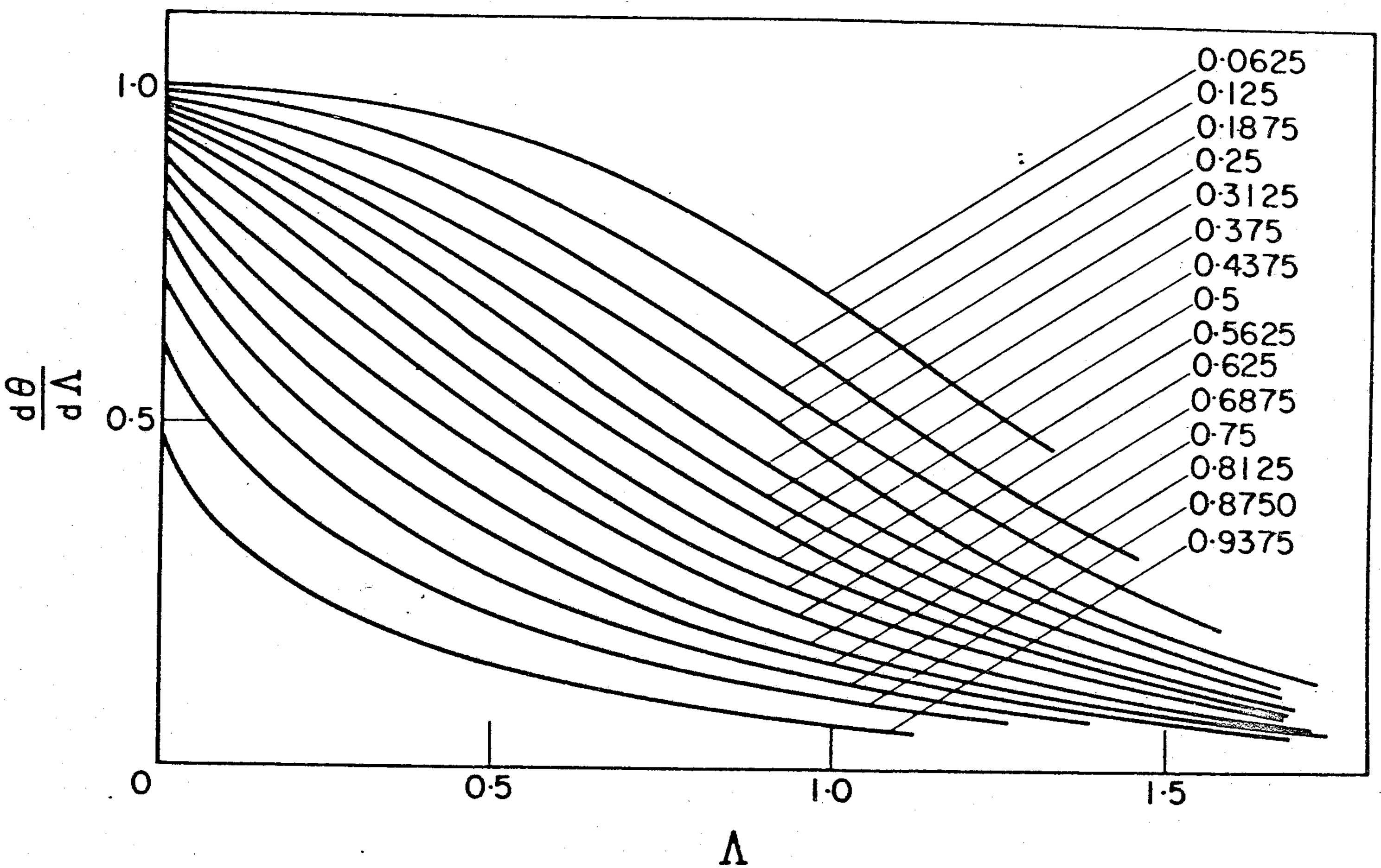

FIG.14 Dθ/DΛ vs. Λ FOR VARIOUS VALUES OF CUT, $\gamma = 1.4$

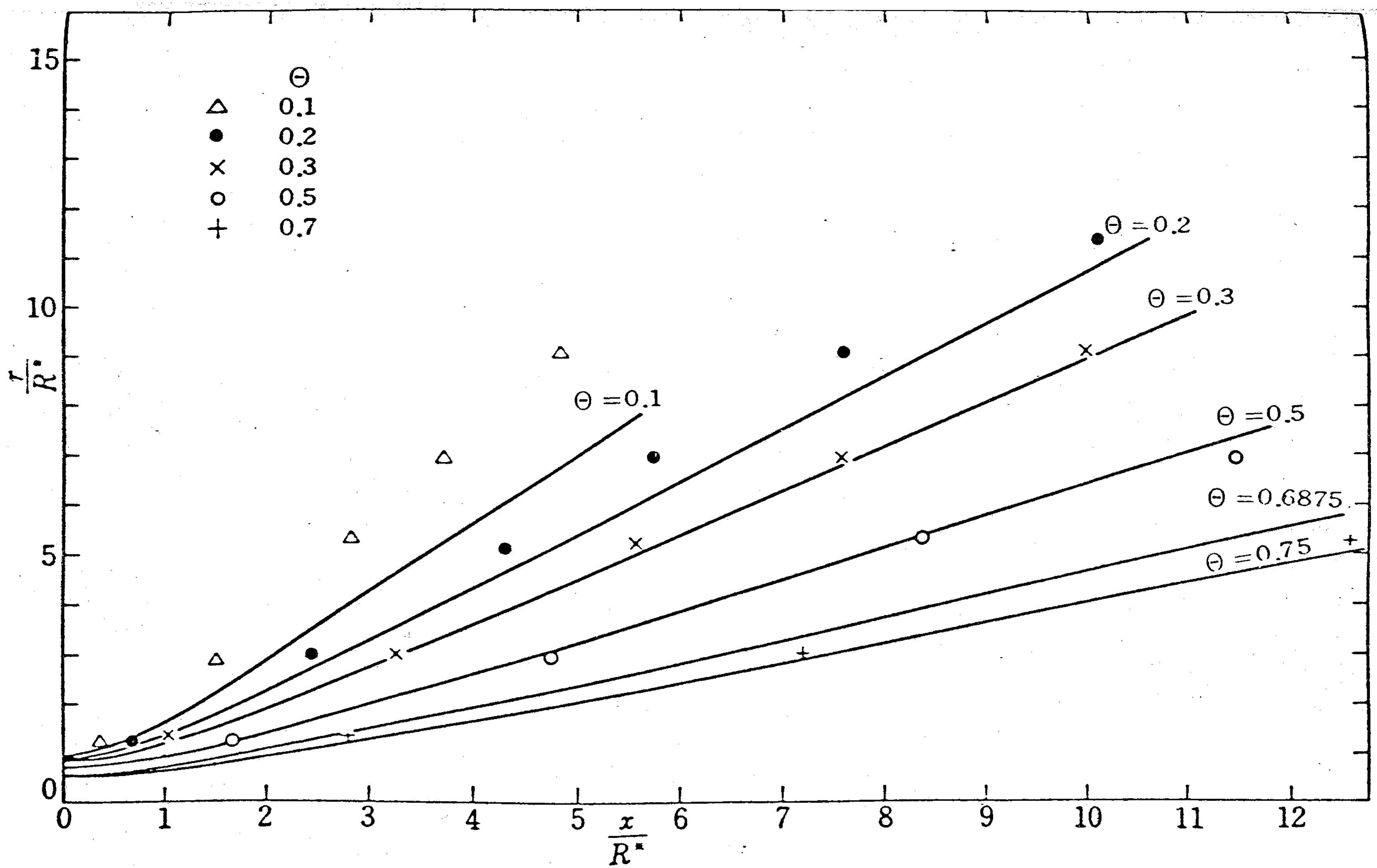

FIG.15 CALCULATED AND EXPERIMENTAL RESULTS ON STREAMLINES CUT AS A PARAMETER, PURE ARGON

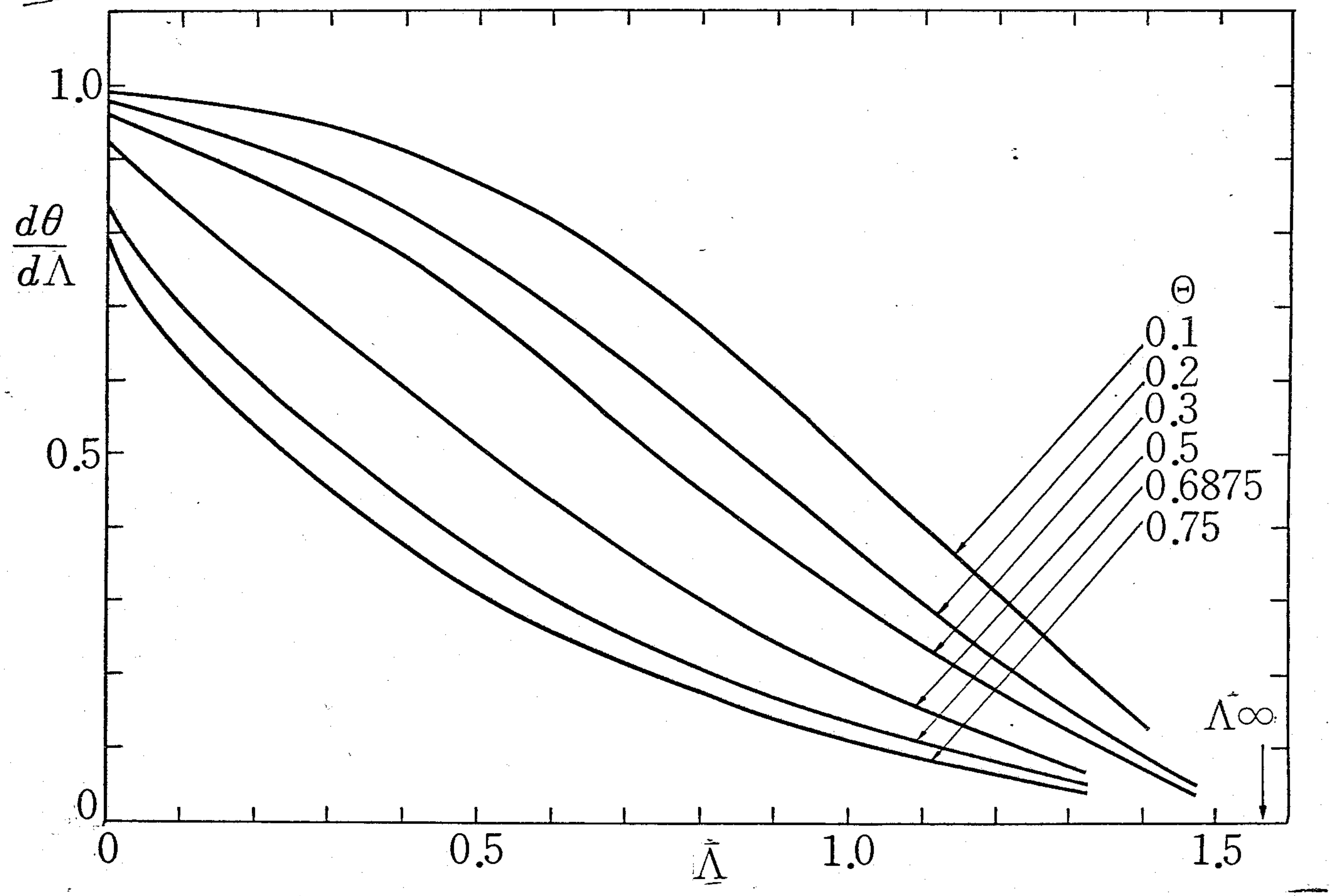

FIG.16 CURVES RELATING $D\theta/D\Lambda$ TO Λ FOR VARIOUS VALUES OF THE CUT (γ = 1.66667)

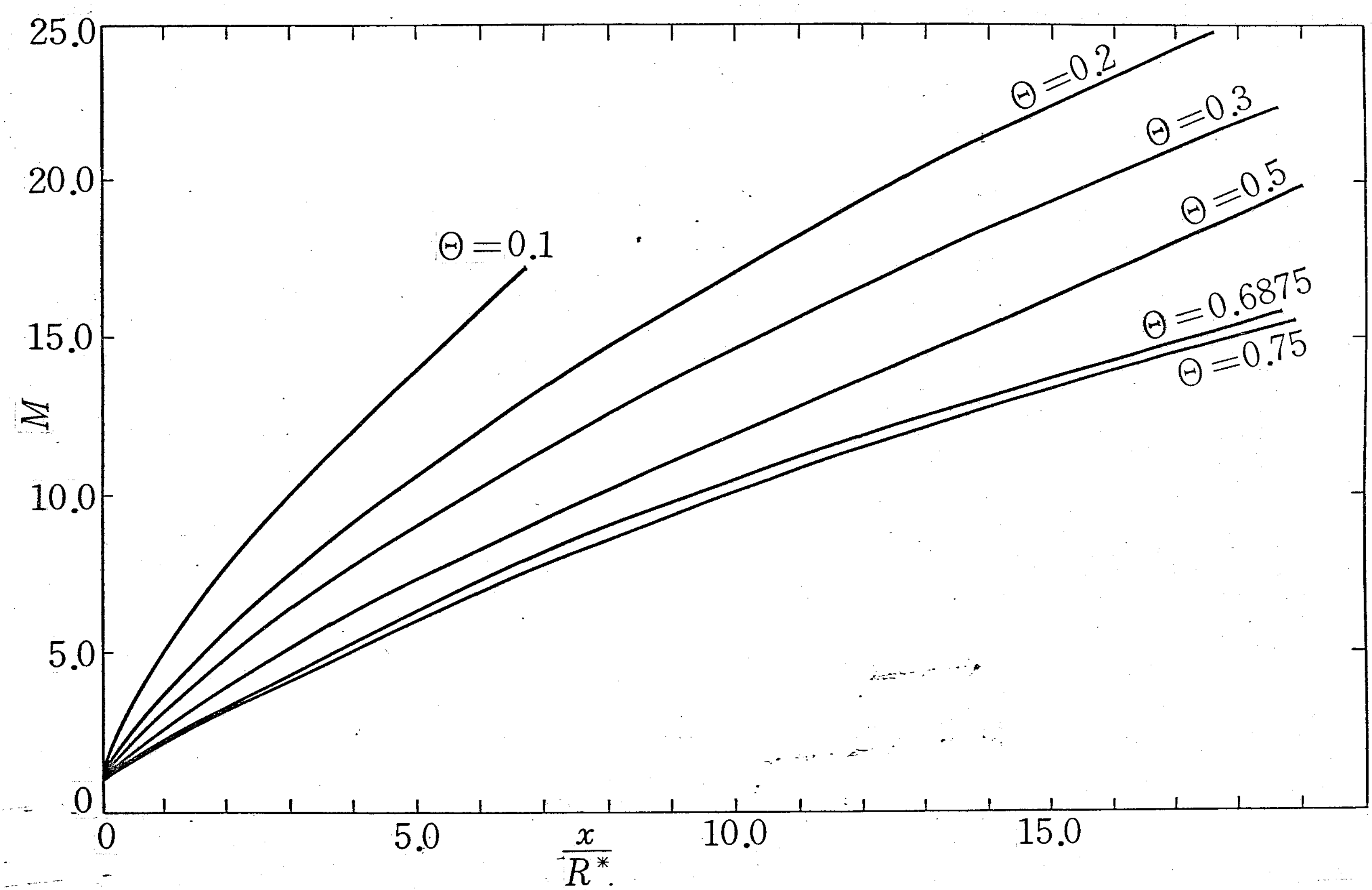

FIG.17 MACH NUMBER DISTRIBUTION IN A FREE JET, PLOTTED WITH THE CUT AS PARAMETER (γ = 1.66667)

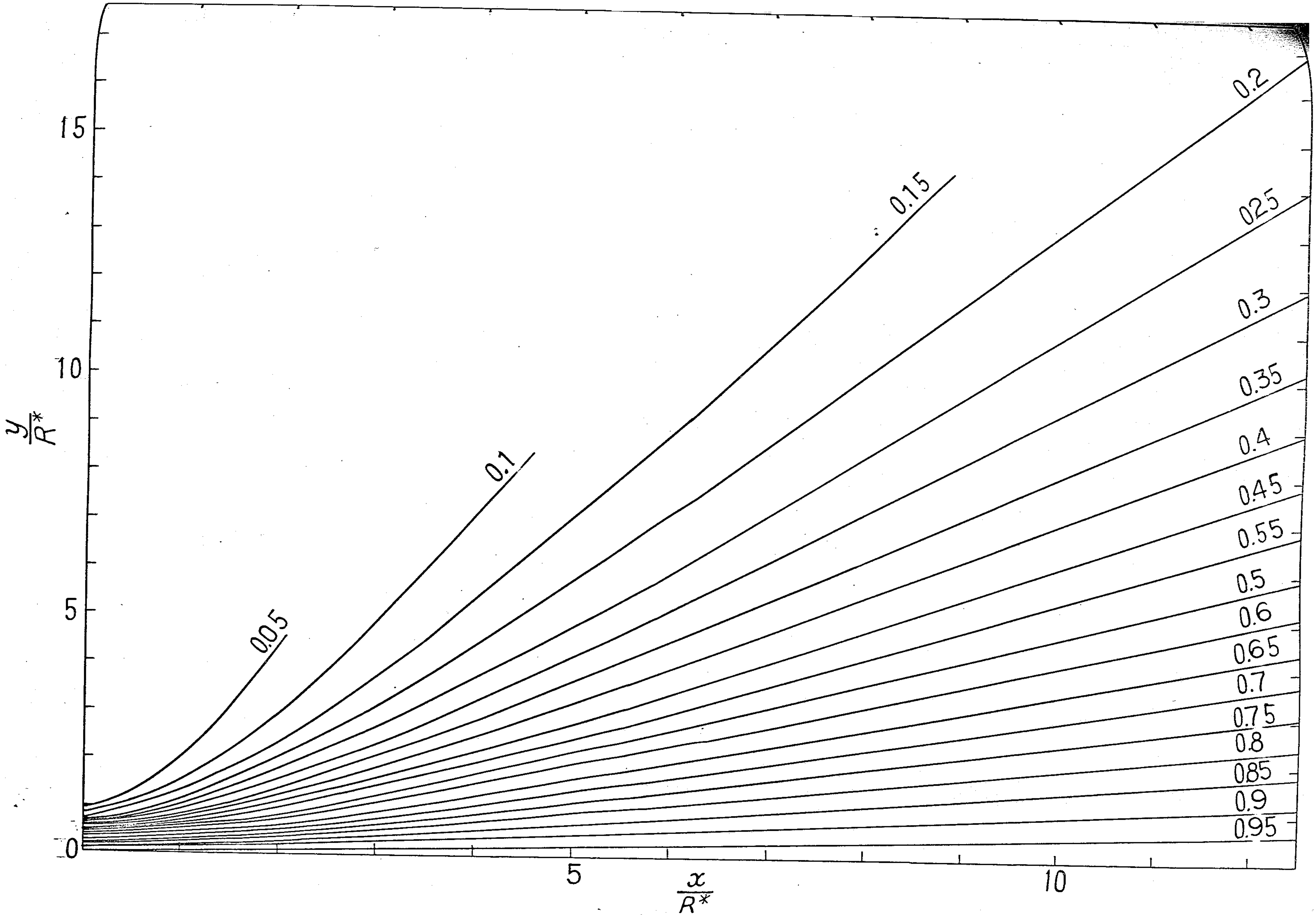

FIG.18 STREAMLINES OF TWO-DIMENSIONAL SUPERSONIC JET INTO VACUUM (γ = 1.4)

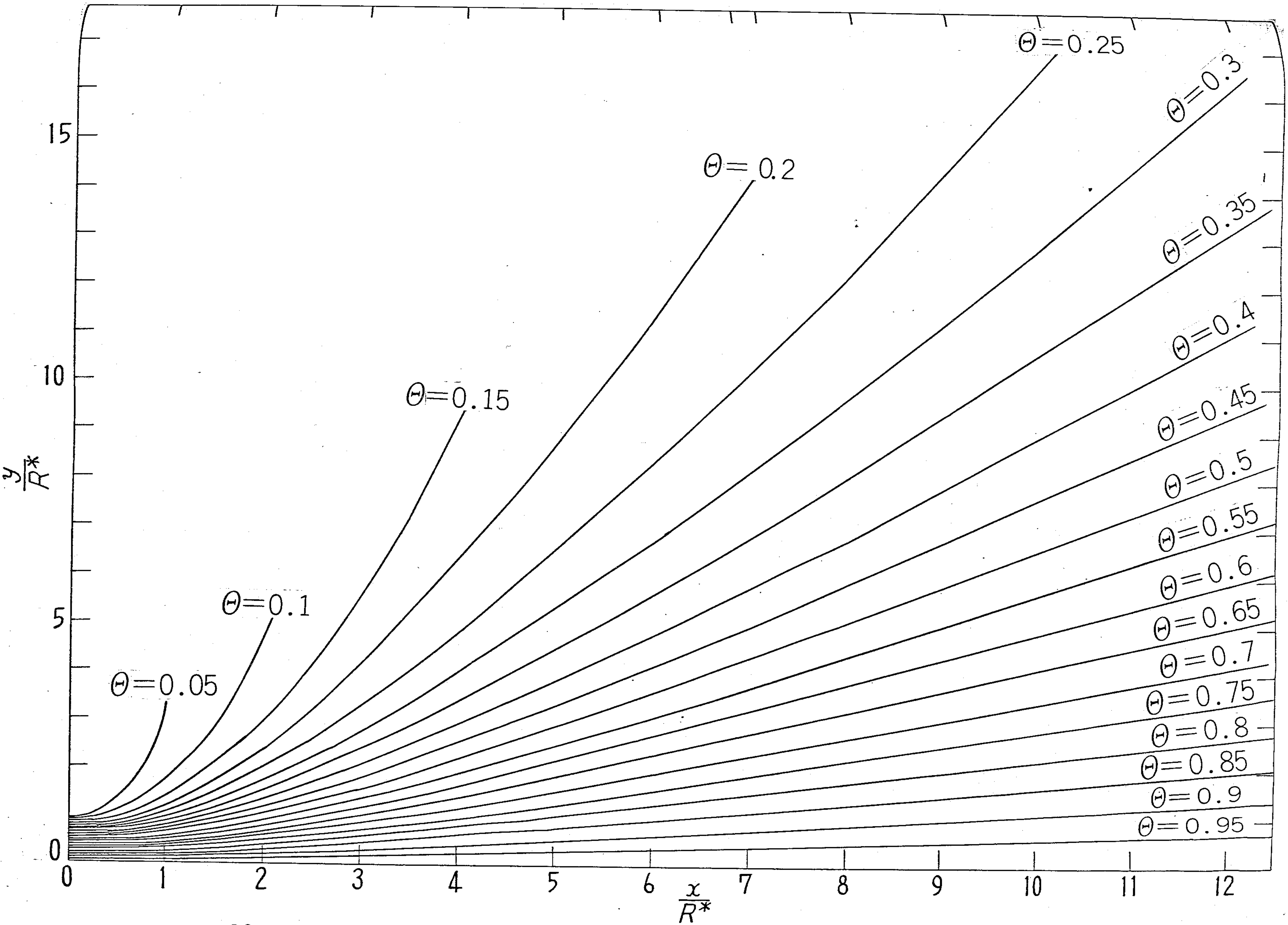

FIG.19 STREAMLINES OF TWO-DIMENSIONAL SUPERSONIC JET INTO VACUUM (γ = 1.067)

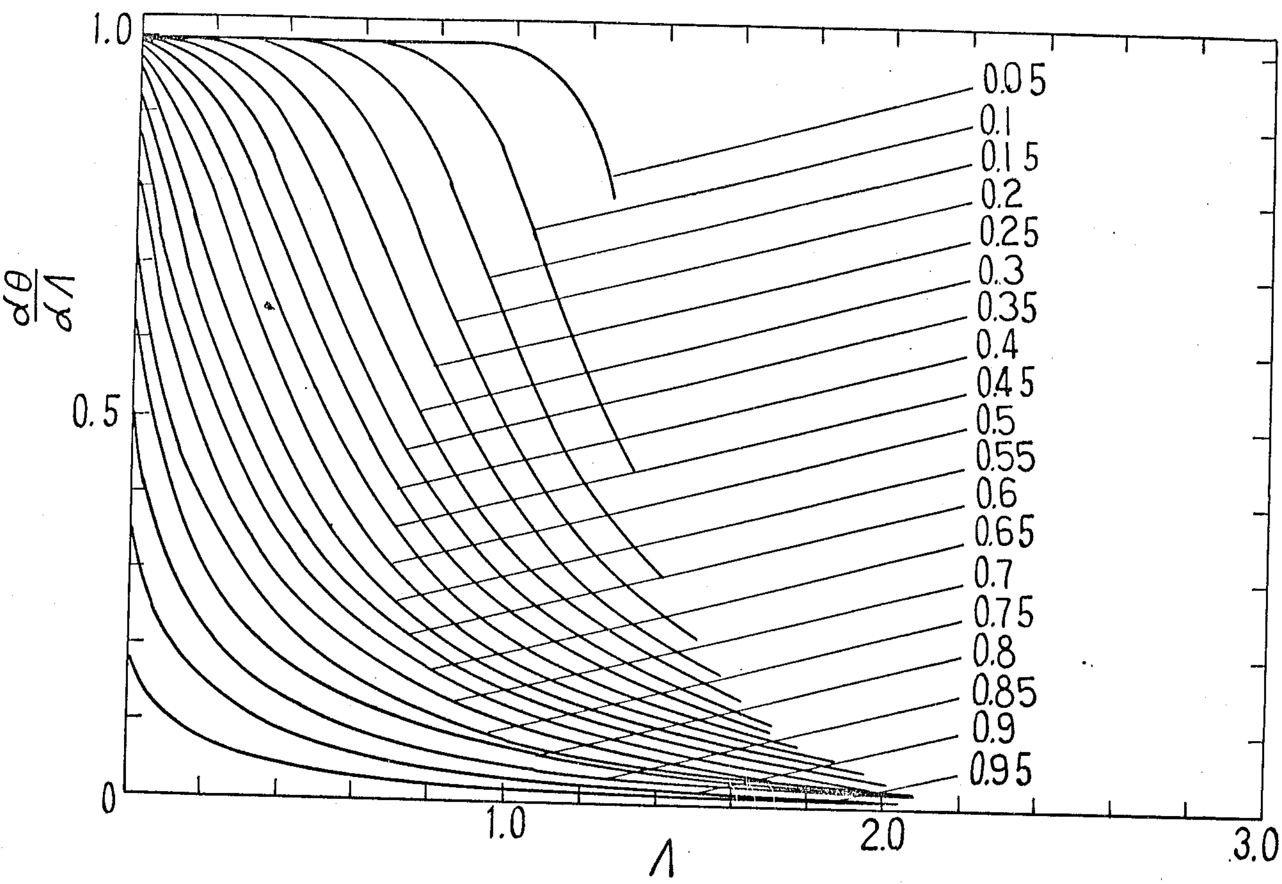

FIG.20 $D\theta/D\Lambda$ vs. Λ FOR VARIOUS VALUES OF THE CUT ($\gamma = 1.4$)

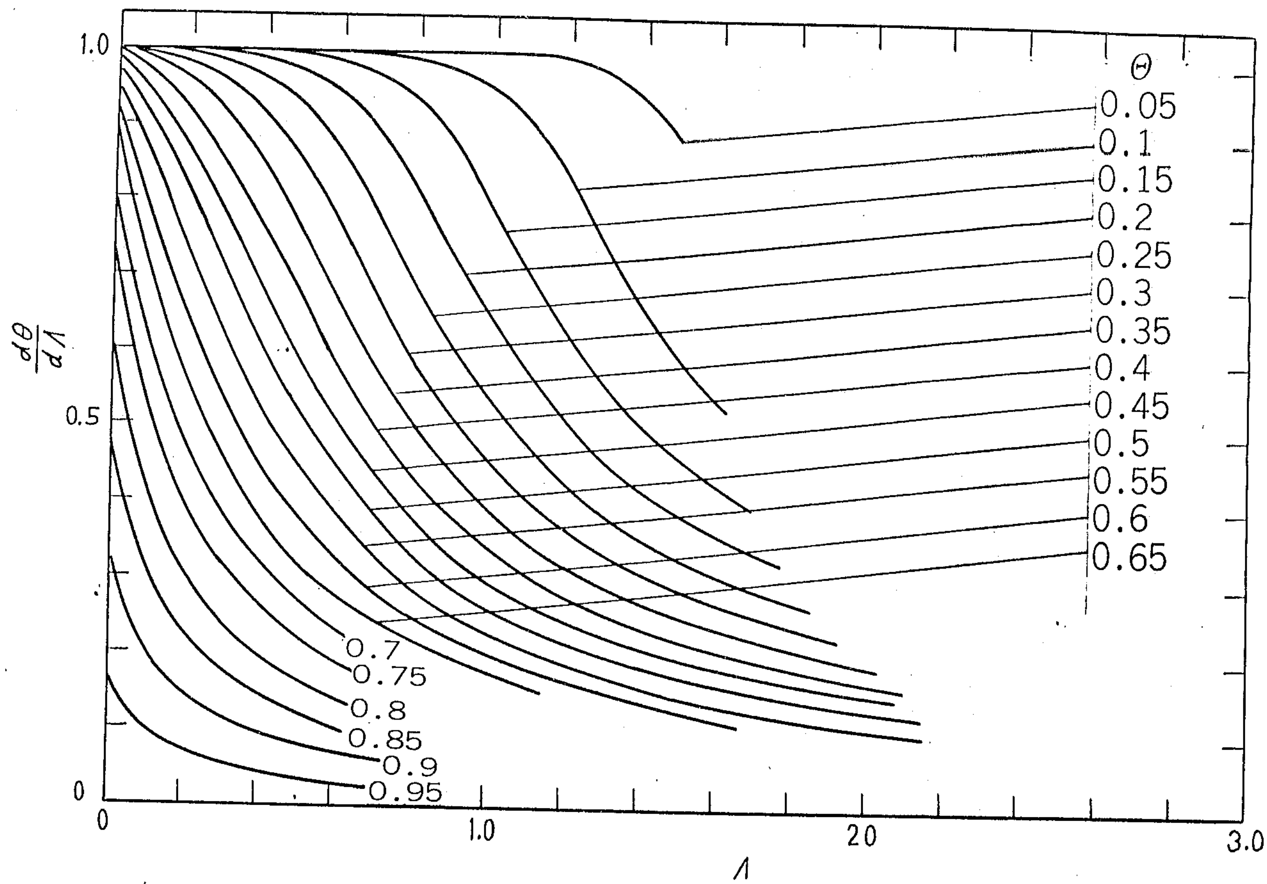

FIG.21 Dθ/DΛ vs. Λ FOR VARIOUS VALUES OF THE CUT
γ = 1.067

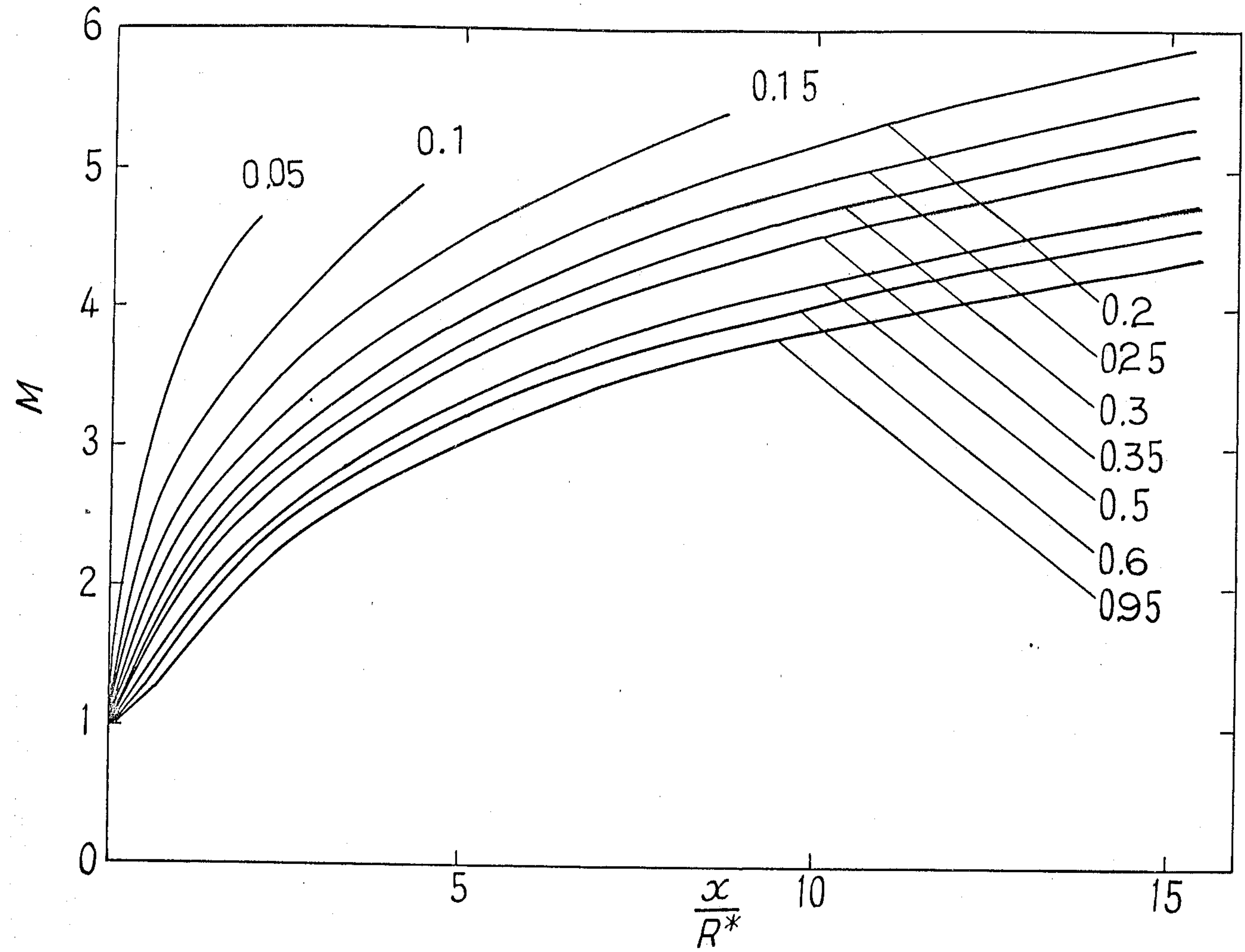

FIG.22 MACH NUMBER DISTRIBUTION IN A FREE JET, PLOTTED WITH THE CUT AS A PARAMETER ($\gamma = 1.4$)

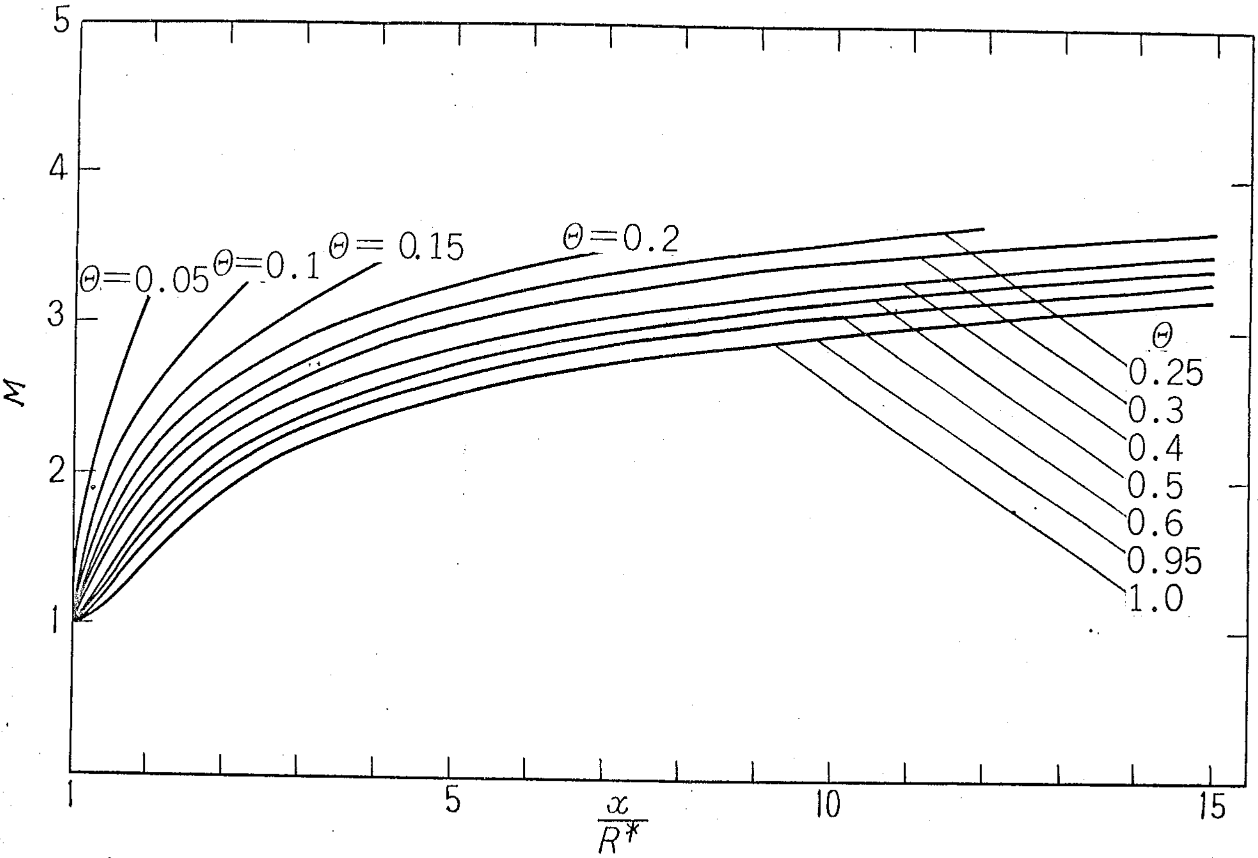

FIG.23 MACH NUMBER DISTRIBUTION IN A FREE JET, PLOTTED WITH CUT, Θ AS PARAMETER (γ = 1.067)

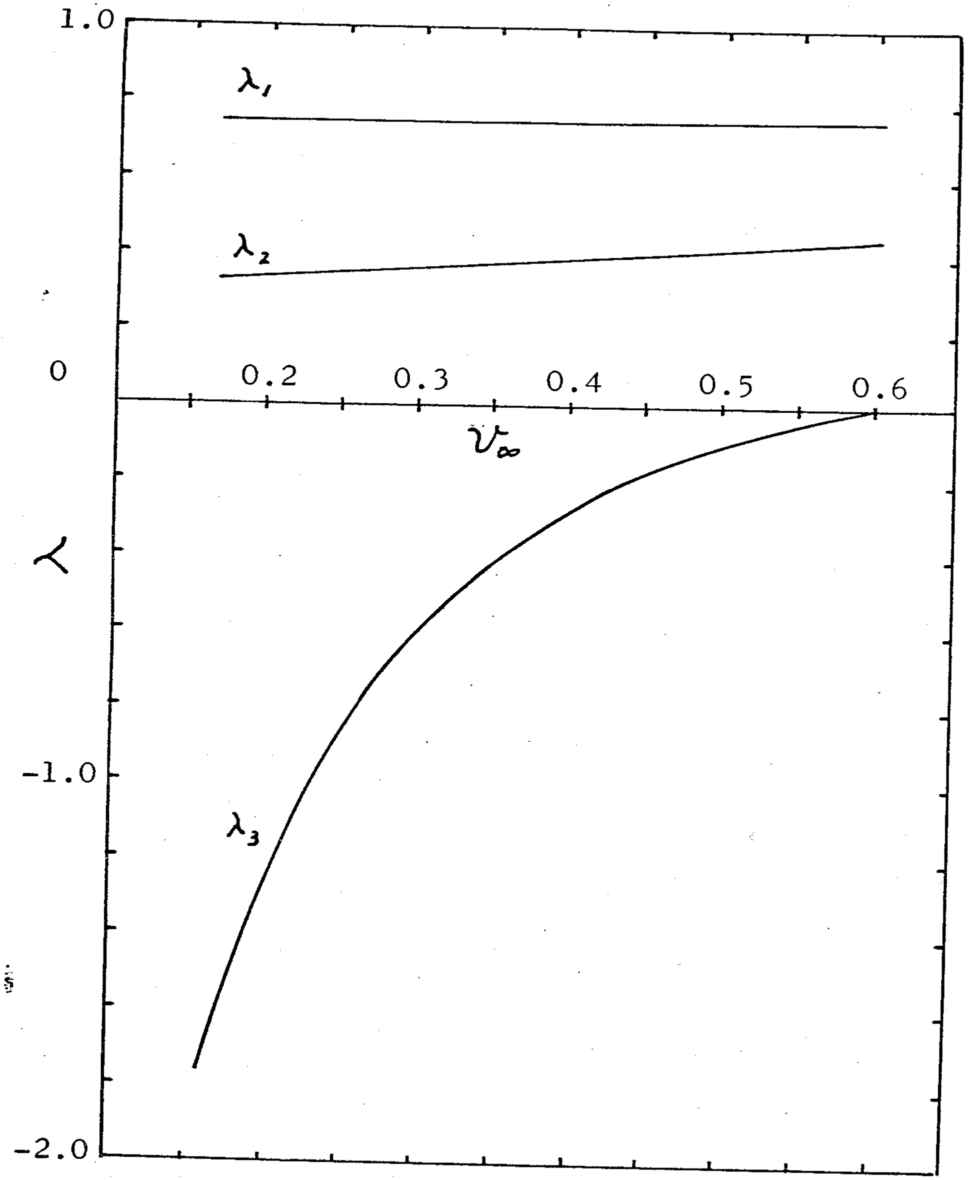

FIG.24 ROOTS OF EQUATION (3.29)
50% H_2-50% N_2 MIXTURE

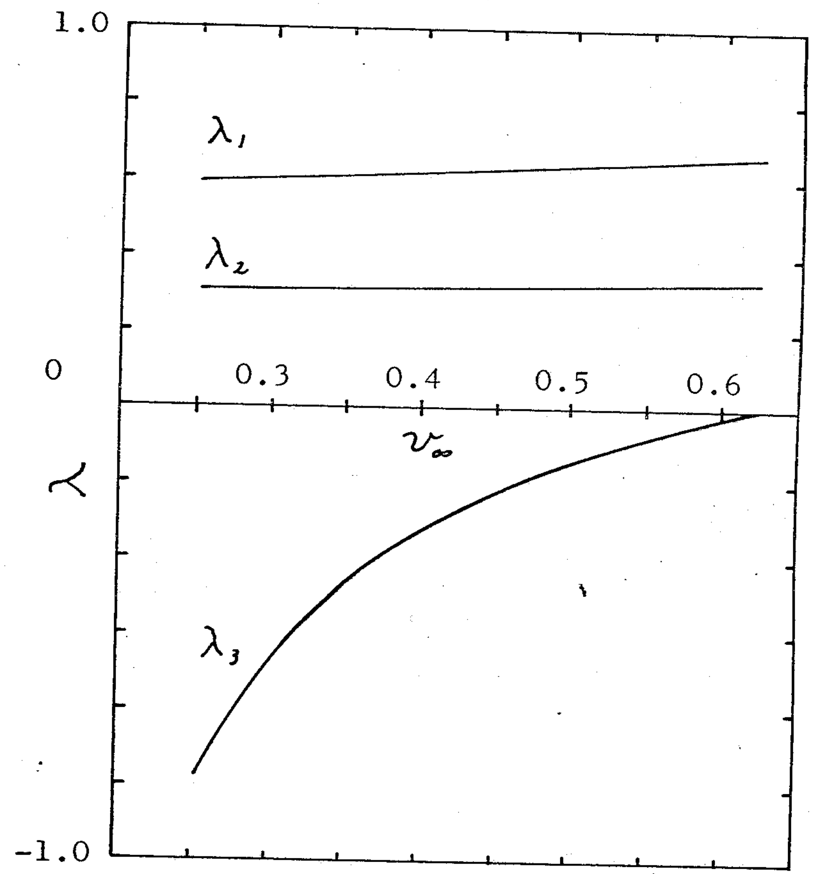

FIG.25 ROOTS OF EQUATION (3.29)
50% He-50% Ar MIXTURE

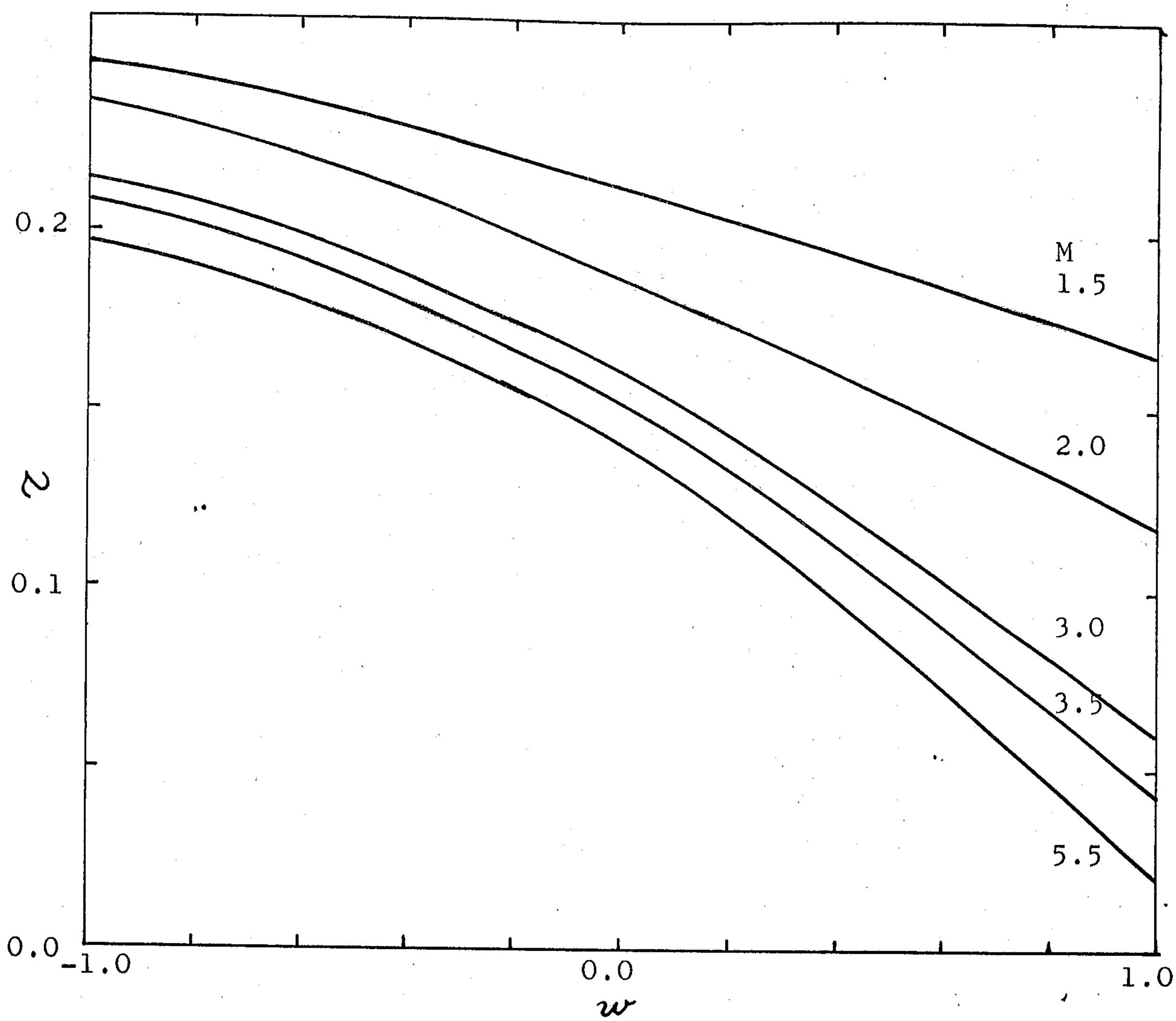

FIG.26 τ vs. W , WHERE $W = \frac{1}{\gamma} \frac{\gamma M_1^2 + 1}{M_1^2 - 1} ((\gamma+1) V - \gamma)$
50% H_2-50% N_2 GAS MIXTURE

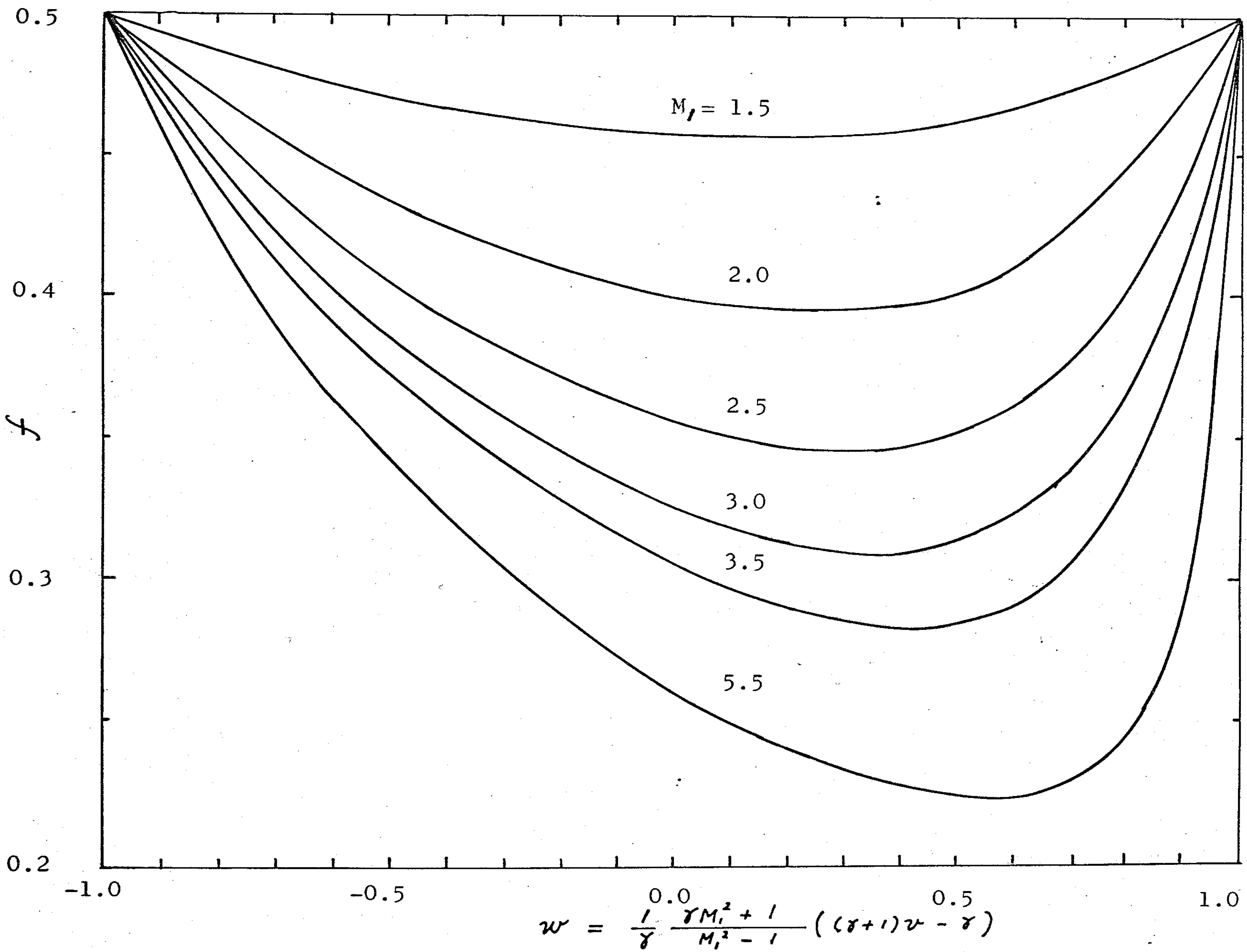

FIG.27 CONCENTRATION PROFILE IN NORMAL SHOCK WAVE (50 % H_2-50 % N_2)

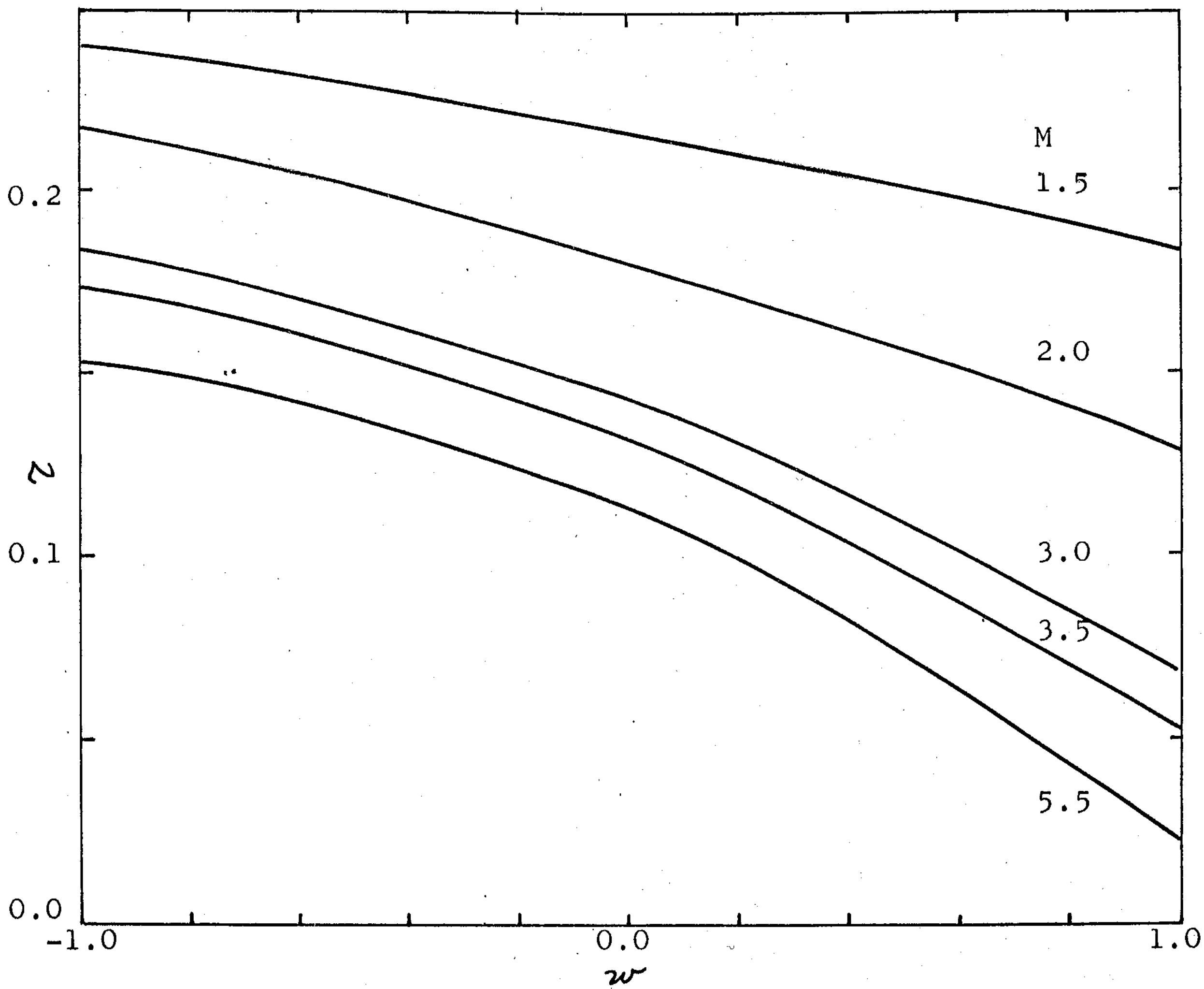

FIG.28 τ vs. W , WHERE $W = \frac{1}{\gamma} \frac{\gamma M_1^2 + 1}{M_1^2 - 1}((\gamma+1)V - \gamma)$
50 % He-50 % Ar GAS MIXTURE

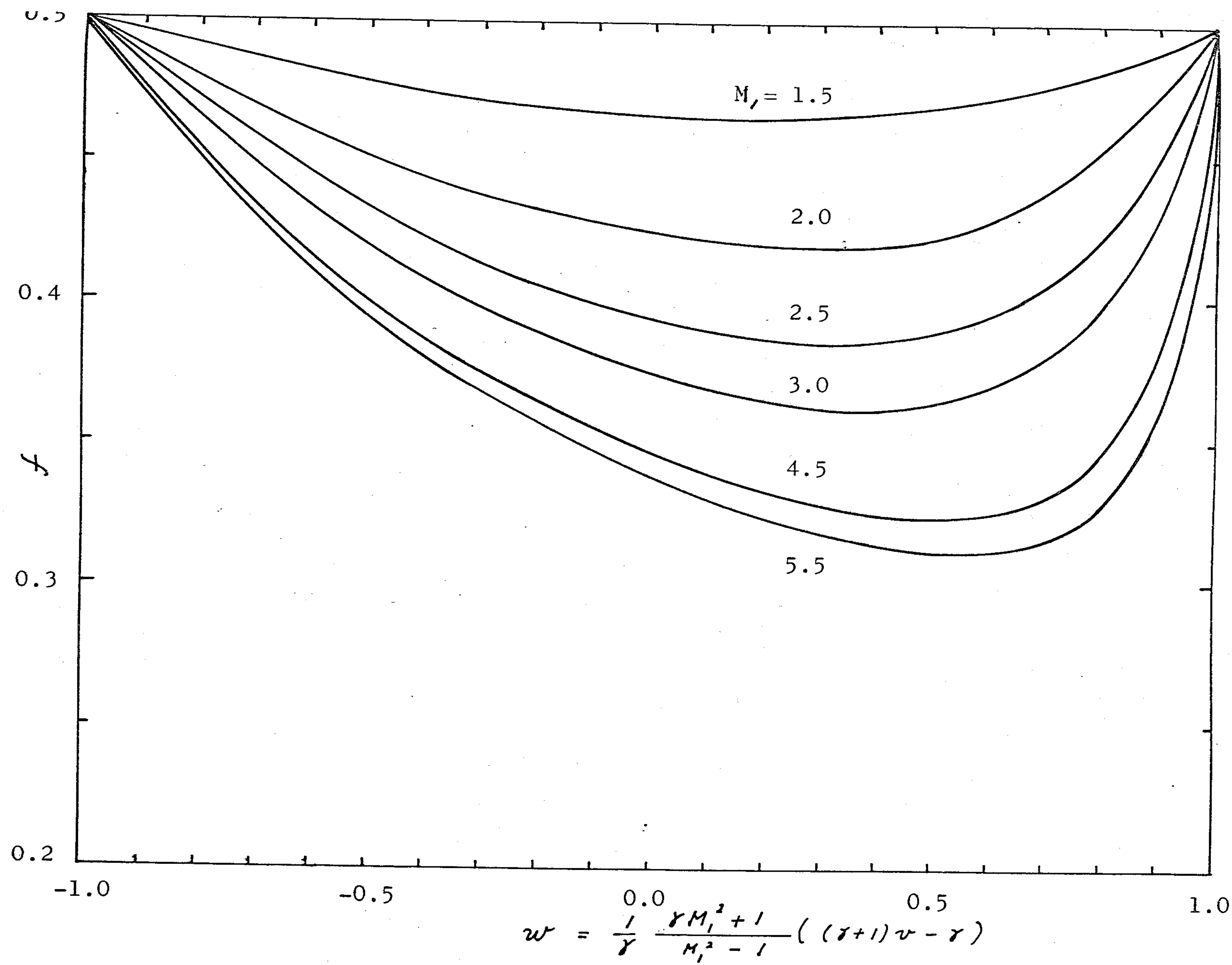

FIG.29 CONCENTRATION PROFILE IN NORMAL SHOCK WAVE (50 % He-50% Ar)

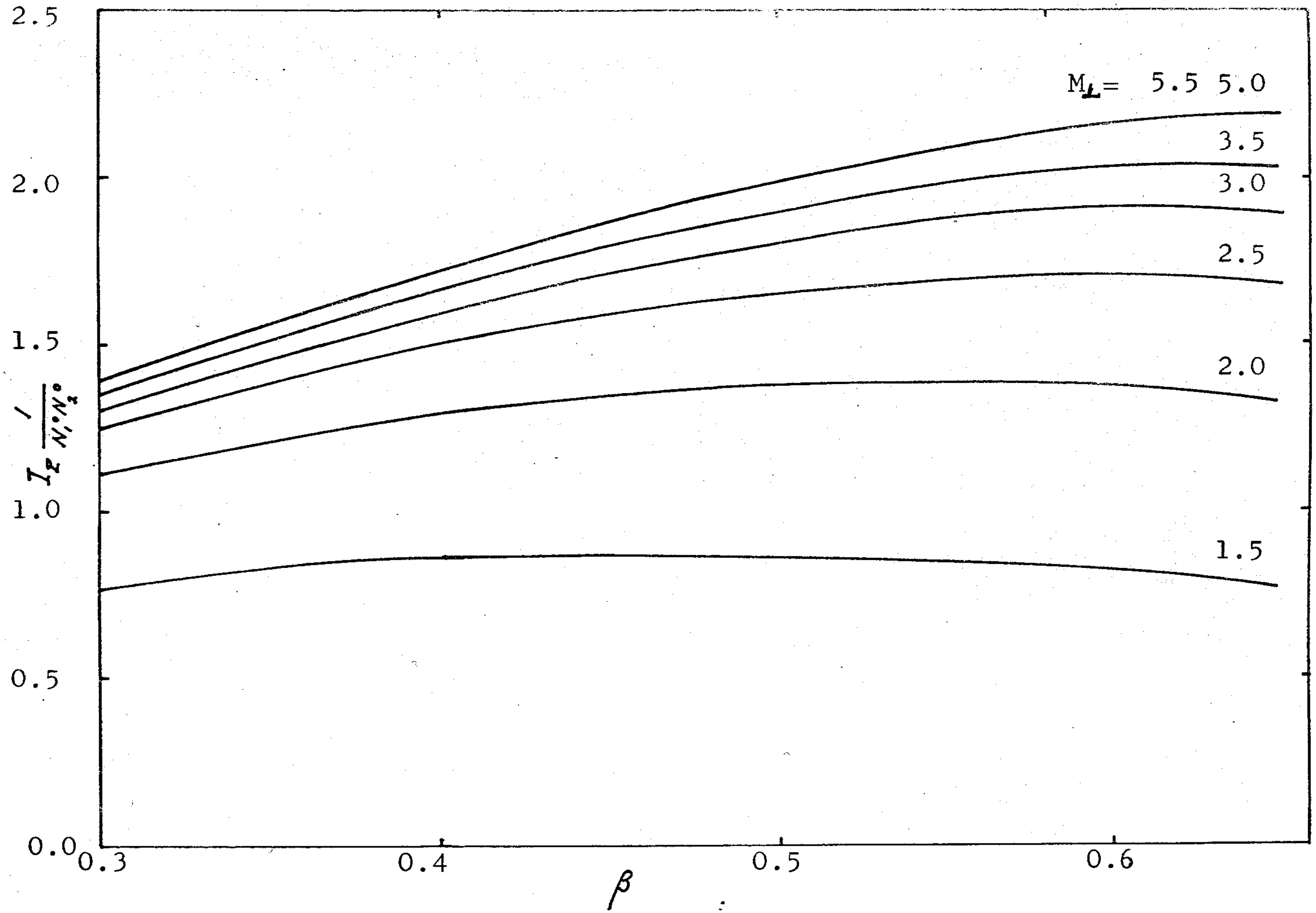

FIG.30 MASS FLUX INTEGRAL IN AN OBLIQUE SHOCK WAVE (50 % H_2-50 % N_2)

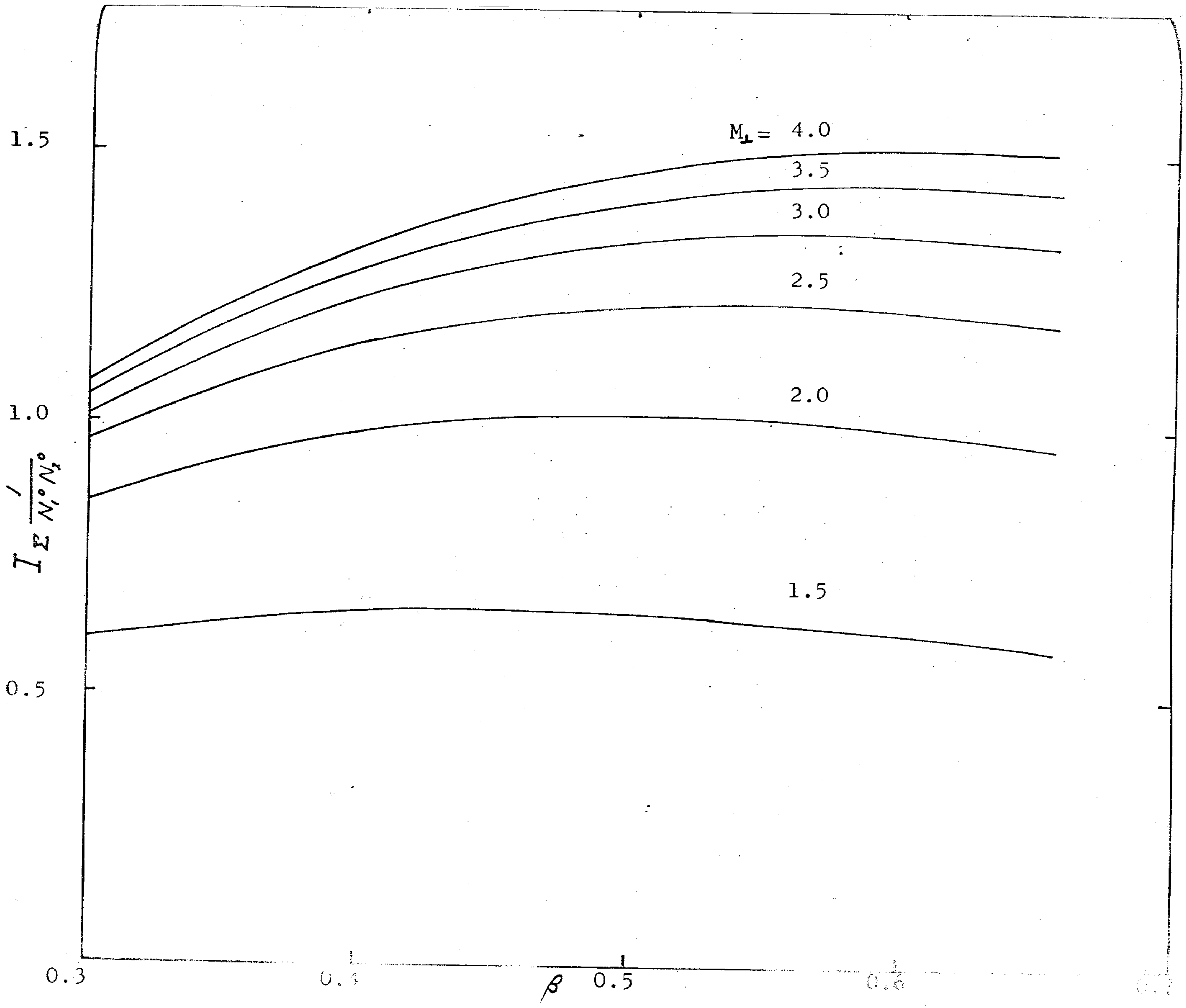

[illegible] IN AN OBLIQUE SHOCK WAVE ([illegible] 50 % Ar)

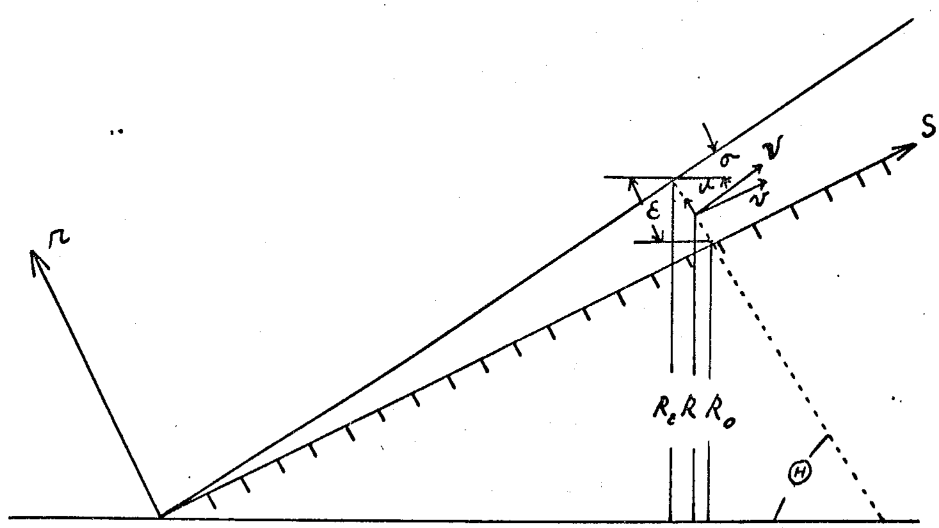

FIG.32 REPRESENTATION OF FLOW WITH ATACHED SHOCK WAVE AND NOTATION USED IN ANALYSIS

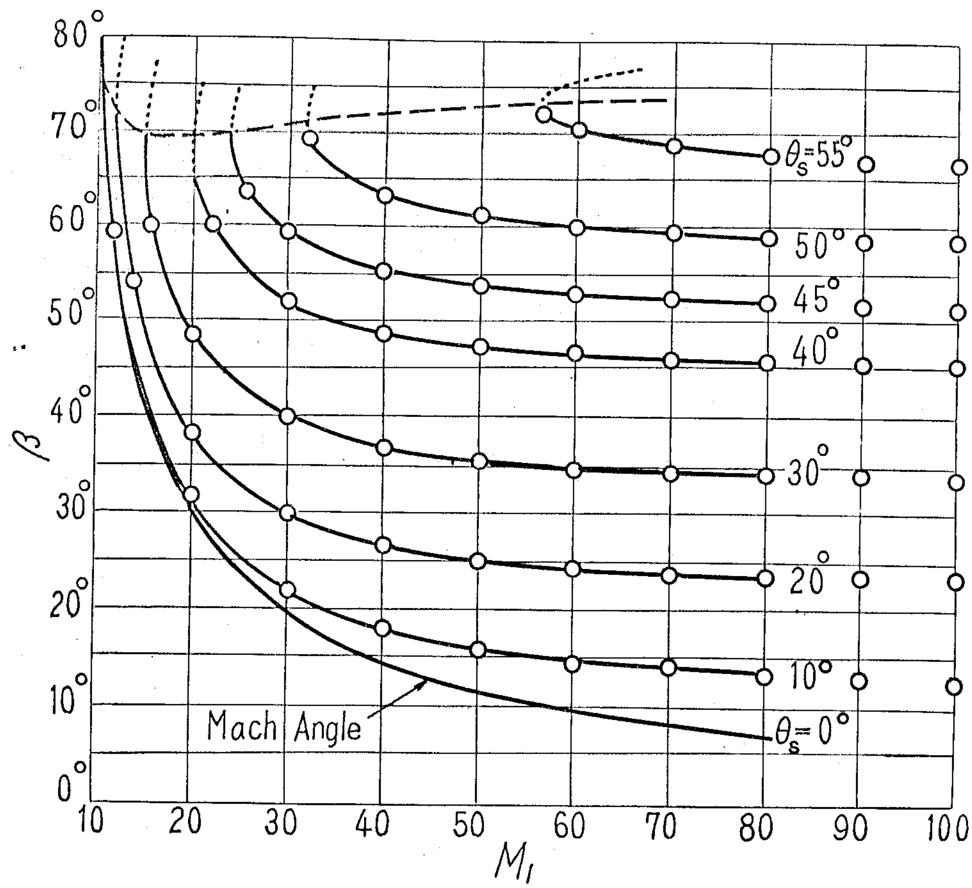

Fig.33 — Variation of shock wave angle with Mach number for different sized cones.

——— TAYLOR MACCOLL

O METHOD OF INTEGRAL RELATION

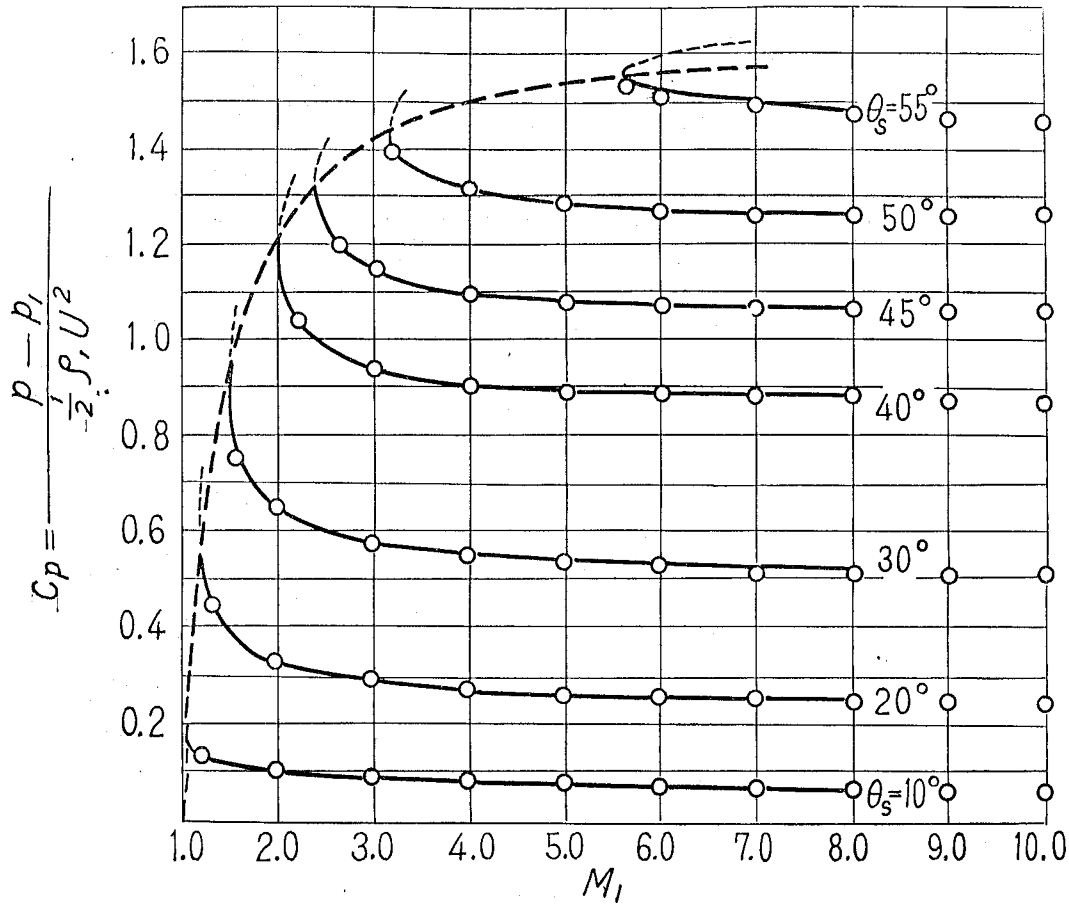

Fig.34—Variation of surface pressure coefficient with Mach number for different sized cones.

——— TAYLOR MACCOLL

O METHOD OF INTEGRAL RELATION

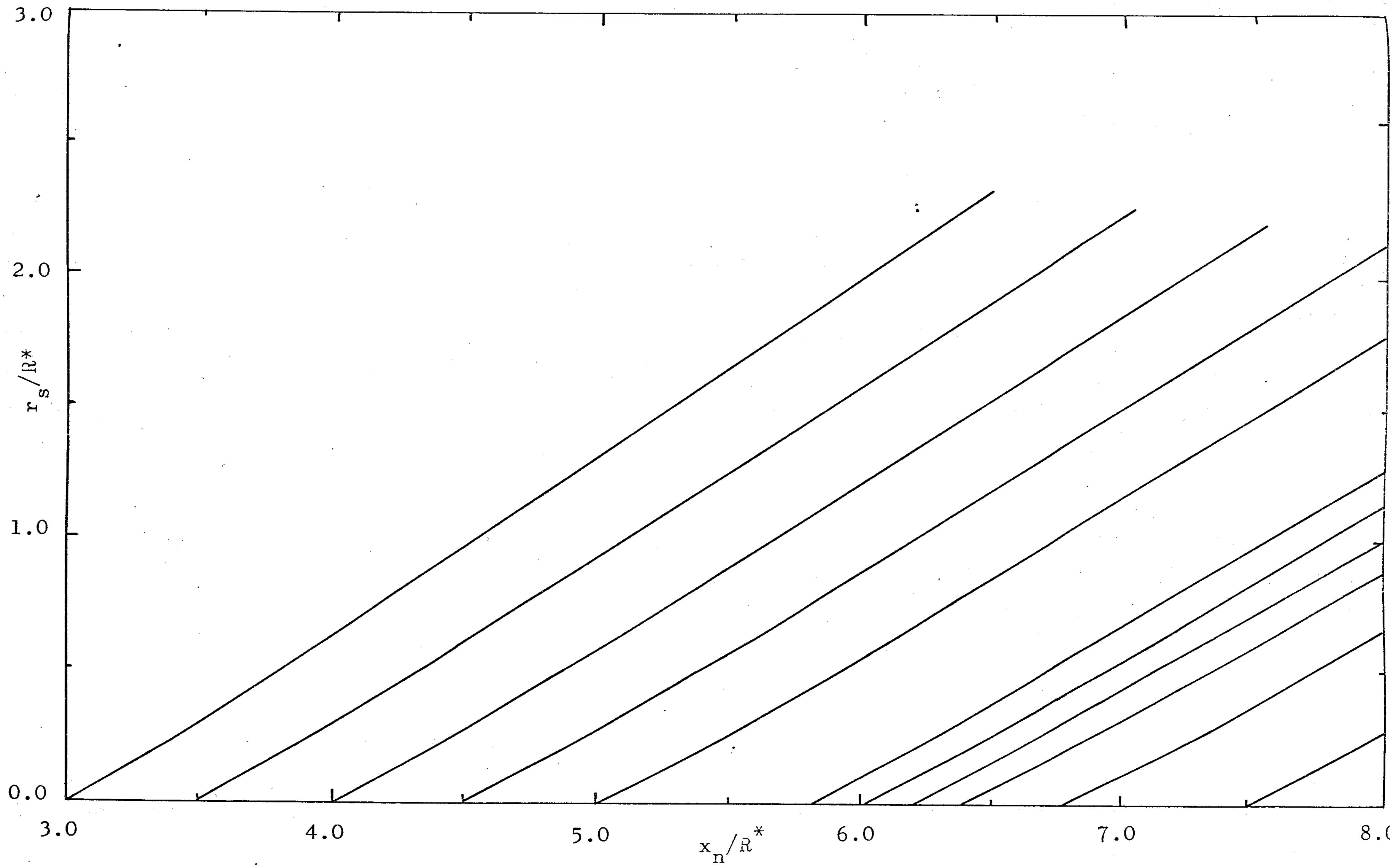

FIG.35 PREDICTED FORM OF ATTACHED SHOCK WAVE AROUND CONE

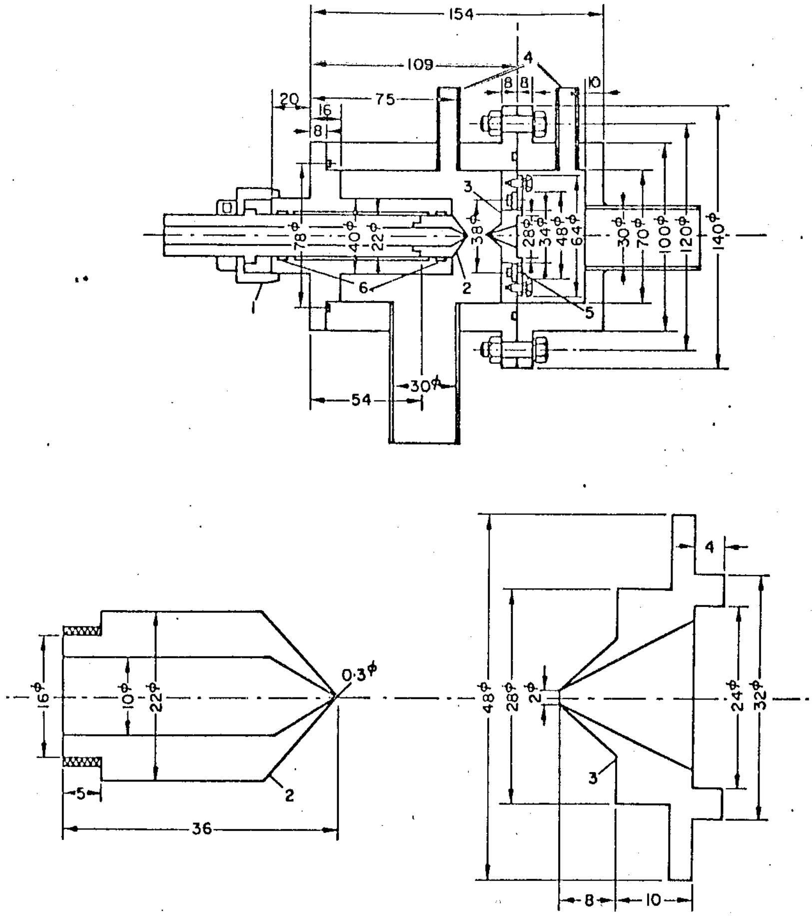

FIG.36 CONSTRUCTIONAL DETAILS OF SUPERSONIC JET APPARATUS.
1. MICROMETER; 2. CONVERGENT NOZZLE; 3. SKIMMER;
4. PRESSURE GAUGE TAP; 5. FLANGE; 6.O-RING

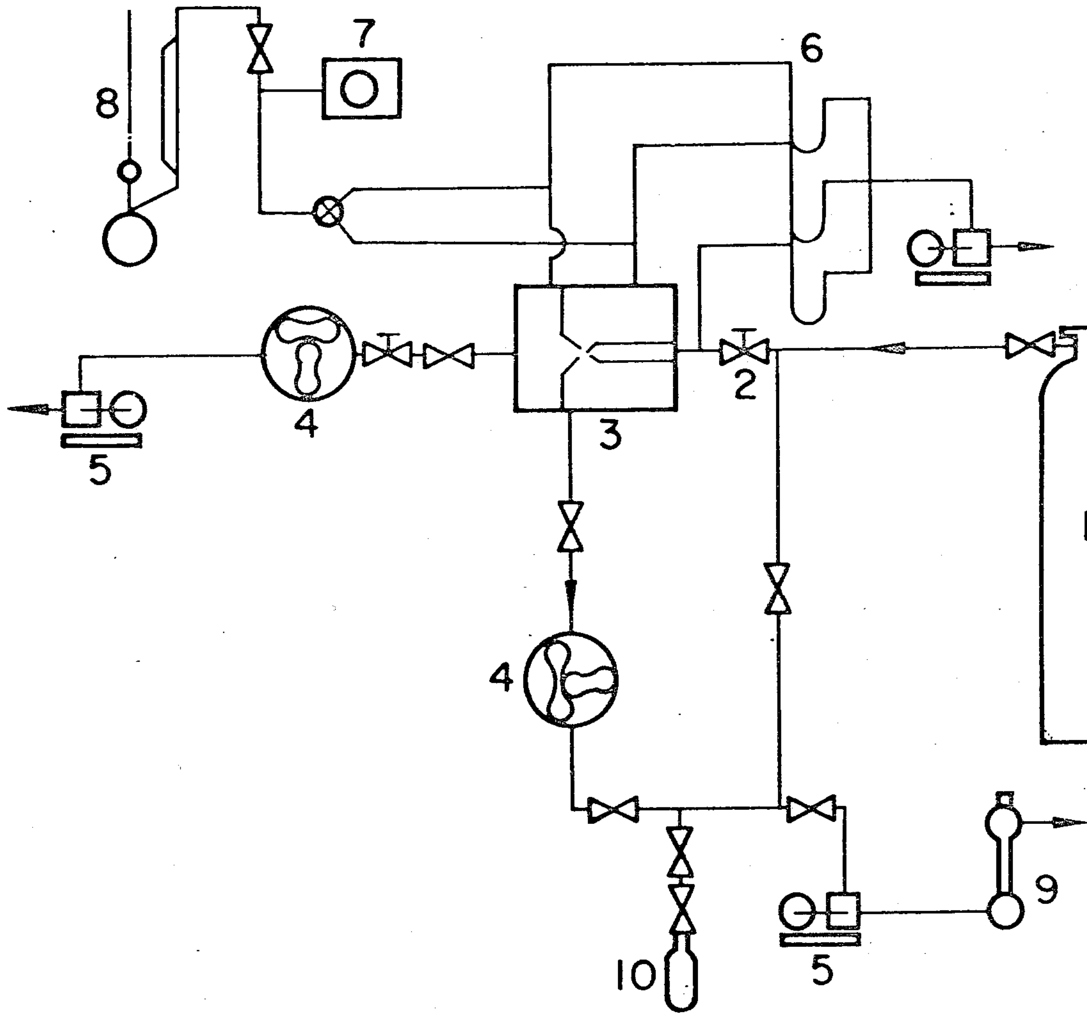

FIG.37 FLOW DIAGRAM OF EXPERIMENTAL EQUIPMENT. 1. GAS MIXTURE CYLINDER; 2. NEEDLE VALVE; 3. SUPERSONIC JET APPARATUS; 4. MECHANICAL BOOSTER; 5. ROTARY VACUUM PUMP; 6. D.O.P. OIL MANOMETER; 7. PIRANI GAUGE; 8. MACLEOD GAUGE; 9. SOAP FILM FLOW METER; 10. SAMPLE BULB.

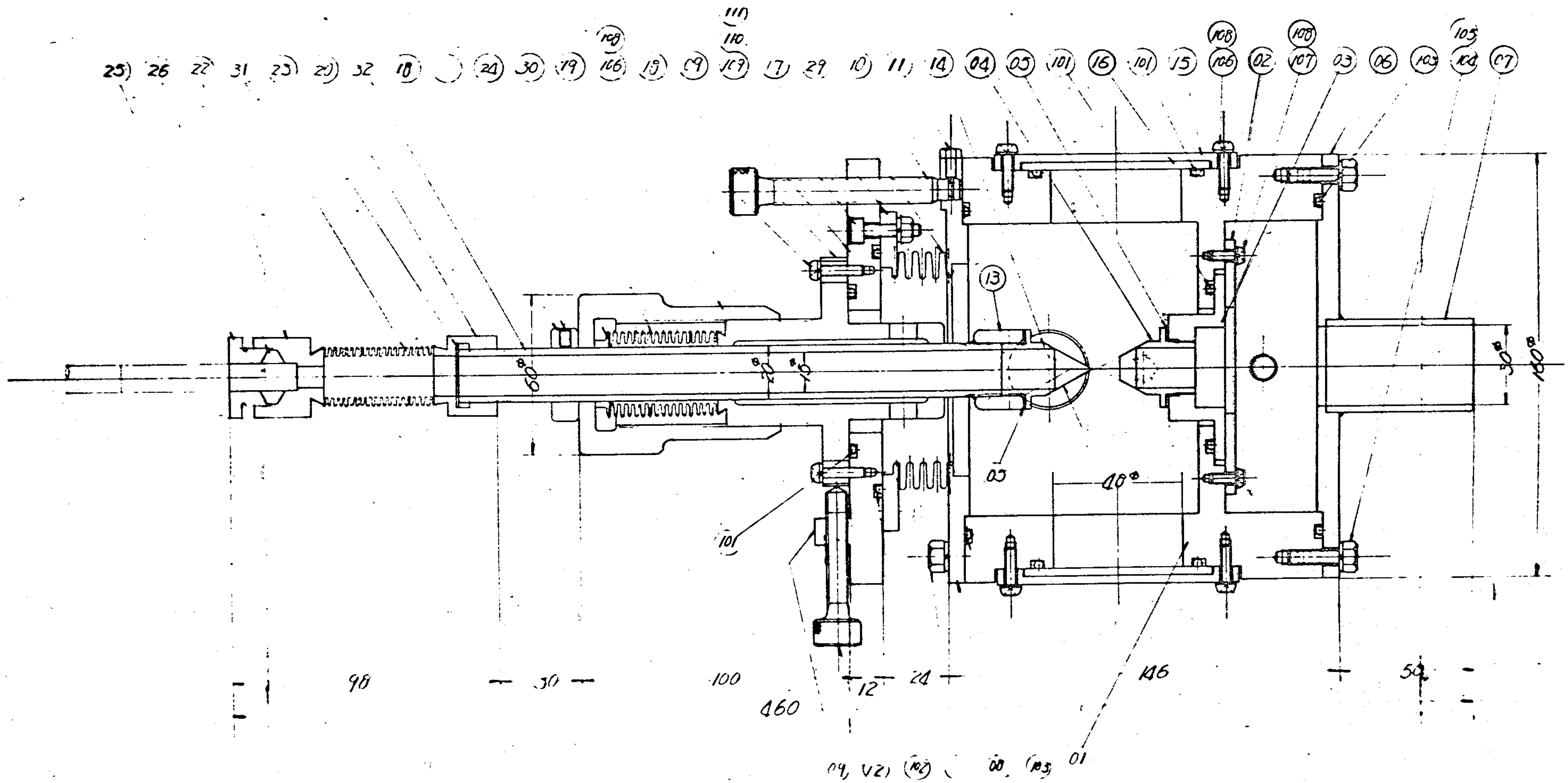

FIG.38 CONSTRUCTIONAL DETAILS OF SUPERSONIC JET APPARATUS.
4. SKIMMER; 5. NOZZLE; 7. SUCTION PIPE; 10. MICROMETER SCREW FOR HORIZONTAL ADJUSTMENT; 12. MICROMETER SCREW FOR VERTICAL ADJUSTMENT; 16. GLASS WINDOW; 29,30,31. BELLOWS; 32. INLET PIPE.

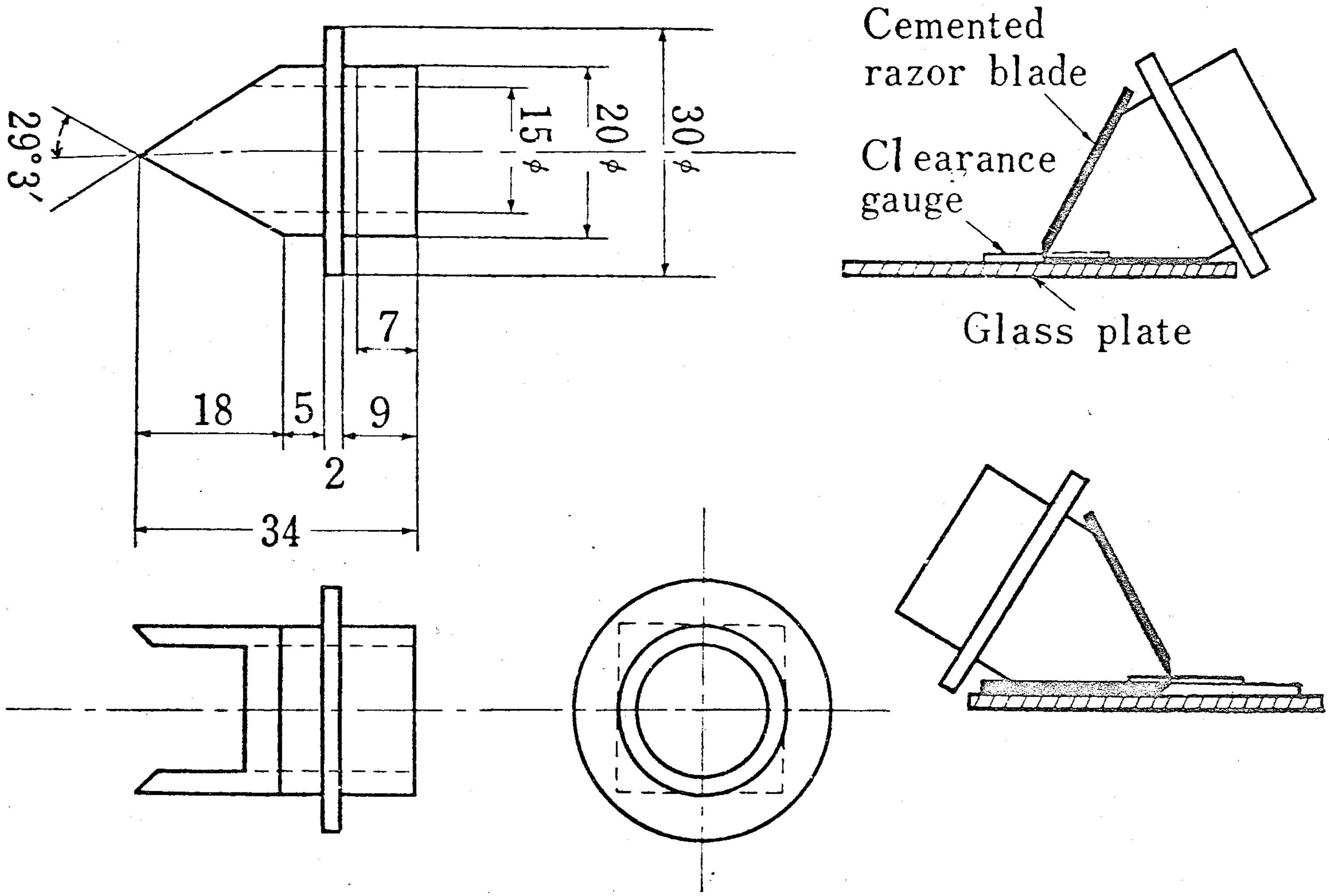

FIG.39 SLIT NOZZLE

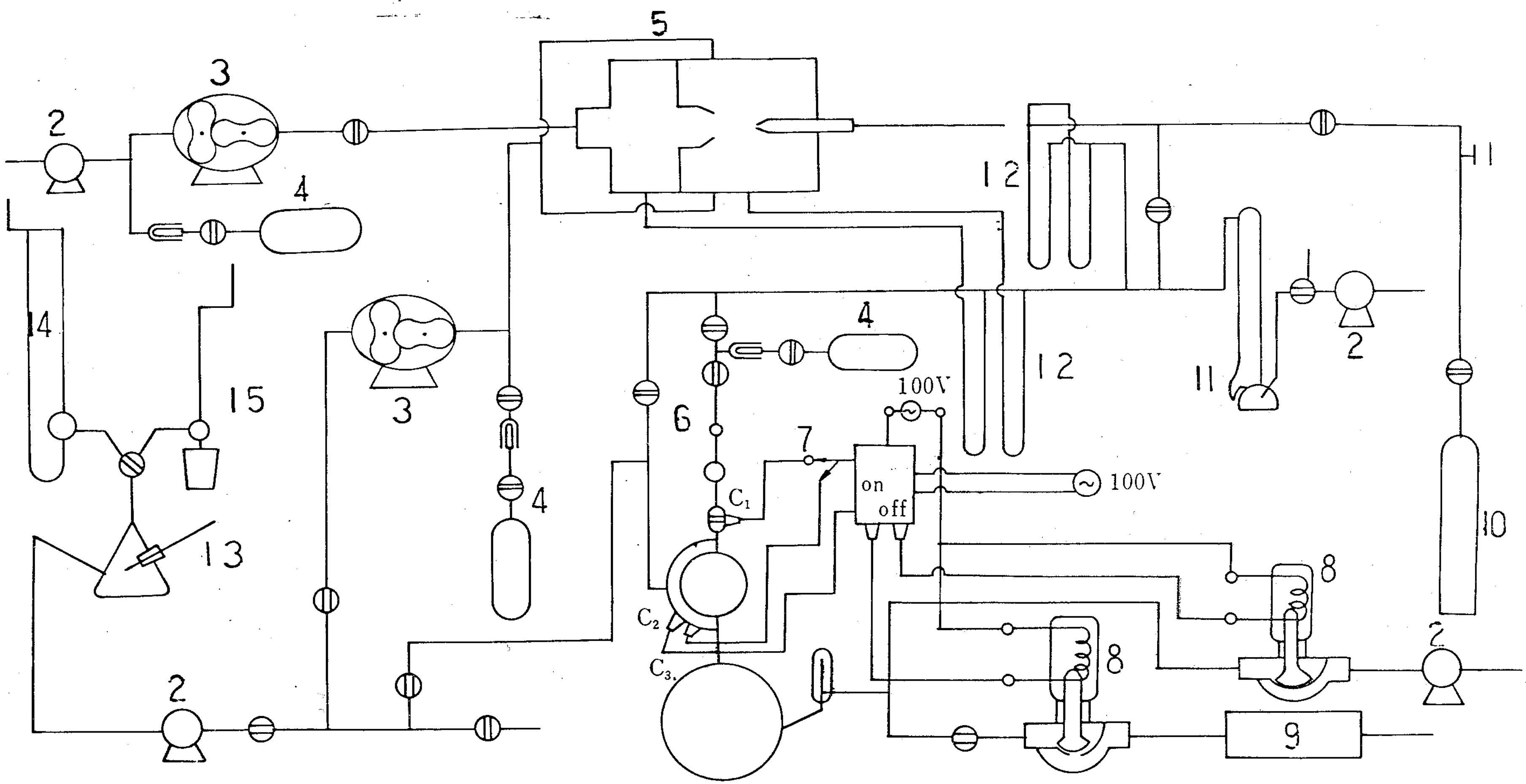

FIG.40 FLOW DIAGRAM OF EXPERIMENTAL EQUIPMENT. 1. NEEDLE VALVE; 2. ROTARY VACUUM PUMP; 3. MECHANICAL BOOSTER; 4. SAMPLE BULB; 5. JET SEPARATION APPARATUS; 6. TÖPLER PUMP; 7. ON-OFF RELAY; 8. MAGNETIC CONTROLLED VALVE; 9. SILICA-GEL PACKED COLUMN; 10. GAS MIXTURE CYLINDER; 11. MERCURY DIFFUSION PUMP; 12. D.O.P. OIL MANOMETER; 13. THERMOMETER; 14. SOAP FILM FLOW METER; 15. SOAP FILM FLOW METER.

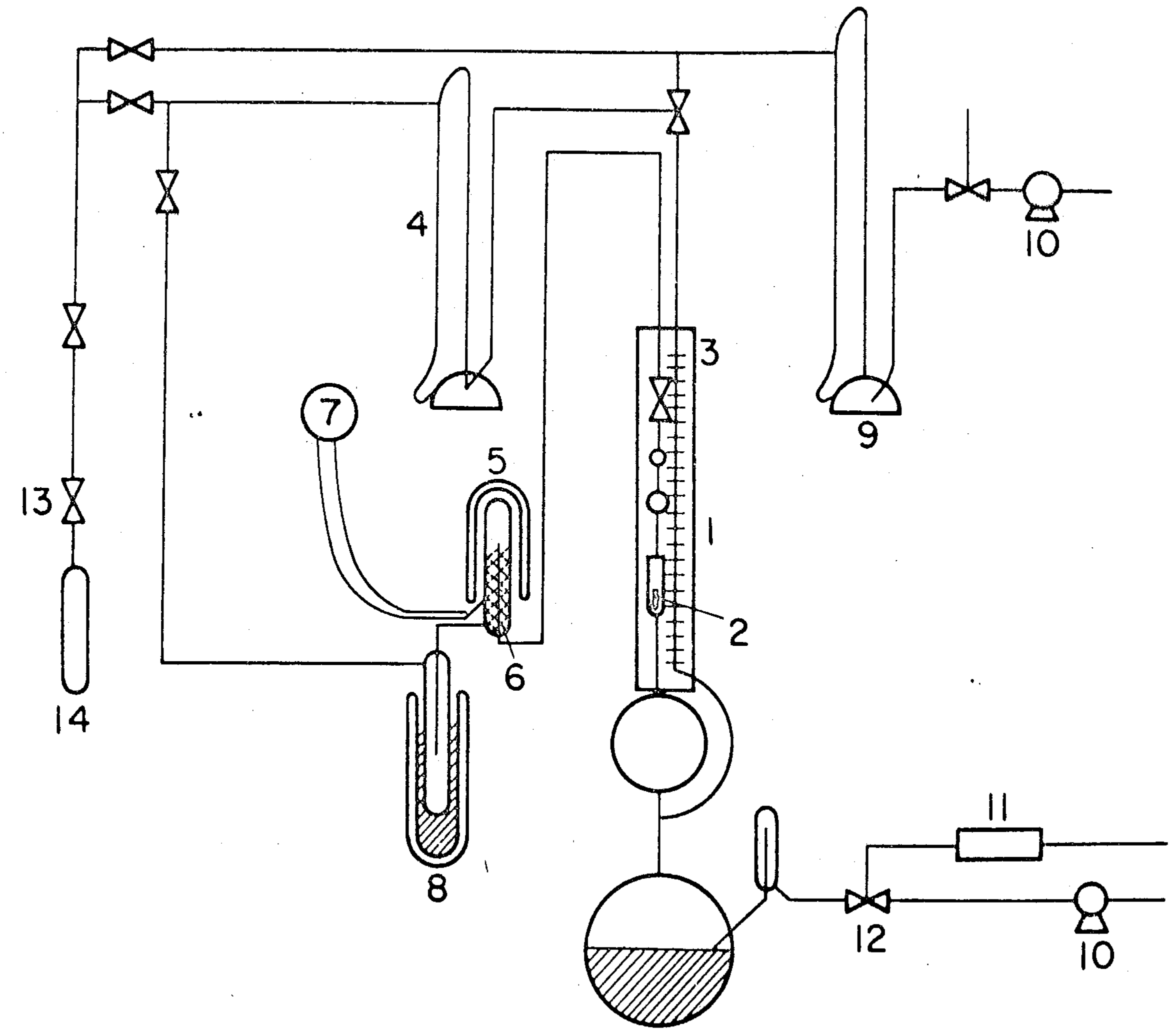

FIG.41 SCHEMATIC DIAGRAM OF GAS ANALYSIS APPARATUS
1. TÖPLER PUMP; 2. MERCURY CUT-OFF; 3. GLASS SCALE;
4. MERCURY DIFFUSION PUMP FOR CIRCULATING GAS MIXTURE;
5. NICHROME WIRE HEATER; 6. COPPER OXIDE; 7. THERMOCOUPLE;
8. LIQUID NITROGEN TRAP; 9. MERCURY DIFFUSION PUMP;
10. ROTARY VACUUM PUMP; 11. SILICA-GEL PACKED COLUMN;
12. THREE WAY COCK; 13. UNIVERSAL JOINT; 14. SAMPLE BULB.

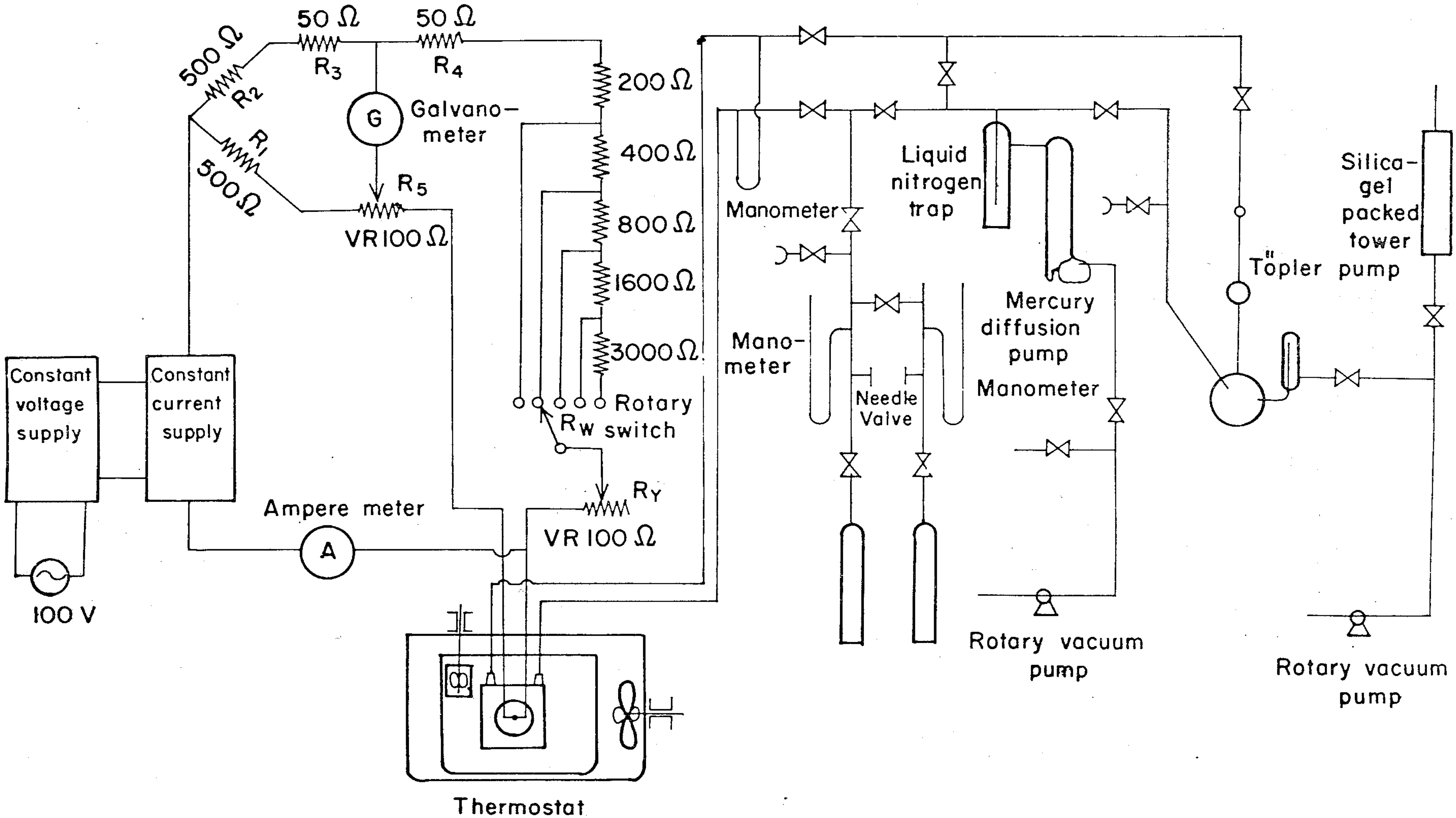

FIG.42 DIAGRAM OF EXPERIMENTAL APPARATUS

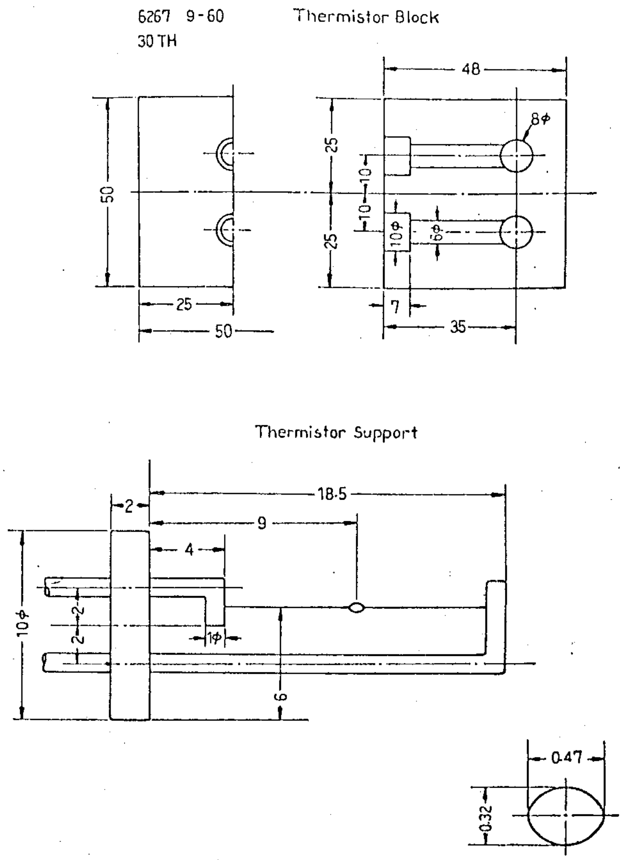

FIG.43 SCHEMATIC DIAGRAM OF CELL BLOCK AND THERMISTOR

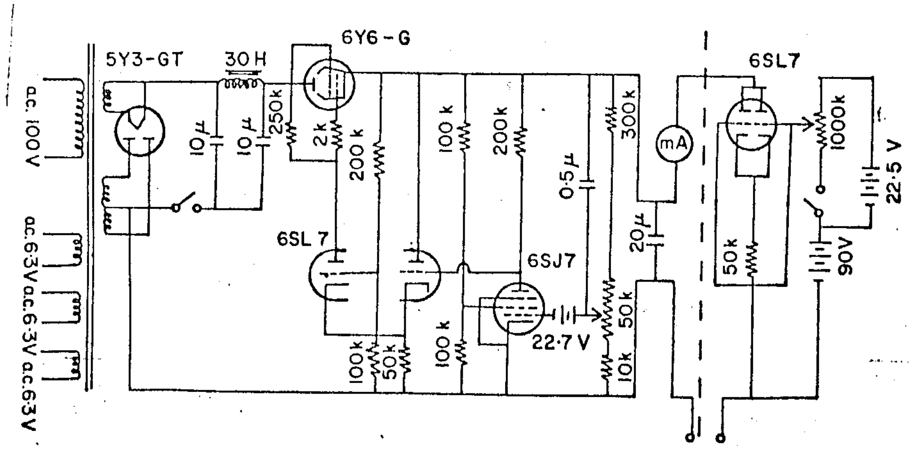

FIG.44 ELECTRONIC CIRCUIT OF CONSTANT D.C. VOLTAGE AND CURRENT REGULATOR

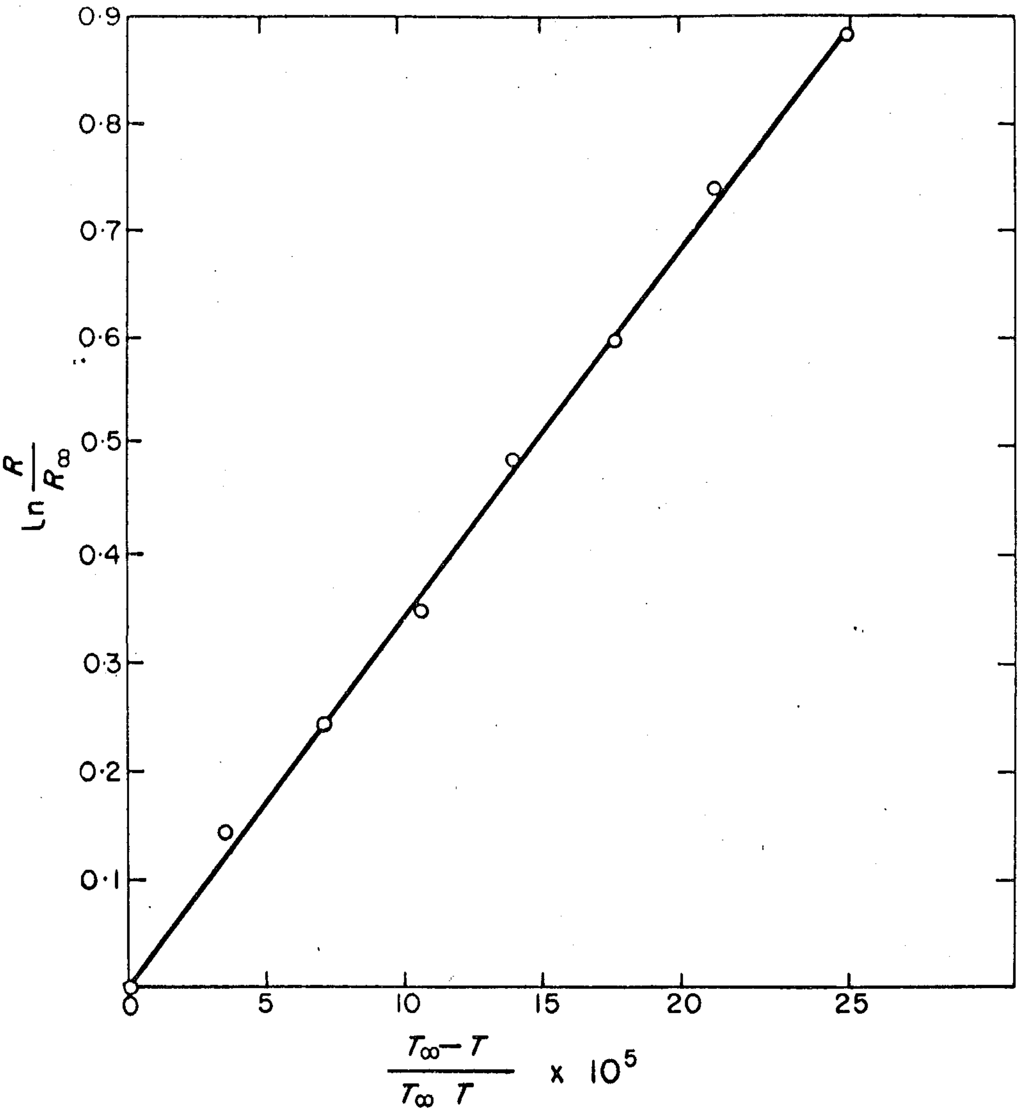

FIG.45 VARIATION OF RESISTANCE OF THERMISTOR WITH TEMPERATURE

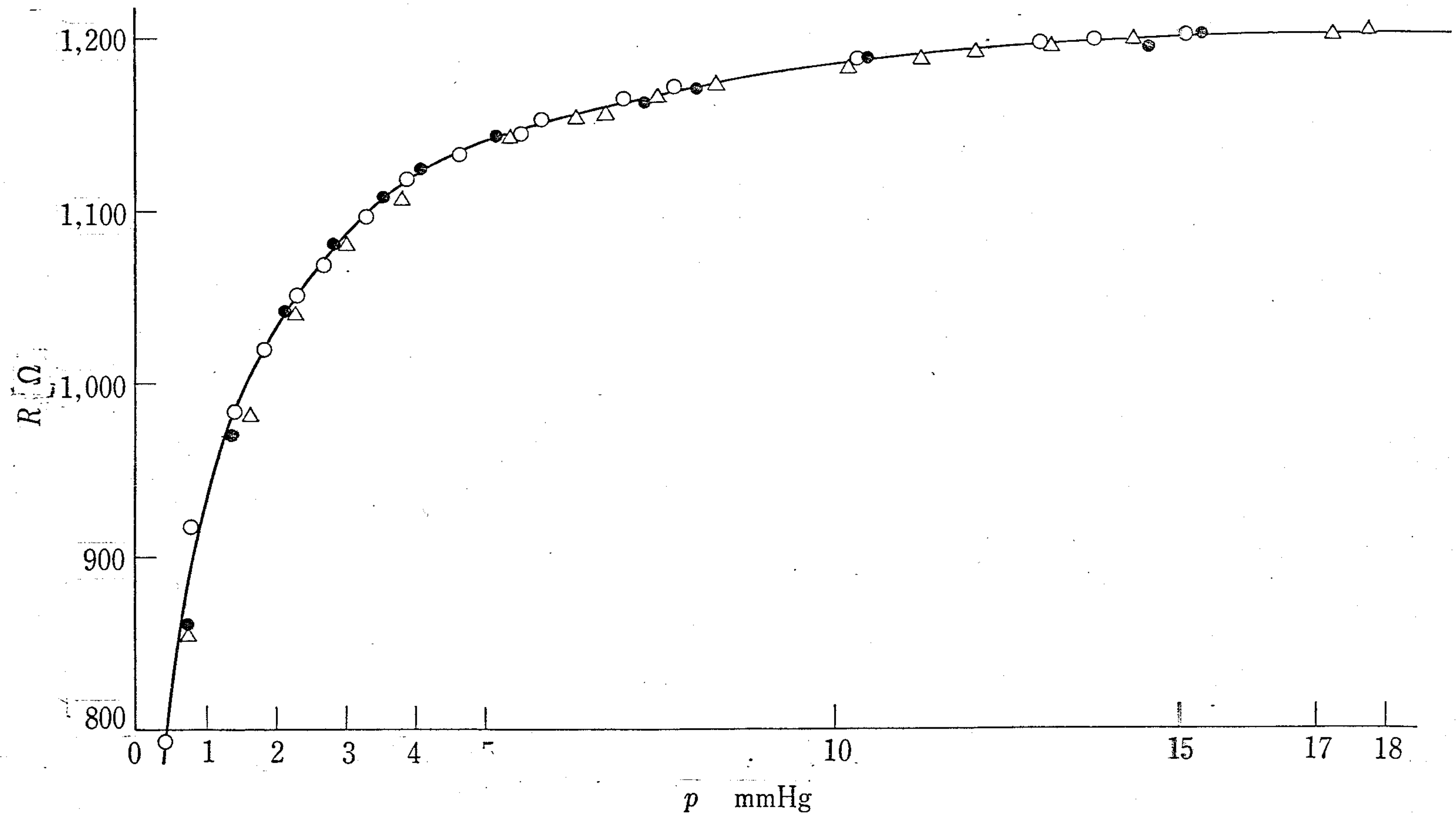

FIG.46 REPRODUCIBILITY TEST BY AIR, (○ ●) BEFORE A SERIES OF EXPERIMENTS WITH HYDROGEN AND NITROGEN GAS MIXTURES, (△) AFTER A SERIES OF EXPERIMENTS WITH HYDROGEN AND NITROGEN GAS MIXTURES

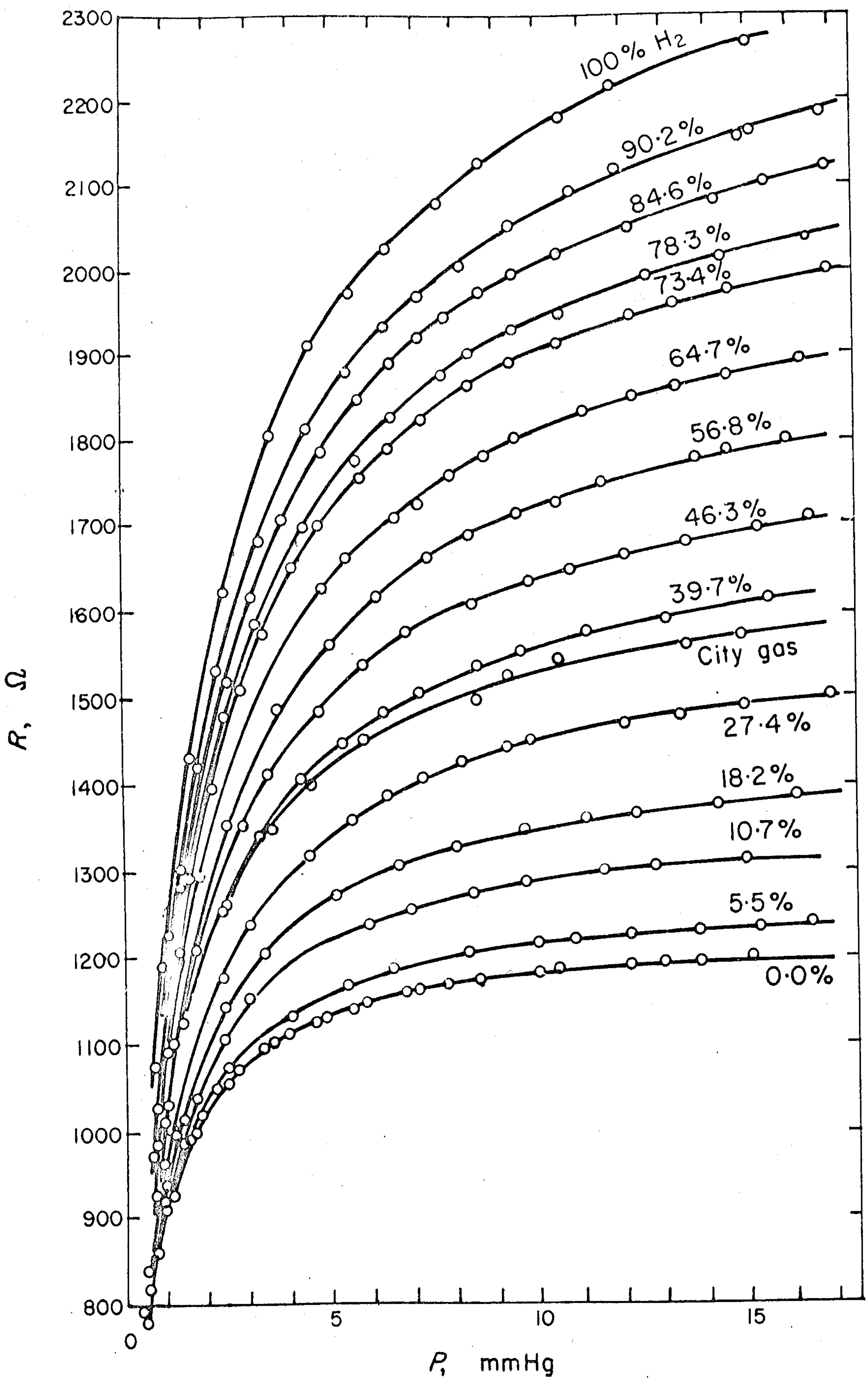

FIG.47 RELATION BETWEEN RESISTANCE AND PRESSURE FOR H_2-N_2 GAS MIXTURES OF VARIOUS CONCENTRATIONS WITH VALUES OF CONCENTRATION AS A PARAMETER

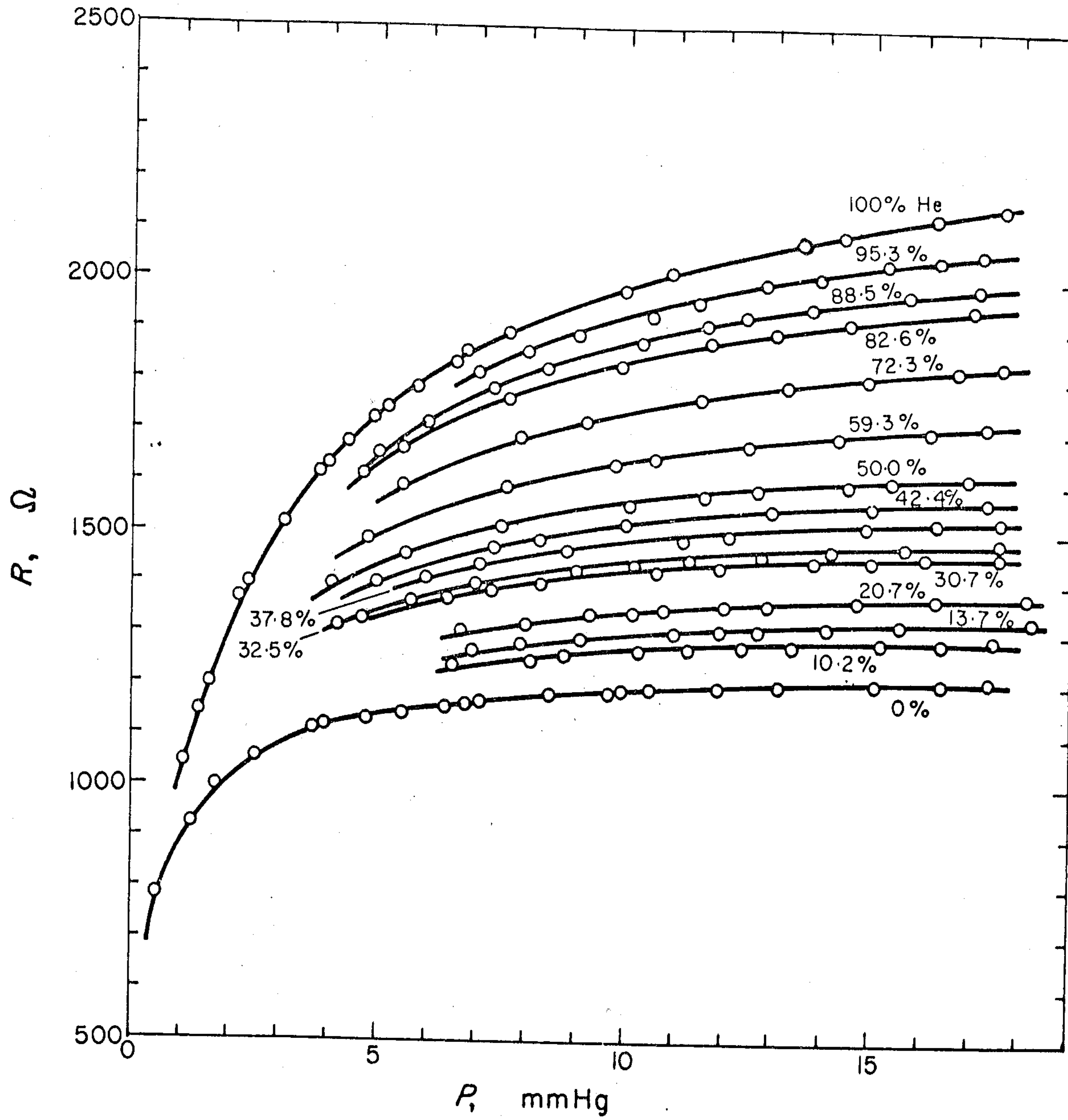

FIG.48 RELATION BETWEEN RESISTANCE AND PRESSURE FOR $He-N_2$ GAS MIXTURES OF VARIOUS CONCENTRATIONS WITH VALUES OF CONCENTRATION AS A PARAMETER

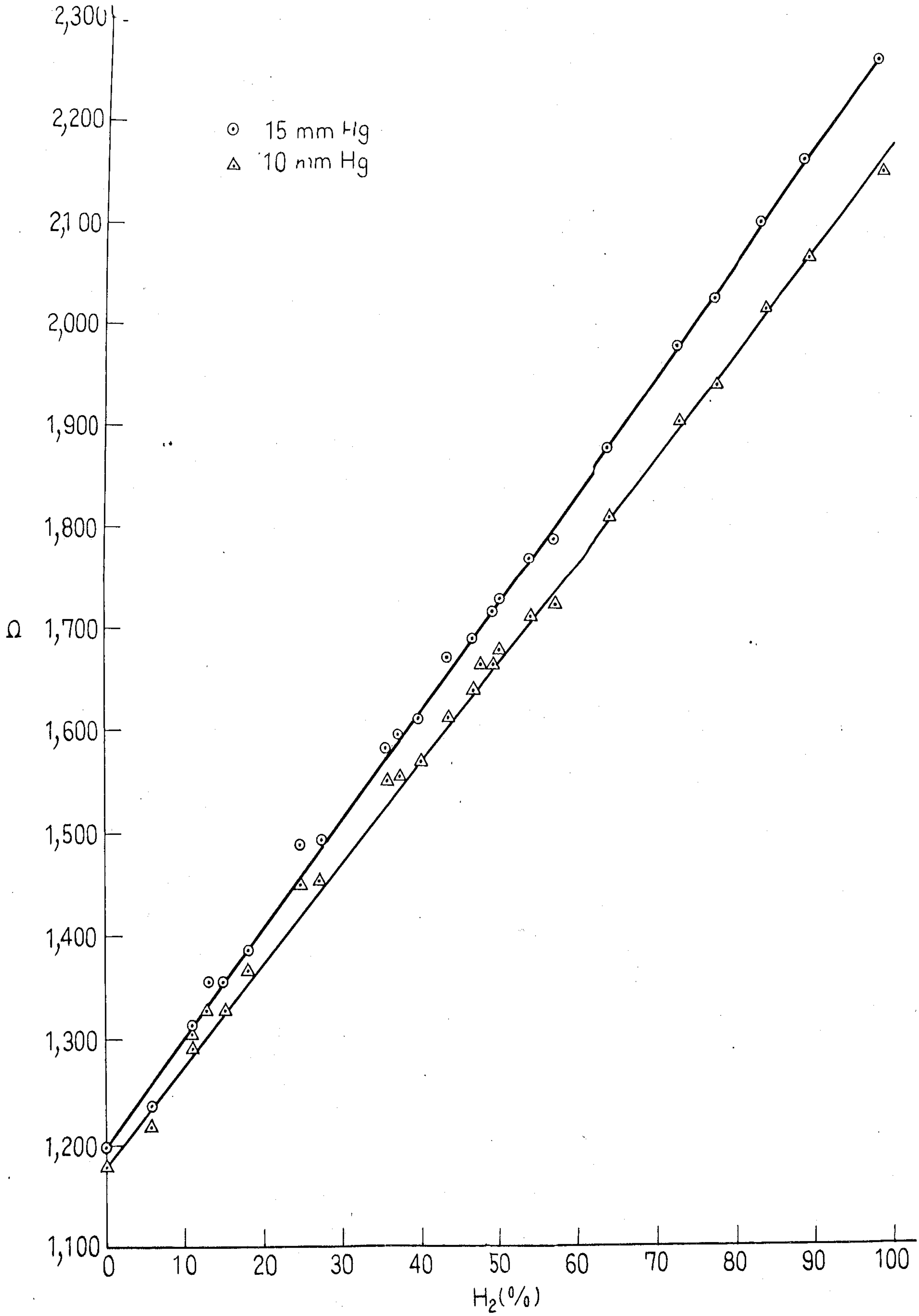

FIG.49 RELATION BETWEEN RESISTANCE AND CONCENTRATION OF H_2

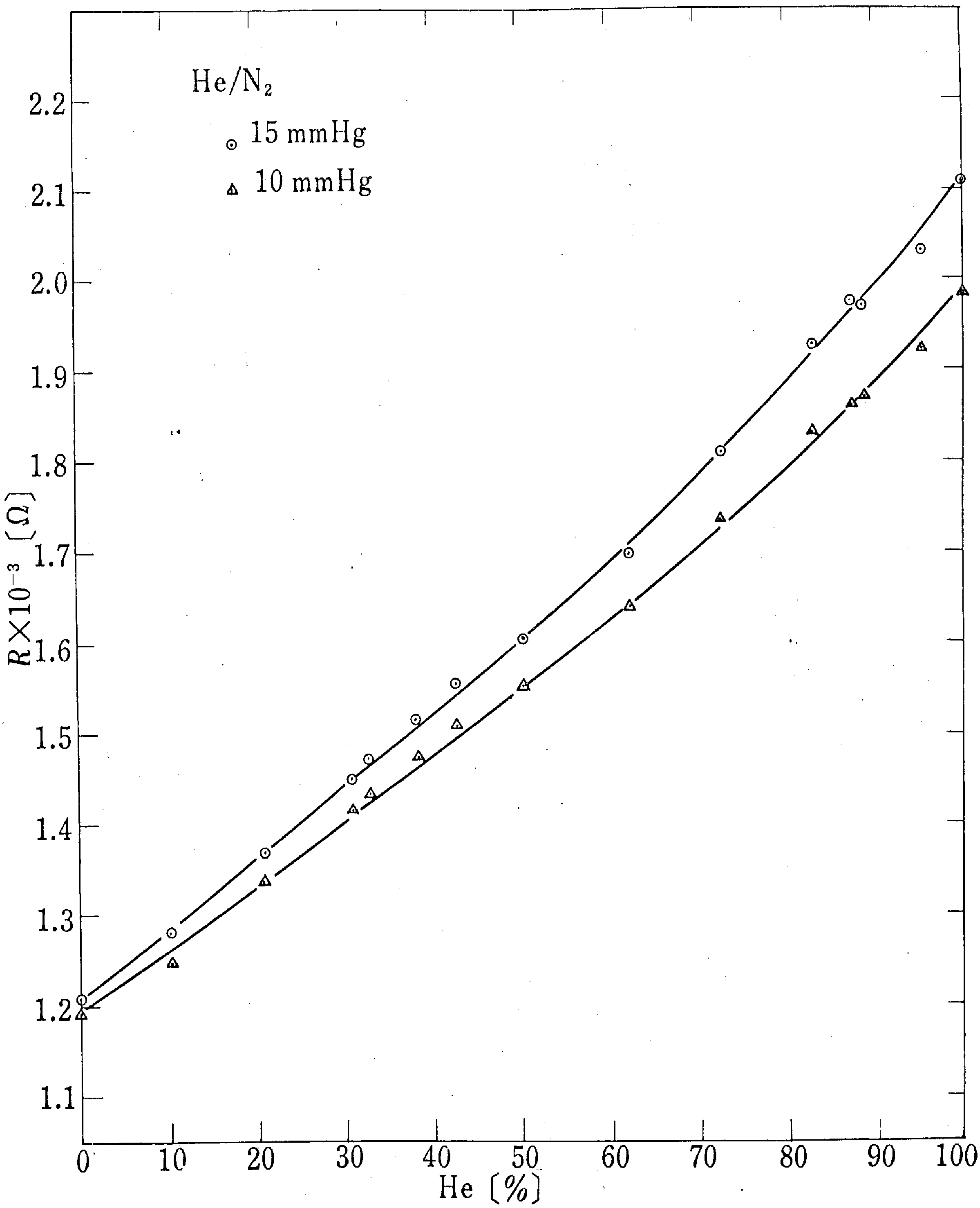

FIG.50 RELATION BETWEEN RESISTANCE AND CONCENTRATION OF He

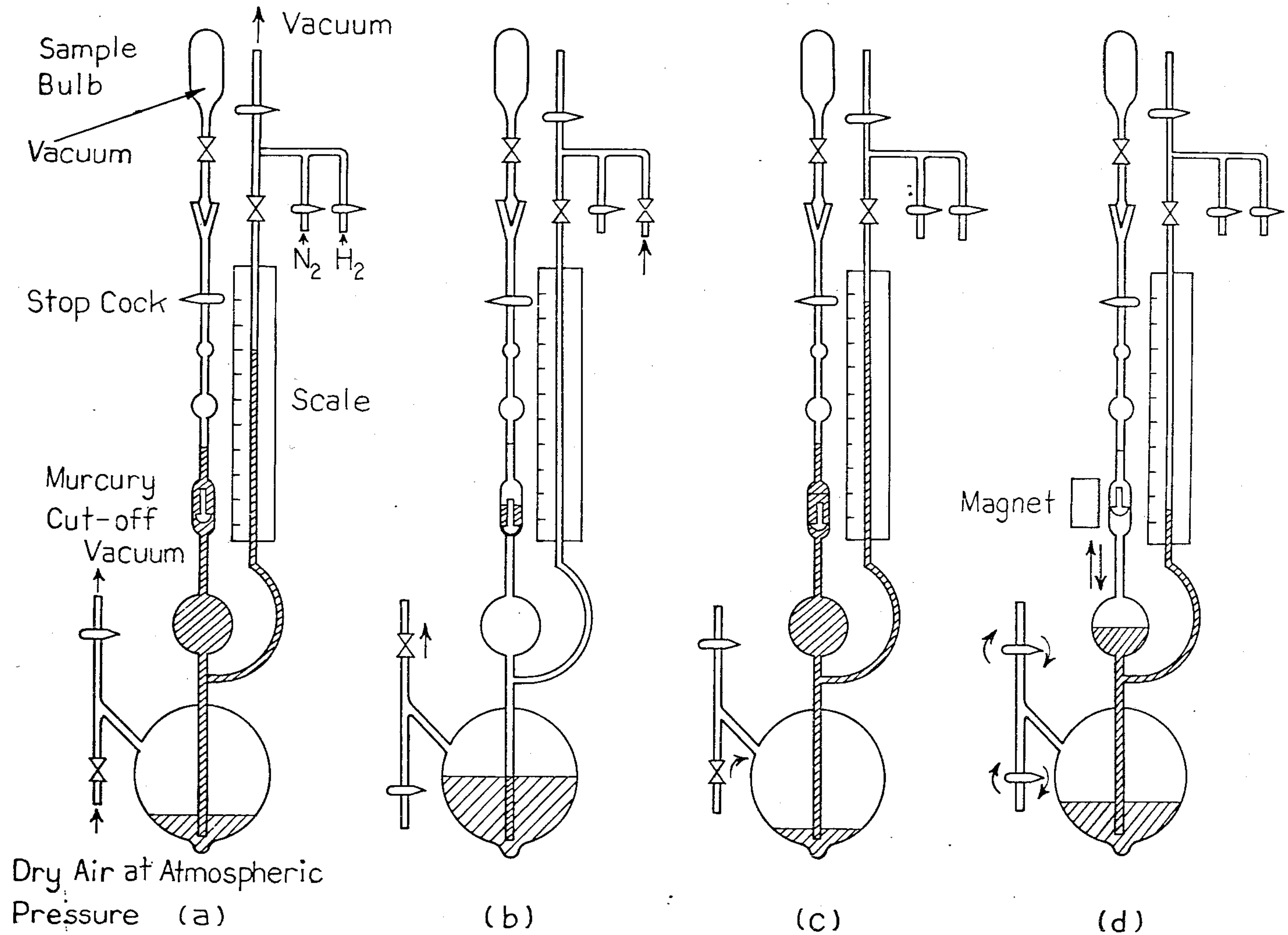

FIG.51 METHOD OF MIXING

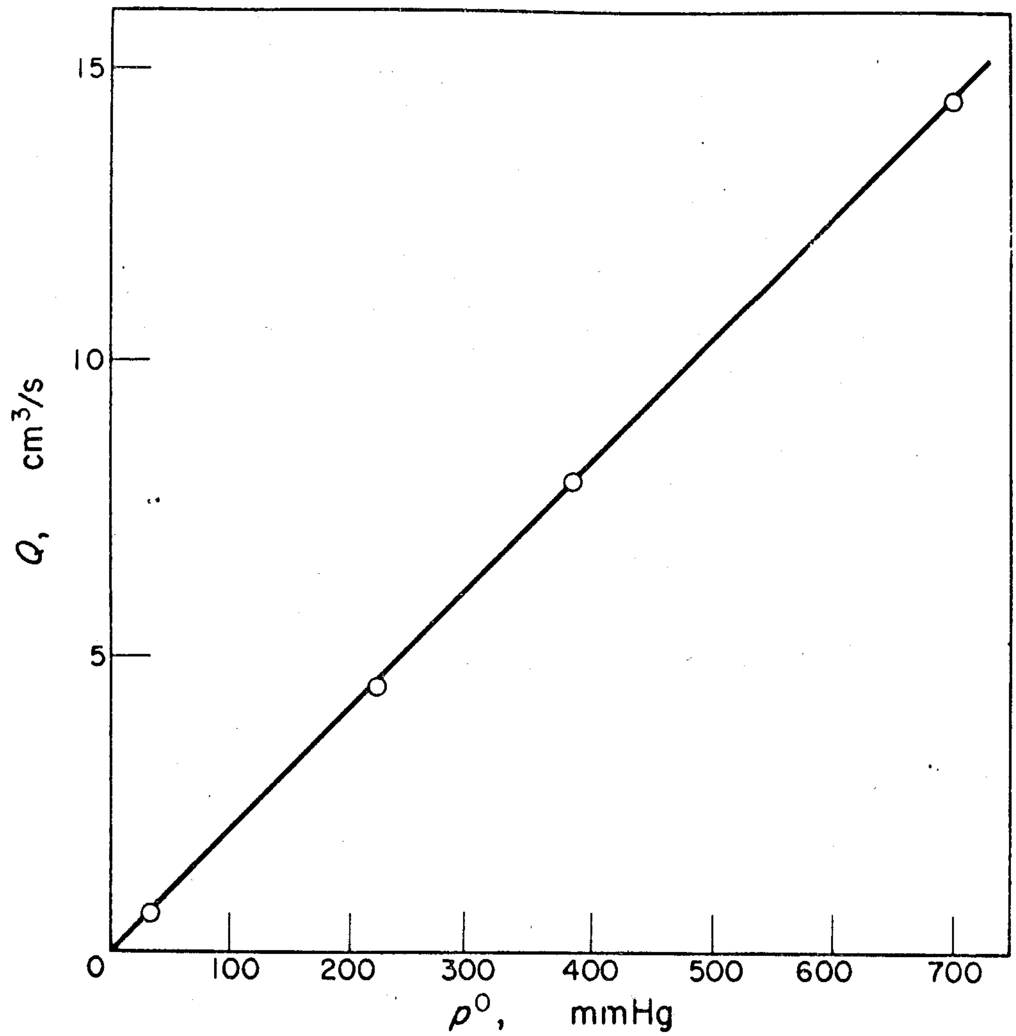

FIG.52 VOLUME FLOW RATE THROUGH NOZZLE VERSUS INLET PRESSURE

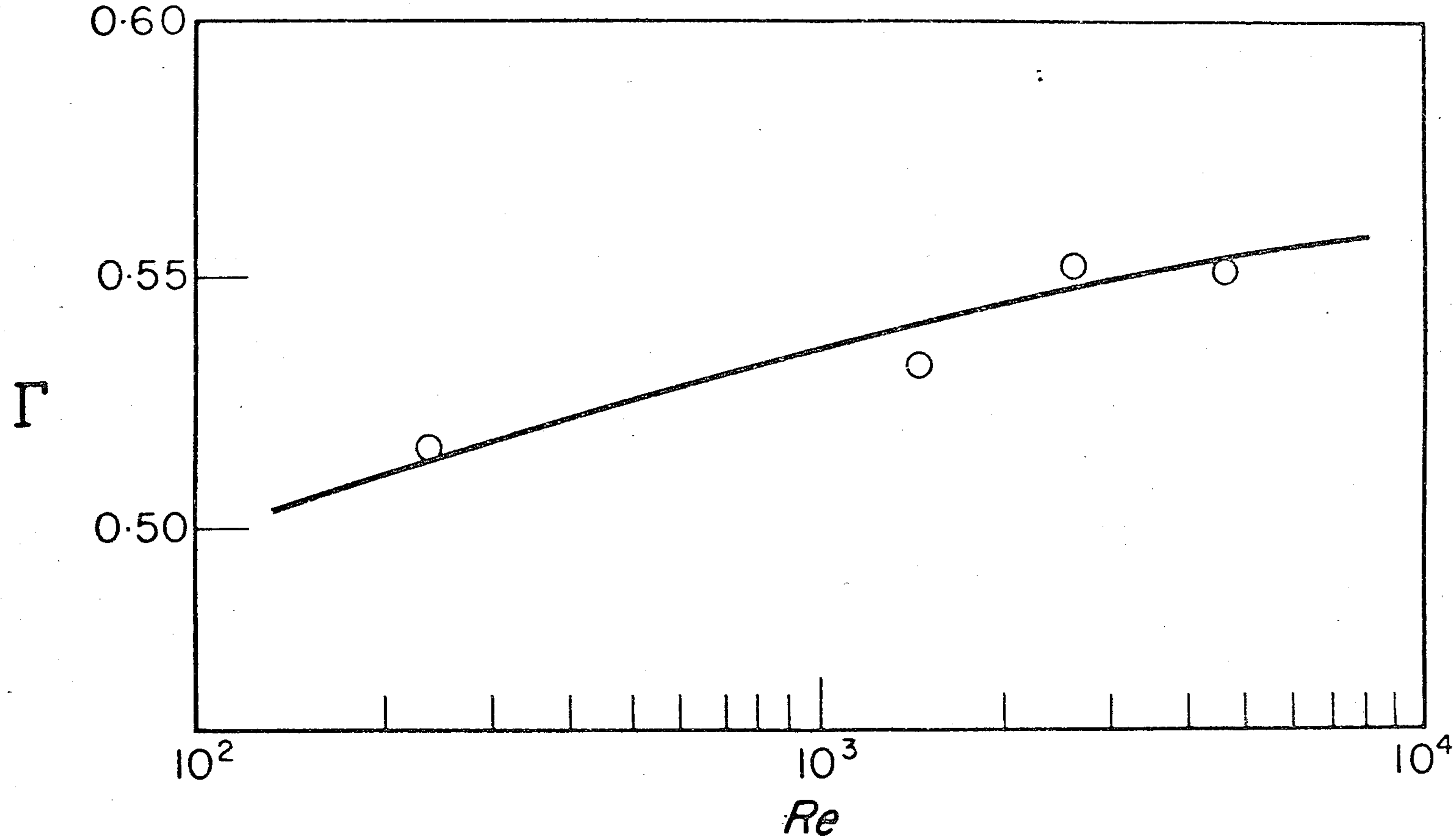

FIG.53 RELATIONSHIP BETWEEN DISCHARGE COEFFICIENT AND REYNOLDS NUMBER

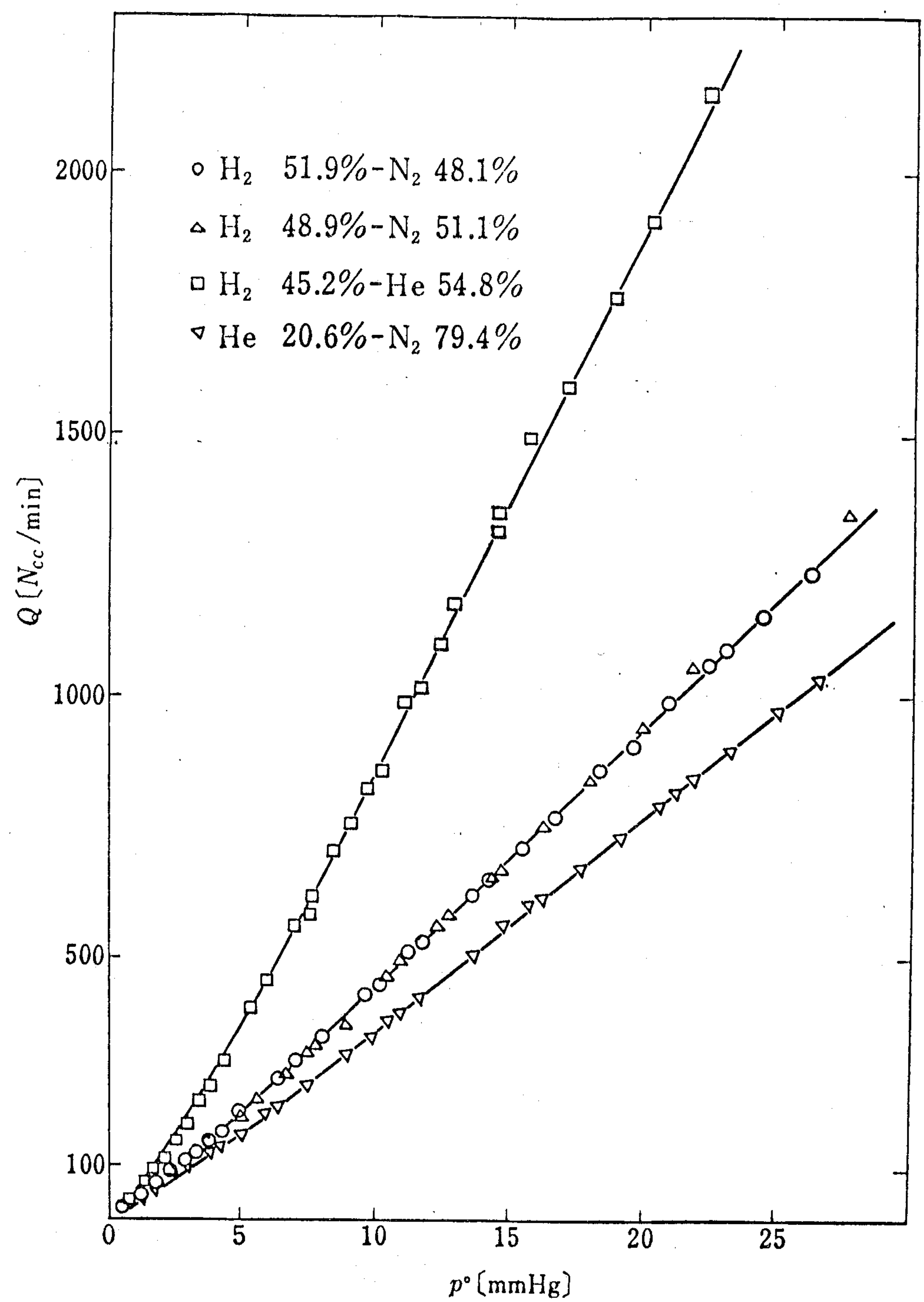

FIG.54 VOLUME FLOW RATE VERSUS INLET PRESSURE

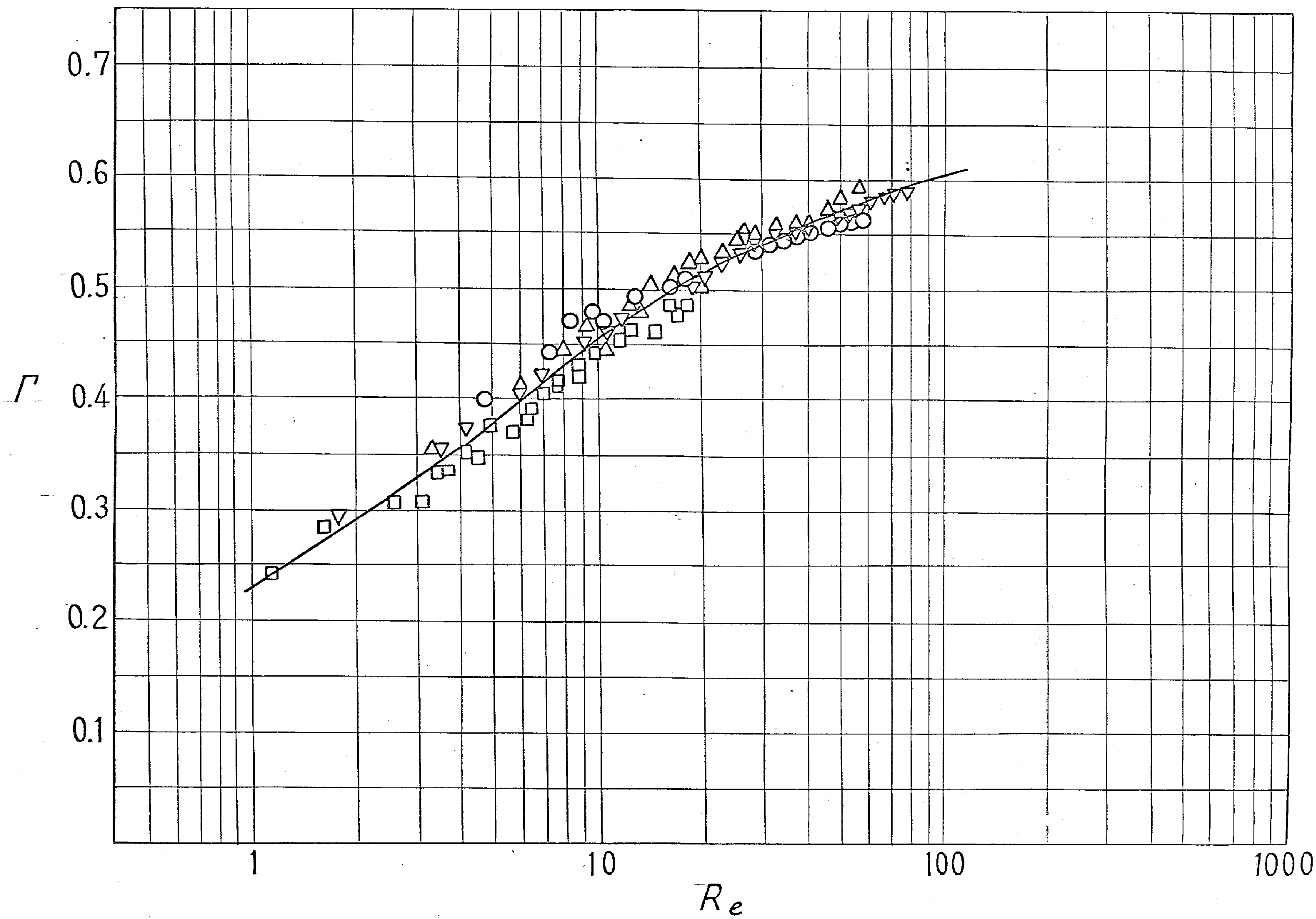

FIG.55 RELATIONSHIP BETWEEN DISCHARGE COEFFICIENT AND REYNOLDS NUMBER

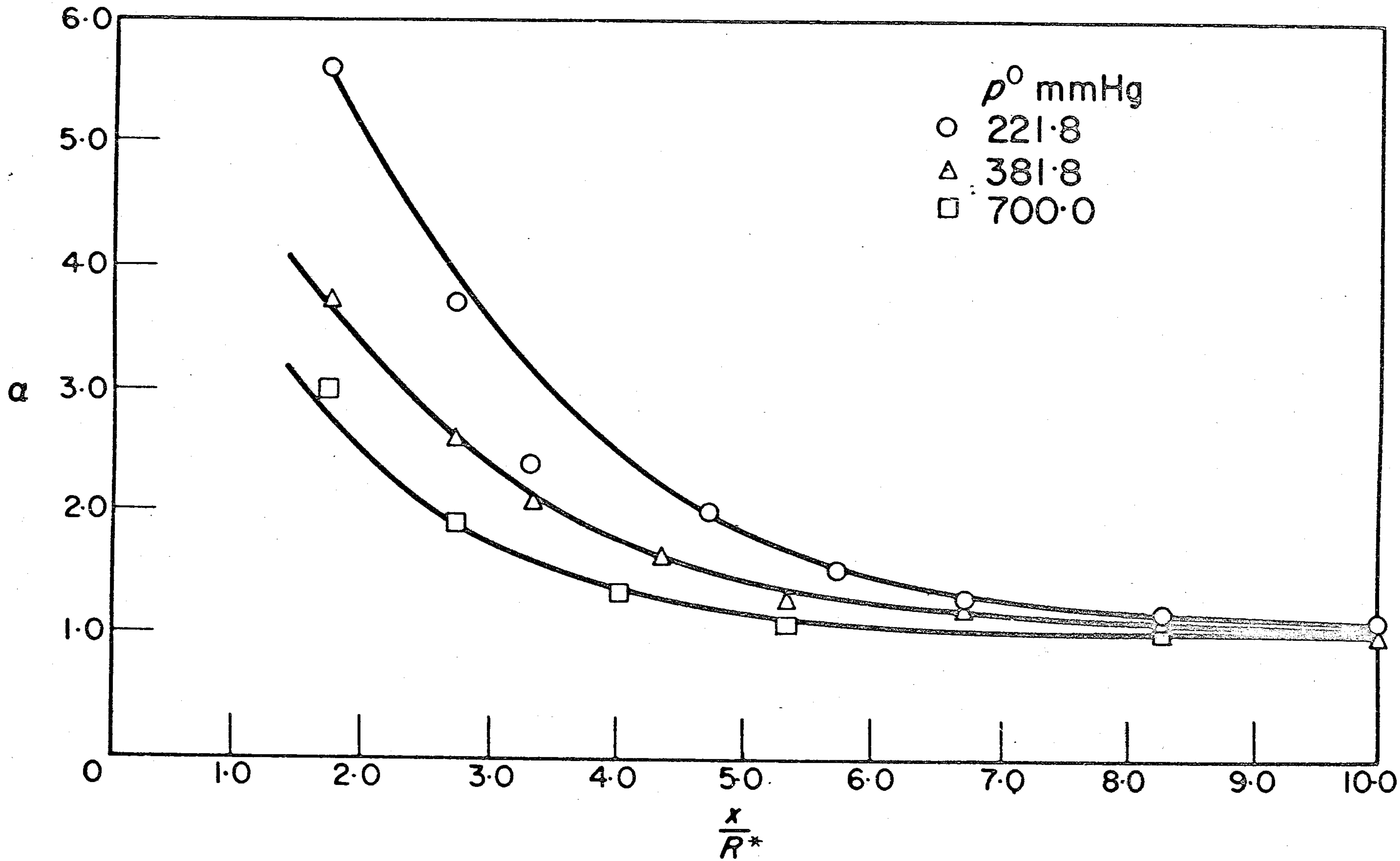

FIG.56 SEPARATION COEFFICIENT AS A FUNCTION OF DISTANCE BETWEEN NOZZLE EXIT AND SKIMMER

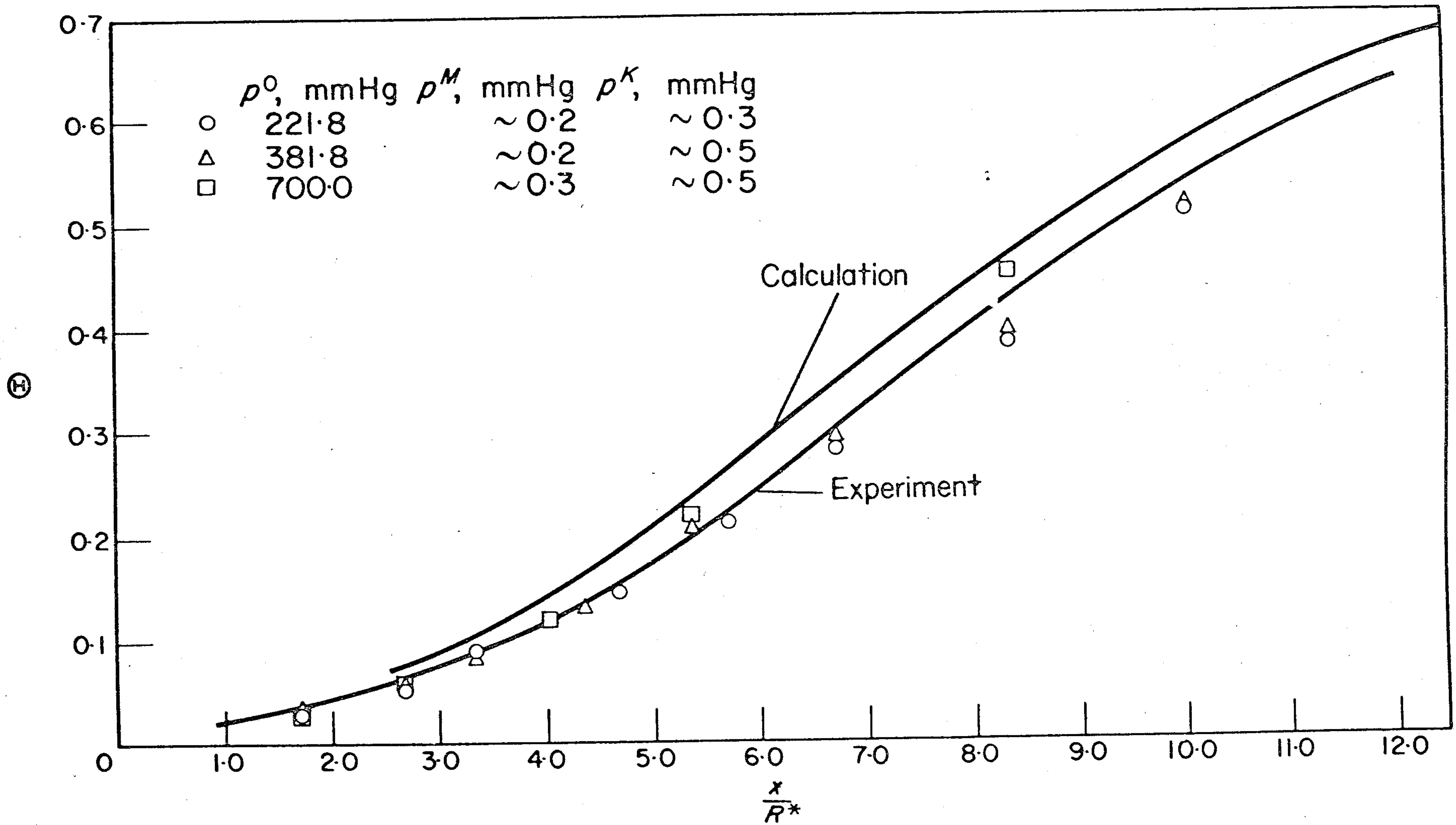

FIG.57 CUT AS A FUNCTION OF DISTANCE BETWEEN NOZZLE EXIT AND SKIMMER

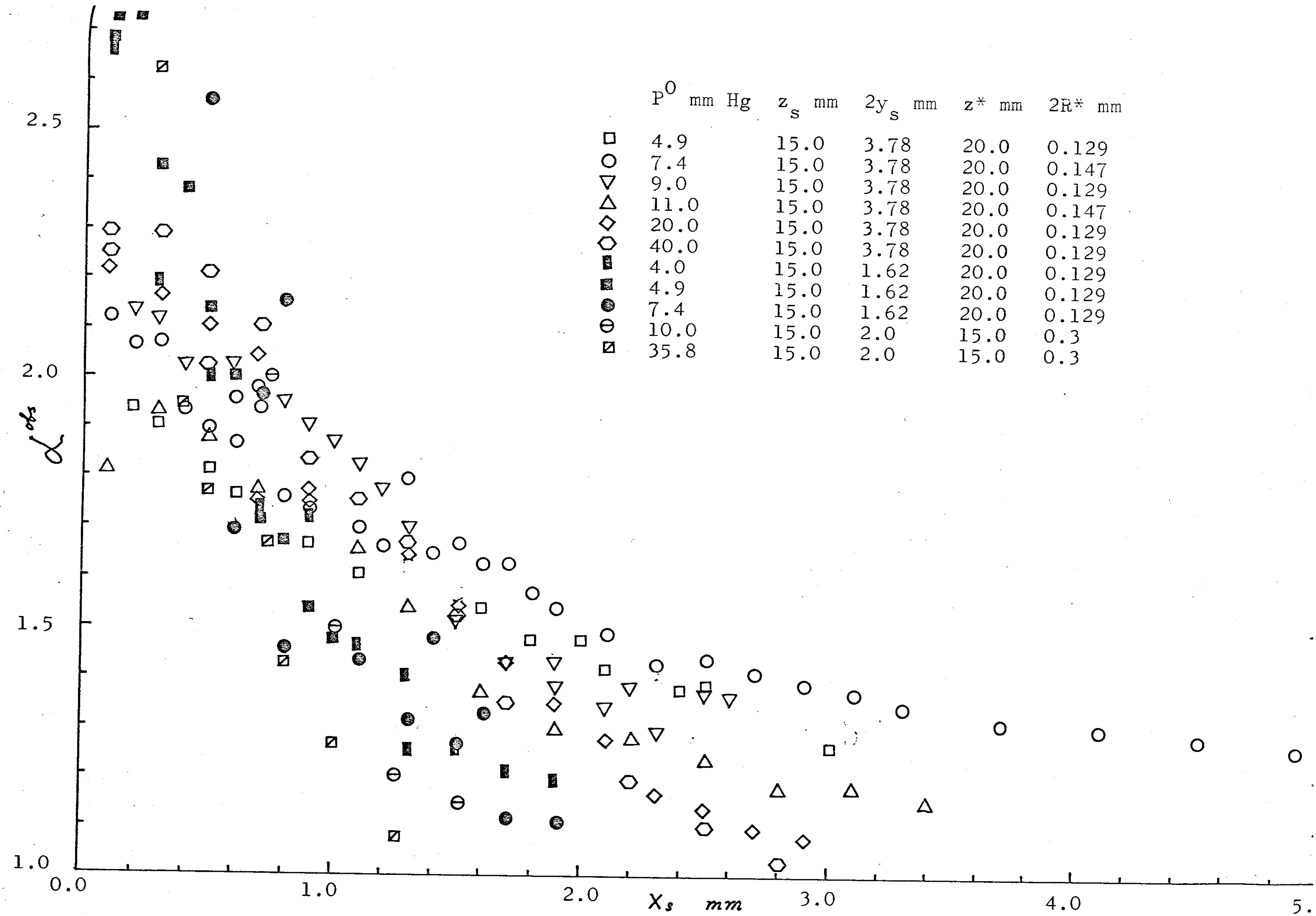

FIG.58 SEPARATION COEFFICIENT AS A FUNCTION OF NOZZLE-SKIMMER DISTANCE (50 % H_2-50 % N_2)

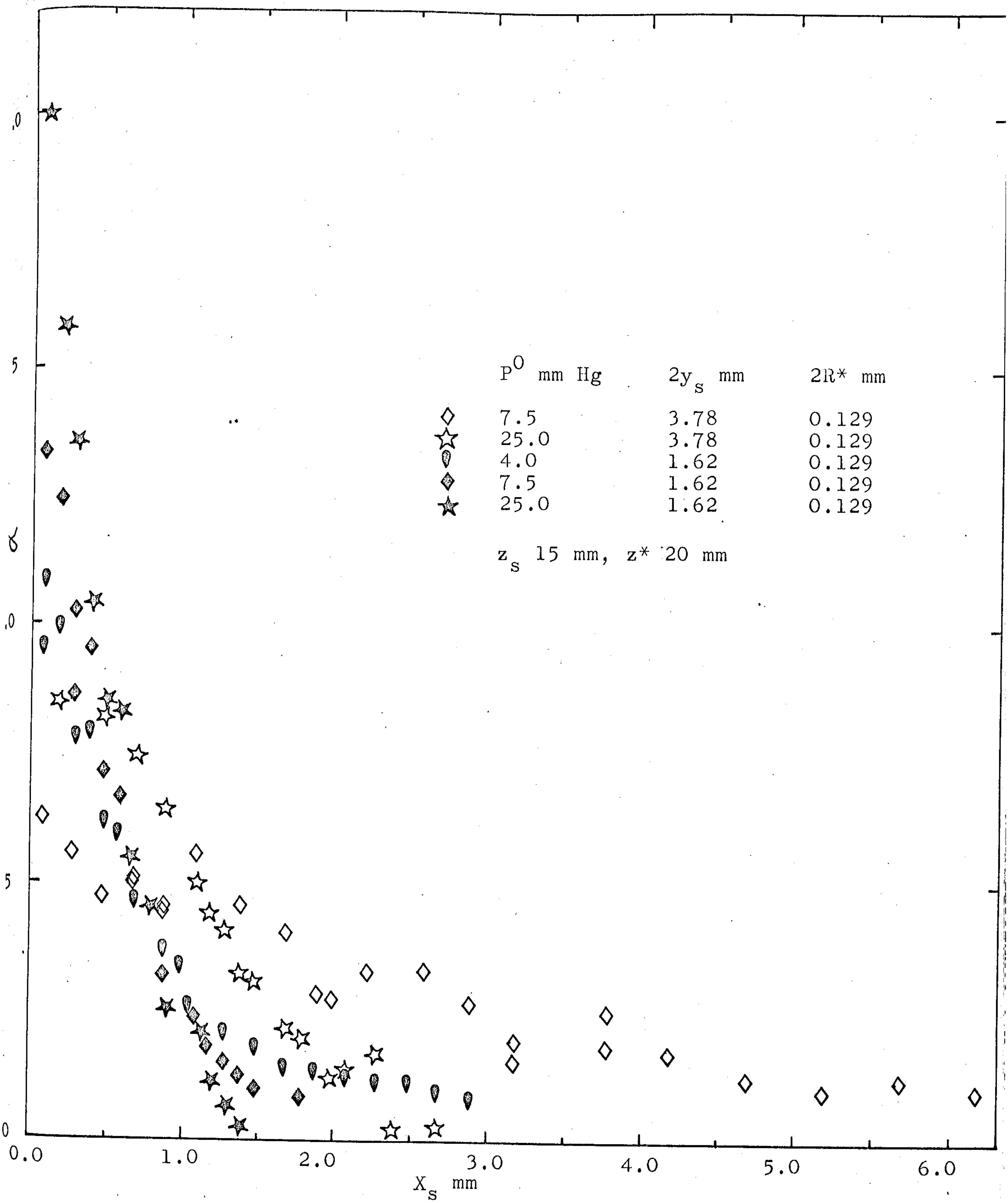

FIG.59 SEPARATION COEFFICIENT AS A FUNCTION OF NOZZLE – SKIMMER DISTANCE ($20\,\%$ He–$80\,\%$ N_2)

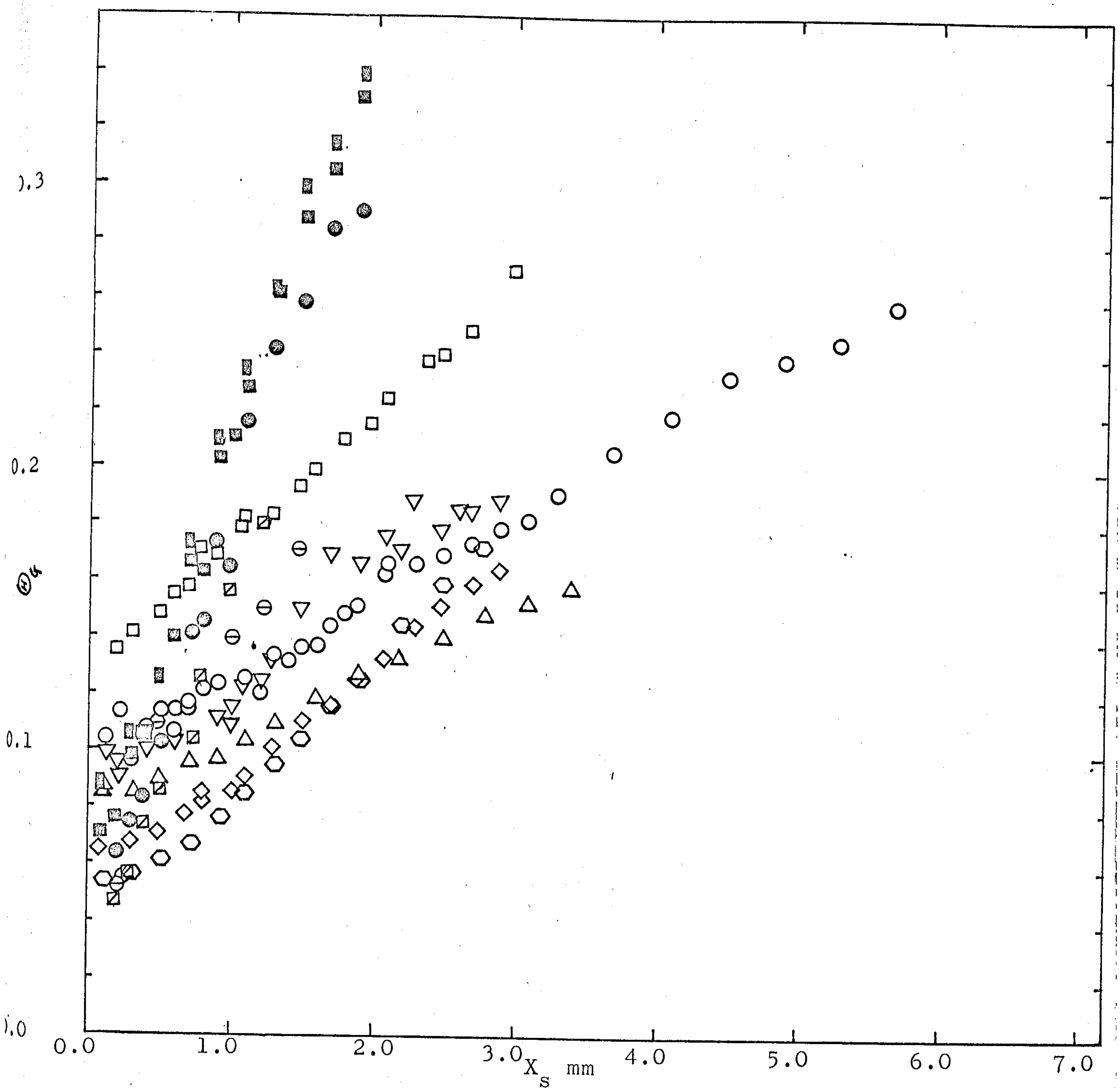

FIG.60 CUT AS A FUNCTION OF NOZZLE-SKIMMER DISTANCE ($50\% H_2$-$50\% N_2$)

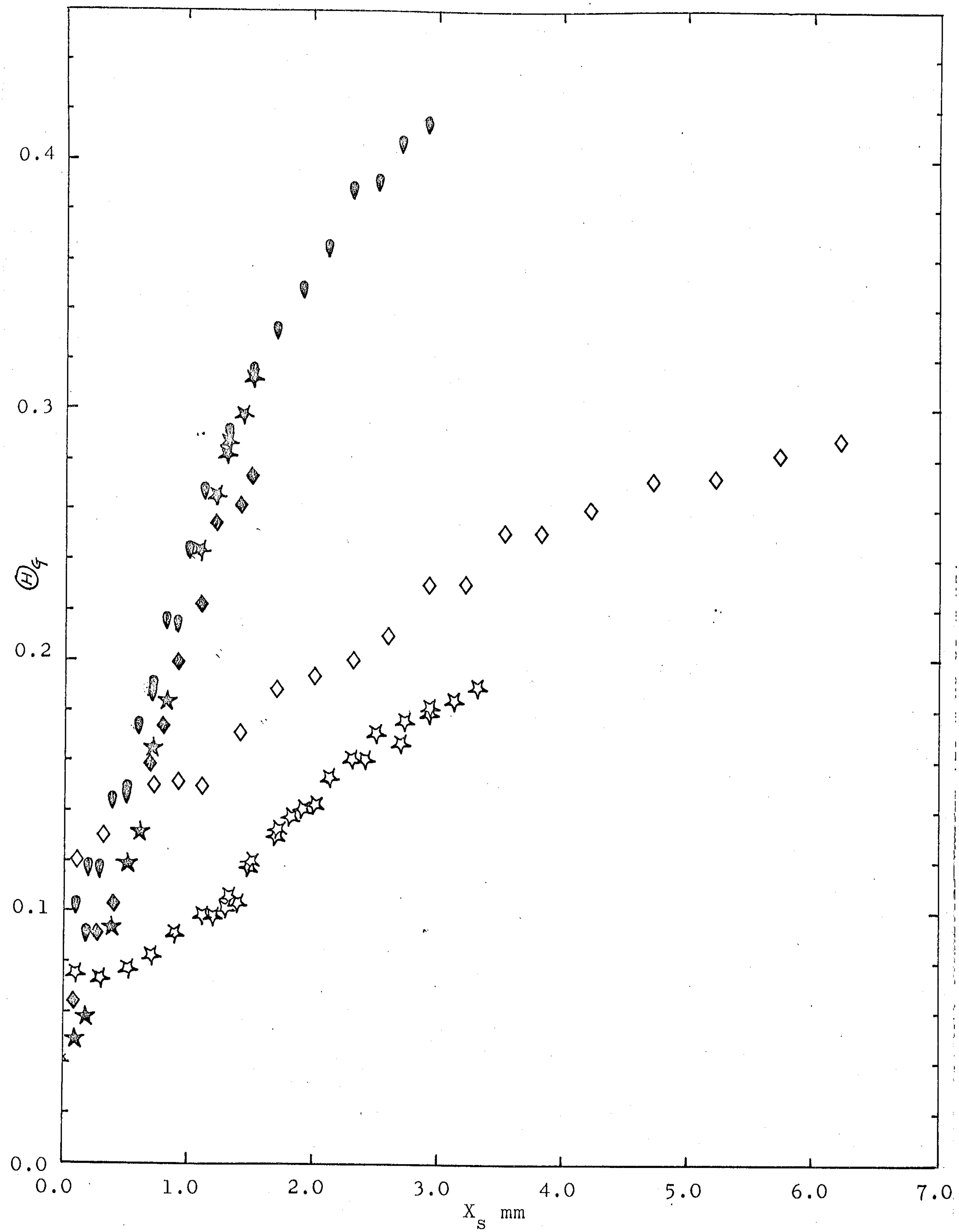

FIG.61 CUT AS A FUNCTION OF NOZZLE-SKIMMER DISTANCE
($20\,\%$ He-$80\,\%$ N_2)

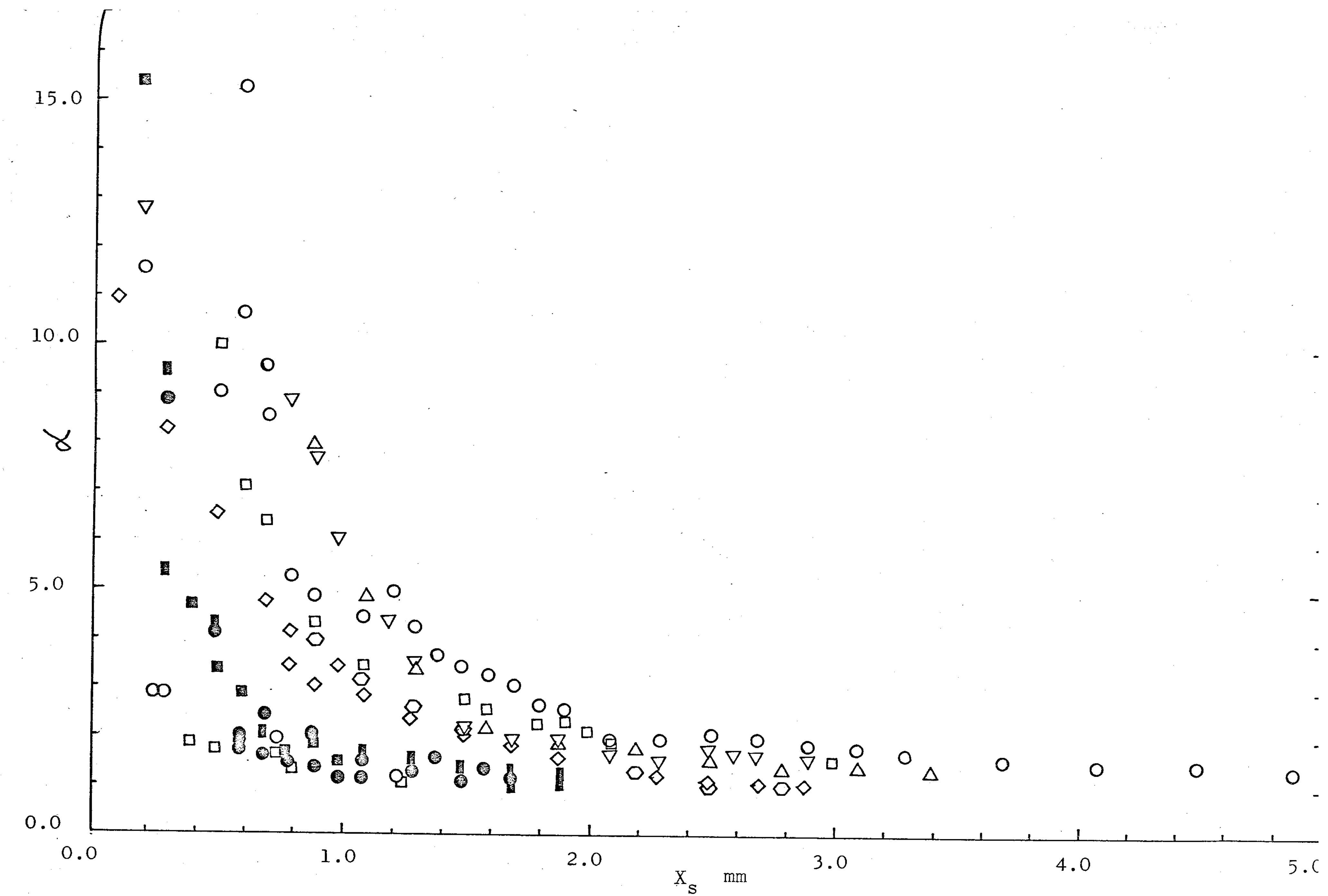

FIG.62 α vs. X_s, CORRECTED VALUES ($50\% H_2 - 50\% N_2$)

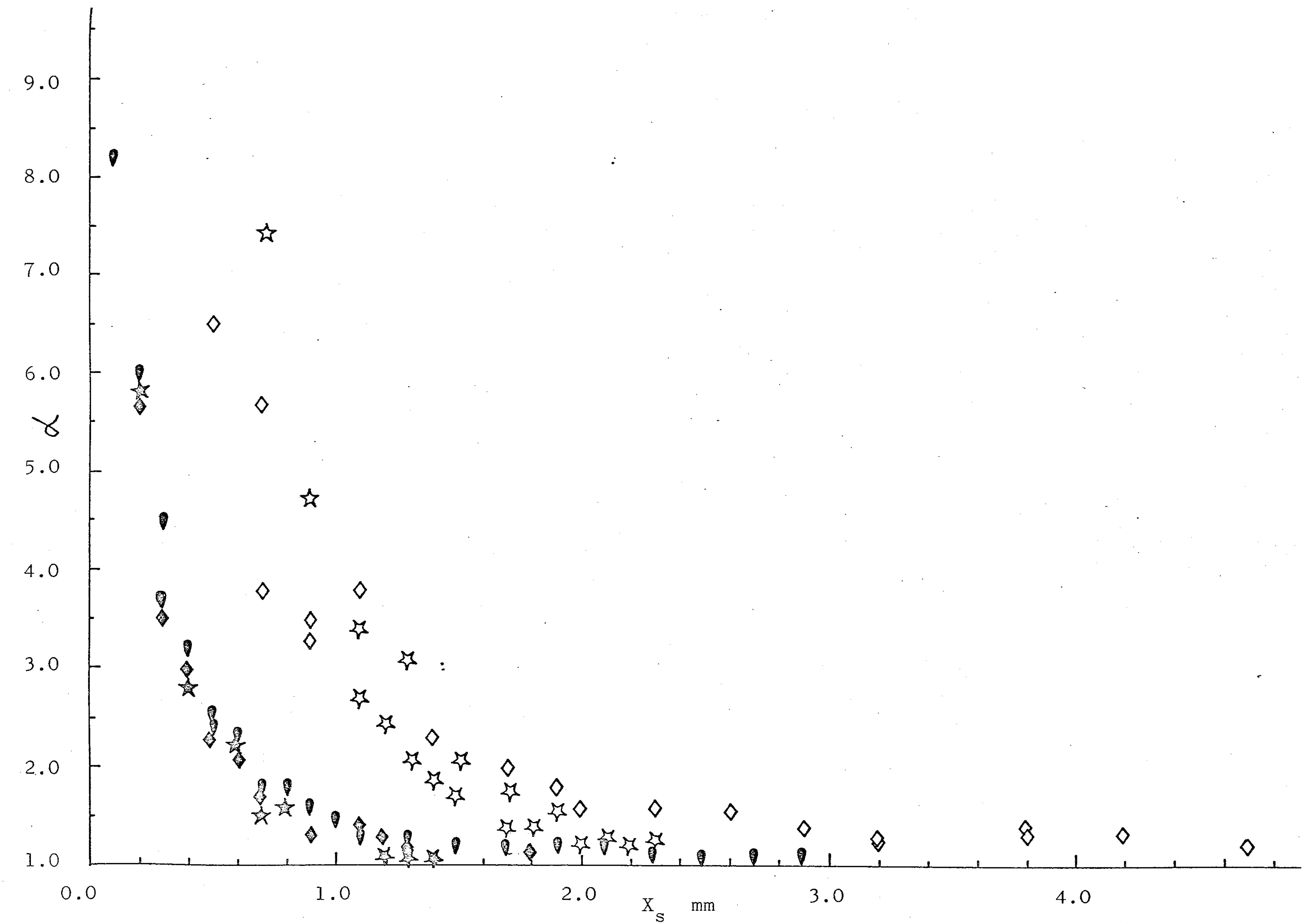

FIG.63 α vs. X_s CORRECTED VALUES (20 % He-80 % N)

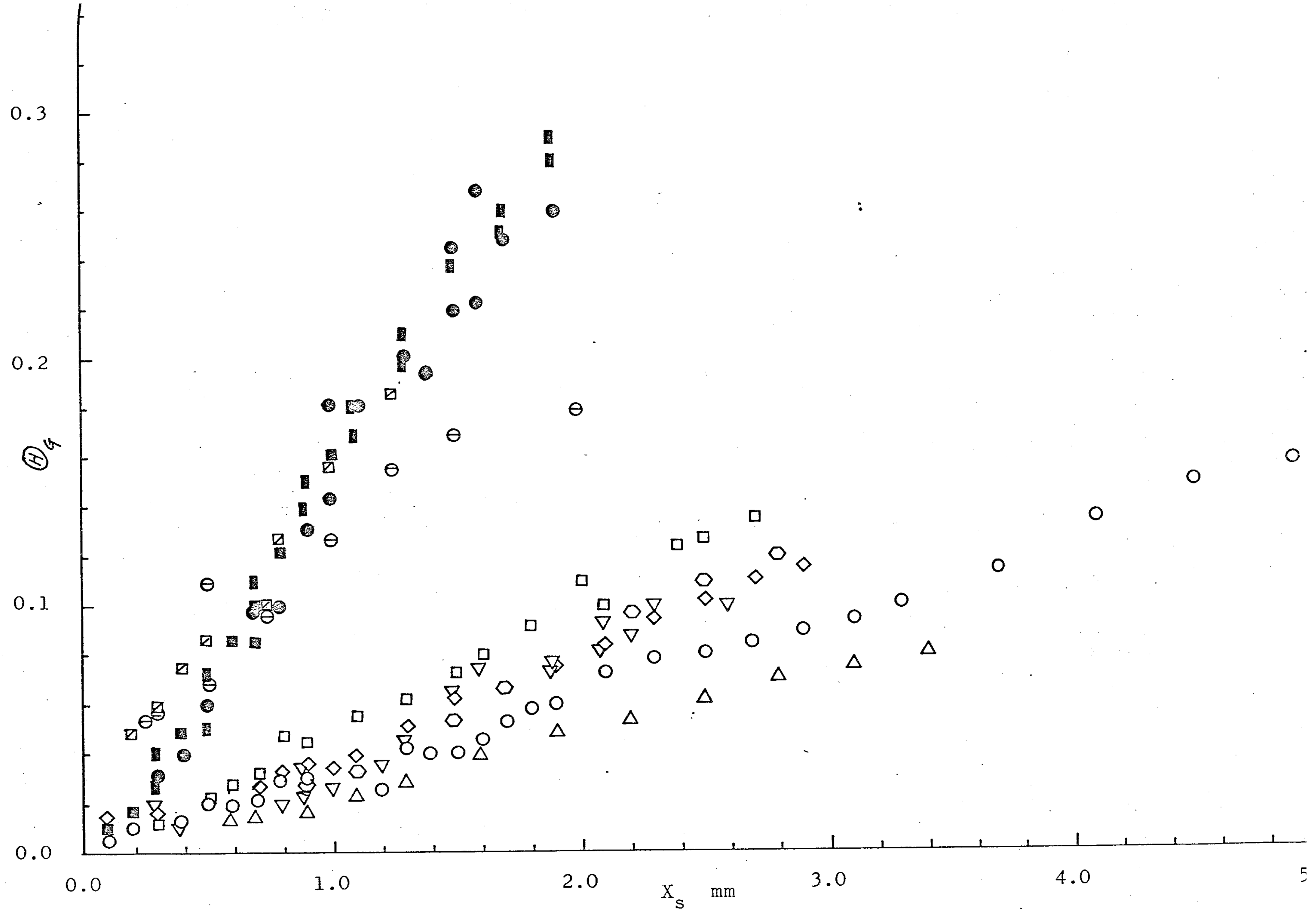

FIG.64 Θ_g vs. X_s, CORRECTED VALUES (50% H_2-50% N_2)

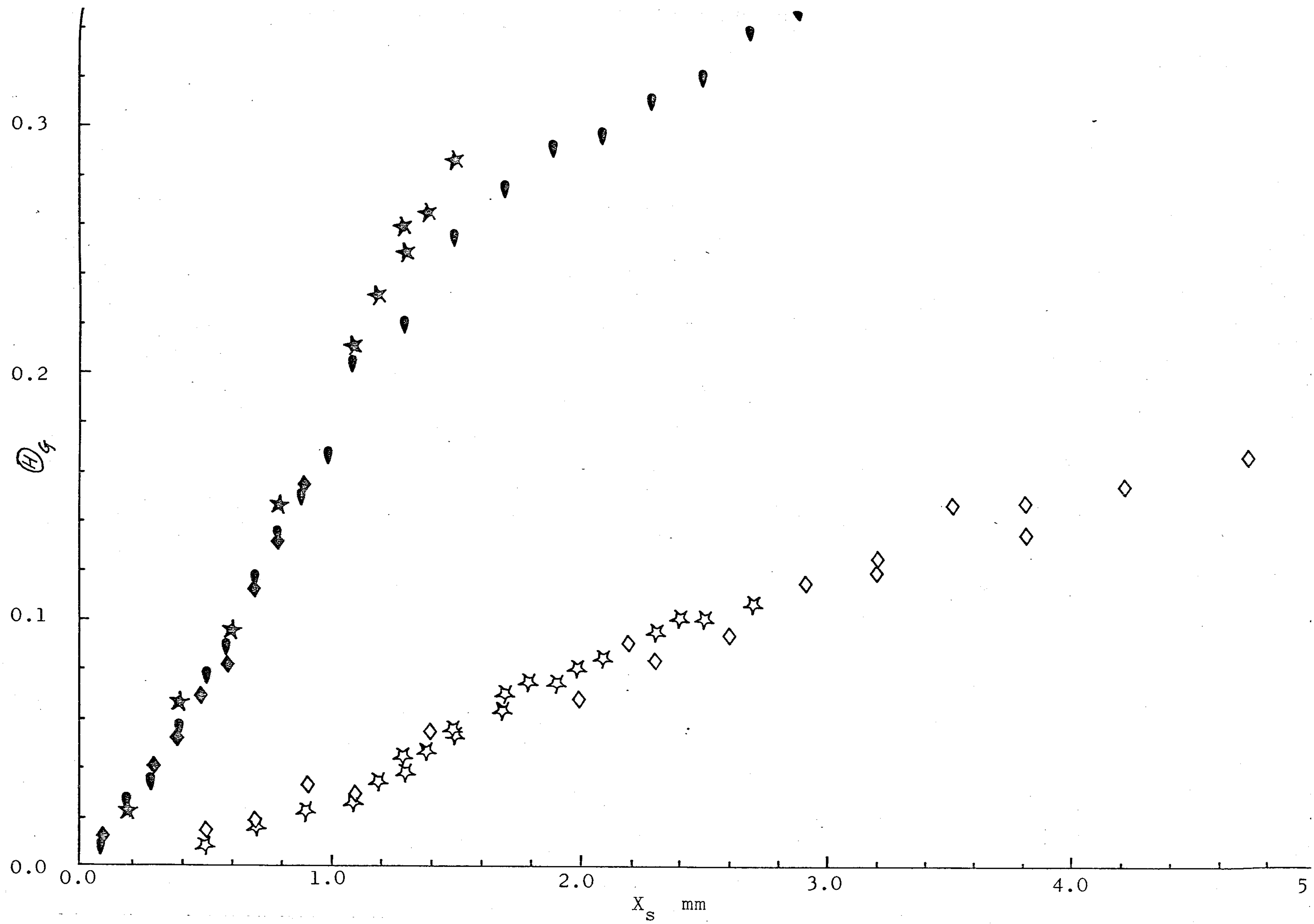

FIG.65 Θ_g vs. X_s, CORRECTED VALUES (20 % He-80 % N_2)

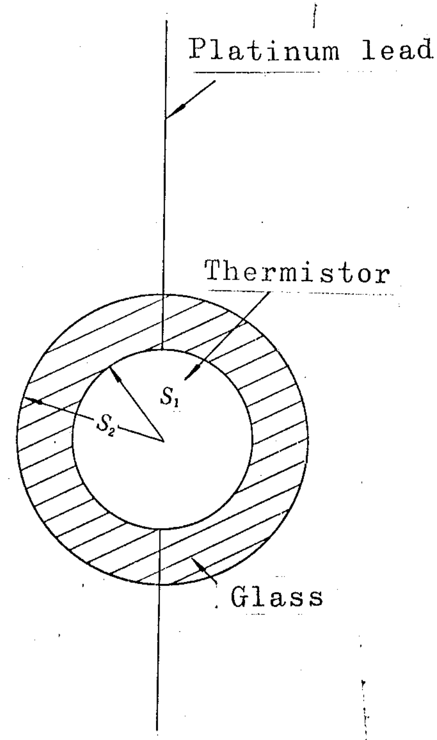

FIG.66 SCHEMATIC DIAGRAM OF THERMISTOR ELEMENT
$S_1/S_2 \simeq 1.0$

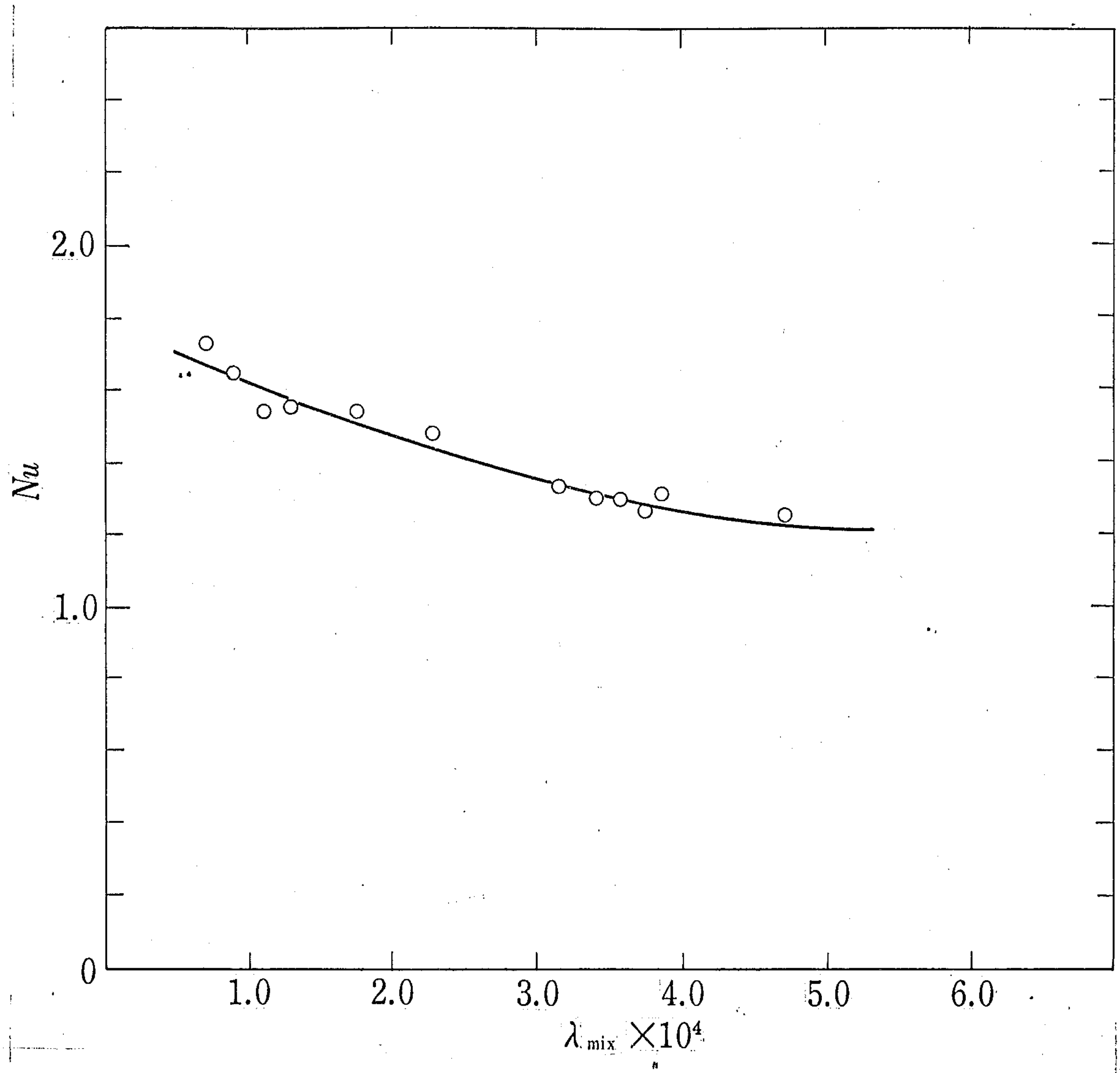

FIG.67 APPARENT NUSSELT NUMBER AS A FUNCTION OF THERMAL CONDUCTIVITY OF GAS

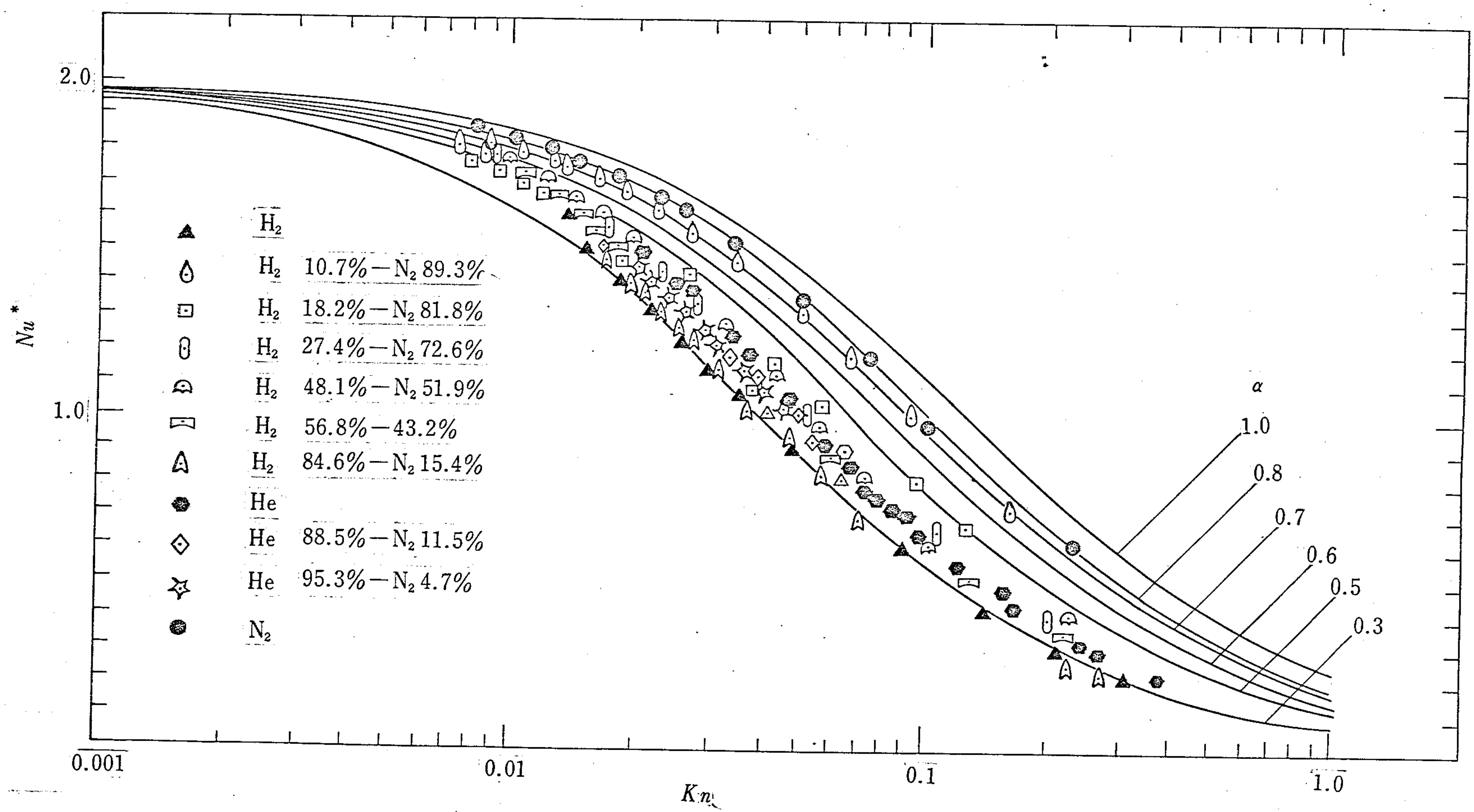

FIG.68 RELATION BETWEEN Nu* AND Kn FOR VARIOUS GAS MIXTURES

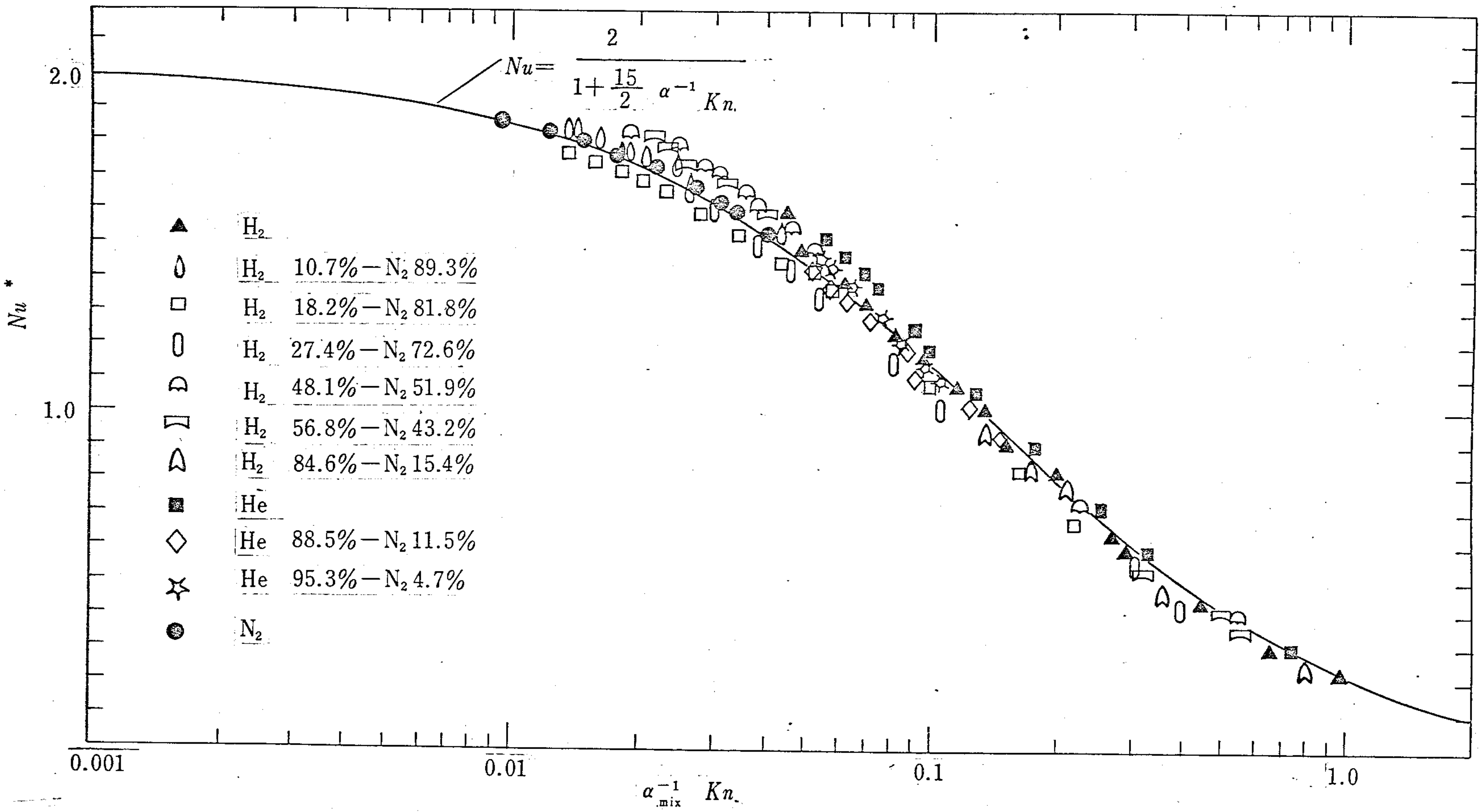

FIG.69 RELATION BETWEEN Nu*AND $Kn\alpha_{mix}^{-1}$

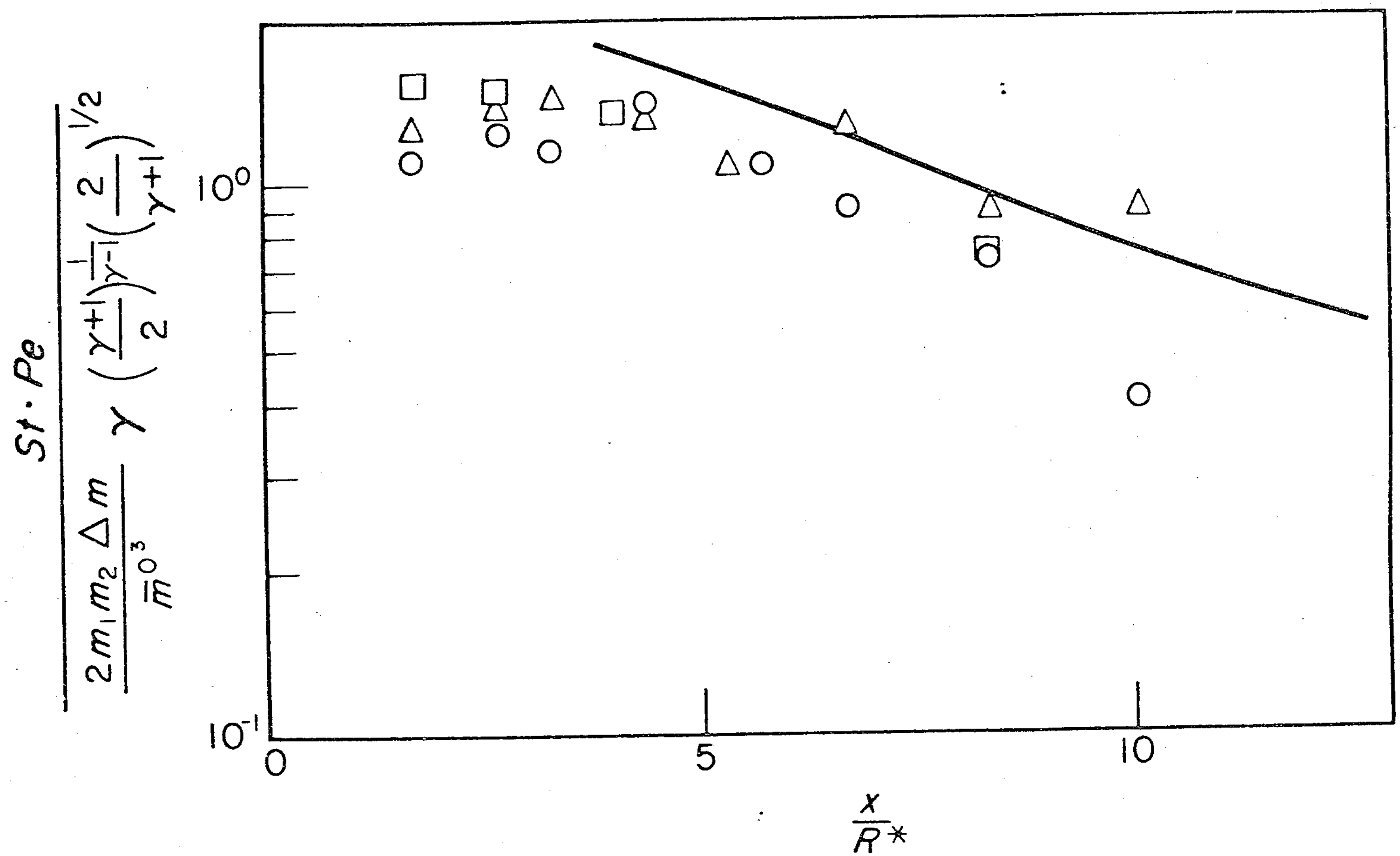

FIG.70 SUMMARY OF THE SEPARATION RESULTS

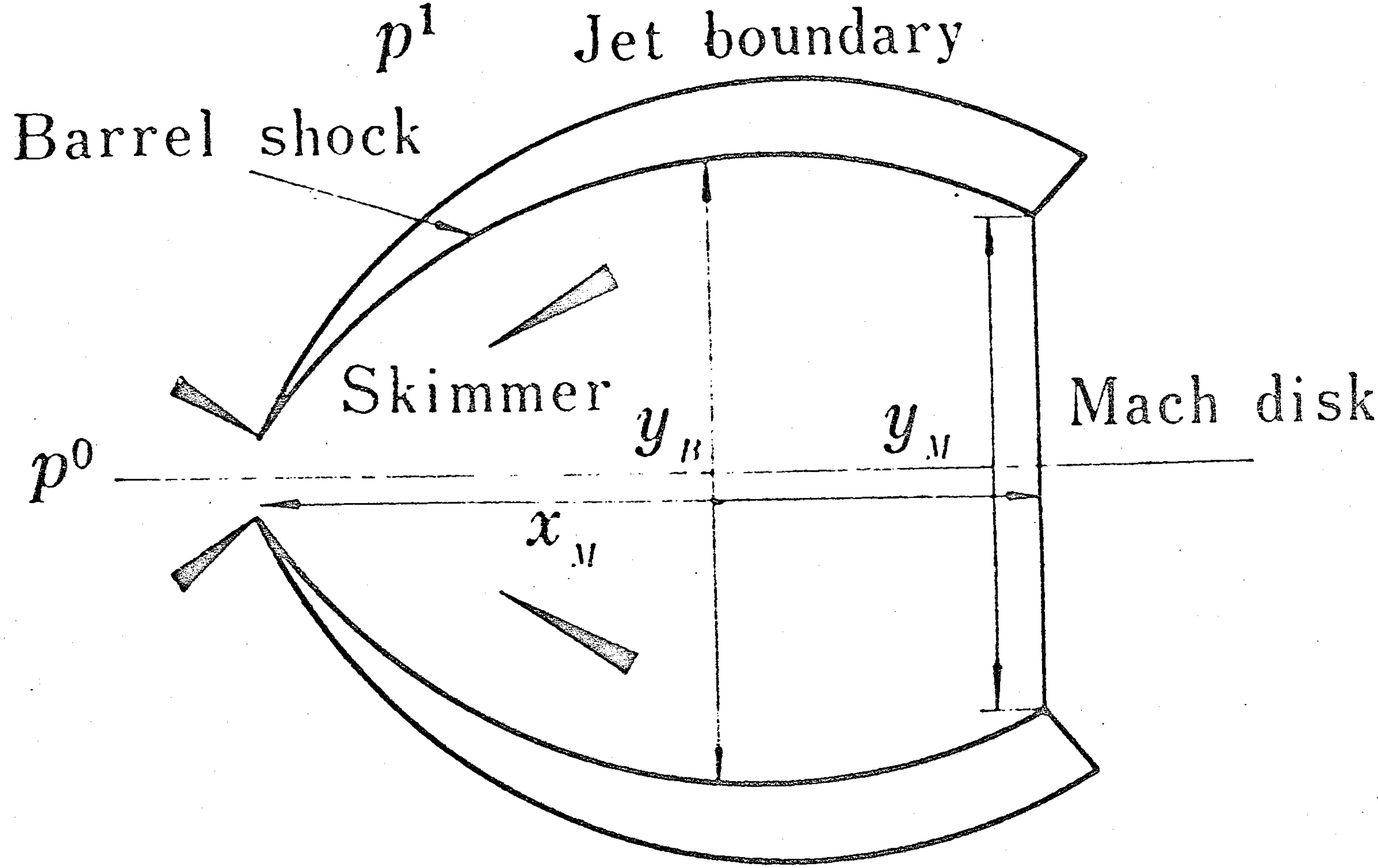

FIG.71 FLOW GEOMETRY OF SUPAERSONIC FREE JET

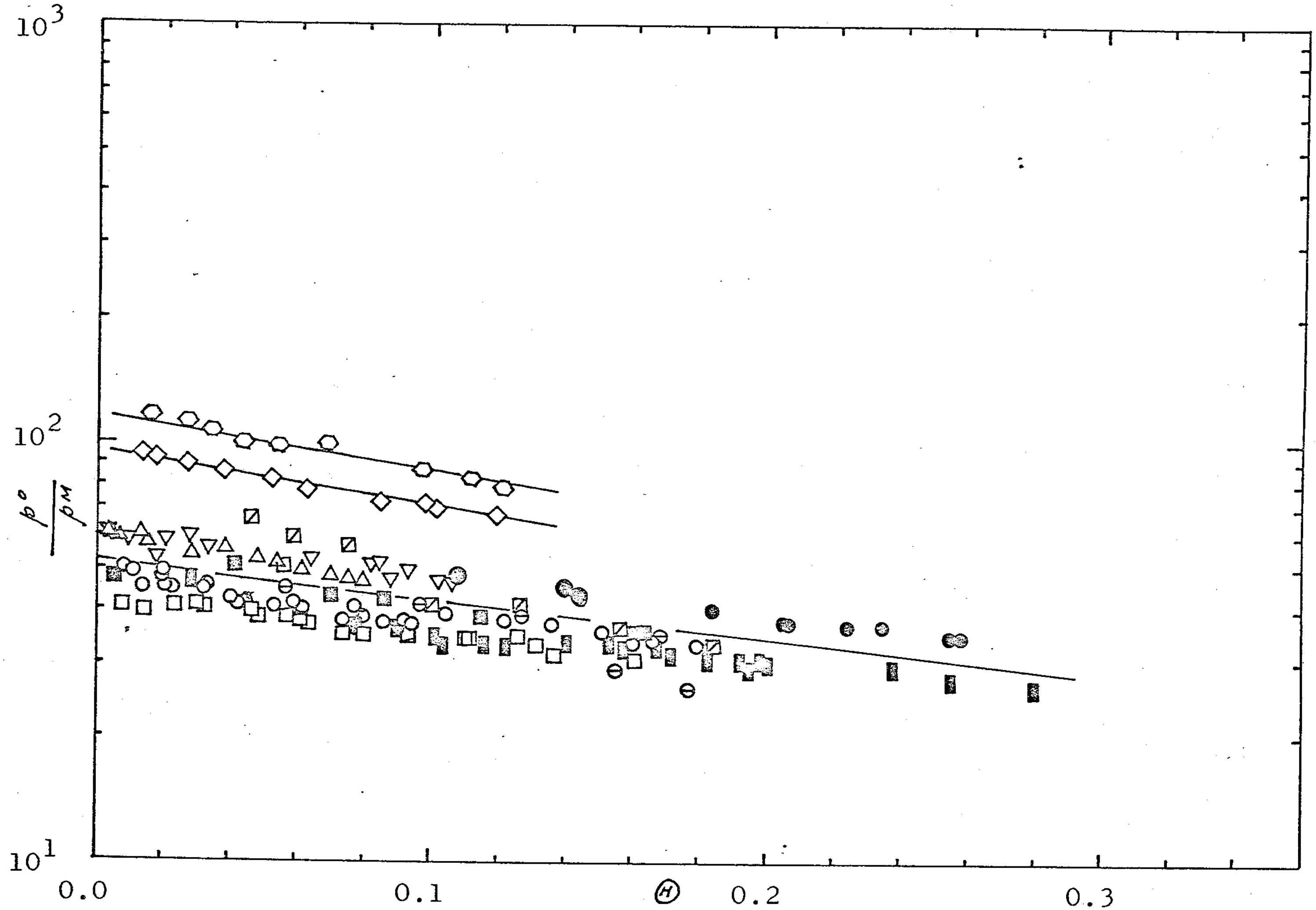

FIG.72 EXPANSION PRESSURE RATIO AS A FUNCTION OF CUT (50 % H_2-50 % N_2)

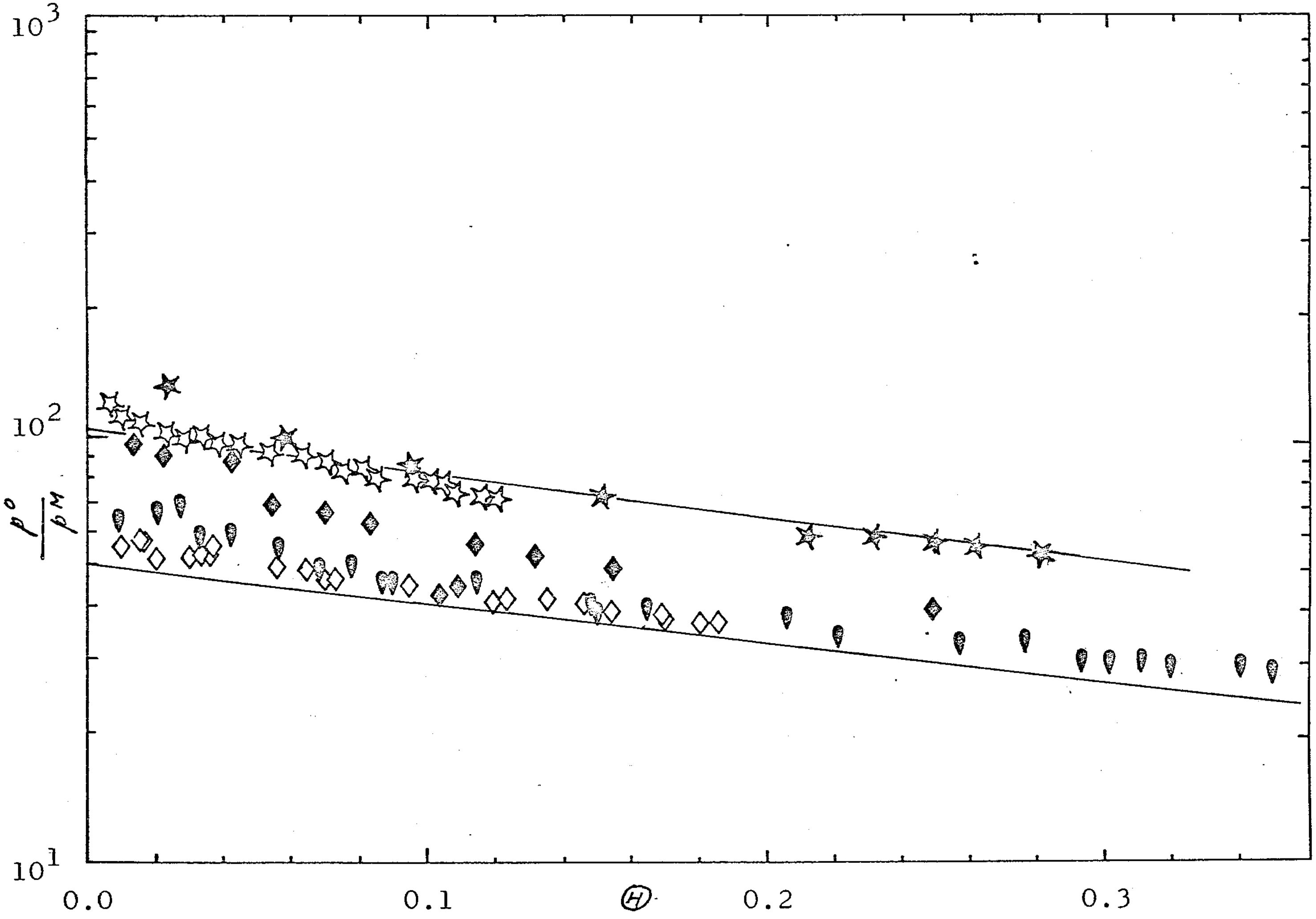

FIG.73 EXPANSION PRESSURE RATIO AS A FUNCTION OF CUT (20 % He-80 % N_2)

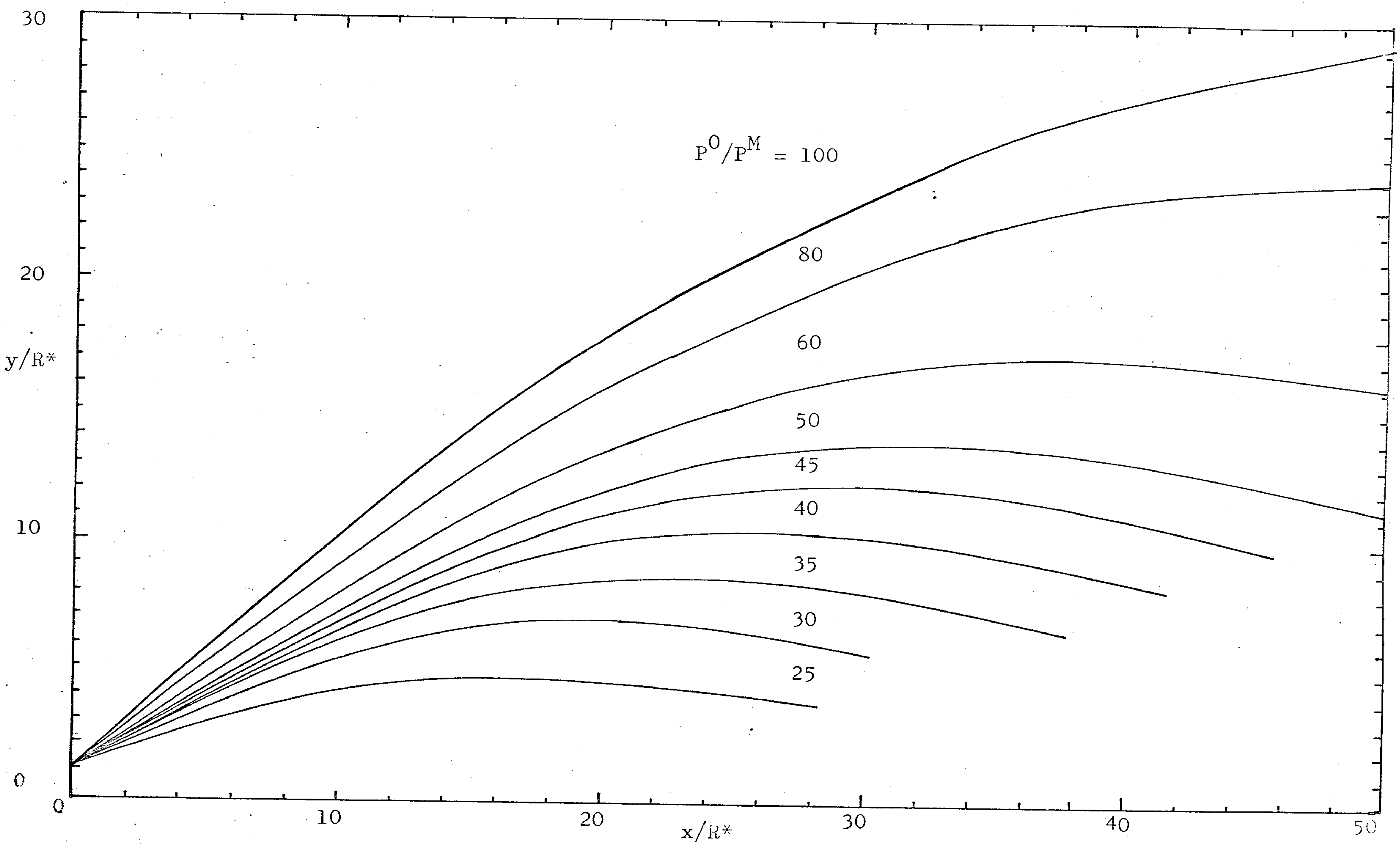

FIG.74 BARREL SHOCK PROFILE IN A TWO-DIMENSIONAL SUPERSONIC JET

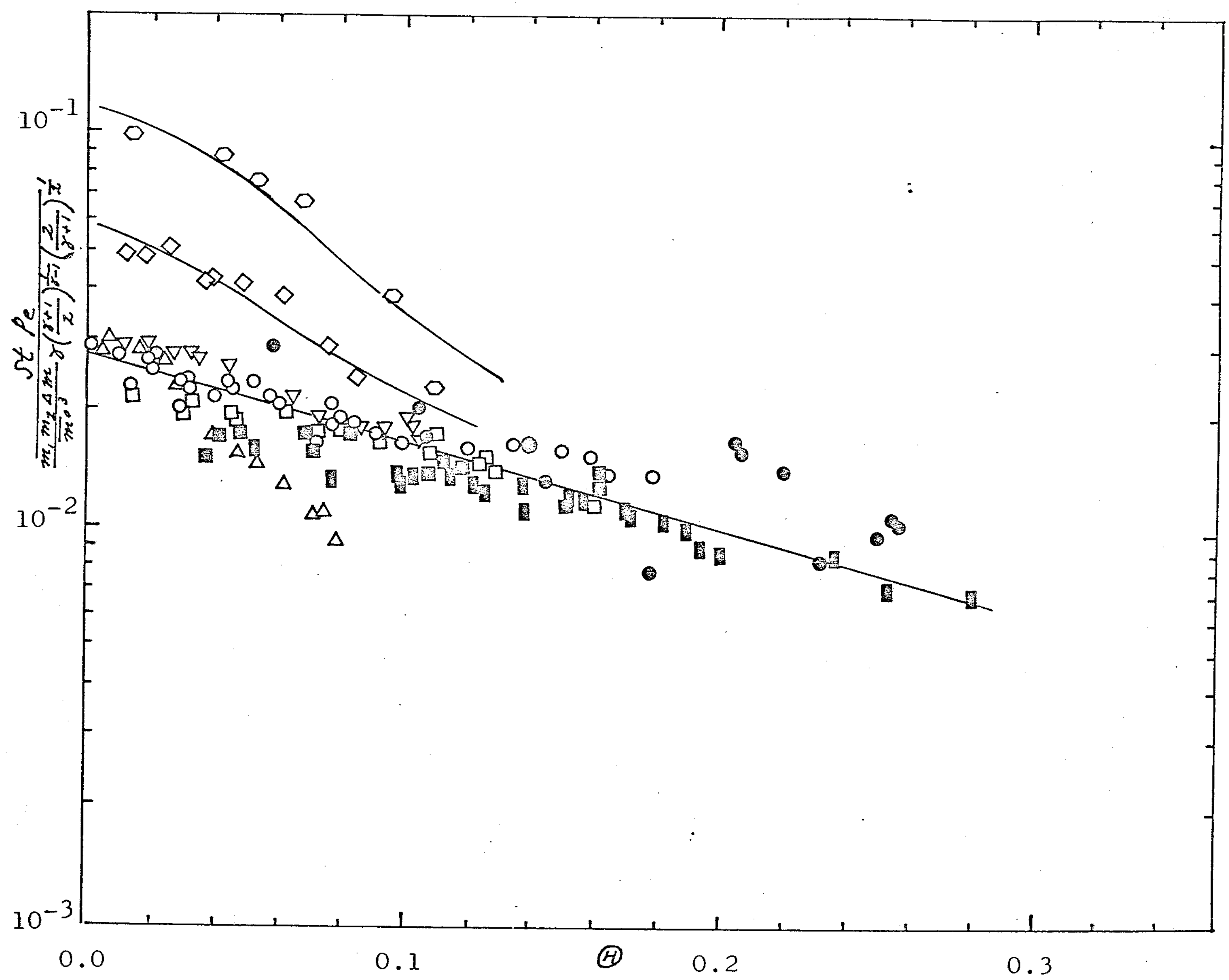

FIG.75 INTEGRAL MASS FLUX AS A FUNCTION OF CUT ($50\%\ H_2-50\%\ N_2$)

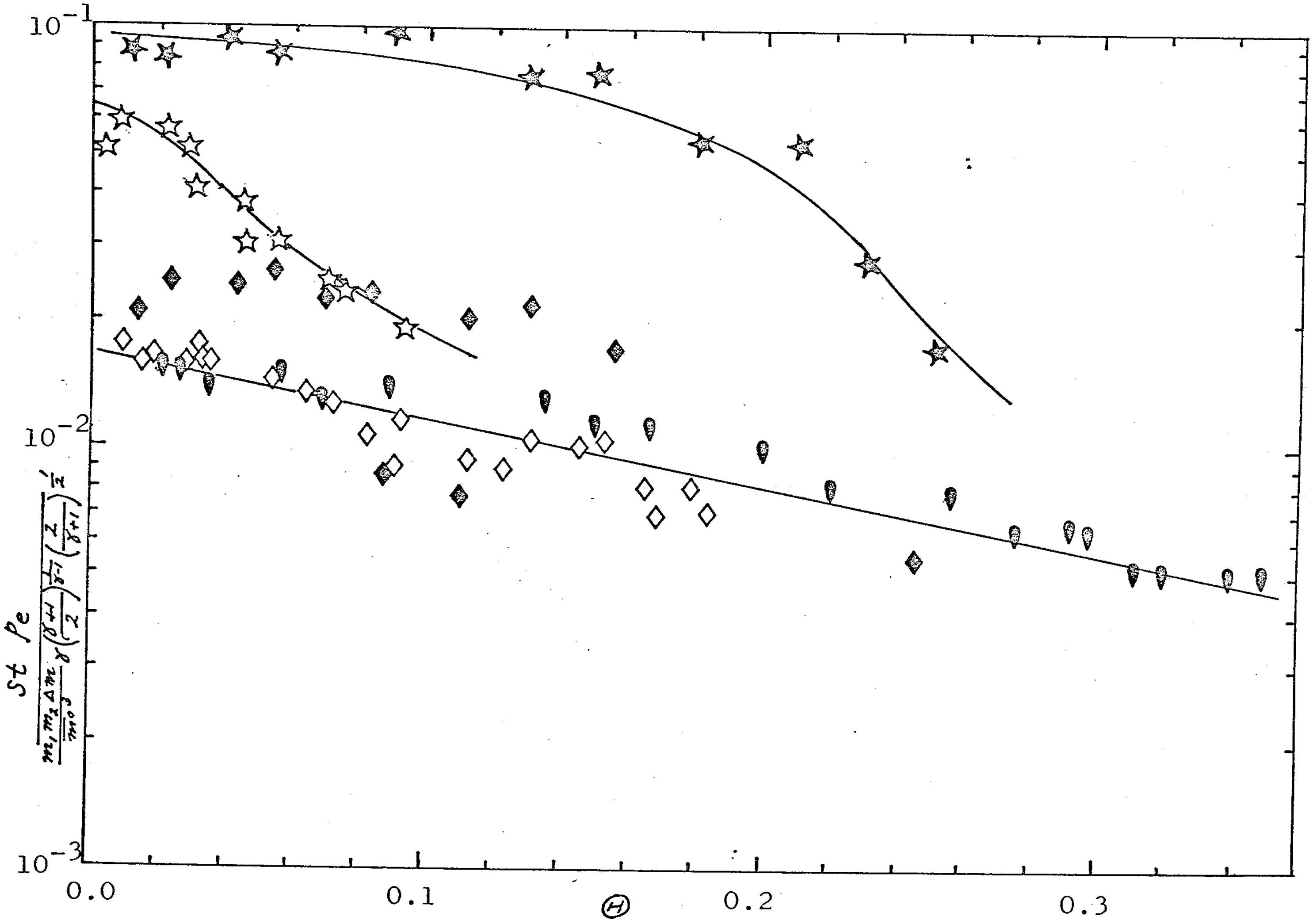

FIG.76 INTEGRAL MASS FLUX AS A FUNCTION OF CUT (20 % He-80 % N_2)

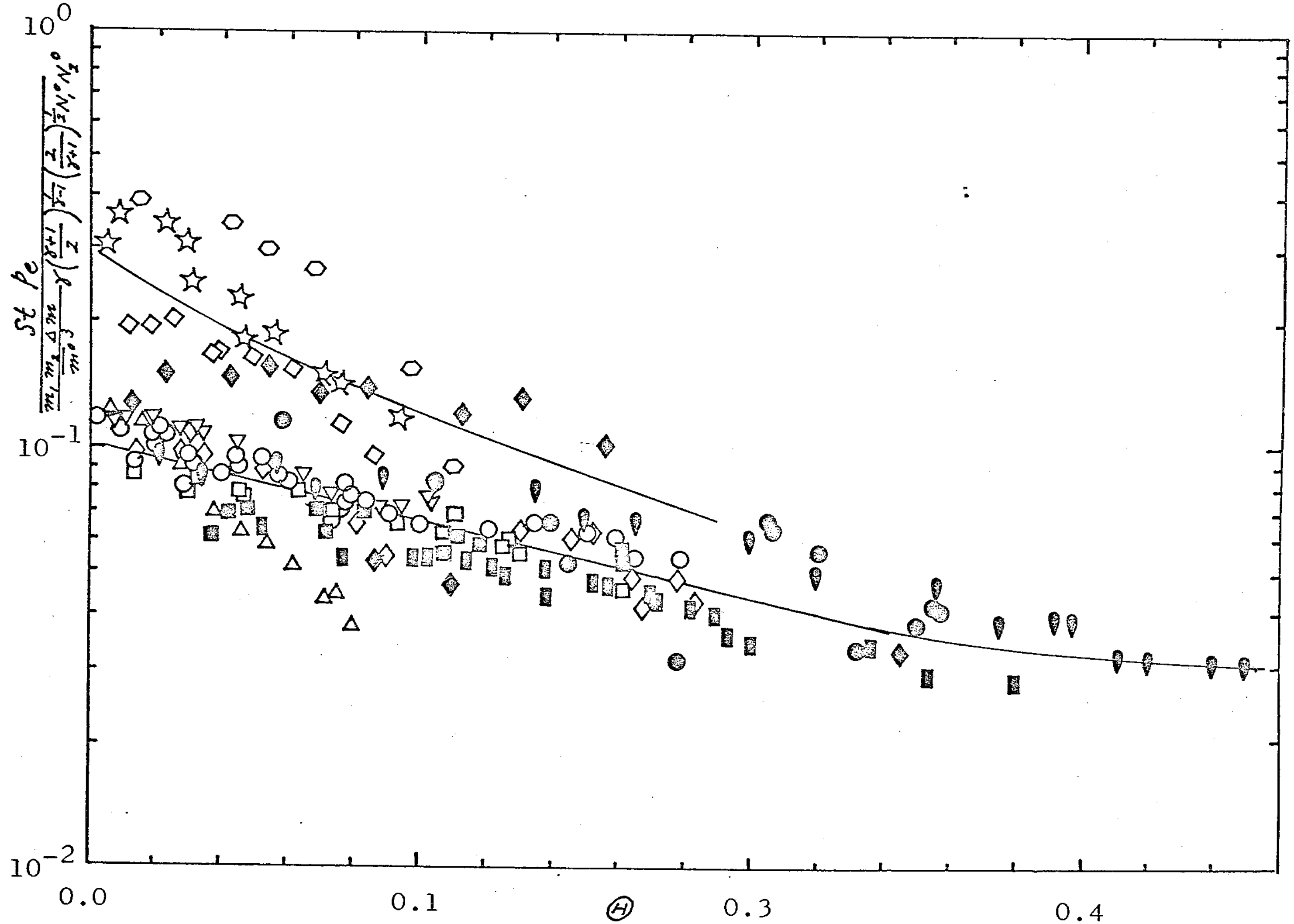

FIG.77 SUMMARY OF EXPERIMENTAL DATA FOR INTEGRAL MASS FLUX

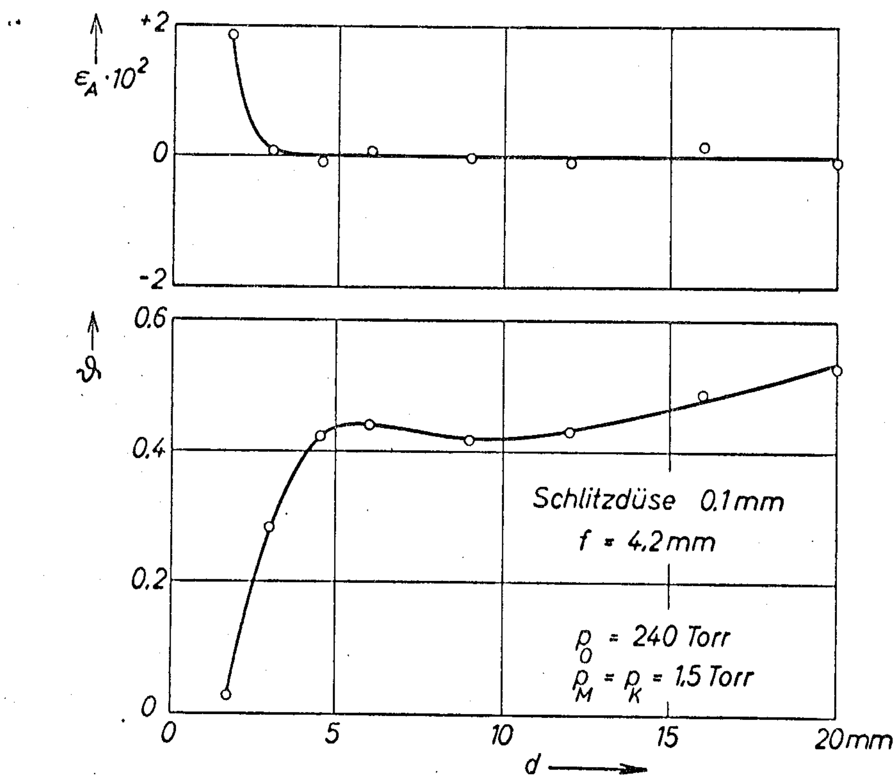

FIG.78. BIER'S EXPERIMENTAL DATA FOR $^{36}Ar/^{40}Ar$ ISOTOPE MIXTURE
Zeitschrift für Naturforschung, 15a, 714 (1960)

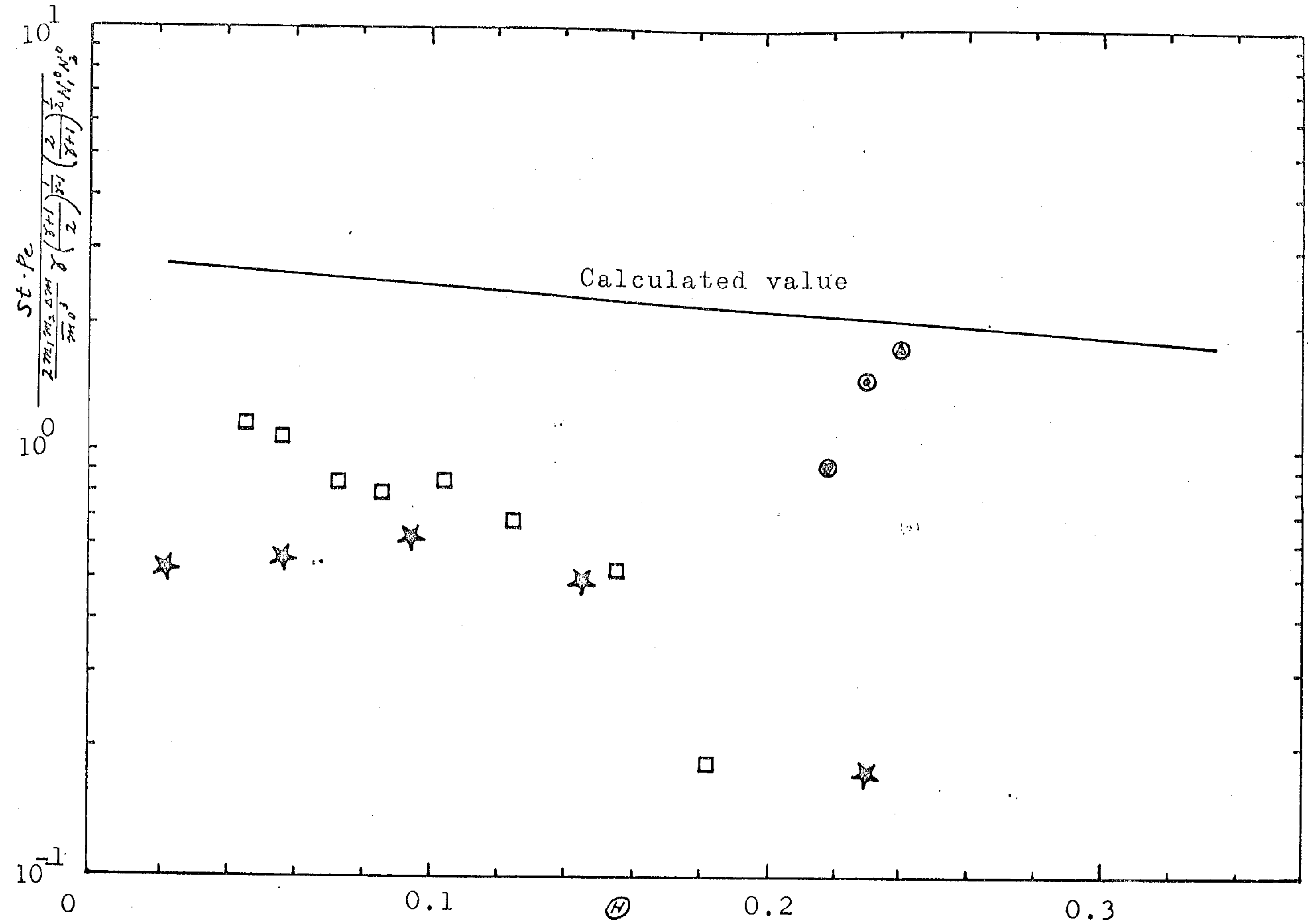

FIG.79 COMPARISON OF DIFFUSIVE SEPARATION BETWEEN EXPERIMENTAL DATA AND THEORETICAL PREDICTION
SYMBOLS ⊗ ⊙ AND ⊗ DENOTE BECKER'S EXPERIMENTAL DATA FOR Ar/UF_6 MIXTURE, $2R^*=0.05$ mm, $x_s=0.05$ mm, $y_s=0.05$ mm, $P^o/P^M = P^o/P^K = 20$.

	P^0
⊗	30 mm Hg
⊙	40 mm Hg
⊗	120 mm Hg

Z. Naturforschg. 18a, 246 (1963)

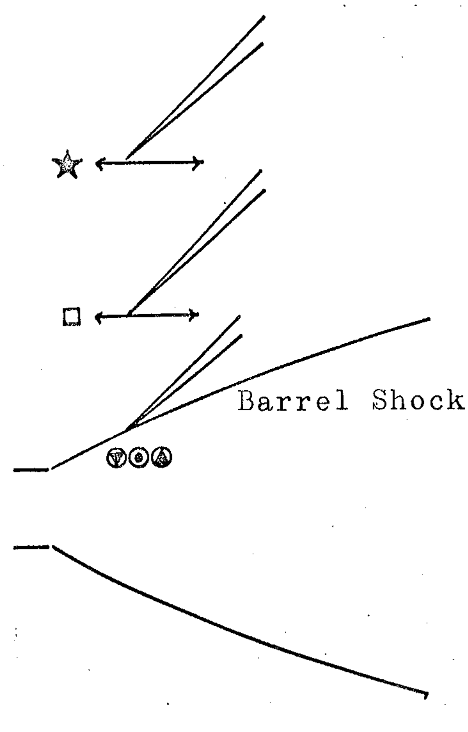

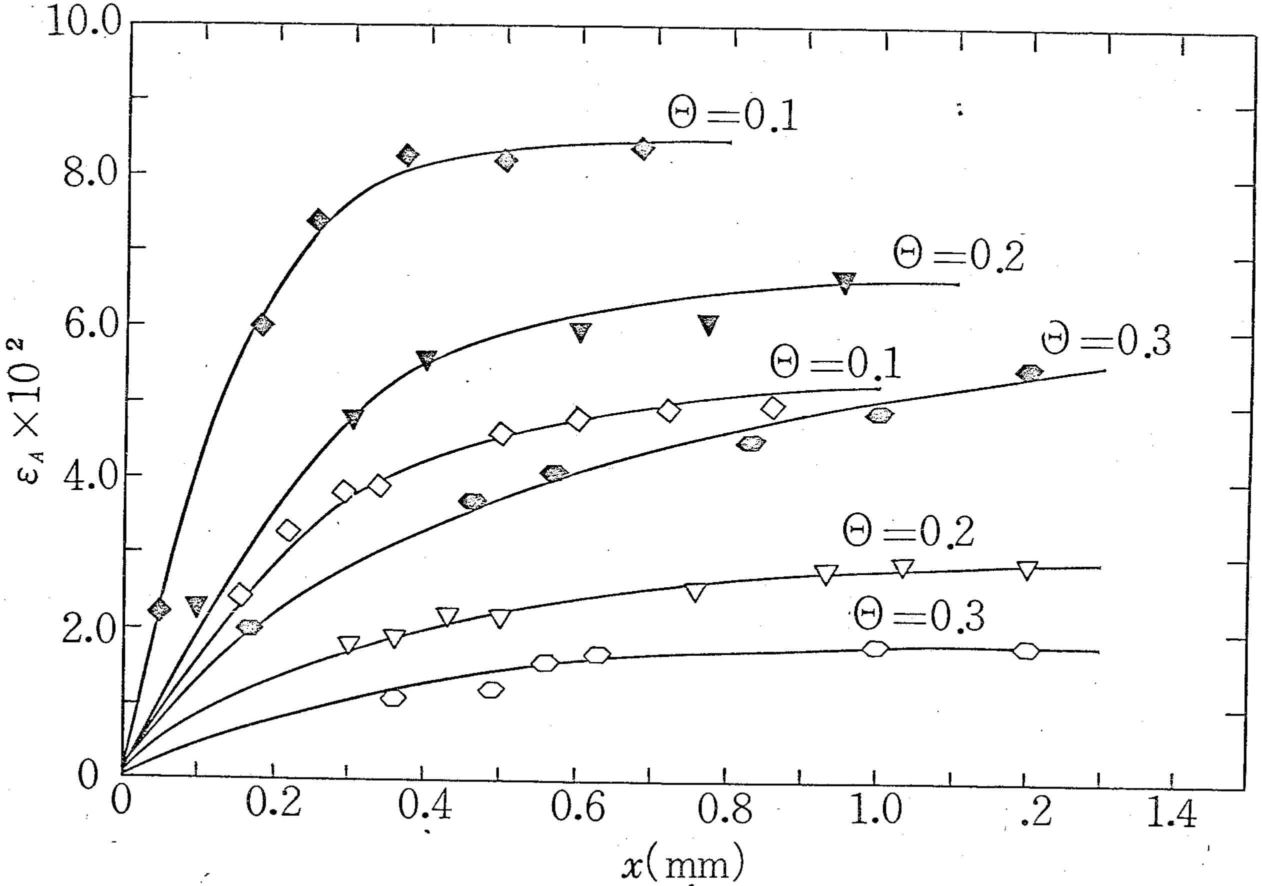

FIG. 80 EXPERIMENTAL DATA OBTAINED ON SEPARATION EFFECT ε_A FOR $^{36}A/^{40}A$ MIXTURE, OBTAINED BY BECKER, ET AL.(51). $p°$ =30 mmHg(◆▼⬣) AND $p°$=80 mmHg(◇▽⬡)

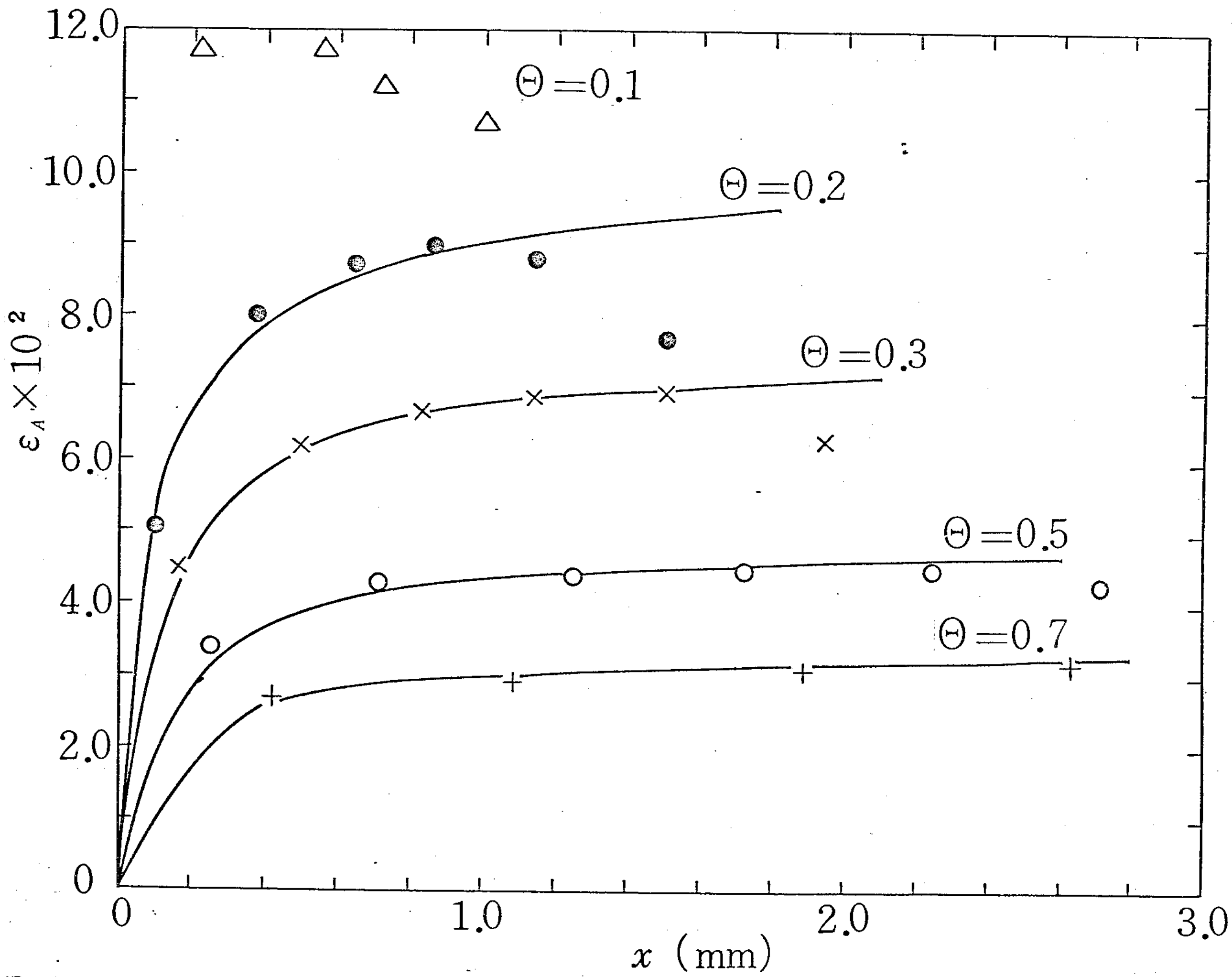

FIG. 81 EXPERIMENTAL DATA OBTAINED ON SEPARATION EFFECT ε_A FOR $^{36}A/^{40}A$ MIXTURE, OBTAINED BY BECKER, ET AL. (29) p°=1 6 mmHg

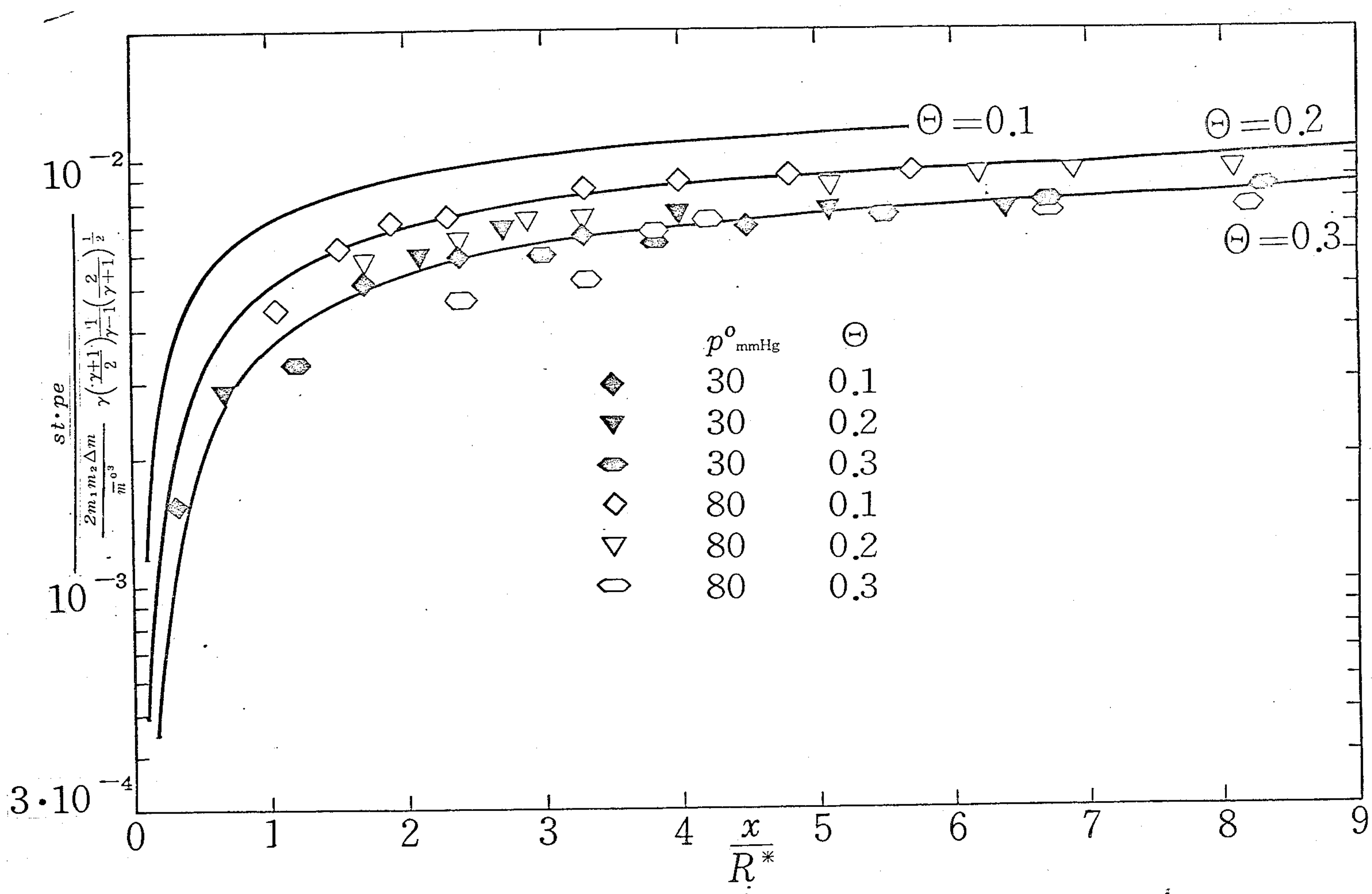

FIG.82 COMPARISON OF EXPERIMENTAL DATA ON DIFFUSIVE SEPARATION WITH THEORETICAL PREDICTIONS

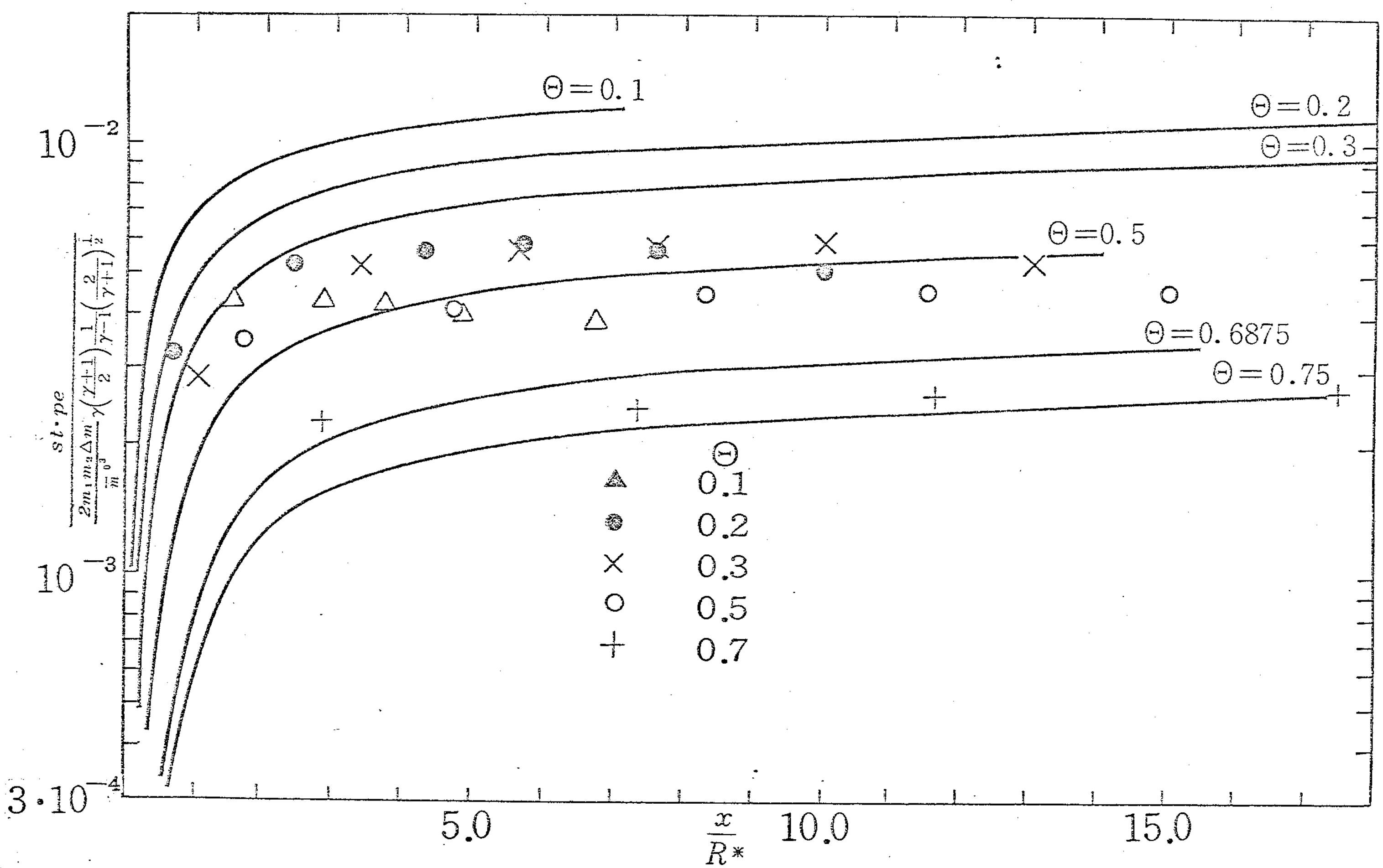

FIG.83 COMPARISON OF EXPERIMENTAL DATA ON DIFFUSIVE SEPARATION WITH THEORETICAL PREDICTIONS

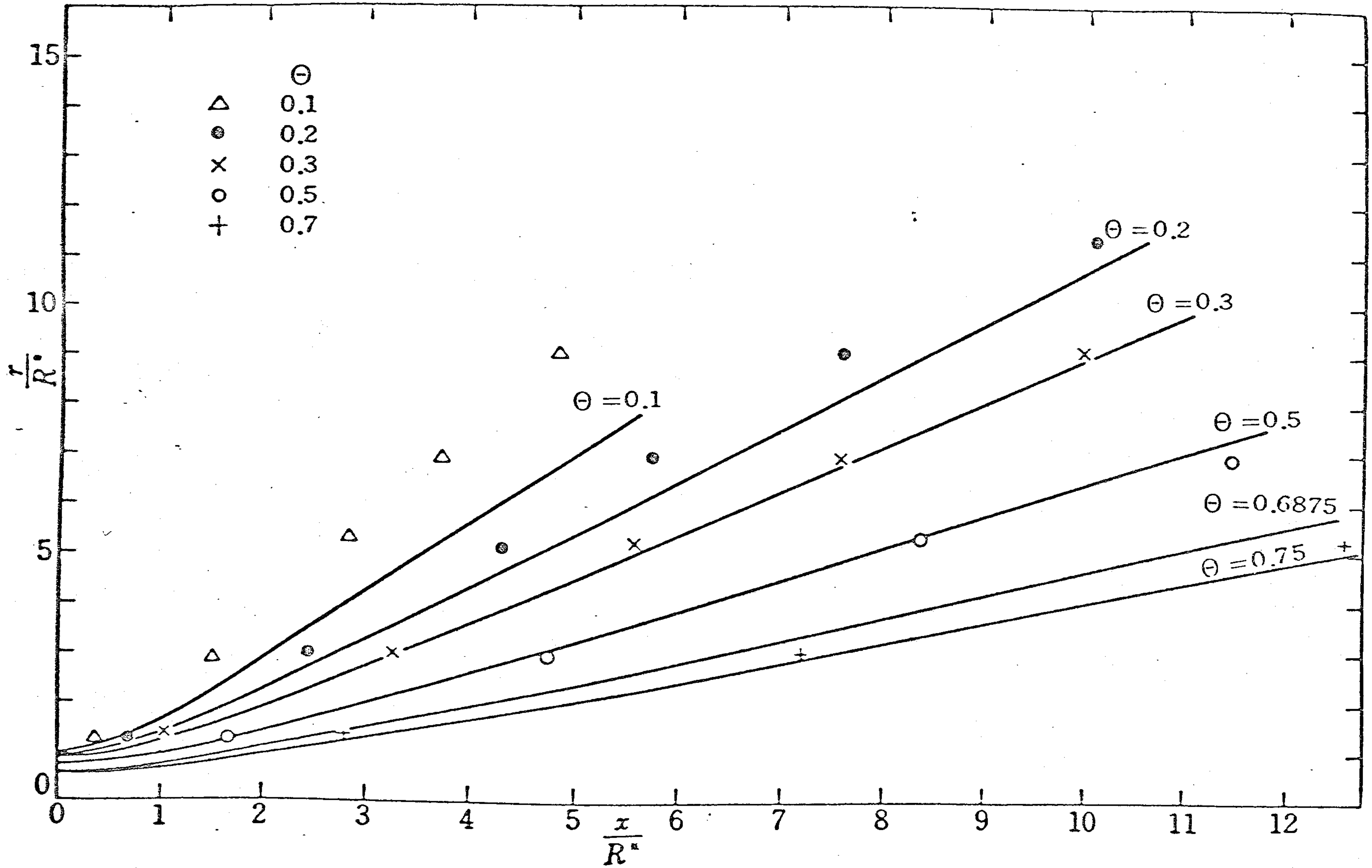

FIG. 84 CALCULATED AND EXPERIMENTAL RESULTS ON STREAMLINES
CUT AS A PARAMETER, PURE ARGON

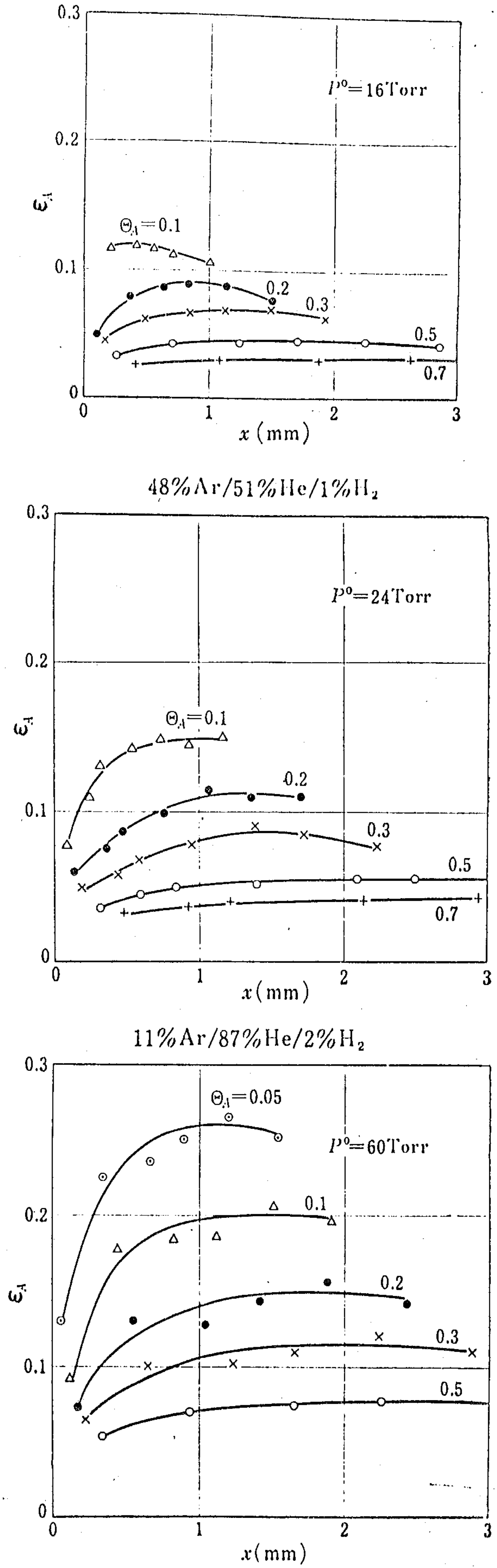

FIG.85 SEPARATION DATA FOR ARGON ISOTOPES BECKER ET AL.(29)

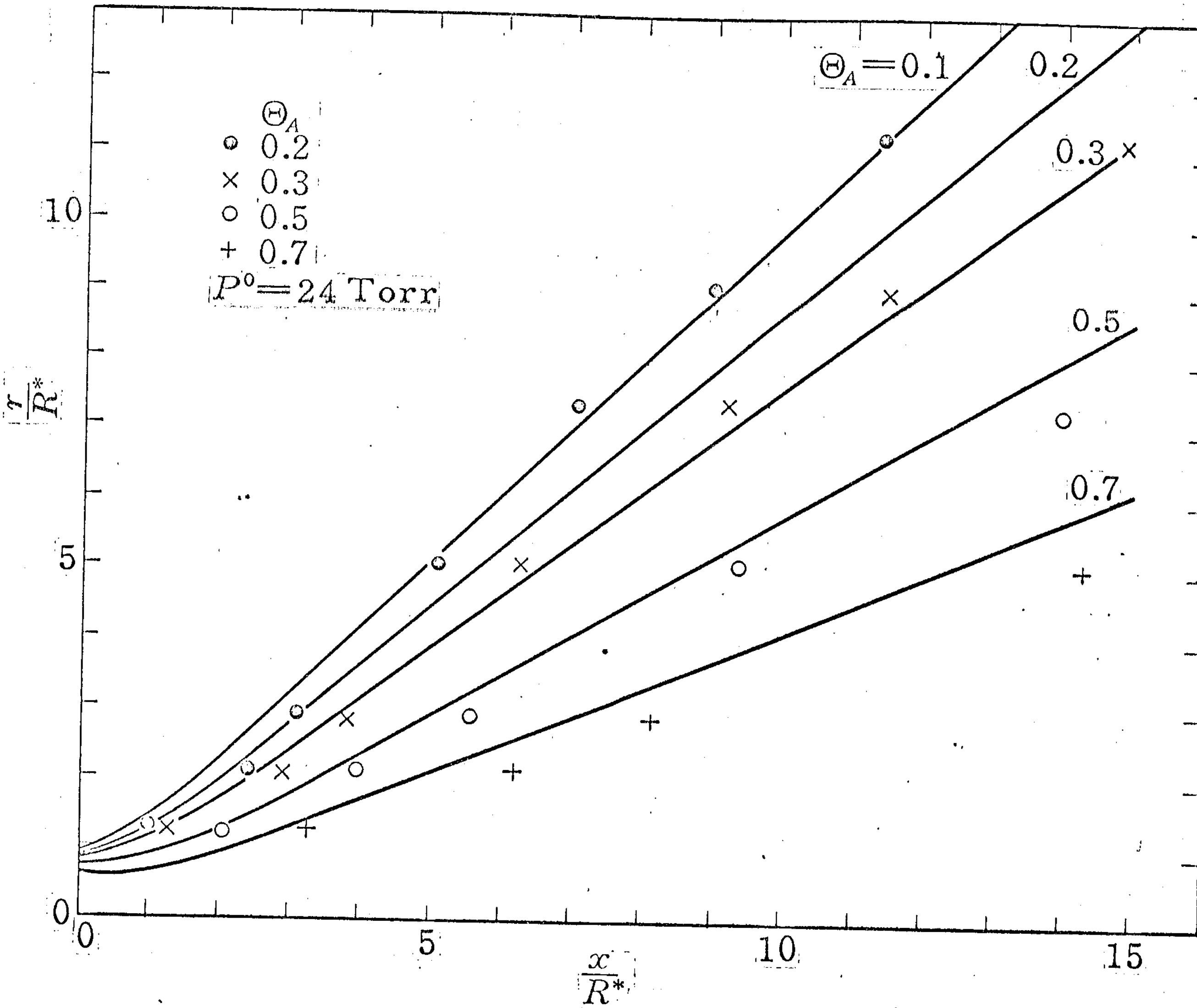

FIG. 86 CALCULATED AND EXPERIMENTAL RESULTS ON STREAMLINES OF ARGON GAS
CUT OF ARGON AS A PARAMETER
CASE I ●, ×, ○, +,
EXPERIMENTAL DATA ORESENTED BY BECKER ET AL. FOR $Ar(0.48)$, $H_2(0.01)$, AND $He(0.51)$ GAS MIXTURE, WHERE NUMERICAL VALUES IN BRANCKETS MEAN MOLE FRACTIONS AT NOZZLE INLET

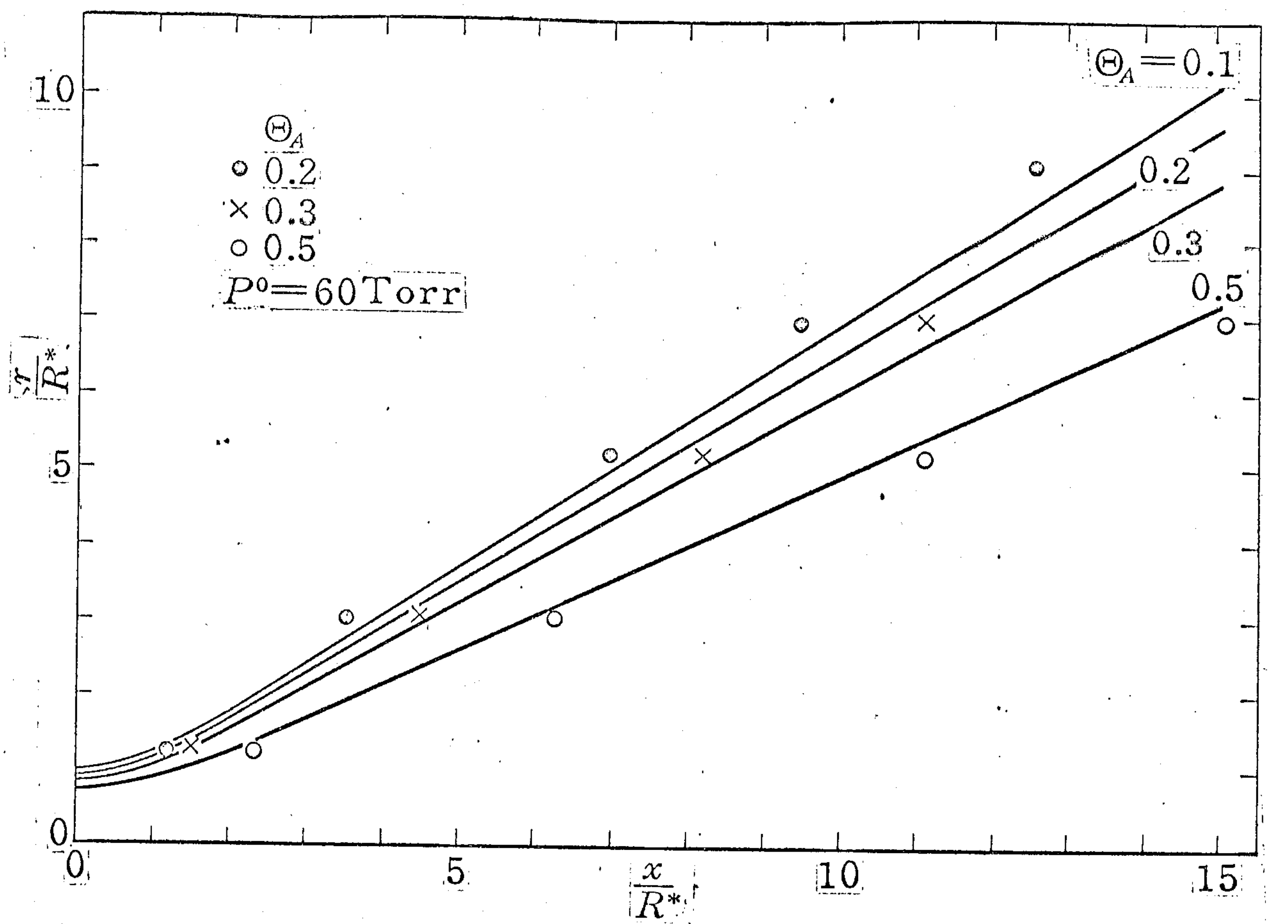

FIG.87 CALCULATED AND EXPERIMENTAL RESULTS ON STREAMLINES OF ARGON GAS
CUT OF ARGON AS A PARAMETER
CASE II ● , × , ○ , EXPERIMENTAL DATA BY BECKER ET AL. FOR Ar(0.11), H_2(0.02), AND He(0.87) GAS MIXTURE

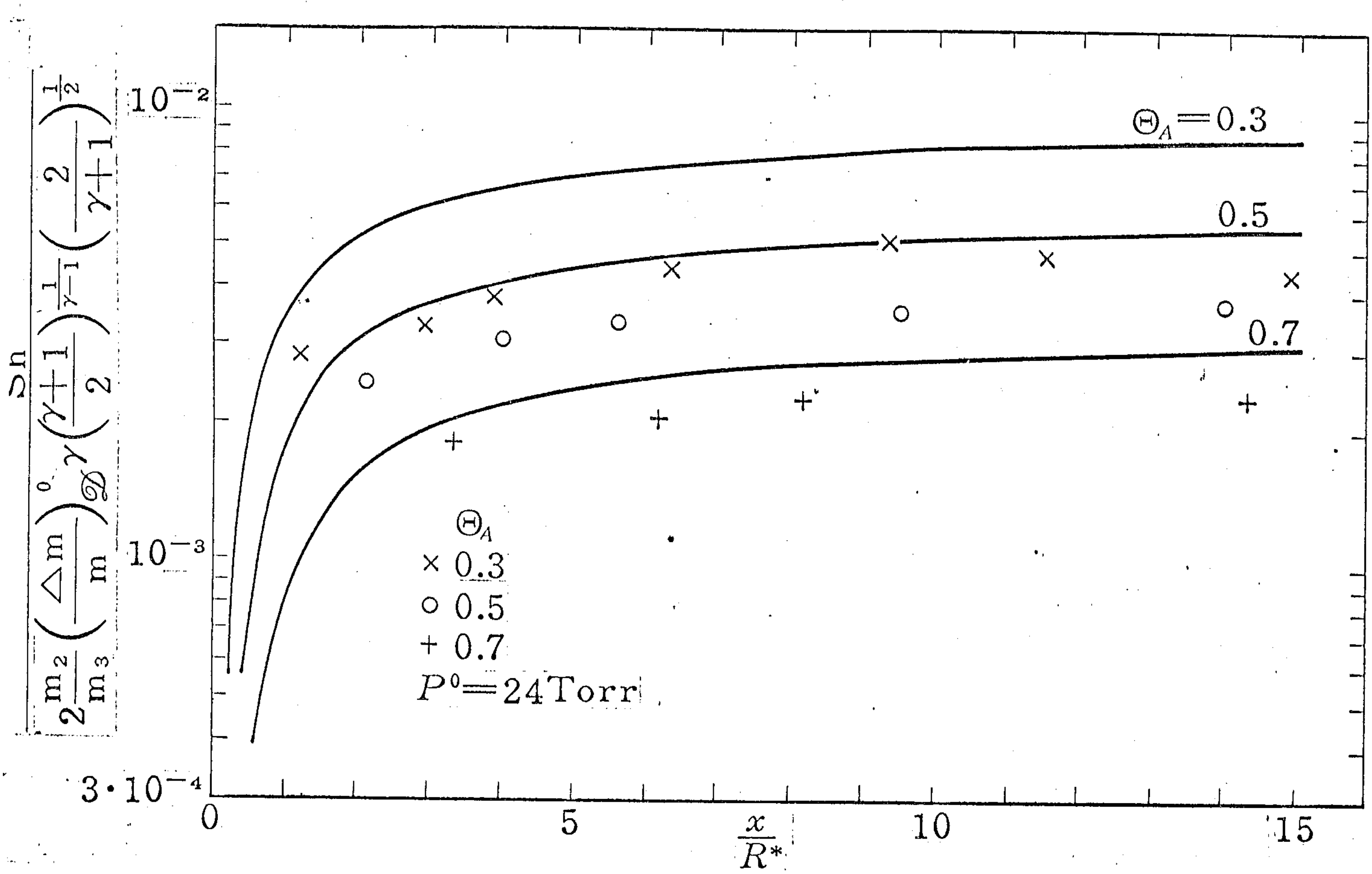

FIG.88 COMPARISON OF EXPERIMENTAL DATA ON DIFFUSIVE SEPARATION OF ARGON ISOTOPES WITH THEORETICAL PREDICTIONS . CASE I

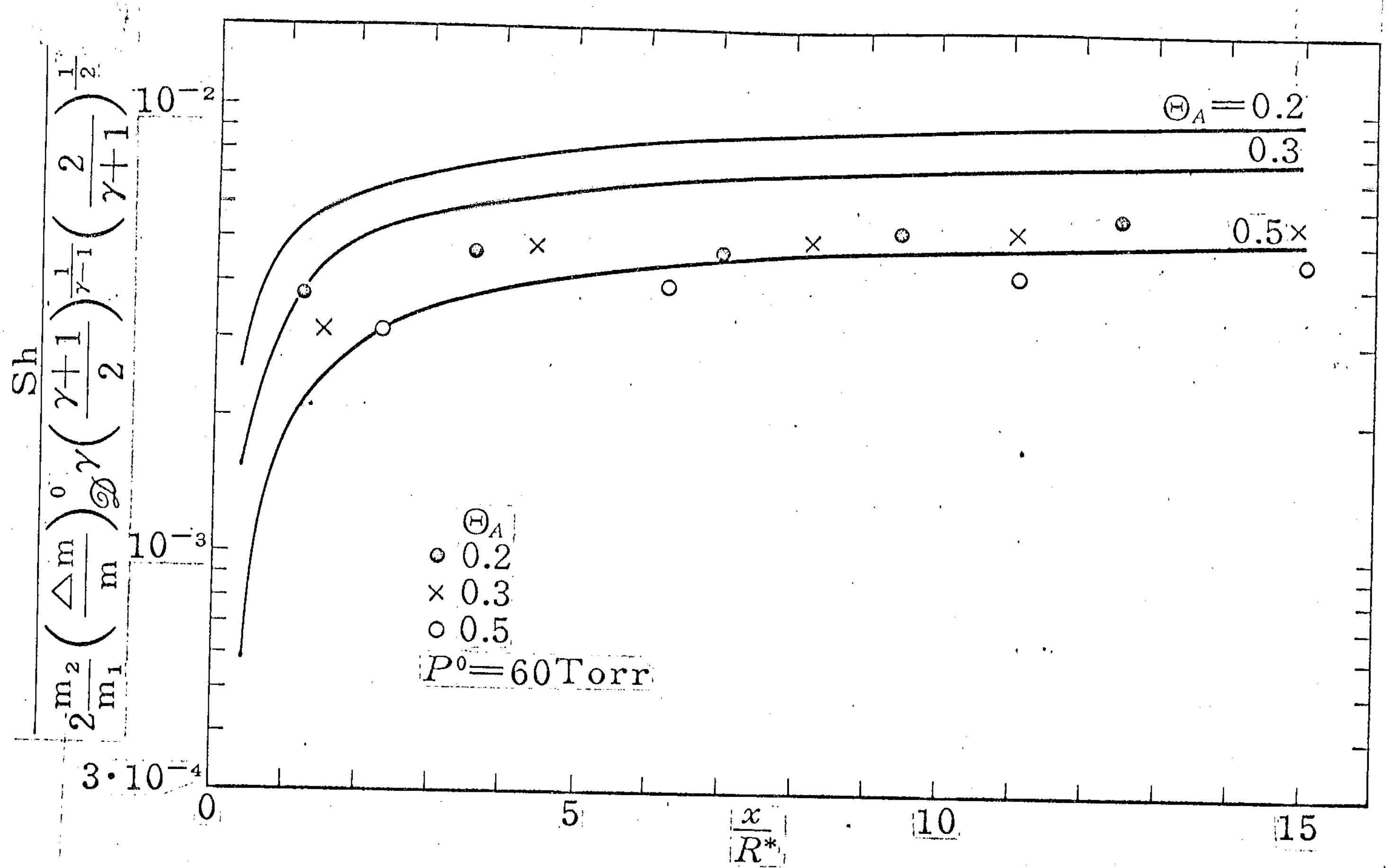

FIG. 89 COMPARISON OF EXPERIMENTAL DATA OF DIFFUSIVE SEPARATION OF ARGON ISOTOPES WITH THEORETICAL PREDICTIONS CASE II

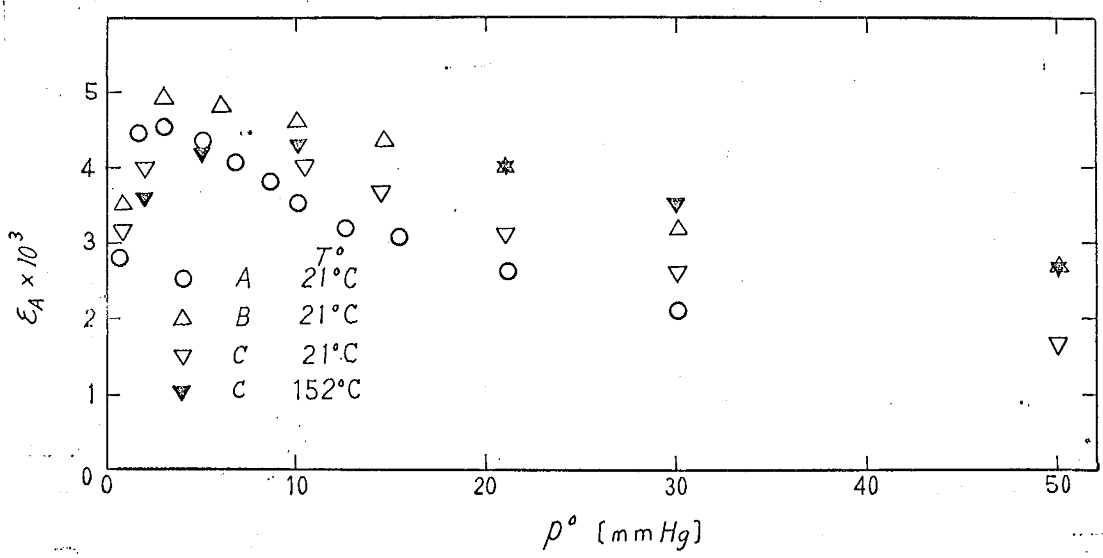

FIG. 90 EXPERIMENTAL DATA ON SEPARATION EFFECT FOR $^{235}UF_6/^{238}UF_6$ MIXTURE, AFTER BECKER ET AL.(53)

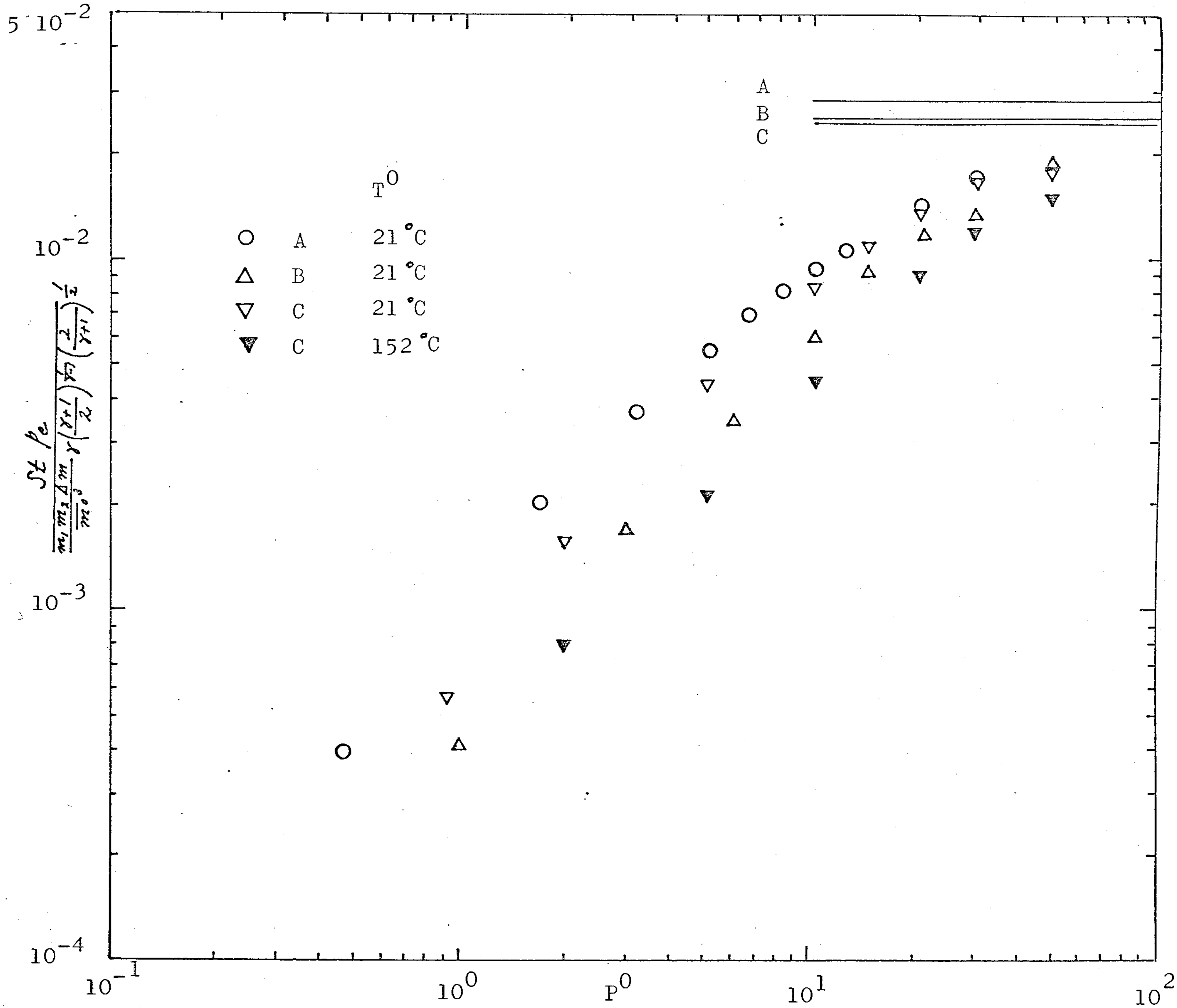

FIG.91 COMPARISON OF DIFFUSIVE SEPARATION BETWEEN EXPERIMENTAL DATA AND THEORETICAL PREDICTION

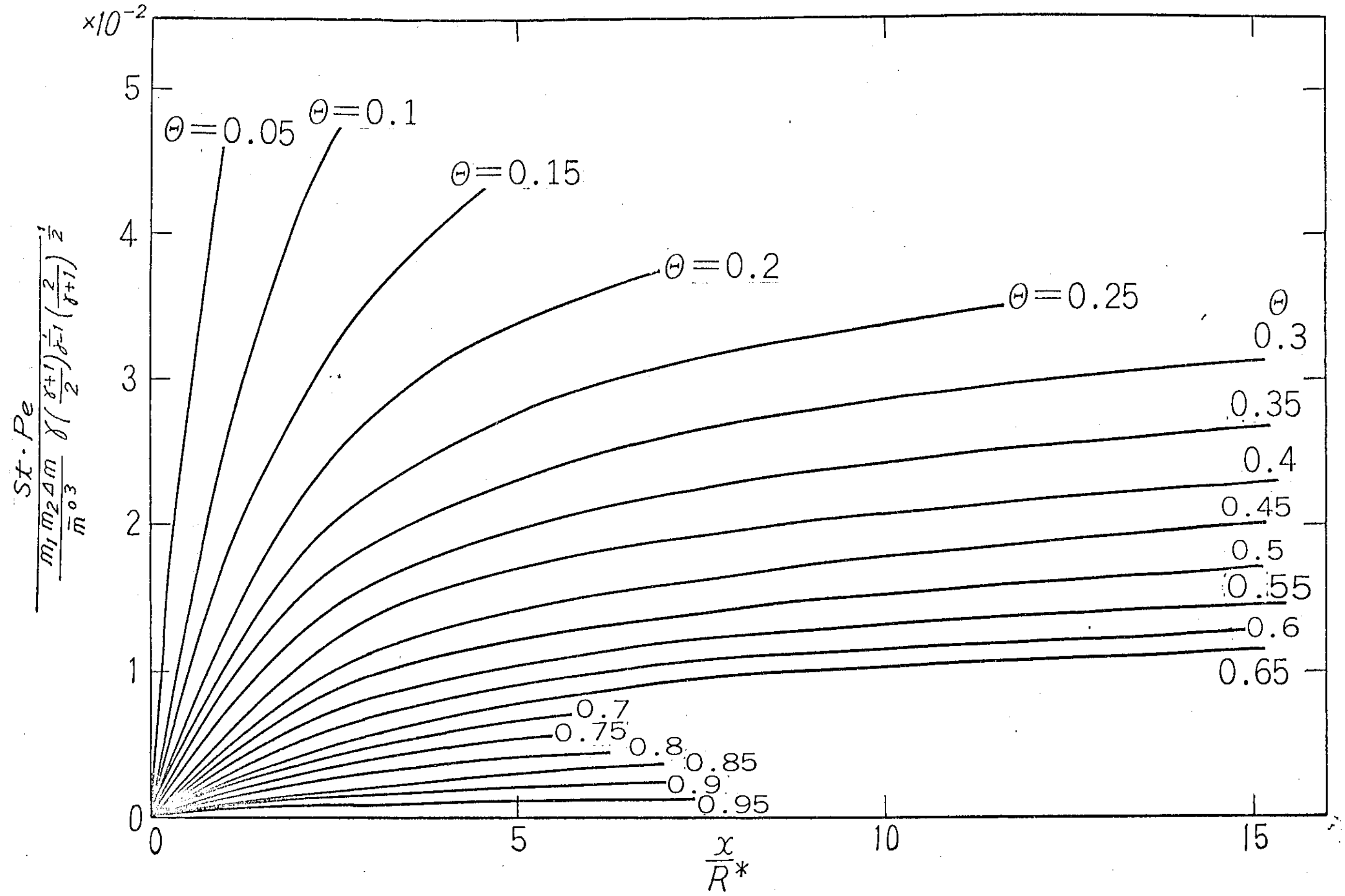

FIG. 92 THE INTEGRAL I vs. x/R* FOR VARIOUS VALUES OF CUT, Θ (γ = 1.067)

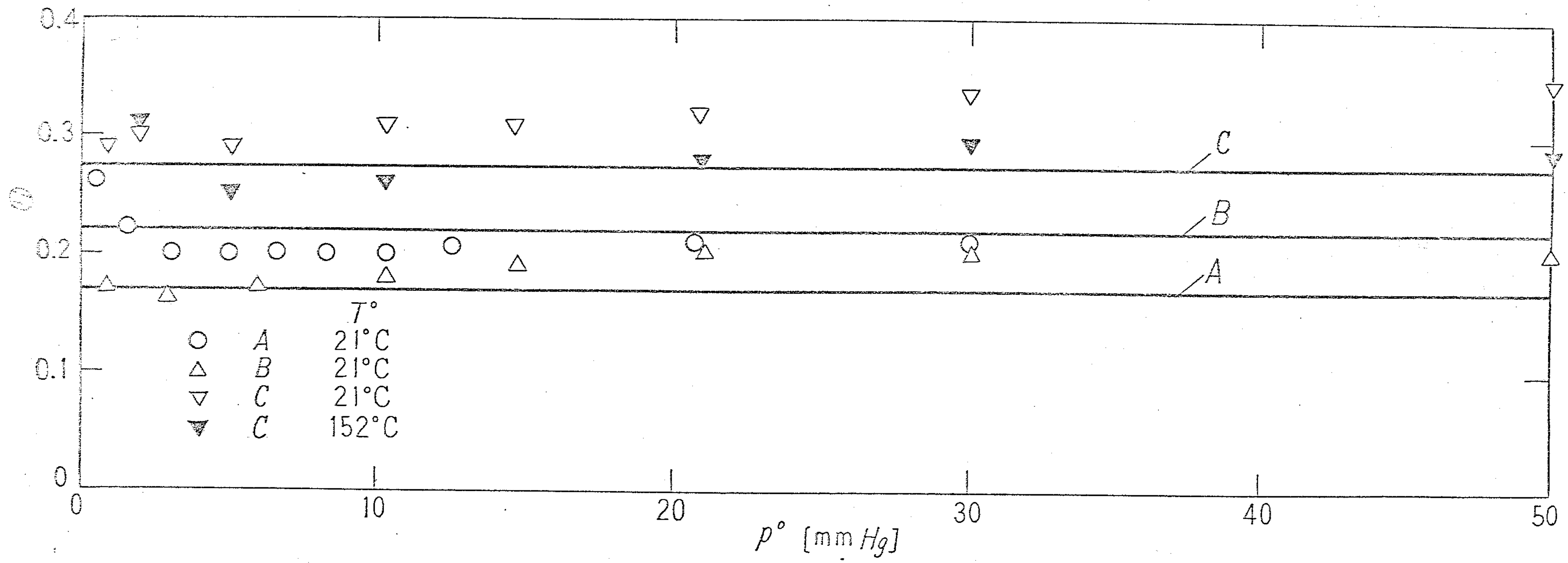

FIG. 93 COMPARISON OF CUT, Θ BETWEEN EXPERIMENTAL DATA AND THEORETICAL PREDICTION

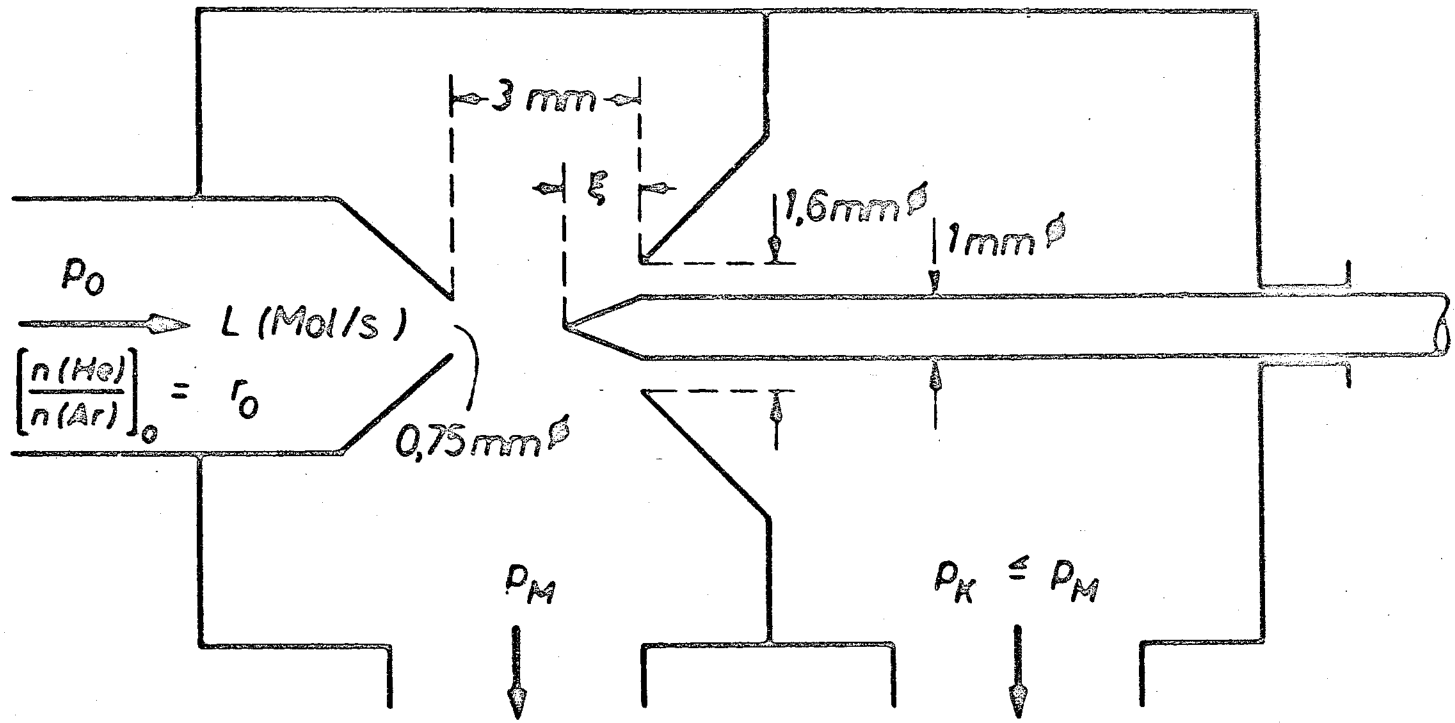

FIG.94 DIAGRAM OF APPARATUS FOR SEPARATION IN SHOCK WAVE BIER AND ZELLER (54)

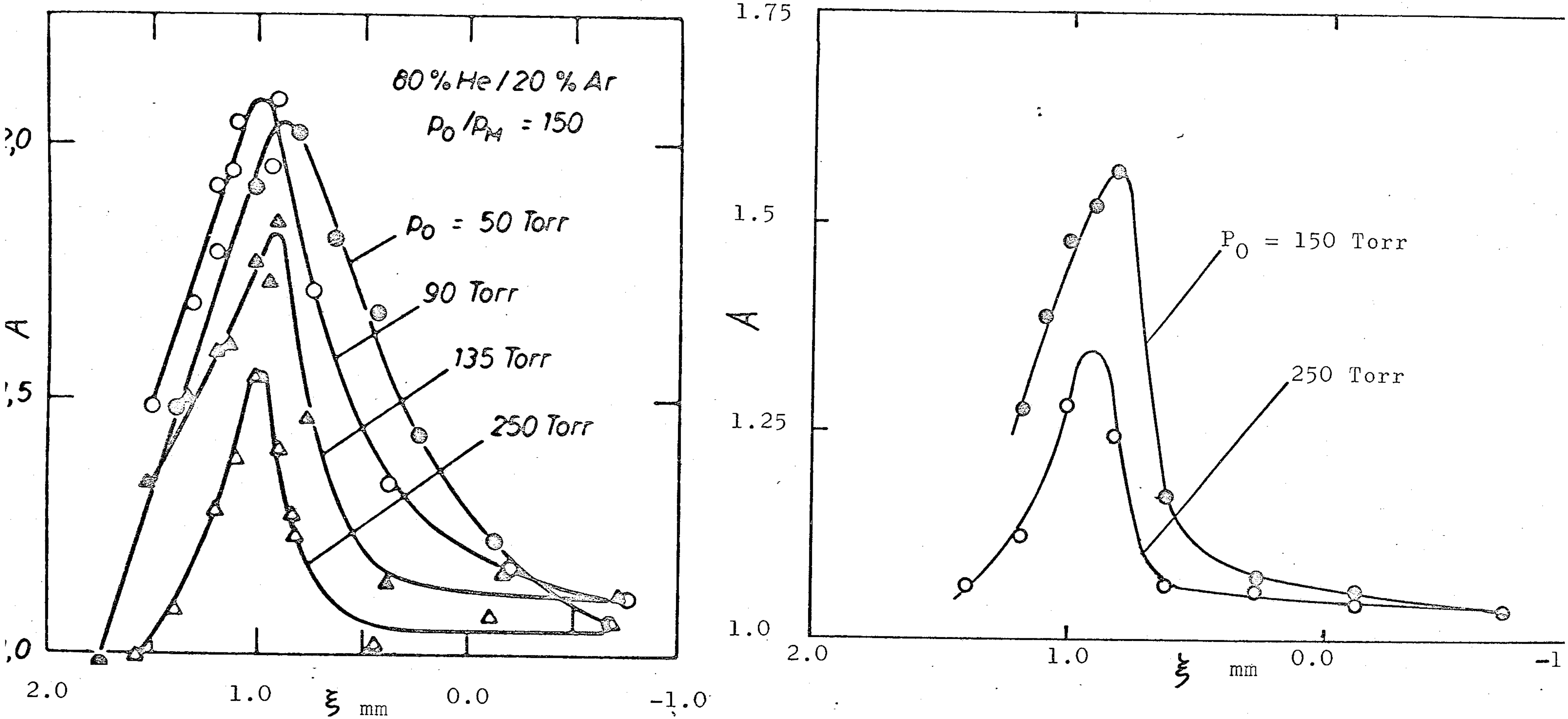

FIG. 95 EXPERIMENTAL DATA FOR SEPARATION COEFFICIENT OBTAINED BY BIER AND ZELLER (54)

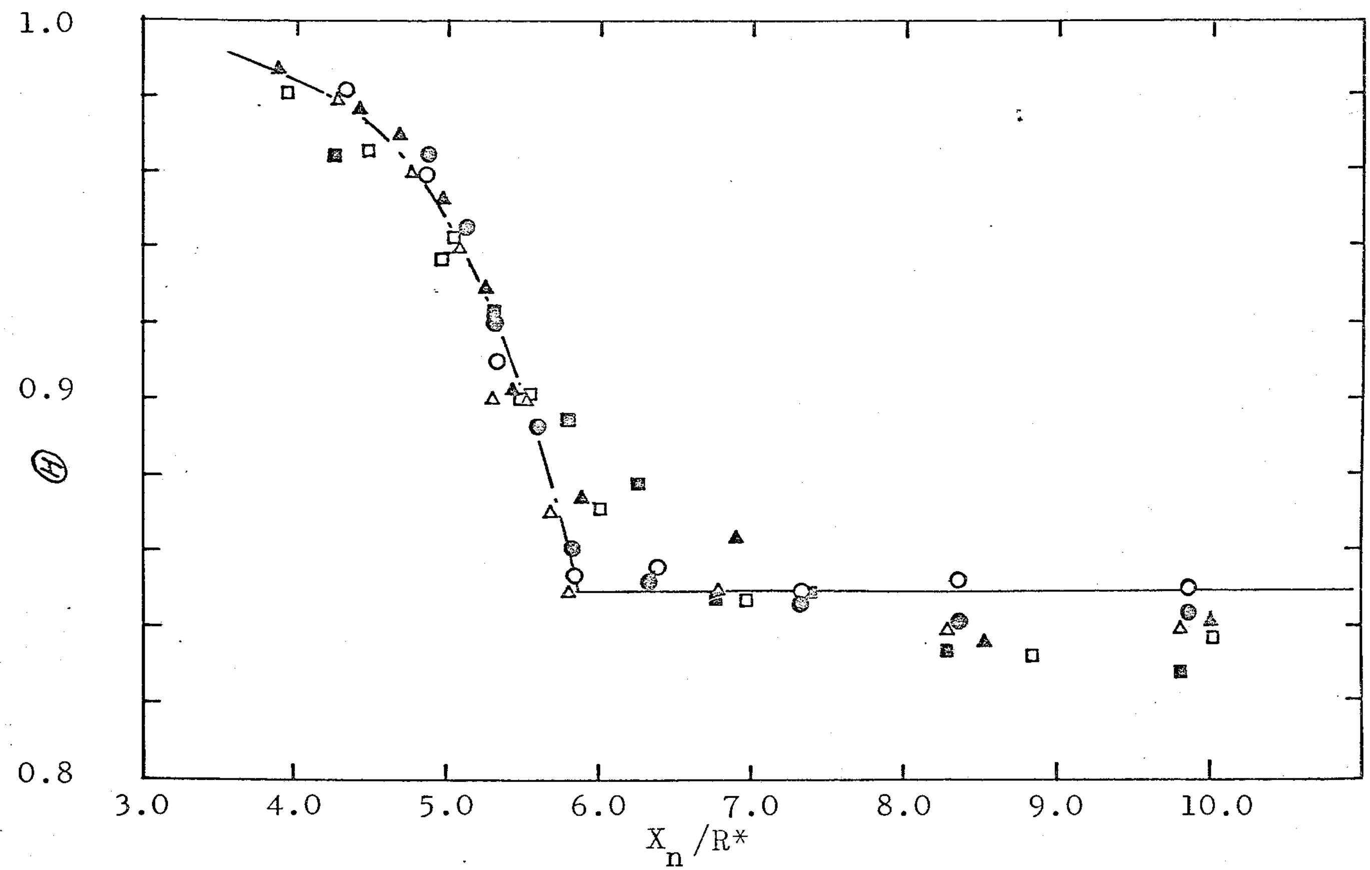

FIG.96 EXPERIMENTAL DATA FOR THE CUT OBTAINED BY BIER AND ZELLER (54)

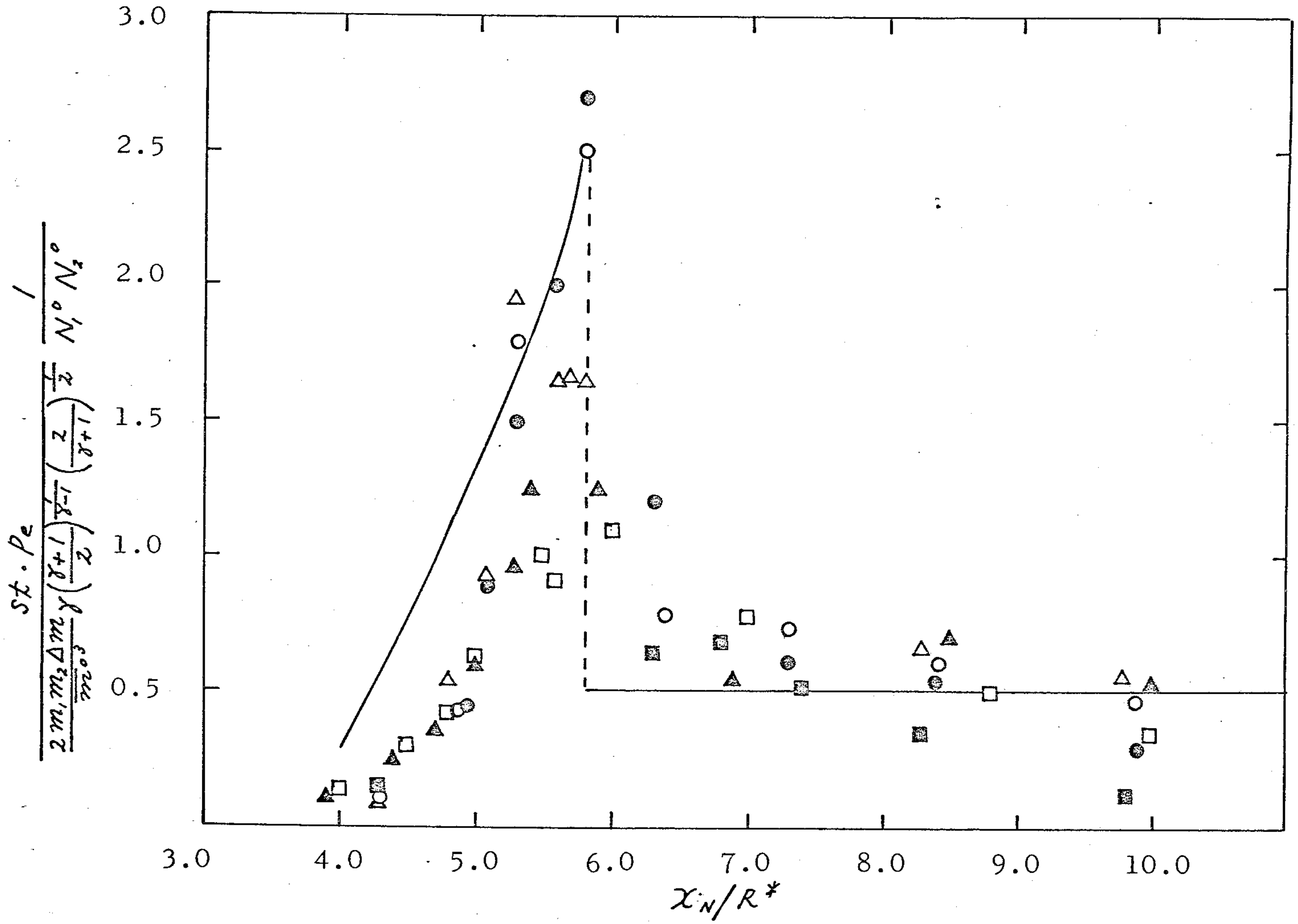

FIG.97 COMPARISON OF EXPERIMENTAL DATA ON DIFFUSIVE SEPARATION IN AN OBLIQUE SHOCK WAVE GIVEN BY BIER AND ZELLER (54) WITH THEORETICAL PREDICTION

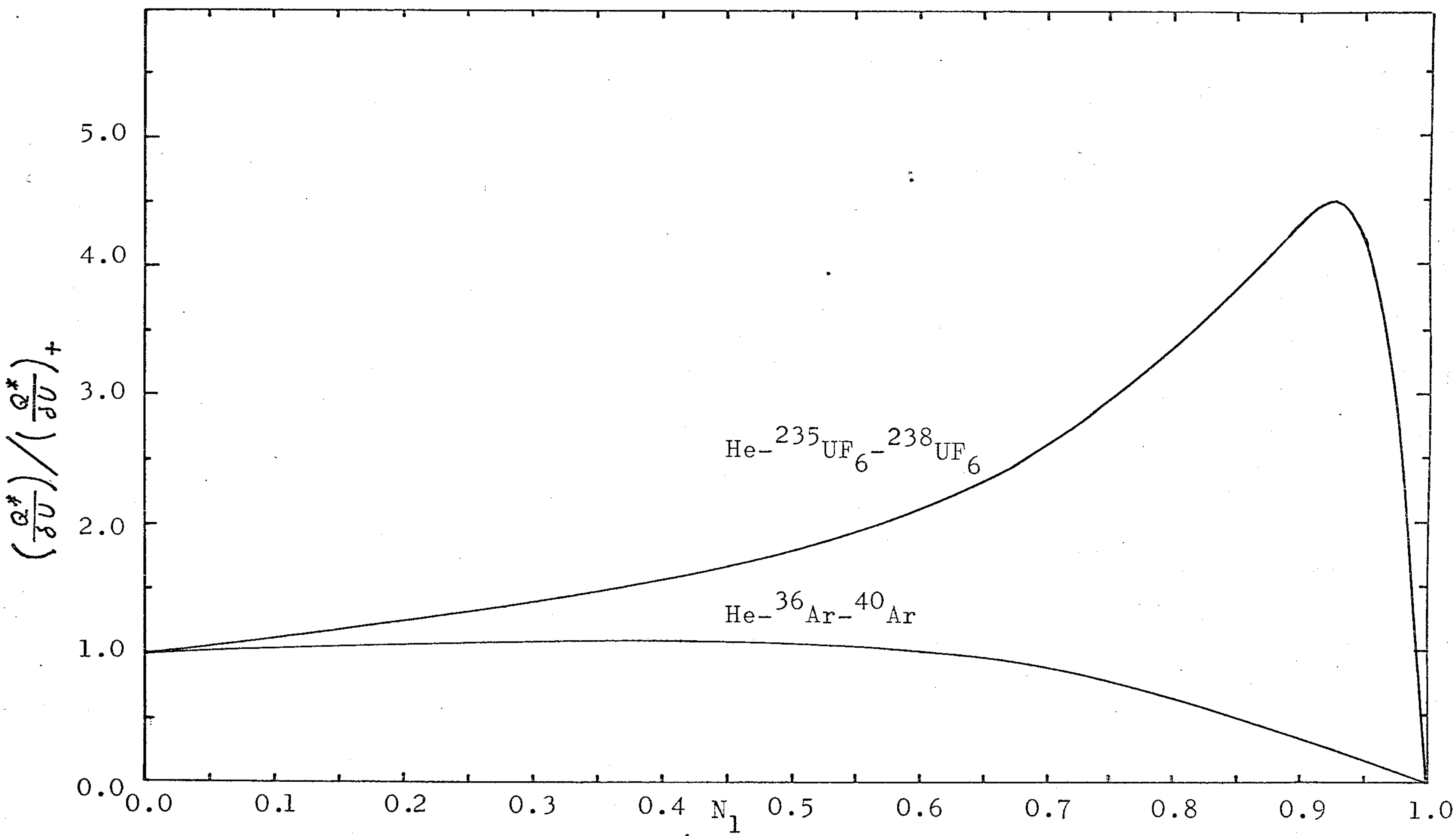

FIG.98 SPECIFIC SUCTION VOLUME AS A FUNCTION OF MOLE FRACTION OF HELIUM

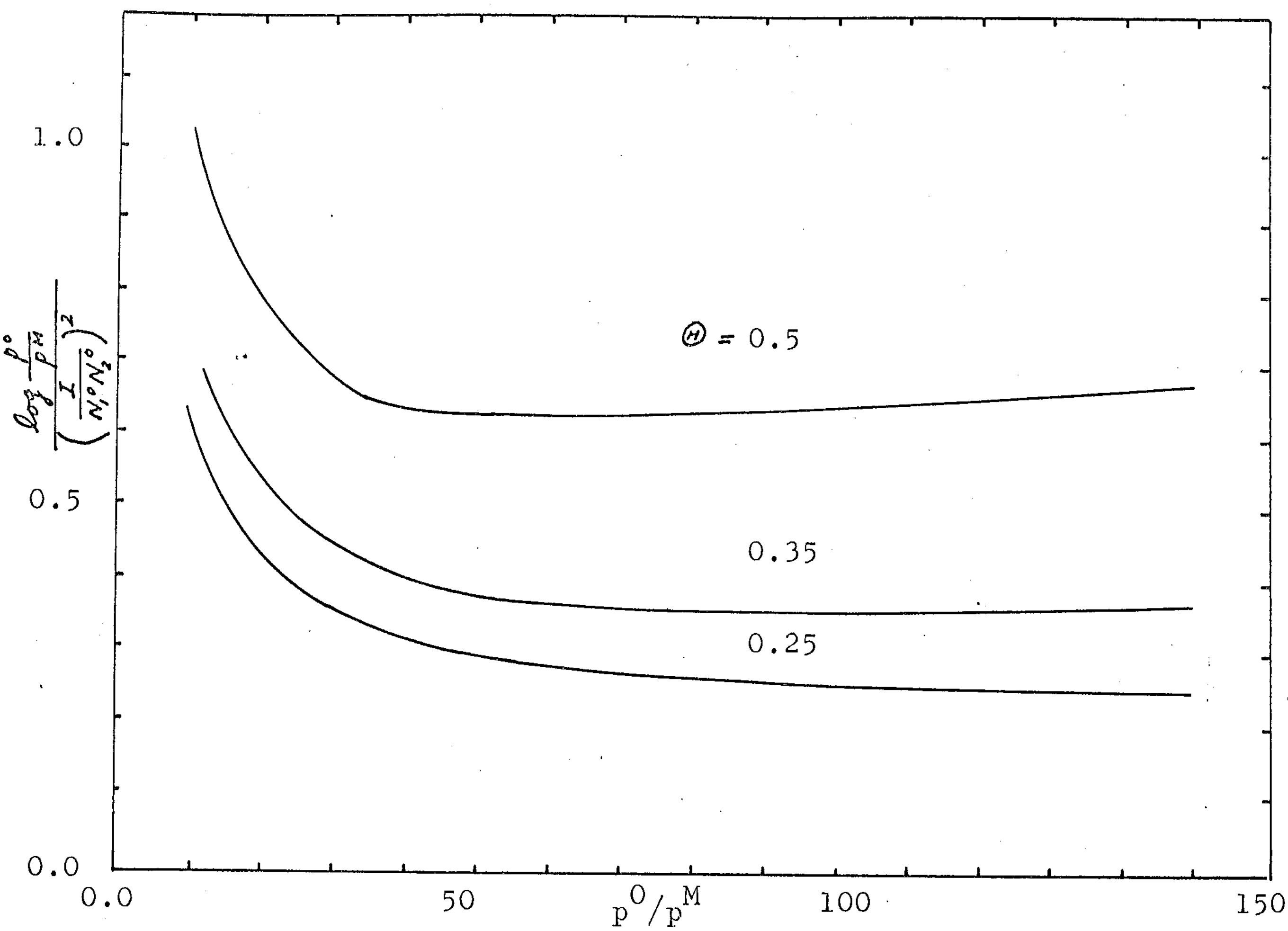

FIG.99 $\log \frac{p^o}{p^M} \Big/ \left(\frac{I}{N_1^o N_2^o}\right)^2$ AS A FUNCTION OF EXPANSION PRESSURE RATO WITH CUT AS A PARAMETER $\gamma = 1.4$

Appendix A

Difference Equations for Flow of Axisymmetric Supersonic Jet

The difference equations for axisymmetric supersonic jet based on Eq. (3.5) are given in the following equations.

$$r_3 = \frac{r_2 - m n r_1 + n(x_1 - x_2)}{(1 - mn)} \tag{A-1}$$

$$x_3 = x_1 + m(r_3 - r_1) \tag{A-2}$$

$$\beta_3 = \frac{1}{K \cdot F + I \cdot E}\{E[I\beta_2 + F(\zeta_1 - \zeta_2) - N(x_3 - x_2)] + F(K\beta_1 - L(r_3 - r_1))\} \tag{A-3}$$

$$\zeta_3 = \zeta_1 - \frac{1}{E}[K(\beta_3 - \beta_1) + L(r_3 - r_1)]\} \tag{A-4}$$

$$m = \frac{1}{2}\left(\frac{\beta_1 - \zeta_1}{\beta_1\zeta_1 + 1} + \frac{\beta_3 - \zeta_3}{\beta_3\zeta_3 + 1}\right) \tag{A-5}$$

$$n = \frac{1}{2}\left(\frac{\beta_2\zeta_2 - 1}{\beta_2 + \zeta_2} + \frac{\beta_3\zeta_3 - 1}{\beta_3 + \zeta_3}\right) \tag{A-6}$$

$$E = \frac{1}{2}\left(\frac{1}{1 + \zeta_1^2} + \frac{1}{1 + \zeta_3^2}\right) \tag{A-7}$$

$$F = \frac{1}{2}\left(\frac{1}{1 + \zeta_2^2} + \frac{1}{1 + \zeta_3^2}\right) \tag{A-8}$$

$$K = -\frac{1}{2}\left(\frac{2\beta_1^2}{(\gamma + 1)(1 + \beta_2^2)(1 + \kappa\beta_2^2)} + \frac{2\beta_3^2}{(\gamma + 1)(1 + \beta_3^2)(1 + \kappa\beta_3^2)}\right) \tag{A-9}$$

$$I = -\frac{1}{2}\left(\frac{2\beta_2^2}{(\gamma + 1)(1 + \beta_2^2)(1 + \kappa\beta_2^2)} + \frac{2\beta_3^2}{(\gamma + 1)(1 + \beta_3^2)(1 + \kappa\beta_3^2)}\right) \tag{A-10}$$

$$L = \frac{1}{2}\left(\frac{\zeta_1}{(\beta_1\zeta_1 + 1)r_1} + \frac{\zeta_3}{(\beta_3\zeta_3 + 1)r_3}\right) \tag{A-11}$$

$$N = \frac{1}{2}\left(\frac{\zeta_2}{(\beta_2\zeta_2 + 1)r_2} + \frac{\zeta_3}{(\beta_3\zeta_3 + 1)r_3}\right) \tag{A-12}$$

The above formulas can be used for calculating interior point from two noncentral points. Special consideration is necessary for calculating central point.

As $r \to 0$ along a characteristic, ζ/r is given by

$$\lim_{r \to 0} \frac{\zeta}{r} = \left(\frac{d\zeta}{dr}\right)_{r=0} = \left(\frac{d\theta}{dr}\right)_{\pm,\, r=0} \tag{A-13}$$

$(d\theta/dr)_{\pm,\, r=0}$ can be obtained by making use of Eq. (3.5), which is rewritten to

$$\sec^2\theta \left(\frac{d\theta}{dr}\right)_{\pm} \mp \frac{2\beta^2(1+\zeta^2)}{(\gamma+1)(1+\beta^2)(1+\kappa\beta^2)} \times \left(\frac{d\beta}{dr}\right) \pm \frac{\zeta(1+\zeta^2)}{(\beta\zeta \pm 1)r} = 0 \tag{A-14}$$

As $r \to 0$, the above equation becomes

$$\left(\frac{d\theta}{dr}\right)_{\pm} \mp \frac{2\beta^2}{(\gamma+1)(1+\beta^2)(1+\kappa\beta^2)}\left(\frac{d\beta}{dr}\right) \pm \left(\frac{d\theta}{dr}\right)_{\pm} = 0 \tag{A-15}$$

Then $(d\theta/dr)_{\pm,\, r=0}$ are given by

$$\left(\frac{d\theta}{dr}\right)_{\pm,\, r=0} = \frac{\beta^2}{(\gamma+1)(1+\beta^2)(1+\kappa\beta^2)}\left(\frac{d\beta}{dr}\right)_{r=0} \tag{A-16}$$

The expressions for ζ_1/r_1 and ζ_3/r_3 on the axis become

$$\frac{\zeta_1}{r_1} = \frac{\beta_1^2}{(\gamma+1)(1+\beta_1^2)(1+\kappa\beta_1^2)} \, \frac{\beta_3-\beta_1}{r_3} \tag{A-17}$$

$$\frac{\zeta_3}{r_3} = \frac{\beta_3^2}{(\gamma+1)(1+\beta_3^2)(1+\kappa\beta_3^2)} \, \frac{\beta_3-\beta_2}{r_2} \tag{A-18}$$

Appendix B

Difference Equations for Flow of Two-Dimensional Supersonic Jet

The difference equations describing a two-dimensional supersonic flow of perfect gas are given by for $|\beta\zeta - 1| \gg 0$ by

$$y_3 = \frac{n y_2 - m y_1 + x_1 - x_2}{n - m} \tag{B-1}$$

$$x_3 = x_1 + m(y_3 - y_1) \tag{B-2}$$

$$m = \frac{1}{2}\left(\frac{\beta_1 - \zeta_1}{1 + \beta_1\zeta_1} + \frac{\beta_3 - \zeta_3}{1 + \beta_3\zeta_3}\right) \tag{B-3}$$

$$n = \frac{1}{2}\left(\frac{\beta_2 + \zeta_2}{\beta_2\zeta_2 - 1} + \frac{\beta_3 + \zeta_3}{\beta_3\zeta_3 - 1}\right) \tag{B-4}$$

and for $|\beta\zeta - 1| \simeq 0$ by

$$y_3 = \frac{y_2 - mny_1 + n(x_1 - x_2)}{(1 - mn)} \tag{B-5}$$

$$x_3 = x_1 + m(y_3 - y_1) \tag{B-6}$$

$$m = \frac{1}{2}\left(\frac{\beta_1 - \zeta_1}{1 + \beta_1\zeta_1} + \frac{\beta_3 - \zeta_3}{1 + \beta_3\zeta_3}\right) \tag{B-7}$$

$$n = \frac{1}{2}\left(\frac{\beta_2\zeta_2 - 1}{\beta_2 + \zeta_2} + \frac{\beta_3\zeta_3 - 1}{\beta_3 + \zeta_3}\right) \tag{B-8}$$

$$\beta_3 = \frac{1}{KF + IE}\left\{E\left[I\beta_2 + F(\zeta_1 - \zeta_2)\right] + FK\beta_1\right\} \tag{B-9}$$

$$\zeta_3 = \zeta_1 - \frac{K}{E}(\beta_3 - \beta_1) \tag{B-10}$$

$|\beta\zeta - 1| \gg 0$:

$$Z_3 = Z_2 - \frac{1}{2}\left(\beta_2 w_2 \frac{(1+\zeta_2^2)^{\frac{1}{2}}}{\beta_2 + \zeta_2} - \beta_3 w_3 \frac{(1+\zeta_3^2)^{\frac{1}{2}}}{\beta_3\zeta_3 - 1}\right)(y_3 - y_2) \tag{B-11}$$

$|\beta \zeta - 1| \simeq 0$:

$$z_3 = z_2 - \frac{1}{2}\left(\rho_2 w_2 \frac{(1+\zeta_2^2)^{\frac{1}{2}}}{\beta_2 + \zeta_2} + \rho_3 w_3 \frac{(1+\zeta_3^2)^{\frac{1}{2}}}{\beta_3 + \zeta_3}\right)(x_3 - x_2) \tag{B-12}$$

$$E = \frac{1}{2}\left(\frac{1}{1+\zeta_1^2} + \frac{1}{1+\zeta_3^2}\right) \tag{B-13}$$

$$F = \frac{1}{2}\left(\frac{1}{1+\zeta_2^2} + \frac{1}{1+\zeta_3^2}\right) \tag{B-14}$$

$$K = -\frac{1}{2}\left(\frac{2\beta_1^2}{(\gamma+1)(1+\beta_1^2)(1+K\beta_1^2)} + \frac{2\beta_3^2}{(\gamma+1)(1+\beta_3^2)(1+K\beta_3^2)}\right) \tag{B-15}$$

and

$$I = -\frac{1}{2}\left(\frac{2\beta_2^2}{(\gamma+1)(1+\beta_3^2)(1+K\beta_3^2)} + \frac{2\beta_3^2}{(\gamma+1)(1+\beta_3^2)(1+K\beta_3^2)}\right) \tag{B-16}$$

If P_3 lies on the jet axis, the difference equations become

$$x_3 = x_2 + \frac{1}{2} y_2 \left(\beta_3 - \frac{\beta_2 + \zeta_2}{\beta_2 \zeta_2 - 1}\right) \tag{B-17}$$

$$\beta_3 = \beta_2 - \frac{1}{I} \zeta_2 \frac{1}{2}\left(\frac{1}{1+\zeta_2^2} + 1\right) \tag{B-18}$$

$$I = -\left(\frac{\beta_2^2}{(\gamma+1)(1+\beta_2^2)(1+K\beta_2^2)} + \frac{\beta_3^2}{(\gamma+1)(1+\beta_3^2)(1+K\beta_3^2)}\right) \tag{B-19}$$

Appendix C

Two-Dimensional Supersonic Jet near Sonic Nozzle Exit

Supersonic jet flows from a two-dimensional sonic nozzle are practically applied in jet separation process, fluid amplifiers, pneumatic control and logic systems. The properties of the flow field can be calculated by the numerical method of characteristics if the flow properties near sonic nozzle exit are known. This report presents the latter solution obtained by the same procedure as what Katskova, et al. (26) have carried out for the axisymmetric case.

Basic Equations

The equations describing the isentropic compressible flow of perfect gas are expressed in the natural coordinate system as follows (27)

$$\frac{\partial \Lambda}{\partial s} - \tan\mu \frac{\partial \theta}{\partial n} = 0 \qquad \text{(C-1)}$$

$$\tan\mu \frac{\partial \Lambda}{\partial n} - \frac{\partial \theta}{\partial s} = 0 \qquad \text{(C-2)}$$

where the velocity of gas is expressed in terms of Prandtl-Meyer function Λ and the inclination angle θ ; The independent variables (s, n) are the streamline coordinates and μ denotes Mach angle (see Fig.). In the characteristic coordinate system, these equations become

$$\frac{\partial(\Lambda + \theta)}{\partial \xi} = 0 \qquad \text{(C-3)}$$

$$\frac{\partial(\Lambda - \theta)}{\partial \eta} = 0 \qquad \text{(C-4)}$$

It is convenient to transform above equations by introducing new independent variables, Z and X which are defined in the manner that a line of Z =const is a streamline, or Z is a stream function, and a line of X =const is a right running characteristic (see Fig.). With the aid of the differential equation for the right running characteristic,

$$\frac{dy}{dx} = \tan(\theta - \mu) \qquad \text{(C-5)}$$

X can be expressed explicity by the equation

$$X = X(s, n) = X(x, y) = \int_0^x \tan(\theta - \mu)\left(\frac{\partial \mu}{\partial y}\right)_X dx + \frac{\pi}{2}$$

$$= \frac{\pi}{2} - \alpha_{Z=1} \qquad \text{(C-6)}$$

where the integration is carried out along the characteristic and x , y denote Cartesian coordinates.

By the definition, we have

$$d\chi = \frac{\partial \chi}{\partial x}dx + \frac{\partial \chi}{\partial y}dy = -\rho v\,dx + \rho u\,dy$$

$$= \rho w\,(\cos\theta\,dy - \sin\theta\,dx) \qquad \text{(C-7)}$$

then we obtain by using Eq. (C-5)

$$\left(\frac{\partial y}{\partial \chi}\right)_X + \frac{1}{\rho w}\frac{\sin(\theta-\mu)}{\sin\mu} = 0 \qquad \text{(C-8)}$$

which is rewritten in the form

$$\beta\left(\frac{\partial y}{\partial \chi}\right)_X + \sin(\theta-\mu) = 0 \qquad \text{(C-9)}$$

where

$$\beta = \rho w \sin\mu = \left(\frac{\gamma+1}{2}\right)^{\frac{1}{2}\frac{\gamma+1}{\gamma-1}}\left(\frac{1-\cos 2\mu}{\gamma-\cos 2\mu}\right)^{\frac{1}{2}\frac{\gamma+1}{\gamma-1}} \qquad \text{(C-10)}$$

Similarly,

$$\beta\left(\frac{\partial x}{\partial \chi}\right)_X + \cos(\theta-\mu) = 0 \qquad \text{(C-11)}$$

On the other hand, from Eq. (C-3) we have

$$\left(\frac{\partial \Lambda}{\partial \chi}\right)_X + \left(\frac{\partial \theta}{\partial \chi}\right)_X = \frac{d\Lambda}{d\mu}\left(\frac{\partial \mu}{\partial \chi}\right)_X + \left(\frac{\partial \theta}{\partial \chi}\right)_X = 0 \qquad \text{(C-12)}$$

By applying the relation.

$$\frac{d\Lambda}{d\mu} = -\frac{1+\cos 2\mu}{\gamma-\cos 2\mu}\left(\frac{\partial \mu}{\partial \chi}\right)_X \qquad \text{(C-13)}$$

Eq. (C-12) is rewritten in the form

$$\left(\frac{\partial \theta}{\partial \chi}\right)_X - \frac{1+\cos 2\mu}{\gamma-\cos 2\mu}\left(\frac{\partial \mu}{\partial \chi}\right)_X = 0 \qquad \text{(C-14)}$$

In order to transform Eq. (C-2), we make use of the equation (27)

$$\tan\mu\,\frac{\partial \Lambda}{\partial n} = \frac{\partial \Lambda}{\partial s} - \sec\mu\,\frac{\partial \Lambda}{\partial \xi} \qquad \text{(C-15)}$$

which relates the derivative of Λ in the natural coordinate system and in the characteristic coordinate system. Combining Eq. (C-2) and Eq. (C-15) we have

$$\left(\frac{\partial \Lambda}{\partial s}\right)_n - \sec\mu\left(\frac{\partial \Lambda}{\partial \xi}\right)_\eta - \left(\frac{\partial \theta}{\partial s}\right)_n = 0 \qquad \text{(C-16)}$$

which is rewritten in the form

$$\left[\frac{d\Lambda}{d\mu}\left(\frac{\partial \mu}{\partial \chi}\right)_Z - \left(\frac{\partial \theta}{\partial \chi}\right)_Z\right]\left(\frac{\partial \chi}{\partial s}\right)_Z - \sec\mu\left(\frac{\partial \Lambda}{\partial Z}\right)_\chi\left(\frac{\partial Z}{\partial \xi}\right)_\chi$$

$$= \left[\frac{d\Lambda}{d\mu}\left(\frac{\partial \mu}{\partial \chi}\right)_Z - \left(\frac{\partial \theta}{\partial \chi}\right)_Z\right] - \left(\frac{\partial s}{\partial \chi}\right)_Z \sec\mu\left(\frac{d\Lambda}{d\mu}\right)\left(\frac{\partial \mu}{\partial Z}\right)_\chi\left(\frac{\partial Z}{\partial y}\right)_\chi\left(\frac{\partial y}{\partial \xi}\right)_\chi = 0 \qquad \text{(C-17)}$$

With the aid of the relations

$$\left(\frac{\partial y}{\partial \xi}\right)_\chi = \sin(\theta - \mu) \qquad \text{(C-18)}$$

$$\left(\frac{\partial s}{\partial \chi}\right)_Z = \left(\frac{\partial s}{\partial y}\right)_Z\left(\frac{\partial y}{\partial \chi}\right)_Z = \frac{1}{\sin\theta}\left(\frac{\partial y}{\partial \chi}\right)_Z \qquad \text{(C-19)}$$

and by using Eqs. (C-9) and (C-13), Eq. (C-17) is expressed as

$$\sin\theta\left[\left(\frac{\partial \theta}{\partial \chi}\right)_Z + \frac{1+\cos 2\mu}{\gamma - \cos 2\mu}\left(\frac{\partial \mu}{\partial \chi}\right)_Z\right] + \frac{2\cos\mu}{\gamma - \cos 2\mu}\,\beta\left(\frac{\partial y}{\partial \chi}\right)_Z\left(\frac{\partial \mu}{\partial Z}\right)_\chi = 0 \qquad \text{(C-20)}$$

Now, it will be useful to summarize the basic equations:

$$\left(\frac{\partial \theta}{\partial Z}\right)_\chi - \frac{1+\cos 2\mu}{\gamma - \cos 2\mu}\left(\frac{\partial \mu}{\partial Z}\right)_\chi = 0 \qquad \text{(C-21)}$$

$$\beta\,\frac{2\cos\mu}{\gamma - \cos 2\mu}\left(\frac{\partial y}{\partial \chi}\right)_Z\left(\frac{\partial \mu}{\partial Z}\right)_\chi + \left[\left(\frac{\partial \theta}{\partial \chi}\right)_Z + \frac{1+\cos 2\mu}{\gamma - \cos 2\mu}\left(\frac{\partial \mu}{\partial \chi}\right)_Z\right]\sin\theta = 0 \qquad \text{(C-22)}$$

$$\beta\left(\frac{\partial y}{\partial Z}\right)_\chi + \sin(\theta - \mu) = 0 \qquad \text{(C-23)}$$

$$\beta\left(\frac{\partial x}{\partial Z}\right)_\chi + \cos(\theta - \mu) = 0 \qquad \text{(C-24)}$$

in which the first two equations are the equations of motion in the (Z, χ) coordinate system and the last two equations give the relation between Cartesian coordinates and (Z, χ) coordinates.

Solution near Sonic Nozzle Exit

Near nozzle exit, we assume that flow variables μ, θ, and y are expressed in terms of power series in χ with coefficients as undetermined functions of Z:

$$\mu = \frac{\pi}{2} + \mu_1(Z)\chi + \mu_2(Z)\chi^2 - \cdots \qquad \text{(C-25)}$$

$$\theta = \theta_1(z)\chi + \theta_2(z)\chi^2 + \theta_3(z)\chi^3 + \theta_4(z)\chi^4 + \cdots \tag{C-26}$$

$$y = z + y_1(z)\chi + y_2(z)\chi^2 + y_3(z)\chi^3 + y_4(z)\chi^4 + y_5(z)\chi^5 + \cdots \tag{C-27}$$

Boundary conditions are given by

$$\mu = \frac{\pi}{2}, \quad \theta = 0, \quad x = 0 \qquad \text{at} \quad \chi = 0 \tag{C-28}$$

$$\mu = \frac{\pi}{2} - \chi, \quad y = 1 \qquad \text{at} \quad z = 1 \tag{C-29}$$

$$\theta = 0, \quad y = 0 \qquad \text{at} \quad z = 0 \tag{C-30}$$

On the other hand, the related functions $f = \dfrac{1 + \cos 2\mu}{\gamma - \cos 2\mu}$, $g = \dfrac{2\cos\mu}{\gamma - \cos 2\mu}$ and β are expanded as

$$f = f_2\chi^2 + \cdots = \frac{2}{\gamma + 1}\mu_1^2\chi^2 + \cdots \tag{C-31}$$

$$g = g_1\chi + \cdots = -\frac{2}{\gamma + 1}\mu_1\chi + \cdots \tag{C-32}$$

$$\begin{aligned}\beta &= 1 + \beta_2\chi^2 + \beta_4\chi^4 + \cdots \\ &= 1 - \frac{1}{2}\mu_1^2\chi^2 + \left[\frac{1}{4!}\mu_1^4 - \frac{1}{2}(2\mu_1\mu_3 - \mu_2^2) - \frac{1}{2}\frac{1}{(\gamma+1)}\mu_1^4\right]\chi^4 + \cdots\end{aligned} \tag{C-33}$$

Substituting Eqs. (C-21), (C-22), (C-23), (C-31), (C-32) and (C-33) into Eq. (C-22), we have

$$g_1 y_1 \mu_1' \chi^2 + \cdots + \theta_1^2\chi + \cdots + f_2\mu_1\theta_1\chi^3 + \cdots = 0 \tag{C-34}$$

thus,

$$\theta_1 = 0 \tag{C-35}$$

Similarly, from Eq. (C-21)

$$\theta_2'\chi^2 + \cdots - f_2\mu_1'\chi^3 + \cdots = 0 \tag{C-36}$$

thus,

$$\theta_2' = 0 \tag{C-37}$$

Since $\theta = 0$, $z = 0$

$$\theta_2 = 0 \tag{C-38}$$

Substituting the expansion

$$S = S_1 \chi + S_2 \chi^2 + \cdots \tag{C-39}$$

into the equation

$$\left(\frac{\partial y}{\partial \chi}\right)_z = \left(\frac{\partial S}{\partial \chi}\right)_z \sin\theta \tag{C-40}$$

we can obtain the equation

$$y_1 + 2y_2\chi + 3y_3\chi^2 + \cdots = (S_1 + 2S_2\chi + 3S_3\chi^2 + \cdots)(\theta_3\chi^3 + \theta_4\chi^4 + \cdots) \tag{C-41}$$

Thus,

$$y_1 = 0 \tag{C-42}$$

$$y_2 = 0 \tag{C-43}$$

$$y_3 = 0 \tag{C-44}$$

From Eq. (C-21), we have

$$\theta_3'\chi^3 + \cdots - (f_2\chi^2\mu_1'\chi + \cdots) = 0 \tag{C-45}$$

and terms of order χ^3 give

$$\frac{d\theta_3}{dz} - \frac{2}{\gamma+1}\mu_1^2\frac{d\mu_1}{dz} = 0 \tag{C-46}$$

From Eq. (C-22), we have

$$g_1\chi\, 4y_4\chi^3\mu_1'\chi + \cdots + (3\theta_3\chi^2 + \cdots + f_2\chi^2\mu_1 + \cdots)(\theta_3\chi^3 + \cdots) = 0 \tag{C-47}$$

and terms of χ^5 gives

$$\frac{8}{\gamma+1}y_4\mu_1\frac{d\mu_1}{dz} - \theta_3\left(3\theta_3 + \frac{2}{\gamma+1}\mu_1^3\right) = 0 \tag{C-48}$$

With the aid of the expansion

$$\sin(\theta-\mu) = -1 + \frac{1}{2}\mu_1^2\chi^2 + \mu_1\mu_2\chi^3 + \left[\frac{1}{2!}(2\mu_1\mu_3 + \mu_2^2) - \theta_3\mu_1 - \frac{1}{4!}\mu_1^4\right]\chi^4 + \cdots \tag{C-49}$$

we get from Eq. (C-23)

$$(1 + \beta_2\chi^2 + \beta_4\chi^4 + \cdots)(1 + y_4'\chi^4 + \cdots)$$

$$-1 + \frac{1}{2}\mu_1^2\chi^2 + \mu_1\mu_2\chi^3 + \left[\frac{1}{2!}(2\mu_1\mu_3 + \mu_2^2) - \theta_3\mu_1 - \frac{1}{4!}\mu_1^4\right] + \cdots = 0 \tag{C-50}$$

Terms of order χ^3 give

$$\mu_2 = 0 \tag{C-51}$$

and terms of order χ^4 give

$$y_4' + \beta_4 + \left[-\mu_1\theta_3 - \frac{1}{4!}\mu_1^4 - \frac{1}{2}(2\mu_1\mu_3 + \mu_2^2) \right] = \frac{dy_4}{dz} - \frac{1}{2}\frac{\mu_1^4}{(\gamma+1)} - \mu_1\theta_3 = 0 \quad \text{(C-52)}$$

From Eq. (C-21), we have

$$(\theta_3'\chi^3 + \theta_4'\chi^4 + \cdots) - (\mu_1'\chi + \mu_3'\chi^3 + \cdots)(f_2\chi^2 + f_4\chi^4 + \cdots) = 0 \quad \text{(C-53)}$$

Terms of order χ^4 give

$$\theta_4 = 0 \quad \text{(C-54)}$$

From Eq. (C-22), we have

$$(1 + \beta_2\chi^2 + \beta_4\chi^4 + \cdots)(g_1\chi + g_3\chi^3 + \cdots)(4y_4\chi^3 + 5y_5\chi^4 + 6y_6\chi^5 + \cdots)(\mu_1'\chi + \mu_3'\chi^3 + \cdots)$$

$$+ [3\theta_3\chi^2 + 4\theta_4\chi^3 + \cdots + (f_2\chi^2 + f_4\chi^4 + \cdots)(\mu_1 + 2\mu_2\chi + 3\mu_3\chi^2 + \cdots)]$$

$$\times \left[(\theta_3\chi^3 + \cdots) - \frac{1}{3!}(\theta_3\chi^3 + \cdots)^3 + \cdots \right] = 0 \quad \text{(C-55)}$$

Terms of order χ^6 give

$$10\mu_1 \frac{d\mu_1}{dz} y_5 = 0 \quad \text{(C-56)}$$

and hence

$$y_5 = 0 \quad \text{(C-57)}$$

The preceding results are summarized below.
Near nozzle exit, flow variables μ, θ and y are expressed in terms of power series in χ in the forms

$$\mu = \frac{\pi}{2} + \mu_1(z)\chi + O(\chi^3) \quad \text{(C-58)}$$

$$\theta = \theta_3(z)\chi^3 + O(\chi^5) \quad \text{(C-59)}$$

$$y = z + y_4(z)\chi^4 + O(\chi^6) \quad \text{(C-60)}$$

and from Eq. (C-11), we get

$$\chi = -\int^{z} \frac{1}{\rho}\cos(\theta - \mu)\, dz \quad \text{(C-61)}$$

Undetermined functions μ_1, θ_3 and y_4 can be obtained by solving the system of differential equations

$$\frac{d\theta_3}{dz} - \frac{2}{\gamma+1}\mu_1^2 \frac{d\mu_1}{dz} = 0 \quad \text{(C-62)}$$

$$\frac{8}{\gamma+1} y_4 \mu_1 \frac{d\mu_1}{dz} - \theta_3 \left(3\theta_3 + \frac{2}{\gamma+1} \mu_1^3 \right) = 0 \qquad \text{(C-63)}$$

$$\frac{dy_4}{dz} - \frac{1}{2} \frac{\mu_1^4}{(\gamma+1)} - \mu_1 \theta_3 = 0 \qquad \text{(C-64)}$$

under the boundary conditions

$$\mu_1(1) = -1, \quad y_4(1) = 0, \quad \theta_3(0) = 0, \quad y_4(0) = 0 \qquad \text{(C-65)}$$

By introducing a new dependent variable, $\omega = \dfrac{4y_4}{\theta_3}$, we have, from Eq. (C-62)

$$\mu_1 = \omega' \qquad \text{(C-66)}$$

and from Eq. (C-64)

$$\theta_3 = \frac{2}{3(\gamma+1)} \omega' (\omega\omega'' - \omega'^2) \qquad \text{(C-67)}$$

Hence,

$$y_4 = \frac{1}{6(\gamma+1)} \omega\omega' (\omega\omega'' - \omega'^2) \qquad \text{(C-68)}$$

Then, Eq. (C-63) is written in the form

$$\omega''' = \frac{1}{\omega\omega'} \omega'' (5\omega'^2 - \omega\omega'') \qquad \text{(C-69)}$$

and boundary conditions become

$$\omega'(1) = -1, \quad \omega(1) = 0, \quad \omega(0)\omega''(0) - \omega'^2(0) = 0 \qquad \text{(C-70)}$$

Calculation of $\omega(z)$, $\omega'(z)$ and $\omega''(z)$

The form of Eq. (C-67) is not changed by making the following change of variables

$$\omega = \Omega \bar{\omega} \qquad \text{(C-71)}$$

$$\zeta = \frac{\Omega'}{\Omega} z \qquad \text{(C-72)}$$

where Ω and Ω' are constants to be evaluated later. Thus, the equation for $\bar{\omega}$ is given by

$$\bar{\omega}''' = \frac{1}{\bar{\omega}\bar{\omega}'} \bar{\omega}'' (5\bar{\omega}'^2 - \bar{\omega}\bar{\omega}'') \qquad \text{(C-73)}$$

and boundary conditions are expressed as

$$\left(\frac{d\bar{\omega}}{d\zeta}\right)_{\zeta=\frac{\Omega'}{\Omega}} = -\frac{1}{\Omega'} \tag{C-74}$$

$$\bar{\omega}\left(\frac{\Omega'}{\Omega}\right) = 0 \tag{C-75}$$

$$\bar{\omega}(0)\,\bar{\omega}''(0) - \bar{\omega}'^{2}(0) = 0 \tag{C-76}$$

Solving Eq. (C-73) under the boundary conditions

$$\bar{\omega}(0) = 1 \tag{C-77}$$

$$\left(\frac{d\bar{\omega}}{d\zeta}\right)_{\zeta=0} = 1 \tag{C-78}$$

$$\left(\frac{d^2\bar{\omega}}{d\zeta^2}\right)_{\zeta=0} = \frac{\bar{\omega}'^{2}(0)}{\bar{\omega}(0)} = 1 \tag{C-79}$$

we can obtain the values of ζ^* and of $\left(\frac{d\bar{\omega}}{d\zeta}\right)_{\zeta=\zeta^*}$ at which $\bar{\omega}$ becomes zero.

Then, Ω and Ω' are determined by the equations

$$\Omega' = -\frac{1}{\left(\frac{d\bar{\omega}}{d\zeta}\right)_{\zeta=\zeta^*}} \tag{C-80}$$

$$\Omega = \frac{\Omega'}{\zeta^*} \tag{C-81}$$

The numerical solution to Eq. (C-73) was obtained by Runge-Kutta-Gill method. The values of ζ^* and $\left(\frac{d\bar{\omega}}{d\zeta}\right)_{\zeta=\zeta^*}$ were computed to be -1.214325 and 0.7937005, respectively. Some numerical values of $\omega(\zeta)$, $\omega'(\zeta)$ and $\omega''(\zeta)$ thus obtained are given in Table $C-1$

Tables of $\omega(\zeta)$, $\omega'(\zeta)$ and $\omega''(\zeta)$ for ζ =0.0 (0.001) 1.0 are available on request.

In order to test the validity of this calculation, the values of the derivative $\left(\frac{d\theta}{d\Lambda}\right)_{\Lambda=0}$ along streamline were calculated as a functions of ζ and compared with the values obtained by solving the hodograph equation of motion. The derivative, $\left(\frac{d\theta}{d\Lambda}\right)_{\Lambda=0}$ can be expressed in terms of ω as

$$h = \left(\frac{d\theta}{d\Lambda}\right)_{\Lambda=0} = \left(\frac{\partial\theta}{\partial\mu}\right)_{\zeta,\,\mu=\frac{\pi}{2}}\left(\frac{d\mu}{d\Lambda}\right)_{\Lambda=0} = \frac{\left(\frac{\partial\theta}{\partial\chi}\right)_{\chi=0}}{\left(\frac{\partial\mu}{\partial\chi}\right)_{\chi=0}}\left(\frac{d\mu}{d\Lambda}\right)_{\Lambda=0} = \frac{(\omega'^2-\omega\omega'')}{\omega'^2} \tag{C-82}$$

On the other hand, the partial differential equation for Z in the modified hodograph plane (Λ , θ) is given by (55)

$$\frac{\partial^2 Z}{\partial \Lambda^2} - \frac{\partial^2 Z}{\partial \theta^2} + k(\Lambda)\frac{\partial Z}{\partial \Lambda} = 0 \qquad \text{(C-83)}$$

and

$$k(\Lambda) = \frac{d}{d\Lambda} \ln \frac{\rho^0}{\rho}(M^2 - 1) \qquad \text{(C-84)}$$

which approaches to $\frac{1}{3\Lambda}$ as $\Lambda \to 0$.

Then, Eq. (C-84) reduces to

$$\frac{\partial^2 Z}{\partial \Lambda^2} - \frac{\partial^2 Z}{\partial \theta^2} + \frac{1}{3\Lambda}\frac{\partial Z}{\partial \Lambda} = 0 \qquad \text{(C-85)}$$

A solution to Eq. (C-84) was obtained by Rudnev (55)

$$Z(h) = \frac{1}{c_1}\int_0^h (1 - x^2)^{-\frac{5}{6}} dx \qquad \text{(C-86)}$$

where

$$c_1 = \frac{1}{2}\frac{\Gamma(\frac{1}{2})\Gamma(\frac{1}{6})}{\Gamma(\frac{2}{3})} \qquad \text{(C-87)}$$

The function $Z(h)$ can be expressed as a series:

$$Z(h) = \frac{1}{c_1}\sum_{n=0}^{\infty} \frac{\left(-\frac{5}{6}\right)\left(-\frac{5}{6}-1\right)\cdots\left(-\frac{5}{6}-n+1\right)}{n!}\frac{(-1)^n}{(2n+1)} h^{2n+1} \qquad \text{(C-88)}$$

or

$$Z(h) = 1 - \frac{1}{c_1}\frac{1}{2}(1 - h^2)^{\frac{1}{6}}\sum_{n=0}^{\infty}\frac{(2n-1)!!}{(2n)!!}\frac{(1+h^2)^n}{\left(\frac{1}{6}+n\right)} \qquad \text{(C-89)}$$

Table $C-2$ gives the results of calculation obtained by Eq. (C-82) and by Eqs. (C-88) or (C-89). It is seen that there is good agreement between both results.

Conclusion

Two tables were given. Table C-1 shows numerical values of the functions $\omega(Z)$, $\omega'(Z)$ and $\omega''(Z)$ from which we can calculate the flow field of two-dimensional supersonic jet near sonic nozzle exit.

Table C-2 gives numerical values of the derivative $\left(\frac{d\theta}{d\Lambda}\right)_{\Lambda=0}$ along streamline as a function of z.
These numerical values are useful in practical calculations of flow field of two-dimensional supersonic jet.

Table C-1 $\omega(z)$, $\omega'(z)$, $\omega''(z)$ as a function of z

z	$\omega(z)$	$\omega'(z)$	$\omega''(z)$	z	$\omega(z)$	$\omega'(z)$	$\omega''(z)$
1.0	0.0	−1.0	0.0	0.49	0.5103424	−1.004699	0.05523991
0.99	0.0100000	−1.000000	$0.0^{9}1611612$	0.48	0.5203923	−1.005279	0.06086225
0.98	0.0200000	−1.000000	$0.0^{8}5132000$	0.47	0.5304482	−1.005917	0.06693187
0.97	0.0300000	−1.000000	$0.0^{7}3891775$	0.46	0.5405108	−1.006619	0.07347460
0.96	0.0400000	−1.000000	$0.0^{6}1641218$	0.45	0.5505808	−1.007388	0.08051720
0.95	0.0500000	−1.000000	$0.0^{6}5009473$	0.44	0.5606588	−1.008231	0.08808736
0.94	0.0600000	−1.000000	$0.0^{5}1354035$	0.43	0.5707457	−1.009152	0.09621369
0.93	0.0700000	−1.000000	$0.0^{5}2694412$	0.42	0.5808422	−1.010157	0.1049257
0.92	0.0800000	−1.000000	$0.0^{5}5253240$	0.41	0.5909491	−1.011253	0.1142539
0.91	0.0900000	−1.000000	$0.0^{5}9466544$	0.40	0.6010675	−1.012444	0.1242297
0.90	0.1000000	−1.000000	$0.0^{4}1603170$	0.39	0.6111984	−1.013739	0.1348854
0.89	0.1100000	−1.000000	$0.0^{4}2581924$	0.38	0.6213427	−1.015145	0.1462542
0.88	0.1200000	−1.000001	$0.0^{4}3989205$	0.37	0.6315016	−1.016667	0.1583704
0.87	0.1300000	−1.000001	$0.0^{4}5952465$	0·36	0.6416764	−1.018315	0.1712690
0.86	0.1400000	−1.000002	$0.0^{4}8934605$	0.35	0.6518684	−1.020095	0.1849861
0.85	0.1500001	−1.000003	$0.0^{3}1217408$	0.34	0.6620788	−1.022017	0.1995587
0.84	0.1600001	−1.000004	$0.0^{3}1681046$	0.33	0.6723092	−1.024089	0.2150244
0.83	0.1700002	−1.000006	$0.0^{3}2276270$	0.32	0.6825611	−1.026321	0.2314222
0.82	0.1800002	−1.000009	$0.0^{3}3029294$	0.31	0.6928362	−1.028721	0.2487915
0.81	0.1900003	−1.000013	$0.0^{3}3969599$	0.30	0.7031361	−1.031300	0.2671729
0.80	0.2000005	−1.000017	$0.0^{3}5130126$	0.29	0.7134628	−1.034068	0.2866078
0.79	0.2100007	−1.000023	$0.0^{3}6547475$	0.28	0.7238182	−1.037036	0.3071383
0.78	0.2200010	−1.000030	$0.0^{3}8262090$	0.27	0.7342042	−1.040214	0.3288076
0.77	0.2300013	−1.000040	$0.0^{2}1031845$	0.26	0.7446232	−1.043616	0.3516596
0.76	0.2400018	−1.000051	$0.0^{2}1276527$	0.25	0.7550773	−1.047252	0.3758391
0.75	0.2500023	−1.000065	$0.0^{2}1565569$	0.24	0.7655691	−1.051135	0.4010918
0.74	0.2600031	−1.000083	$0.0^{2}1904745$	0.23	0.7761009	−1.055278	0.4277641
0.73	0.2700040	−1.000104	$0.0^{3}2300310$	0.22	0.7866755	−1.059695	0.4558036
0.72	0.2800052	−1·000129	$0.0^{2}2759018$	0.21	0.7972958	−1.064399	0.4852585
0.71	0.2900066	−1.000159	$0.0^{3}3288142$	0.20	0.8079645	−1.069405	0.5161782
0.70	0.3000083	−1.000195	$0.0^{2}3895493$	0.19	0.8186849	−1.074727	0.5486127
0.69	0.3100105	−1.000237	$0·0^{2}4589436$	0.18	0.8294602	−1.080382	0.5826135
0.68	0.3200131	−1.000287	$0.0^{2}5378914$	0.17	0.8402937	−1.086385	0.6182329
0.67	0.3300163	−1.000345	$0.0^{2}6273461$	0.16	0.8511891	−1.092752	0.6555242
0.66	0.3400200	−1.000413	$0.0^{2}7283225$	0.15	0.8621500	−1.099501	0.6945424
0.65	0.3500246	−1.000491	$0.0^{2}8299417$	0.14	0.8731804	−1.106649	0.7353436
0.64	0.3600299	−1.000582	$0.0^{2}9692163$	0.13	0.8842844	−1.114214	0.7779853
0.63	0.3700362	−1.000685	0.01111486	0.12	0.8954662	−1.122215	0.8225268
0.62	0.3800437	−1.000804	0.01269985	0.11	0.9067302	−1.130671	0.8690292
0.61	0.3900524	−1.000940	0.01446062	0.10	0.9180812	−1.139603	0.9175555
0.60	0.4000625	−1.001094	0.01641137	0.09	0.9295239	−1.149029	0.9681709
0.59	0.4100743	−1.001269	0.01856703	0.08	0.9410635	−1.158973	1.020943
0.58	0.4200880	−1.001466	0.02094331	0.07	0.9527052	−1.169456	1.075943
0.57	0.4301037	−1.001689	0.02355666	0.06	0.9644545	−1.180500	1.133243
0.56	0.4401219	−1.001938	0.02642433	0.05	0.9763171	−1.192129	1.192921
0.55	0.4501426	−1.002218	0.02956438	0.04	0.9882991	−1.204366	1.255058
0·54	0.4601663	−1.002531	0.03299566	0.03	1.000407	−1.217238	1.319737
0.53	0.4701933	−1.002879	0.03673788	0.02	1.012646	−1.230770	1.387049
0.52	0.4802240	−1.003266	0.04081159	0.01	1.025024	−1.244988	1.457088
0.51	0.4902588	−1.003696	0.04523817	0.0	1.037548	−1.259921	1.529954
0.50	0.5002981	−1.004172	0.05003989				

Table C-2 $(d\theta/d\Lambda)_{=0}$ vs. z

First column: The values calculated from Eq.(C-81)

Second column: The values calculated from Eq.(C-89) or Eq.(C-90)

z	$\left(\frac{d\theta}{d\Lambda}\right)_{\Lambda=0}$	$\left(\frac{d\theta}{d\Lambda}\right)_{\Lambda=0}$	z	$\left(\frac{d\theta}{d\Lambda}\right)_{\Lambda=0}$	$\left(\frac{d\theta}{d\Lambda}\right)_{\Lambda=0}$
0.05	0.1804865	0.1804857	0.55	0.9867506	0.9867506
0.1	0.3513561	0.3513559	0.6	0.9934487	0.9934487
0.15	0.5046748	0.5046753	0.65	0.9970560	0.9970560
0.2	0.6353238	0.6353239	0.7	0.9988319	0.9988317
0.25	0.7413126	0.7413130	0.75	0.9996086	0.9996086
0.3	0.8233712	0.8233705	0.8	0.9998974	0.9998974
0.35	0.8841776	0.8841171	0.85	0.9999818	0.9999818
0.4	0.9271538	0.9271537	0.9	0.9999985	0.9999985
0.45	0.9563167	0.9563165	0.95	1.0000000	1.0000000
0.5	0.9751726	0.9751726	1.0	1.0000000	1.0000000

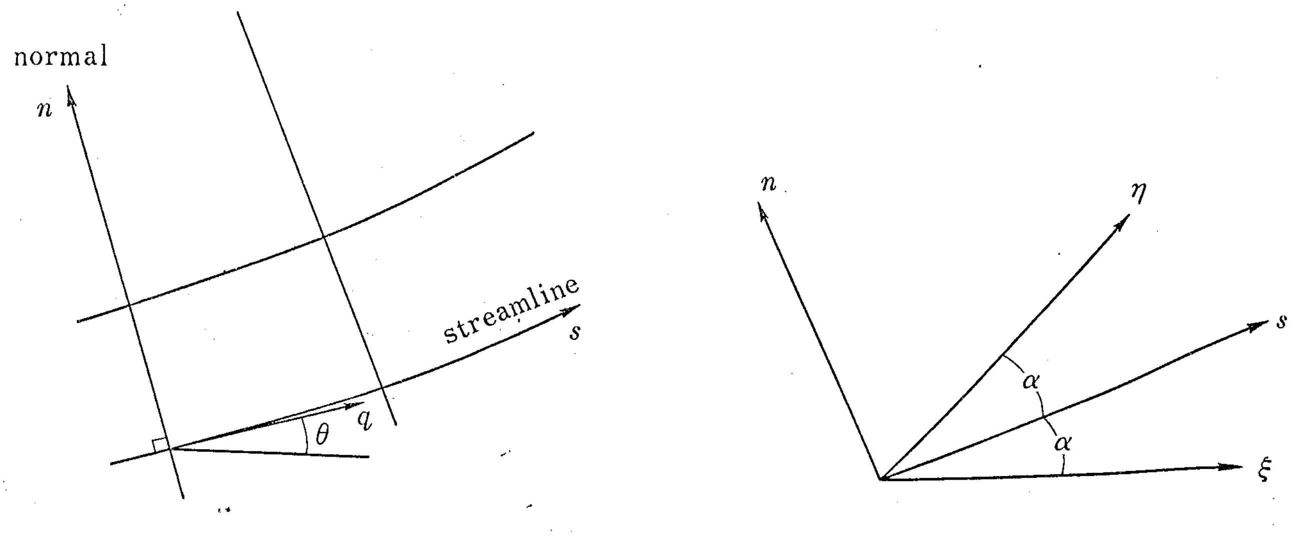

(a) natural coordinates

(b) characteristic coordinates

FIG.C-1 COORDINATES FOR TWO-DIMENSIONAL SUPERSONIC FLOW

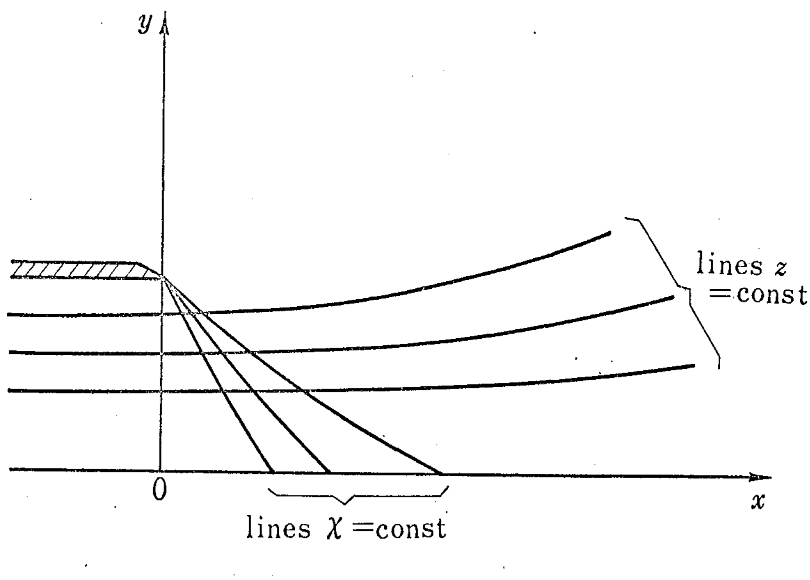

FIG.C-2 COORDINATES FOR TWO-DIMENSIONAL SUPERSONIC JET

Appendix D

The Equations of Motion for a Steady One-Dimensional Shock Wave of Binary Gas Mixture (24, 30)

The conservation equations of mass, momentum and energy in a one-dimensional shock wave of binary gas mixture are given by

$$\rho u = \rho_1 u_1 - \rho_2 u_2 = m \tag{D-1}$$

$$\rho u^2 + p - \frac{4}{3}\mu \frac{du}{dx} = P = \rho_\infty u_\infty^2 + p_\infty \tag{D-2}$$

$$\rho u \left(h + \frac{1}{2}u^2\right) - \frac{4}{3}\mu u \frac{du}{dx} + q_x = \frac{1}{2}Q = m\left(h_\infty + \frac{1}{2}u_\infty^2\right) \tag{D-3}$$

with

$$q_x = -\lambda \frac{dT}{dx} + \rho_1 (u_1 - u)\left(h_1 - h_2 + \frac{M^2}{M_1 M_2}\frac{p}{\rho}\alpha\right) \tag{D-4}$$

where ρ, u, p, T, h, M, α and λ, respectively denote density, velocity, pressure, temperature, enthalpy, molecular weight, thermal diffusion factor and coefficient of thermal conductivity. Subscript 1 denotes the heavier molecular component, 2 denotes the lighter, and subscript ∞ denotes quantities outside the shock.

Sherman combines the above continum flow conservation equations with the equation for diffusion velocity given by the Chapman-Enskog theory. The latter equation is written in the form:

$$V_1 = u_1 - u = \frac{\rho M_1 M_2}{\rho_1 M^2}\mathcal{D}_{12}\left\{f(1-f)\left[\frac{M_1 - M_2}{M}\frac{d}{dx}\ln p - \alpha \frac{d}{dx}\ln T\right] - \frac{df}{dx}\right\} \tag{D-5}$$

where f is the mole fraction of the heavier species; $M = fM_1 + (1-f)M_2$ is the mean molecular mass; $\mathcal{D}_{12}$ is the binary diffusion coefficient; V_1 is the diffusion velocity of the heavy species defined by

$$V_1 = u_1 - u \tag{D-6}$$

where u_1 is the mass average velocity of the heavy species and u is the center of mass velocity of an element of the gas mixture. The equation of state for ideal gas is written in the form:

$$p = \frac{M_\infty}{M} \rho \tilde{R} T \tag{D-7}$$

where

$$\tilde{R} \equiv \frac{p_\infty}{\rho_\infty T_\infty} \tag{D-8}$$

Furthermore, Sherman introduced following dimensionless variables and parameters:

$v = m u / P$

$\tau = m^2 \tilde{R} T / P^2$

$a = m Q / P^2$

$\theta = M_1 / M_2$

f_∞ = mole fraction of heavy molecules outside the shock and the reference length $L = \mu / m$

Then, with the aid of Eqs. (D-1) and (D-7), Eqs. (D-2), (D-3) and (D-5) are rewritten in the forms:

$$L \frac{dv}{dx} = \frac{3}{4} \left\{ v - \frac{1 + (\theta - 1) f_\infty}{1 + (\theta - 1) f} \frac{\tau}{v} - 1 \right\} \tag{D-9}$$

$$L \frac{d\tau}{dx} = \frac{\gamma - 1}{2\gamma} \frac{\mu C_p}{\lambda} \left\{ 2v - v^2 - a + 2\tau \times \left[\frac{\gamma}{\gamma - 1} - \frac{1 + (\theta - 1) f_\infty}{1 + (\theta - 1) f} + (f_0 - f)\alpha \right] \right\} \tag{D-10}$$

$$L \frac{df}{dx} = - \frac{\mu}{\rho \mathcal{D}_{12}} \frac{(f_\infty - f)[1 + (\theta - 1) f]^3}{[1 + (\theta^2 - 1) f][1 + (\theta - 1) f_\infty]} - L \frac{f(1-f)[1 + (\theta - 1) f]}{1 + (\theta^2 - 1) f} \times \left\{ (\theta - 1) \frac{d}{dx} \ln v - \left[(\theta - 1) - \alpha \{ 1 + (\theta - 1) f \} \right] \frac{d}{dx} \ln \tau \right\} \tag{D-11}$$

The independent variables x can be eliminated by dividing Eqs. (D-10) and (D-11) by Eq. (D-9). This yields two direction field equations for $d\tau / dv$ and df / dv for which we seek a solution.

On the other hand, the coefficients a_i, b_i, and c_i (i=1, 2, 3) are expressed as follows:

$$a_1 = \frac{3}{4}\left(1 - \frac{\tau_\infty}{v_\infty^2}\right) \quad \text{(D-12)}$$

$$a_2 = \frac{3}{4}\frac{\tau_\infty}{v_\infty}\frac{(\theta - 1)}{1 + (\theta - 1)f_o} \quad \text{(D-13)}$$

$$a_3 = -\frac{3}{4}\frac{1}{v_\infty} \quad \text{(D-14)}$$

$$b_1 = -\frac{\gamma - 1}{2\gamma} P_r^\infty\, 2(1 - v_\infty) \quad \text{(D-15)}$$

$$b_2 = -\frac{\gamma - 1}{2\gamma} P_r^\infty\, 2\tau_\infty\left[\alpha - \frac{(\theta - 1)}{1 + (\theta - 1)f_o}\right] \quad \text{(D-16)}$$

$$b_3 = \frac{1}{\gamma} P_r^\infty \quad \text{(D-17)}$$

$$c_1 = \frac{f_o(1 - f_o)[1 + (\theta - 1)f_o]}{[1 + (\theta^2 - 1)f_o]}\frac{(\theta - 1)}{v_\infty} \quad \text{(D-18)}$$

$$c_2 = S_c^\infty \frac{[1 + (\theta - 1)f_o]^2}{[1 + (\theta^2 - 1)f_o]} \quad \text{(D-19)}$$

$$c_3 = \frac{f_o(1 - f_o)[1 + (\theta - 1)f_o]}{[1 + (\theta^2 - 1)f_o]}[(\theta - 1) - \alpha\{1 + (\theta - 1)f_o\}]\frac{1}{\tau_\infty}$$

(D-20)

Appendix E The Differential Equations for Shock Profile

The differential equations which determine the attached shock shape ahead of a cone placed in a supersonic flow have been given by Bartyenev and Shirshov (32), in the following forms:
(The reader is referred to Fig.)

$$\frac{dv_0}{ds} = \frac{\frac{\gamma-1}{\gamma+1}(1-v_0^2)}{R_0\rho_0\left(\frac{\gamma-1}{\gamma+1}-v_0^2\right)}\left[\frac{s}{\varepsilon}\cos\Theta\tan\left(\sigma+\Theta-\frac{\pi}{2}\right)(\rho_\varepsilon v_\varepsilon^- - \rho_0 v_0^-)\right.$$
$$\left. - 2\rho_\varepsilon u_\varepsilon\left(\frac{s}{\varepsilon}\cos\Theta+\sin\Theta\right) - \cos\Theta\left(\rho_\varepsilon v_\varepsilon^- + \rho_0 v_0^-\right)\right]$$
$$- \frac{\frac{\gamma-1}{\gamma+1}(1-v_0^2)}{\rho_0\left(\frac{\gamma-1}{\gamma+1}-v_0^2\right)}\;\frac{1}{1+\frac{\varepsilon}{s}\tan\Theta}\left(\rho_\varepsilon\frac{dv_\varepsilon}{ds}+v_\varepsilon\frac{d\rho_\varepsilon}{ds}\right) \tag{E-1}$$

$$\frac{d\sigma}{ds} = \frac{1}{\varepsilon\left(\cos\Theta+\frac{\varepsilon}{s}\sin\Theta\right)(\rho_\varepsilon v_\varepsilon^- F_1+\rho_\varepsilon u_\varepsilon F_5+u_\varepsilon v_\varepsilon^- F_9)}\times$$
$$\times\left[\left(\frac{\varepsilon}{s}\sin\Theta+2\cos\Theta\right)\frac{\gamma-1}{2\gamma}(p_0-p_\varepsilon) - 2\rho_\varepsilon u_\varepsilon^2\left(\sin\Theta\frac{\varepsilon}{s}+\cos\Theta\right)\right.$$
$$\left. +\rho_\varepsilon u_\varepsilon v_\varepsilon^-\tan\left(\sigma+\Theta-\frac{\pi}{2}\right)\cos\Theta\left(1-\frac{\varepsilon}{s\tan\left(\sigma+\Theta-\frac{\pi}{2}\right)}\right)\right] \tag{E-2}$$

$$\frac{d\varepsilon}{ds} = \tan\left(\sigma+\Theta-\frac{\pi}{2}\right)$$

with

$$\frac{du_\varepsilon}{ds} = F_1\frac{d\sigma}{ds} + F_2\frac{d\theta}{ds} + F_4\frac{dM_\infty}{ds} \tag{E-3}$$

$$\frac{dv_\varepsilon}{ds} = F_5\frac{d\sigma}{ds} + F_6\frac{d\theta}{ds} + F_8\frac{dM_\infty}{ds} \tag{E-4}$$

$$\frac{d\rho_\varepsilon}{ds} = F_9\frac{d\sigma}{ds} + F_{10}\frac{d\theta}{ds} + F_{11}\frac{dM_\infty}{ds} \tag{E-5}$$

where σ , v_0 , and ε , respectively denote angle of shock inclination, velocity on cone surface and distance to shock along r axis; s axis is in the direction of generatrix of cone and r axis perpendicular to it; subscript ε denote quantities just behind the shock. The coefficients , F_i are given as follows:

$$F_1 = \frac{\partial u_\varepsilon}{\partial \sigma} = \frac{2V_\infty}{\gamma+1}\left\{\sin(2\sigma+\theta-\Theta) + \frac{\sin(\Theta+\theta)}{M_\infty^2 \sin^2(\sigma-\theta)}\right\} \tag{E-6}$$

$$F_2 = \frac{\partial u_\varepsilon}{\partial \theta} = V_\infty\left\{\sin(\Theta+\theta) - \left[1 + \frac{1}{M_\infty^2 \sin^2(\sigma-\theta)}\right]\frac{2\sin(\sigma+\Theta)\cos(\sigma-\theta)}{\gamma+1}\right\} \tag{E-7}$$

$$F_3 = \frac{\partial u_\varepsilon}{\partial \Theta} = V_\infty\left\{\left[1 - \frac{1}{M_\infty^2 \sin^2(\sigma-\theta)}\right]\frac{2\sin(\sigma-\theta)\cos(\sigma+\theta)}{\gamma+1} + \sin(\Theta+\theta)\right\} \tag{E-8}$$

$$F_4 = \frac{\partial u_\varepsilon}{\partial M} = \frac{2u_\varepsilon}{M_\infty[(\gamma-1)M_\infty^2+2]} + \frac{4V_\infty}{M_\infty^3(\gamma+1)}\cdot\frac{\sin(\sigma+\Theta)}{\sin(\sigma-\theta)} \tag{E-9}$$

$$F_5 = \frac{\partial v_\varepsilon}{\partial \sigma} = \frac{2V_\infty}{\gamma+1}\left\{\cos(2\sigma+\Theta-\theta) + \frac{\cos(\Theta+\theta)}{M_\infty^2 \sin^2(\sigma-\theta)}\right\} \tag{E-10}$$

$$F_6 = \frac{\partial v_\varepsilon}{\partial \theta} = V_\infty\left\{\cos(\Theta+\theta) - \left[1 + \frac{1}{M_\infty^2 \sin^2(\sigma-\theta)}\right]\frac{2\cos(\sigma+\Theta)\cos(\sigma-\theta)}{\gamma+1}\right\} \tag{E-11}$$

$$F_7 = \frac{\partial v_\varepsilon}{\partial \Theta} = V_\infty\left\{\cos(\Theta+\theta) - \left[1 - \frac{1}{M_\infty^2 \sin^2(\sigma-\theta)}\right]\frac{2\sin(\sigma-\Theta)\sin(\sigma+\Theta)}{\gamma+1}\right\} \tag{E-12}$$

$$F_8 = \frac{\partial v_\varepsilon}{\partial M} = \frac{2v_\varepsilon}{M_\infty[(\gamma-1)M_\infty^2+2]} + \frac{4V_\infty}{M_\infty^3(\gamma+1)}\cdot\frac{\cos(\sigma+\Theta)}{\sin(\sigma-\theta)} \tag{E-13}$$

$$F_9 = \frac{\partial \rho_\varepsilon}{\partial \sigma} = \rho_\varepsilon\left[2\cot(\sigma-\theta) - \frac{\frac{\gamma-1}{\gamma+1}M_\infty^2 \sin 2(\sigma-\theta)}{\left(1-\frac{\gamma-1}{\gamma+1}\right) + \frac{\gamma-1}{\gamma+1}M_\infty^2\sin^2(\sigma-\theta)}\right] \tag{E-14}$$

$$F_{10} = \frac{\partial \rho_\varepsilon}{\partial \theta} = -F_9 \tag{E-15}$$

$$F_{11} = \frac{\partial \rho_\varepsilon}{\partial M} = 2\rho_\varepsilon\left\{\frac{2+(\gamma-2)M_\infty^2}{M_\infty[2+(\gamma-1)M_\infty^2]} - \frac{M_\infty\frac{\gamma-1}{\gamma+1}\sin^2(\sigma-\theta)}{\left(1-\frac{\gamma-1}{\gamma+1}\right) + \frac{\gamma-1}{\gamma+1}M_\infty^2\sin^2(\sigma-\theta)}\right\} \tag{E-16}$$

where M_∞ denotes the initial Mach number;

$$V_\infty^2 = \frac{(\gamma-1)M_\infty^2}{2+(\gamma-1)M_\infty^2} \; . \tag{E-17}$$

Appendix F An Analysis of Conductive Heat Transfer from a Sphere to Rarefied Gas

In this section, Nusselt number was calculated analytically as a function of Knudsen number on the basis of the same procedure of Lees and Liu (56). This procedure is to solve the Maxwell integral equation of transport utilizing the two-sided Maxwellian distribution function. Maxwell's equation for a physical quantity ψ which depends on the velocity of a molecule is given as follows: (40 , 57)

$$\frac{\partial n\overline{\psi}}{\partial t} + div_r\, n\overline{\psi V} - n\,\overline{\frac{\partial \psi}{\partial t}} + \overline{V \cdot grad_r \psi} + \frac{X}{m} \cdot \overline{grad_V \psi} = \Delta \psi \qquad \text{(F-1)}$$

where a bar script denotes the mean quantity by averaging over all velocity space, and $\Delta\psi$, is the change of ψ produced by collisions.

We consider a sphere of radius R_0 placed in an infinite gaseous media of single component at an arbitrary pressure. The temperature on the surface is set T_w and the temperature at infinity, T_∞ (see Fig.F-1). In the spherical coordinate system. Eq. (F-1) can be written in the following form:

$$\frac{1}{r^2}\frac{\partial}{\partial r} r^2 \int f V_r \psi \, dV + \frac{1}{r \tan\theta} \int f V_\theta \psi \, dV$$
$$+ \int f \left(\frac{1}{r} V_\varphi V_r + \frac{1}{r \tan\theta} V_\varphi V_\theta \right) \frac{\partial \psi}{\partial V_\varphi} dV$$
$$+ \int f \left(\frac{1}{r} V_\theta V_r - \frac{1}{r \tan\theta} V_\varphi^2 \right) \frac{\partial \psi}{\partial V_\theta} dV$$
$$- \int f \left(\frac{1}{r} V_\theta^2 + \frac{1}{r} V_\varphi^2 \right) \frac{\partial \psi}{\partial V_\varphi} dV = \Delta \psi \qquad \text{(F-2)}$$

By applying Lee's model, the velocity distribution function was assumed as follows:

$$f_1 = n_1 \left(\frac{\beta_1}{\pi}\right)^{\frac{3}{2}} exp(-\beta_1 V^2), \quad or$$
$$f_2 = n_2 \left(\frac{\beta_2}{\pi}\right)^{\frac{3}{2}} exp(-\beta_2 V^2) \qquad \text{(F-3)}$$

according as

$$0 \leq \mu \leq \frac{\pi}{2} - \alpha, \quad or \quad \frac{\pi}{2} - \alpha \leq \mu \leq \pi$$

where n_1, n_2, $\beta_1 = m/2kT_1$ and $\beta_2 = m/2kT_2$ are unknown functions of radial distance. Setting $\psi = m, mV_r, \frac{1}{2}mV^2 + u$ or $(\frac{1}{2}mV^2+u)V_r$, we obtain the following ordinary differential equations from Eqs. (F-2) and (F-3) on the assumption that internal energy, u is independent of molecular velocity.

$$\bar{n}_1 \bar{T}_1^{\frac{1}{2}} = \bar{n}_2 \bar{T}_2^{\frac{1}{2}} \tag{F-4}$$

$$\bar{n}_1 \bar{T}_1^{\frac{3}{2}} - \bar{n}_2 \bar{T}_2^{\frac{3}{2}} = \omega \tag{F-5}$$

$$\sin^3\alpha \frac{d}{d\bar{r}} (\bar{n}_1 \bar{T}_1 - \bar{n}_2 \bar{T}_2) - \frac{d}{d\bar{r}} (\bar{n}_1 \bar{T}_1 + \bar{n}_2 \bar{T}_2) = 0 \tag{F-6}$$

$$\sin^3\alpha \cdot \frac{d}{dr} (n_1 T_1^2 - n_2 T_2^2) - \frac{d}{dr} (n_1 T_1^2 + n_2 T_2^2) = \frac{4}{15} \frac{R_o}{L_\infty} \frac{1}{\bar{r}^2} \left[n_1 (1 - \sin\alpha) + n_2 (1 + \sin\alpha) \right] \omega \tag{F-7}$$

where all quantities are expressed non-dimensionally by characteristic number density n_∞, temperature T_∞, and the radius of the sphere, and all dimensionless quantities are denoted by a bar superscript, and is an integration constant.

The change of ψ produced by collisions $\Delta\psi$, was expressed from Maxwell's inverse fifth power force law

$$F = m_1 m_2 \frac{\tilde{K}}{r^5} \tag{F-8}$$

Then the mean free path, L_∞ and the viscosity, μ_∞ become (56)

$$L_\infty = \frac{1}{3 A_2 \rho_\infty} \left(\frac{\pi k T_\infty}{\tilde{K}} \right)^{\frac{1}{2}} \tag{F-9}$$

$$\mu = \frac{kT}{\frac{3}{2} A_2 (2m\tilde{K})^{\frac{1}{2}}} \tag{F-10}$$

where A = 1.3682 and

$$\Delta \left(\frac{1}{2} mV^2 + u \right) V_r = \frac{p}{\mu} \left(- \frac{2}{3} q_r^{Tr} \right) \tag{F-11}$$

where p = total pressure, and q_r^{Tr} = radial translational energy flux.

$$p = \frac{1}{2} k \left[n_1 T_1 (1 - \sin\alpha) + n_2 T_2 (1 + \sin\alpha) \right] \tag{F-12}$$

$$q_r^{Tr} = \frac{1}{2} \pi^{-\frac{1}{2}} m \cos^2\alpha \times (n_1 \beta_1^{-\frac{3}{2}} - n_2 \beta_2^{-\frac{3}{2}}) = k n_\infty T_\infty \left(\frac{2k}{\pi m} \right)^{\frac{1}{2}} \omega \left(\frac{R_o}{r} \right)^2 \tag{F-13}$$

The boundary condition at $\bar{r} = 1$ and at $\bar{r} = \infty$ are

$$\frac{T_1 - T_2}{T_w - T_2} = \alpha \ , \quad T = T_2 = T_\infty \ , \quad n = n_2 = n_\infty \qquad \text{(F-14)}$$

where α denotes the accommodation coefficient. In the present investigation, the amount of maximum departure of T_w / T_∞ from unity was only about 0.2, so that it will be valid to assume that

$$\begin{aligned} \bar{n}_1 &= 1 + N_1 \\ \bar{n}_2 &= 1 + N_2 \\ T_1 &= 1 + t_1 \\ T_2 &= 1 + t_2 \\ N_1 , N_2 &, t_1 , t_2 \leqslant 1 \end{aligned} \qquad \text{(F-15)}$$

Upon substitution of Eq. (F-15) into Eqs. (F-4), (F-5), (F-6) and (F-7), one obtains the following set of linearized equations:

$$N_1 + \frac{1}{2} t_1 = N_2 + \frac{1}{2} t_2 \qquad \text{(F-16)}$$

$$(N_1 - N_2) + \frac{3}{2} (t_1 - t_2) = \omega \qquad \text{(F-17)}$$

$$\sin^3 \alpha \frac{d}{d\bar{r}} (N_1 + t_1 - N_2 - t_2) - \frac{d}{d\bar{r}} (N_1 + t_1 + N_2 + t_2) = 0 \qquad \text{(F-18)}$$

$$\sin^3 \alpha \frac{d}{d\bar{r}} (N_1 - N_2 + 2t_1 - 2t_2) - \frac{d}{d\bar{r}} (2 + N_1 + N_2 + 2t_1 + 2t_2) \simeq \frac{8}{15} \frac{R_0}{L_\infty} \frac{1}{\bar{r}^2} \omega \qquad \text{(F-19)}$$

The boundary condition at infinity becomes

$$\bar{r} \longrightarrow \infty ; \quad t_2 = 0 , \quad N_2 = 0 \qquad \text{(F-20)}$$

From Eqs. (F-16) and (F-17)

$$t_1 - t_2 = \omega \qquad \text{(F-21)}$$

$$N_1 - N_2 = -\frac{1}{2} \omega \qquad \text{(F-22)}$$

Then by integrating Eq. (F-18),

$$N_1 + N_2 + t_1 + t_2 = const. = \frac{1}{2} \omega \qquad \text{(F-23)}$$

With the aid of the above equation and the boundary condition at infinity, Eq. (F-19) is integrated to give

$$t_1 + t_2 = \frac{8}{15}\frac{R_0}{L_\infty}\,\omega\,\frac{1}{r} + \omega \tag{F-24}$$

Hence,

$$t_1 = \omega\left(1 + \frac{4}{15}\frac{R_0}{L_\infty}\frac{1}{r}\right) \tag{F-25}$$

$$t_2 = \frac{4}{15}\frac{R_0}{L_\infty}\,\omega\,\frac{1}{r} \tag{F-26}$$

$$\overline{T}_1 = 1 + t_1 = 1 + \omega\left(1 + \frac{4}{15}\frac{R_0}{L_\infty}\right) \tag{F-27}$$

$$\overline{T}_2 = 1 + t_2 = 1 + \frac{4}{15}\frac{R_0}{L_\infty}\,\omega \tag{F-28}$$

The boundary condition at $r = 1$ is

$$\frac{\overline{T}_1 - \overline{T}_2}{\overline{T}_w - \overline{T}_2} = \alpha \tag{F-29}$$

From Eqs. (F-27), (F-28) and (F-29), there follows

$$\omega = \frac{\alpha\left(\overline{T}_w - 1\right)}{\alpha\frac{4}{15}\frac{R_0}{L_\infty} + 1} \tag{F-30}$$

At limit of $K_n \to 0$,

$$\omega_{K_n \to 0} = \frac{15}{4}\frac{L_\infty}{R_0}\frac{T_w - T_\infty}{T_\infty} \tag{F-31}$$

We may assume for the radial heat flux q_r ,

$$q_r = (1 + \theta\kappa)\, q_r^{T_r} \tag{F-32}$$

where denotes the ratio of internal energy to translational energy and $\kappa = (5-3\gamma)/3(\gamma-1)$, θ is a pure number and nearly unity. Therefore, the radial heat flux in the continuum regime, $q_{r,K_n\to 0}$ becomes from Eq. (F-13)

$$q_{r,K_n\to 0} = (1+\theta\kappa)\, k\, n_\infty \left(\frac{2k}{\pi m}\right)^{\frac{1}{2}} \frac{R_0}{r^2}\,\frac{15}{4}\, L_\infty\,(T_w - T_\infty) \tag{F-33}$$

The above expression readily yields the Fourier law of heat conduction,

$$q_{r,K_n\to 0} = \lambda_g \frac{R_0}{r^2}(T_w - T_\infty), \qquad \lambda_g = (1 + \theta\kappa)\,\lambda_g^{(M)} \tag{F-34}$$

as we utilize the relation of $\lambda_g^{(M)} = \frac{15}{4}\mu k/m$ for a monatomic gas and Eqs. (F-9) and (F-10).

As Nu^* is expressed from the definition,

$$Nu^* = \frac{hD}{\lambda_g} = \frac{D}{\lambda_g}\,\frac{q_{r,\bar{r}=1}}{T_w - T_\infty} = \frac{D}{\lambda_g}\,\frac{q_{r,Kn\to 0,\bar{r}=1}}{T_w - T_\infty}$$

$$\times\ \frac{q_{r,\bar{r}=1}}{q_{r,Kn\to 0,\bar{r}=1}} = \frac{D}{\lambda_g}\,\frac{\omega}{\omega_{Kn\to 0}}\,q_{r,Kn\to 0,\bar{r}=1} \qquad \text{(F-35)}$$

we eventually obtain the following expression for Nusselt number as a function of Kn and α with the aid of Eqs. (F-30), (F-31) and (F-33).

$$Nu^* = \frac{2}{1 + \frac{15}{2}Kn\,\alpha^{-1}}\ , \qquad Kn = \frac{L_\infty}{2R_0} \qquad \text{(F-36)}$$

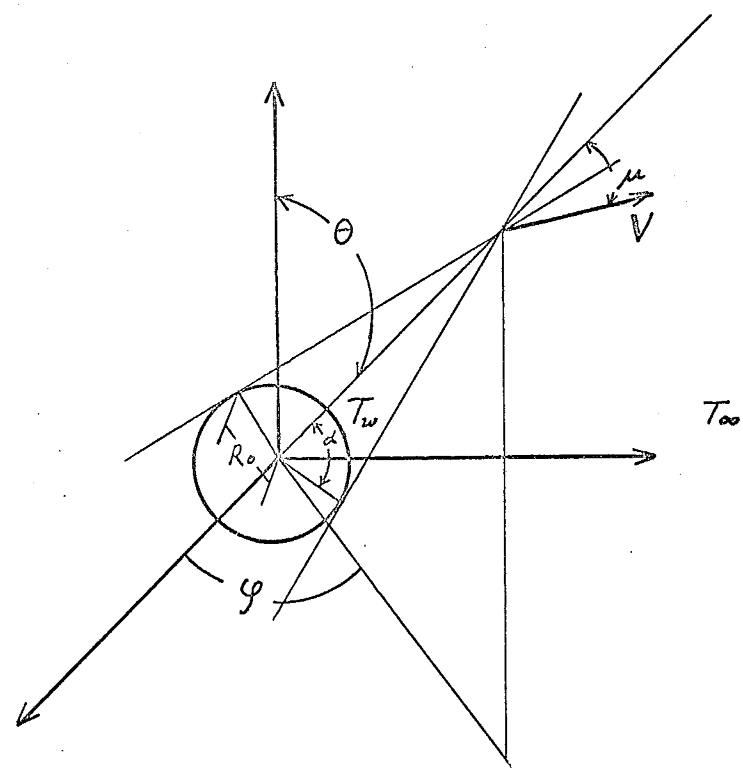

FIG.F-1 DIAGRAM FOR A SPHERE IN THE SPHERICAL POLAR COORDINATE SYSTEM

Appendix G

Comparison of Their Magnitudes between the Three Terms in the Diffusion Flux Equation

The expression for the mass flux, $\dot{j}_i$ consists of three terms describing ordinary diffusion, pressure diffusion, and thermal diffusion as shown in Chapter II, Eq.(2.1). In the present study, the terms of both ordinary diffusion and of thermal diffusion were neglected in comparison with the term of pressure diffusion. Furthermore, the invicid flow field of supersonic jet was applied for evaluating the pressure diffusion flux.

The validity of this simplification can be verified in the manner as described below along the line of analysis made by Sherman (24). In the case of steady flow of a binary gas mixture with zero external body force, the governing equations are as follows:

Total continuity:

$$\mathrm{div}\,\rho \mathbb{V} = \mathrm{div}\,\rho_1 \mathbb{V}_1 + \mathrm{div}\,\rho_2 \mathbb{V}_2 = 0 \qquad \text{(G-1)}$$

Species continuity:

$$\mathrm{div}\,\rho_1 \mathbb{V}_1 = \mathrm{div}\,\rho_1 \mathbb{V} + \mathrm{div}\,\rho_1 \mathbb{V}_1 = 0 \qquad \text{(G-2)}$$

Total momentum:

$$\rho \mathbb{V}\cdot \mathrm{grad}\,\mathbb{V} + \mathrm{grad}\,p = \frac{1}{Re}\left\{ \mathrm{grad}\,\zeta\, \mathrm{div}\,\mathbb{V} + \mathrm{div}\,\mu\, \mathrm{def}\,\mathbb{V} \right\} \qquad \text{(G-3)}$$

Total energy:

$$\rho T \mathbb{V}\cdot \mathrm{grad}\,S = \frac{\gamma}{Re}\left\{ \frac{\gamma-1}{Pr}\mathrm{div}\,\lambda\, \mathrm{grad}\,T + (\zeta\, \mathrm{div}\,\mathbb{V} + \mu\, \mathrm{def}\,\mathbb{V})\cdot \mathrm{grad}\,\mathbb{V} \right\}$$
$$+ \mathrm{div}\left\{ \rho_1 \mathbb{V}_1 \left(\frac{\gamma_1}{\gamma_1 - 1}\frac{m}{m_1} - \frac{\gamma_2}{\gamma_2 - 1}\frac{m}{m_2} + \frac{m^2}{m_1 m_2}\alpha_T \right) T \right\} \qquad \text{(G-4)}$$

Diffusion equation:

$$\rho_1 \mathbb{V}_1 = \frac{1}{Re\,Sc}\frac{m_1 m_2}{m^2} T^{\frac{1}{2}} \frac{1}{\Omega^{(1,1)*}}\left\{ \mathrm{grad}\,N_1 - \frac{\Delta m}{m} N_1 N_2\, \mathrm{grad}\,\ln p - k_T\, \mathrm{grad}\,\ln T \right\} \qquad \text{(G-5)}$$

where all velocities are measured in units of stagnation sound speed and all physical quantities except for mass, mole fraction, and thermal diffusion factor in units of their stagnation quantities, respectively.

Taking the divergence of Eq.(G-5), and using Eqs.(G-2) and (G-1), we get

$$\rho \mathbb{V}\cdot \mathrm{grad}(\rho_1/\rho) = -\frac{1}{Re\, Sc}\,\mathrm{div}\,\frac{m_1 m_2}{m^2} T^{\frac{1}{2}} \frac{1}{\Omega^{(1,1)*}} \times$$
$$\times \left\{ \mathrm{grad}\, N_1 - \frac{\Delta m}{m} N_1 N_2\, \mathrm{grad}\ln p - k_T\, \mathrm{grad}\ln T \right\} \qquad \text{(G-6)}$$

Thus, the expression for mass fraction, $w = \rho_1/\rho$ is given in the form:

$$w - w_0 = -\frac{1}{Re\, Sc}\int_0^s \mathrm{div}\,\frac{m_1 m_2}{m^2} T^{\frac{1}{2}} \frac{1}{\Omega^{(1,1)*}} \times$$
$$\times \left\{ \mathrm{grad}\, N_1 - \frac{\Delta m}{m} N_1 N_2\, \mathrm{grad}\ln p - k_T\, \mathrm{grad}\ln T \right\} \frac{ds}{\rho q} \qquad \text{(G-7)}$$

where the path of integration is a streamline and subscript 0 denotes a quantity under the stagnation condition.
Then all the quantities can be expanded in terms of ε = 1/Re.
These are

$$\left.\begin{aligned}
\rho &= \rho^{(0)} + \varepsilon\rho^{(1)} + \cdots \\
\rho_1 &= \rho_1^{(0)} + \varepsilon\rho_1^{(1)} + \cdots \\
w &= w^{(0)} + \varepsilon w^{(1)} + \cdots \\
\mathbb{V} &= \mathbb{V}^{(0)} + \varepsilon \mathbb{V}^{(1)} + \cdots \\
\mathbb{V}_1 &= \mathbb{V}_1^{(0)} + \varepsilon \mathbb{V}_1^{(1)} + \cdots \\
N_i &= N_i^{(0)} + \varepsilon N_i^{(1)} + \cdots \\
T &= T^{(0)} + \varepsilon T^{(1)} + \cdots
\end{aligned}\right\} \qquad \text{(G-8)}$$

If these series are substituted into Eqs.(G-1) to (G-7) and coefficients of equal power of ε are equated, we obtain the set of equations for $\mathbb{V}_1^{(0)}\ \mathbb{V}_1^{(1)}, \cdots, w^{(0)}, w^{(1)}, \cdots$ etc.
From terms of order ε^0, we get Euler's equation of motion (Eq.(G-3)). To this approximation, the flow is isentropic (Eq.(G-4)) and the mixture remains homogenious (Eq.(G-7)) and mass flux becomes zero (Eq.(G-5)).
Then, the mass flux perturbation, proportinal to 1/Re is given by

$$\rho_1^{(0)}\mathbb{V}_1^{(1)} = \frac{1}{Re\, Sc}\frac{m_1 m_2}{m^2} T^{(0)\frac{1}{2}} \frac{1}{\Omega^{(1,1)*}(T^{*(0)})}$$
$$\times \left\{ -\frac{\Delta m}{m} N_1^{(0)} N_2^{(0)}\, \mathrm{grad}\ln p^{(0)} - k_T\, \mathrm{grad}\ln T^{(0)} \right\} \qquad \text{(G-9)}$$

At high Reynolds number, the first order perturbation will be a good approximation to the exact solution. Then, the ordinary diffusion flux can be safely neglected in comparison with other terms.

Now, let's compare the order of magnitudes of pressure diffusion flux to thermal diffusion flux. For invicid flow, we have

$$p\,T^{\frac{\gamma}{\gamma-1}} = const \tag{G-10}$$

Hence,

$$grad \ln T = \frac{\gamma-1}{\gamma}\, grad \ln p \tag{G-11}$$

Thus the ratio of thermal diffusion flux to the pressure diffusion flux is given by

$$\frac{\gamma-1}{\gamma}\alpha_T \Big/ \frac{\Delta m}{m} \tag{G-12}$$

where α_T denotes the thermal diffusion factor. In the table G-1, the above value is shown for several pairs of molecules. It is seen that thermal diffusion flux can be neglected in first approximation. The more valid expression for the mass flux is written in the form:

$$\begin{aligned} j_1 &= -\left(\frac{\Delta m}{m} N_1^{(0)} N_2^{(0)} + k_T \frac{\gamma-1}{\gamma}\right) grad\, p \\ &= -N_1^{(0)} N_2^{(0)}\left(\frac{\Delta m}{m} + \alpha_T \frac{\gamma-1}{\gamma}\right) grad\, p \end{aligned} \tag{G-13}$$

Table G-1 Ratio of Thermal Diffusion Flux to Pressure Diffusion Flux

	γ	$(\gamma-1)/\gamma\ \alpha_T$	$\Delta m/\bar{m}$	$\frac{\gamma-1}{\gamma}\alpha_T \Big/ \frac{\Delta m}{\bar{m}}$
He - Ar(1:1)	1.66667	0.148	1.636	0.0905
H_2 - N_2(1:1)	1.4	0.0886	1.733	0.0511
^{36}Ar - ^{40}Ar	1.66667	0.00728	0.1	0.0728
$^{235}UF_6$-$^{238}UF_6$	1.067	0.0^4141	0.0 0852	0.00165